Table of Contents

LIST OF TABLES

LIST OF FIGURES

5.0 PHYSICAL ENVIRONMENT

The Project Area is located off the Northeast Newfoundland Slope in the Orphan Basin, is approximately 44,695 km² in size, and encompasses the overall geographic area within which planned Project-related activities will take place (see Figure 2.1 in Section 2.2). Three of the ELs (ELs 1145, 1146, 1148) are in the West Orphan Basin, and EL 1149 is in the East Orphan Basin. The East Orphan Basin is also referred to as the Northern Flemish Pass. The RAA encompasses most of the eastern Newfoundland offshore area and has significant overlap with the Eastern Newfoundland SEA Study Area (Figure 5.1) (Amec 2014).

The following sections provide an overview of the relevant components of the physical environment within the Project Area and in surrounding areas including its geology (including seismicity and bathymetry), climatology, air quality, oceanography, ambient noise, and ice conditions.

Of most relevance to the EIS is information on the physical environment that is used in assessing and evaluating the potential effects of the environment on the Project (Chapter 16). This includes physical environment conditions that could affect Project planning and in-field Project Activities. For this reason, the primary focus of this section is on the Project Area itself.

5.1 Geology

The geology of the Eastern Newfoundland offshore area is complex and dynamic, and the current bedrock and surficial characteristics of the area have been shaped by various natural and human factors and processes over time (Amec 2014). The eastern continental shelf was formed by extension during the breakup of Pangea and the opening of the Atlantic Ocean during the Late Triassic to Cretaceous and is underlain by pre-rift basement rocks (Fader et al. 1989). A combination of rifting and salt tectonics in the area created a series of Mesozoic rift basins. The main sedimentary basins in the area include the Orphan, Flemish Pass, Jeanne d'Arc, and Carson basins (Fader et al. 1989). The following sections provide an overview of the geology, seismicity, and bathymetry of the Project Area and surrounding areas.

5.1.1 Bedrock Geology

The Orphan Basin is a wide continental rift (Enachescu 2006), is approximately 160,000 km² in size (Enachescu et al. 2005) and is bound by the Charlie-Gibbs Transfer Fault Zone to the north, the Continent-Ocean Boundary to the east, the Cumberland Belt Transfer Fault Zone to the south, and the Bonavista Fault Zone to the west (see Figure 5.2) (Enachescu et al. 2005; Enachescu 2006). The Orphan Knoll, in the East Orphan Basin, rises from 3,000 to 1,800 m water depth and is comprised of shallow water marine sediments from the Palaeozoic era overlain by sediments from the Jurassic to Cretaceous periods (Enachescu et al. 2005; Amec 2014).

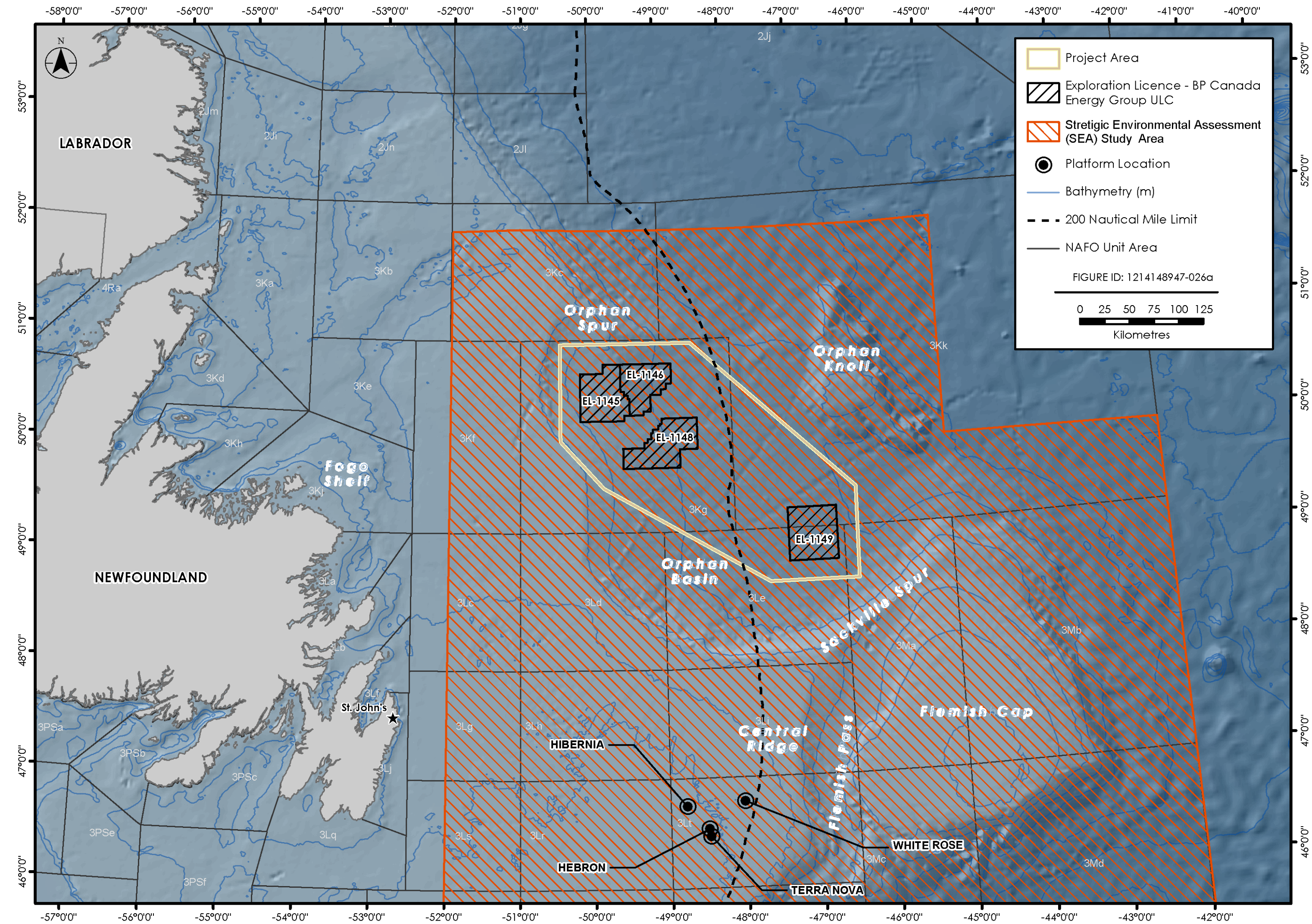

Figure 5.1 Geomorphic Features

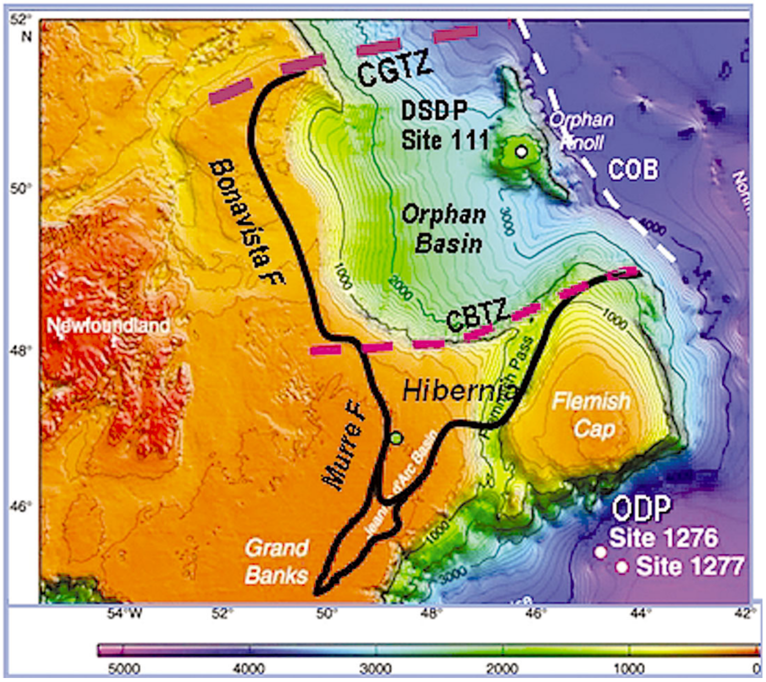

Source: Enachescu 2006
Note: CBZT = Cumberland Belt Transform Fault Zone; CGTZ = Charlie Gibbs Transform Fault Zone; COB = interpreted Continent-Ocean Boundary

Figure 5.2 Basin Boundaries in the Orphan Basin

Prior to the initiation of Mesozoic rifting, the Orphan Basin was part of a broad Paleozoic sedimentary platform within the Avalon terrane of the Appalachian orogenic system (Enachescu 2006). The first phase of rifting, as indicated by seismic stratigraphic relationships, began in the Triassic, and affected the East Orphan Basin (Enachescu 2006). This initial narrow rift (oriented northeast-southwest) expanded during the Late Triassic-Early Jurassic within the Tethys rift system, which extended from the Gulf of Mexico to the Barents Shelf and northern Europe (Enachescu 2006). The rift basin was reactivated, enlarged, and deepened during the Late Jurassic-Early Cretaceous Atlantic rifting phase, after a long thermal subsidence stage (Enachescu 2006). Extension and minor transtension continued during the Aptian-Albian rift phase and into several extensional episodes in the Late Cretaceous and Tertiary (Enchescu 2006). As a result of these extensional episodes, the architecture of Orphan Basin is dominated by alternating ridges of basement block overlain by sediments and deep sub-basins, which are predominantly oriented northeast-southwest or north-south (Enachescu 2006).

The evolution of Orphan Basin involved multiple tectonostratigraphic events that combined to influence the present-day basin morphology and sedimentary fill (Dafoe et al. 2013). Dafoe et al. (2013) provide a list of these events:

- Middle to Late Jurassic rifting, shallow marine deposition, and subsequent deformation
- Tithonian and Early Cretaceous rifting that propagated westward, with shallow marine to shelf deposition

- Development of the central Orphan High and deformation of Tithonian and Lower Cretaceous units around the time of Albian sequence boundary development
- Thinning of continental crust outside of Orphan Knoll and possible contemporaneous development of a major flooding surface in the Albian-Cenomanian
- Santonian sequence boundary development with late crustal faulting in northern Orphan Basin and north of the Charlie-Gibbs Fracture Zone (CGFZ), initiation of transitional crust with true oceanic crust development south of the CGFZ, and major subsidence of the basin in Maastrichtian-Paleocene time
- Magmatism in the northern Orphan Basin
- Tertiary basin filling and shelf-slope development

Considering petroleum potential, and relevant tectono-structural factors, the East Orphan Basin is older than the West Orphan Basin and is a Tethys rift stage remnant with Jurassic, probably Triassic, and Cretaceous sedimentary fill (Enachescu 2006). The East Orphan Basin is situated in deep water (1,500-3,000 m) and is likely to be oil and gas prone (Enachescu 2006). The West Orphan Basin is younger than the East Orphan Basin and evolved during the North Atlantic and Labrador rift stages (Enachescu 2006). The West Orphan Basin contains mostly Cretaceous sedimentary fill, is situated in shallower water (1,000-1,500 m) and is likely to be gas prone (Enachescu 2006). Tertiary cover is thick over West Orphan Basin (4 km) and relatively thin over the East Orphan Basin (2 km) (Enachescu 2006). These two main rift basins (the East and West Orphan Basin) are separated by a major crustal fault zone, the White Sail Fault, which dips eastward and penetrates deeply into the upper crust (Enachescu 2006).

5.1.2 Geomorphology and Surficial Geology

The geomorphology and surficial geology of the Project Area and surrounding areas is a product of modern oceanographic processes and past glacial activity (Statoil Canada Ltd. 2017). The topography of the Orphan Basin is highly diverse, as characterized by depth, location, and physiography. The Orphan Basin proper is in 2,000 to >3,000 m water depth. The West Orphan Basin (ELs 1145, 1146, and 1148) is located on the Northeast Newfoundland Shelf (≤200 m to 2,000 m water depth), and the East Orphan Basin (EL 1149) is located at the northern end of the Flemish Pass (>3,000 m water depth).

Surface seabed features have been mapped for the Continental Margin of Eastern Canada (see Figure 5.3), although they only provide detail for EL 1145. The major geomorphic features in or near the Project Area are described in Table 5.1.

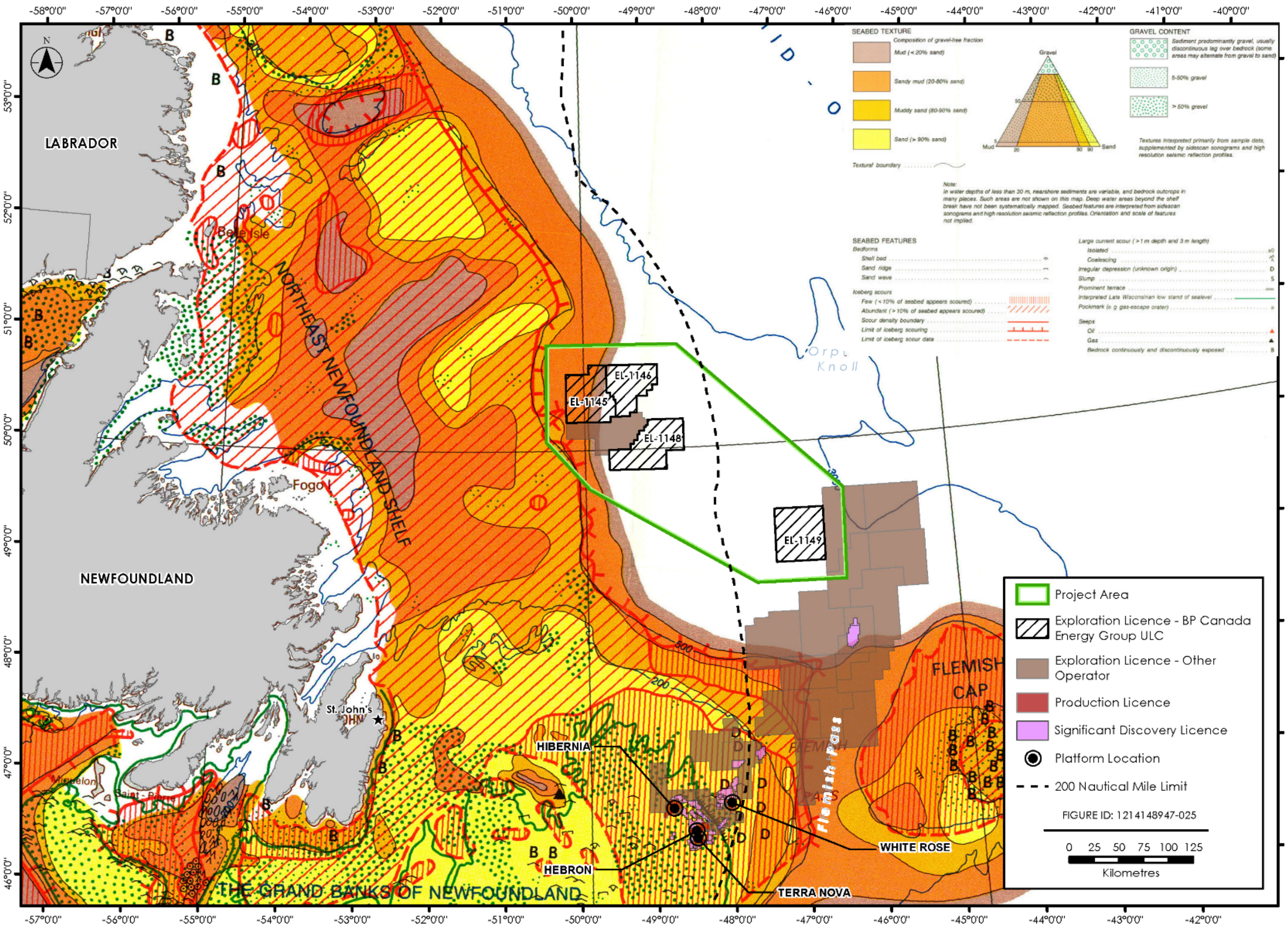

Source: modified from Cameron and Best 1985

Figure 5.3 Eastern Newfoundland Seabed Features

Table 5.1 Geomorphic Features

Feature	Description
Sackville Spur	Prominent contourite drift formed at the northern end of the Flemish Pass during the Neogene-Quaternary that has been incised by numerous canyons[1]
Central Ridge	Faulted intrabasinal high separating the Jeanne d'Arc Basin and the Flemish Pass Basin[2]
Flemish Cap	Large isolated continental basement high separated from the Grand Banks by the Flemish Pass and is the most easterly extension of the North American continental crust[3]
Flemish Pass	Sedimentary basin that forms a terraced continuation of the East Orphan basin[4]
Orphan Knoll	Topographic high that rises 1,000 m above the Orphan Basin to the west, 1,600 m above the Orphan Basin to the south, and drops to 2,200 m to the Labrador Sea Abyssal Plain to the east. The knoll is oriented NNW-SSE and is approximately 75 km in breadth and 190 km long[5]
See Figure 5.1 Sources: [1]Marshall et al. 2014, in Statoil Canada Ltd. 2017; [2]Enachescu 2012, in Statoil 2017; [3]King and Fader 1985, in Statoil Canada Ltd. 2017; [4]Lowe et al. 2011; [5]Ruffman 2011	

Almost the entire upper continental slope off Atlantic Canada is underlain by glacial till (Edinger et al. 2011). In some places, the till is buried up to tens of metres beneath younger proglacial and Holocene sediment (Edinger et al. 2011). Many till samples on the continental shelf and upper slope are composed of sand or mud that was derived from the reworking of Pleistocene or Late Tertiary sediments but include a small proportion of bedrock ranging from pebbles to boulders (Edinger et al. 2011).

In general, eroded Quaternary sediments and authigenic carbonates are thought to be more common than eroded Tertiary bedrock along the shelf break and upper slope of Newfoundland and Labrador (Piper et al. 2005; Edinger et al. 2011). Authigenic carbonates refers to any carbonate mineral precipitated inorganically *in situ*, whether at the water-sediment interface or within sediment pore waters (Schrag et al. 2013). Authigenic carbonates may occur on Orphan Knoll (Enachescu 2004), although the exposed pinnacles on Orphan Knoll could also be eroded remnants of Paleozoic bedrock (Parson et al. 1984; van Hinte et al. 1995).

While the Flemish Cap is not part of the Project Area, it is a notable geomorphic feature within the RAA (see Table 5.1 and Figure 5.1) and is located near the southeast tip of the Project Area. The Flemish Cap is underlain by Avalon terrane bedrock and consists of a central core of Hadrynian rock, including granodiorite, granites, dacites, and an onlapping sequence of Mesozoic- to Cenzoic-aged sediments (King et al. 1986). The Flemish Cap is covered by a veneer of sand up to several metres thick (Weitzman et al. 2014).

The Flemish Pass Basin is also not part of the Project Area but is one the main sedimentary basins in the RAA (see Section 5.4.1) and is located near the southeast tip of the Project Area. Geophysical evidence suggests that the Flemish Pass Basin forms a terraced continuation of the highly stretched and subsided East Orphan Basin, and both Basins are interpreted to have similar geological histories during the Late Jurassic to Early Cretaceous (Lowe et al. 2011). The primary reservoirs are located in shallow marine and fluvial shale and sandstone that was deposited during the late Jurassic and Early Cretaceous periods of the Mesozoic Era (Statoil Canada Ltd. 2017). Deeper basins such as the Flemish Pass Basin are generally silt or clay-filled (Statoil Canada Ltd. 2017). The seabed on the slope of the Flemish Pass generally consists of Holocene silty clay (Statoil Canada Ltd. 2017).

Quaternary deposits in the southern Orphan Basin include complex mass transport deposits (MTD) comprised of both glaciogenic debris flow and blocky MTD (Statoil Canada Ltd. 2017). The surficial sediment in Orphan Basin ranges from fine mud and clay to boulders and bedrock (LGL 2003).

5.2 Seismicity

Eastern Canada is located within a relatively stable area of the North American Plate, where there has been a relatively low level of recorded seismic activity (Amec 2014). There are approximately 450 earthquakes that occur each year in Eastern Canada, and the majority of these have magnitudes between two and three (Amec 2014).

The Seismicity Hazard Map of Canada (see Figure 5.4) shows the probability of earthquake occurrences across Canada, and this Map indicates that the Project Area and RAA are classified as having a low to moderate seismic hazard (NRCan 2016).

According to the National Earthquake Database, 36 earthquakes have occurred in the RAA between 1985 and 2018 (Figure 5.5) (NRCan 2018). Of these, 28 had magnitudes of 2-4, and 8 of these had magnitudes of 4-4.7 (NRCan 2018). Six of these earthquakes occurred within or bordering on the Project Area; three of these had magnitudes of 2-4, and three had magnitudes of 4-4.7. One earthquake of a magnitude of 4-4.7 occurred on the southern border of EL 1145. One earthquake of a magnitude of 4-4.7 occurred on the northern border of EL 1146. There were no recorded earthquakes in ELs 1148 and 1149. Most of the earthquake epicentres, as shown in Figure 5.4, are in the northwest part of the Project Area. A 4.2 magnitude earthquake was recorded west of the Project Area on September 2, 2018, 293 km northeast of Bonavista, NL; no tsunami was generated from the event (CBC 2018).

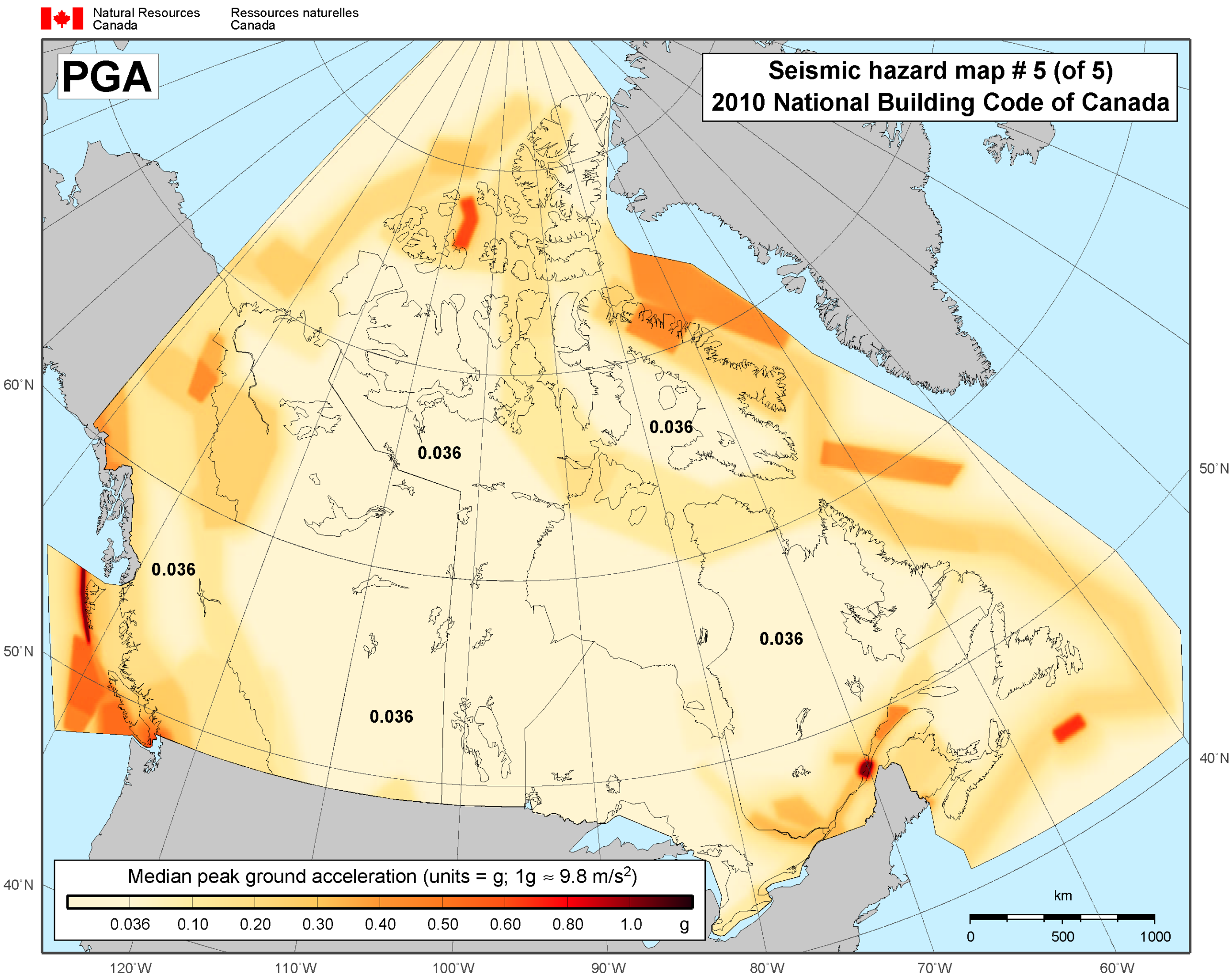

Peak ground acceleration at a probability of 2%/50 years for firm ground conditions (NBCC soil class C).

Source: NRCan 2016

Figure 5.4 Seismicity Hazard Map of Canada – Peak Ground Acceleration

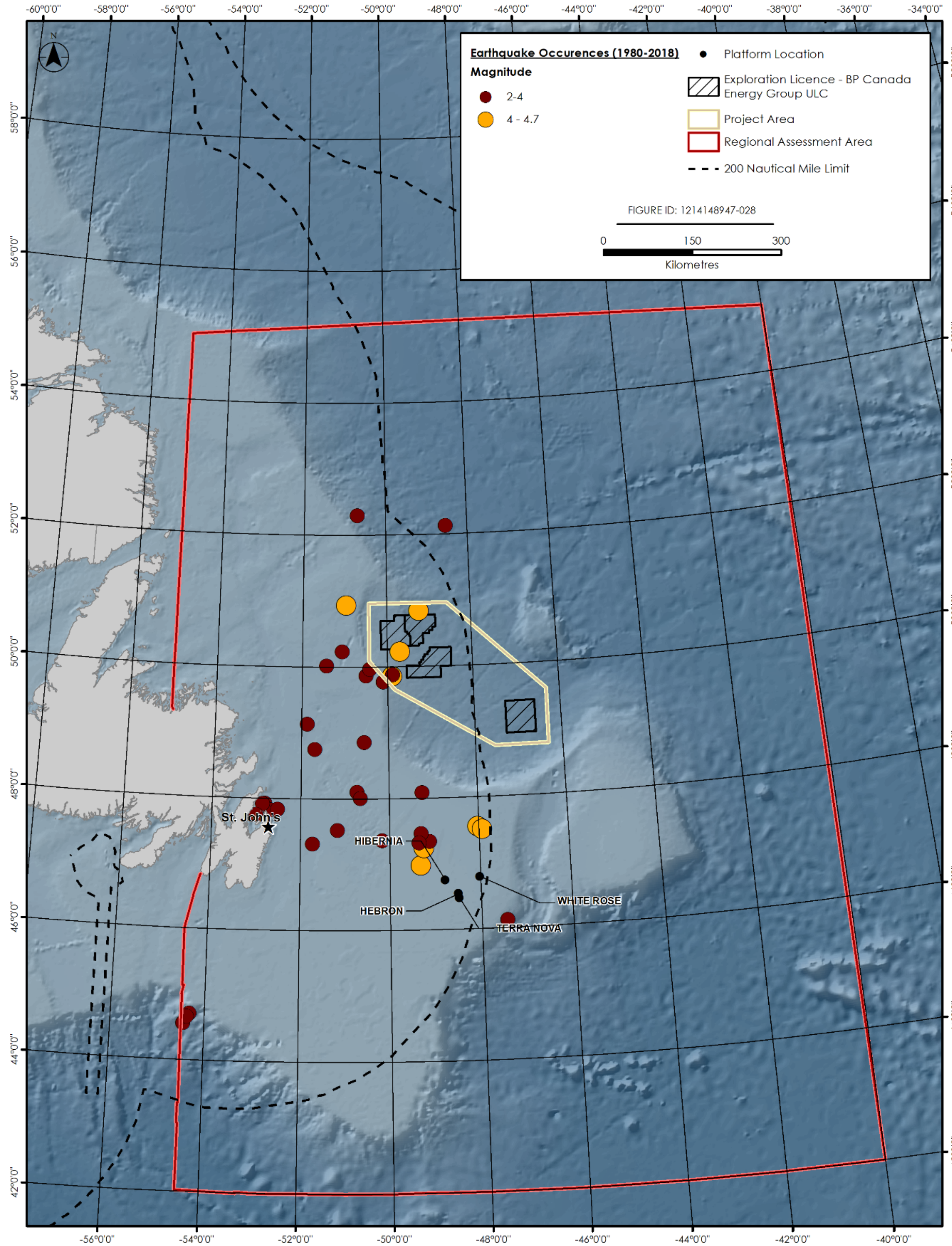

Source: NRCan 2018

Figure 5.5 Earthquake Epicentres (1985 to 2018) in RAA

5.3 Atmospheric Environment

5.3.1 Data Sources

The data sources to describe the wind climatology within the Project Area came from three main sources: The International Comprehensive Ocean-Atmosphere Data Set (ICOADS) (Woodruff et al. 2011), rig observations, and the MSC50 North Atlantic wind and wave climatology database. The locations of the climate data sources are presented in Figure 5.6.

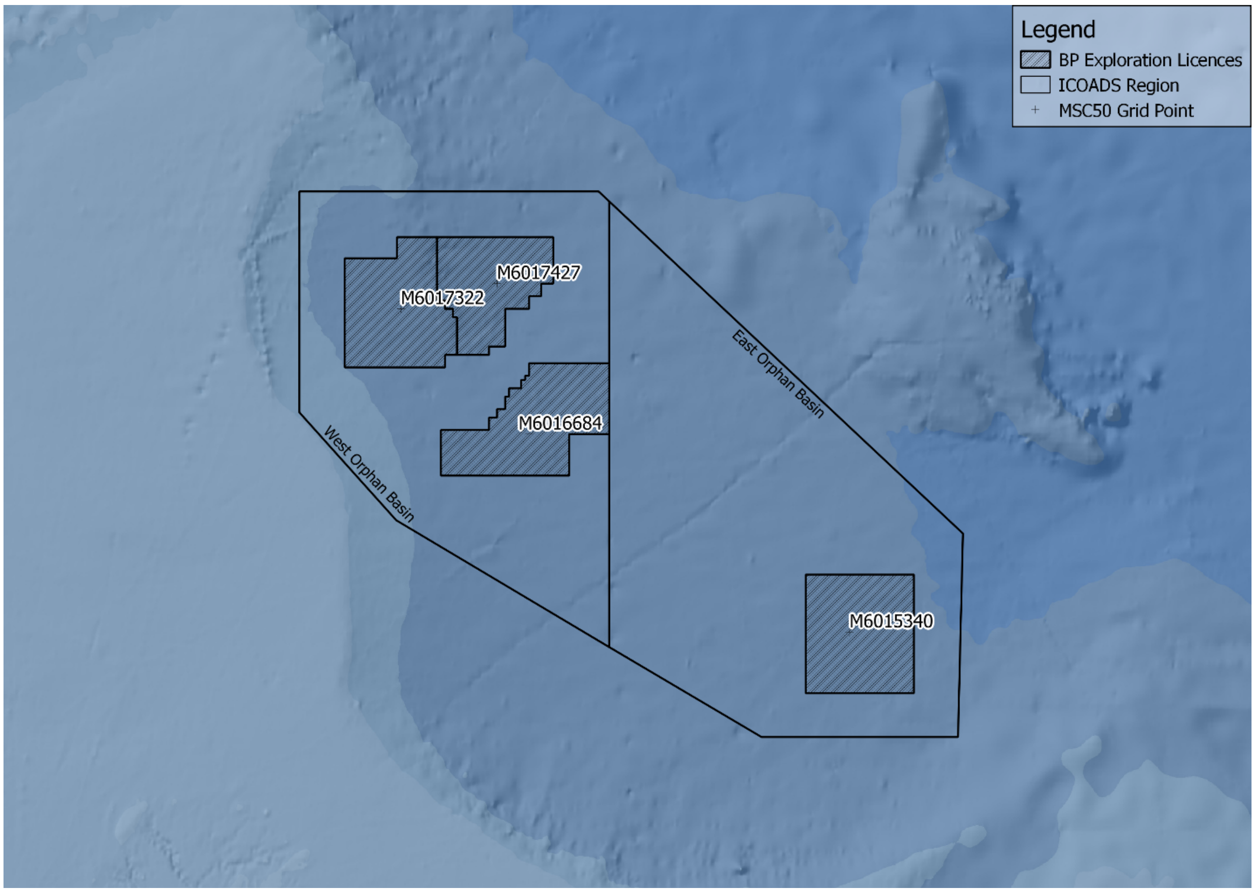

Figure 5.6 Climate Data Source Locations

Wind speeds from the MSC50 and ICOADS data sets are not directly comparable to each other due to their sampling period and the heights at which they were measured. Wind speed is dependent on height since the wind speed increases at increasing heights above sea level. Methods to reduce wind speeds from anemometer level to 10 m have proven ineffective due to atmospheric stability issues. Winds in the ICOADS data set were either estimated or measured by anemometers at various heights above sea level.

Winds speeds from each of the data sources have different averaging periods. The MSC50 winds are 1-hour averages while the ICOADS and MANMAR winds are 10-minute average winds.

5.3.1.1 ICOADS

Wind, wave, air temperature, sea surface temperature, visibility and freezing spray statistics for the area were compiled using data from the ICOADS Release 3.0 (Freeman et al. 2017) Enhanced Trimming data set. A subset of global marine surface observations from ships, drilling rigs, and buoys for the area covering the period from January 1986 to December 2015 was used in this report.

The Enhanced Trimming data set was trimmed to exclude outliers, which fall outside of 4.5 standard deviations from the smoothed median. Despite this analysis, valid observations may still have been excluded from the data set. Conversely, invalid data which fell within the limits of the quality control analysis may have been included in the data set.

While the ship-based reports have been quality controlled to the extent possible, they are likely to contain some observation errors in addition to position report errors, particularly for the older reports. The data set is also known to contain a ‘fair weather bias’, which arises for the following reasons: ship’s captains may choose to avoid areas of heavy weather, and since the reporting program is voluntary, fewer observations are likely to be taken under adverse weather and sea state conditions. This bias is more likely to be present during the winter season and over temperate and northern seas where vessel traffic is light.

Kent et al. (1993) demonstrated various systematic inconsistencies in the meteorological observations from voluntary observing ships. These inconsistencies were mostly dependent on the method of estimation that was used. Sea surface temperature data from engine intake thermometers were found to be biased high by an average of 0.3ºC. The dew point temperatures from fixed thermometer screens were biased high compared to psychrometer readings. The magnitude of the bias was of the order of 1ºC and varied with dew point temperature. Wind speeds from anemometers were biased high compared to visual winds by about two knots for winds up to about 25 knots. It was unknown whether visual winds or anemometer winds were more accurate. Compared to daytime values, visual winds at night were underestimated by about 1 m/s at 15 m/s and 5 m/s at 25 m/s.

The ICOADS data set was subdivided into two regions, covering the East Orphan Basin and West Orphan Basin. This division occurred along the longitudinal line of 48.5°W (Figure 5.6). This line was chosen to be consistent with the oceanographic region division.

5.3.1.2 MSC50 Data Set

Wind and wave climate statistics for the Project Area were extracted from the MSC50 North Atlantic wind and wave climatology database compiled by Oceanweather Inc. under contract to Environment and Climate Change Canada. The MSC50 database consists of continuous wind and wave hindcast data in 1-hour time steps from January 1954 to December 2015, on a 0.1° latitude by 0.1° longitude grid. A subset of the MSC50 data set from 1985 to 2015 for grid points 15340, 16684, 17322 and 17427 was chosen to represent conditions within the area of interest. Wave heights and periods in the MSC50 database are computed using a Pierson Moskowitz spectrum.

Weekly ice data supplied by the Canadian Ice Service was used allowing the MSC50 hindcast to better represent the changing ice conditions (Swail et al. 2006).

5.3.2 Climate Overview

The East and West Orphan Basin regions experience weather conditions typical of a marine environment with the surrounding waters having a moderating effect on temperature. In general, marine climates experience cooler summers and milder winters than continental climates and have a much smaller annual temperature range. A marine climate tends to be fairly humid, resulting in reduced visibilities, low cloud heights, and significant amounts of precipitation.

The climate of the area is very dynamic, largely governed by the passage of high and low-pressure circulation systems. These circulation systems are embedded in, and steered by, the prevailing westerly flow that typifies the upper levels of the atmosphere in the mid-latitudes, which arises because of the normal tropical to polar temperature gradient. The mean strength of the westerly flow is a function of the intensity of this gradient and is considerably stronger in the winter months than during the summer months, due to an increase in the south to north temperature gradient.

At any given time, the upper level flow is a wave-like pattern of large and small amplitude ridges and troughs. These ridges and troughs tend to act as a steering mechanism for surface features and therefore their positions in the upper atmosphere determine the weather at the earth's surface. Upper ridges tend to support areas of high pressure at the surface, while upper troughs lend support to low pressure developments. The amplitude of the upper flow pattern tends to be higher in winter than summer, which is conducive to the development of more intense storm systems.

During the winter months (e.g., December, January, February), an upper level trough tends to lie over Central Canada and an upper ridge over the North Atlantic resulting in three main storm tracks affecting the region: one from the Great Lakes Basin, one from Cape Hatteras, North Carolina and one from the Gulf of Mexico. These storm tracks, on average, bring eight low pressure systems per month over the area. The intensity of these systems ranges from relatively weak features to major winter storms. Studies (Archer and Caldeira 2008) have shown that there exists a poleward shift of the jet stream, and consequently storm tracks, at a rate of 0.17 to 0.19 degrees / decade in the northern hemisphere. This shift has been related to an increase in the equator-to-pole temperature gradient. McCabe et al. (2001) obtained similar results, finding that there has been a decrease in mid-latitude cyclone frequency and an increase in high-latitude cyclone frequency. In addition, McCabe et al. (2001) found that storm intensity has increased in both the high and mid-latitudes.

In the case where the upper level long wave trough lies well west of the region, the main storm track will lie through the Gulf of St. Lawrence or Newfoundland. Under this regime, an east to southeast flow ahead of a warm front associated with a low will give way to winds from the south in the warm sector of the system. Typically, the periods of southerly winds and mild conditions will be of relatively long duration, and in general, the incidence of extended storm conditions is likely to be relatively infrequent. Strong frictional effects in the stable flow from the south results in a marked shear in the surface boundary layer and relatively lower winds at the sea surface; local wind wave development tends to be inhibited under such conditions. Precipitation types are more likely to be in the form of rain or drizzle, with relatively infrequent periods of continuous snow, although periods of snow showers prevail in the unstable air in the wake of cold fronts associated with the lows. Visibility will be reduced at times in frontal and advection fogs, in snow, and in snow shower activity.

At other times, with the upper long wave trough situated further to the east, the main storm track may lie through or to the east of the Orphan Basin. With the lows passing closer to the site and a higher potential for storm development, the incidence of strong gale and storm conditions is greater. Longer bouts of cold, west to northwest winds behind cold fronts occur more frequently, and because the flow is colder than the surface water temperatures, the surface layer is unstable. The shear in the boundary layer is lower, resulting in relatively higher wind speeds near the surface, and consequently relatively higher sea state conditions. With cold air and sea surface temperatures coupled with high winds, the potential for freezing spray will occur quite frequently. In this synoptic situation, a greater incidence of precipitation in the form of snow is likely to occur. Freezing precipitation, either as rain or drizzle, occurs rather infrequently within the region. Visibility will be reduced in frontal and advection fogs, and relatively more frequently by snow.

Frequently, intense low-pressure systems become ‘captured’ and slow down or stall off the coast of Newfoundland and Labrador. This may result in an extended period of little change in conditions that may range, depending on the position, overall intensity and size of the system, from the relatively benign to heavy weather conditions.

By summer, the main storm tracks have moved further north than in winter. Low-pressure systems are less frequent and much weaker. With increasing solar radiation during spring, there is a general warming of the atmosphere that is relatively greater at higher latitudes. This decreases the north-south temperature contrast, lowers the kinetic energy of the westerly flow aloft and decreases the potential energy available for storm development. Concurrently, there is a northward shift of the main band of westerly winds at upper levels and a marked development of the Bermuda-Azores sub-tropical high-pressure area to the south. This warm-core high-pressure cell extends from the surface through the entire troposphere. The main track of the weaker low-pressure systems typically lies through the Labrador region and tends to be oriented from the west-southwest to the east-northeast.

With low pressure systems normally passing to the north of the region in combination with the northwest sector of the sub-tropical high to the south, the prevailing flow across the Orphan Basin is from the southwest to south during the summer season. Wind speed is lower during the summer and the incidence of gale or storm force winds relatively infrequent. There is also a corresponding decrease in significant wave heights.

The prevailing south-westerly flow during the late spring and early summer tends to be moist and it is relatively warmer than the underlying surface waters.

Rapidly deepening storms are a problem south of Newfoundland in the vicinity of the warm water of the Gulf Stream. Sometimes these explosively deepening oceanic cyclones develop into a ‘weather bomb’, defined as a storm that undergoes central pressure falls greater than 24 millibars (mb) over 24 hours. Hurricane force winds near the center, the outbreak of convective clouds to the north and east of the centre during the explosive stage, and the presence of a clear area near the centre in its mature stage (Rogers and Bosart 1986) are typical of weather bombs. After development, these systems will either move across Newfoundland or to the east of Newfoundland producing gale to storm force winds over the Orphan Basin.

5.3.3 Air Quality

Air quality within the Project Area, and in surrounding areas, is anticipated to be good, with occasional exposure to exhaust products from PSVs, other marine traffic, helicopters, and existing offshore oil production facilities in the Jeanne d'Arc Basin (Hibernia, Terra Nova, White Rose, and Hebron). The general area also receives long-range contaminants from the Northeast Seaboard and industrial Midwest of the United States (ExxonMobil Canada Properties 2011, in Husky Energy 2012). There are no site-specific ambient air quality data for the Project Area.

Data were acquired from the National Pollutant Release Inventory (NPRI) Reporting program to characterize the existing ambient air quality surrounding the Project Area. The NPRI Reporting program is regulated under the *Canadian Environmental Protection Act* (CEPA) for criteria air contaminants (CACs) (i.e., carbon monoxide (CO), nitrogen dioxide (NO_2), sulphur dioxide (SO_2), total particulate matter (TPM), particulate matter less than 2.5 and 10.5 microns in diameter ($PM_{2.5}$, PM_{10}), and volatile organic compounds (VOCs)). If a facility meets specified reporting triggers, they must report their emissions of these CACs on an annual basis to ECCC. The CAC emissions for the 2016 reporting year from the Hibernia, Terra Nova, and White Rose platforms are provided in Table 5.2 (CAC data from 2017 was still preliminary at the time of EIS preparation).

Table 5.2 2016 Facility Reported CAC Emissions (NPRI Reporting) – Newfoundland and Labrador Offshore Area Production Platforms

Facility	Air Emissions (tonnes/year)					
	CO	NO_2	TPM	PM_{10}	$PM_{2.5}$	VOC
Hibernia	701	1064	168	168	168	461
Terra Nova	439	2219	118	115	115	116
White Rose (Sea Rose FPSO)	602	2567	168	167	167	436

Source: ECCC 2018

Note: SO_2 (and hydrogen sulphide) emissions have not been reported as the Jeanne d'Arc Basin is not known to contain sour gas.

The GHG Emissions Reporting Program requires existing offshore oil production platforms report their GHGs to the ECCC on an annual basis. The GHG emissions for the 2015 reporting year from the Hibernia, Terra Nova, and White Rose platforms are provided in Table 5.3.

Table 5.3 2016 Facility Reported GHG Emissions – Newfoundland and Labrador Offshore Area Production Platforms

Facility	GHG Emissions (tonnesCO_{2eq}/year)			
	CO_2	CH_4	N_2O	Total
Hibernia	517,524	40,320	4,619	562,463
Terra Nova	527,836	22,556	10,208	560,600
White Rose (Sea Rose FPSO)	401,696	32,669	11,497	445,861
Source: ECCC 2017				

Emissions from vessel traffic, which could also occasionally influence Project Area air quality, are regulated by the International Maritime Organization (IMO) through MARPOL.

5.3.4 Wind Speed and Direction

The Project Area experiences predominately southwest to west flow throughout the year. There is a strong annual cycle in the wind direction. West to northwest winds which are prevalent during the winter months begin to shift counter-clockwise during March and April, resulting in a predominant southwest wind by the summer months. As fall approaches, the tropical-to-polar temperature gradient strengthens, and the winds shift slightly, becoming predominately westerly again by late fall and into winter. Low pressure systems crossing the area are more intense during the winter months. As a result, mean wind speeds tend to peak during this season.

In addition to mid-latitude low pressure systems crossing the Grand Banks, tropical cyclones often move northward out of the influence of the warm waters of the Gulf Stream, passing near the Island of Newfoundland. Once the cyclones move over colder waters they lose their source of latent heat energy and often begin to transform into a fast-moving and rapidly developing extratropical cyclone producing large waves and sometimes hurricane force winds.

Low pressure systems crossing the area are more intense during the winter months, with mean wind speeds tending to peak during this season.

Wind speed statistics for the four MSC50 grid points as well as the ICOADS data set are presented in Table 5.4. Monthly maximum wind speeds for each of the data sets is presented in Table 5.5. Wind roses of the annual wind speed and direction as well as the associated histogram of the wind speed frequency are presented in Figures 5.7 to 5.10.

Table 5.4 Mean Wind Speed (m/s) Statistics

	East Orphan Basin		West Orphan Basin			
	MSC50 Grid Point 15340	ICOADS	MSC50 Grid Point 16684	MSC50 Grid Point 17322	MSC50 Grid Point 17427	ICOADS
January	12.71	14.52	12.62	12.55	12.76	12.16
February	12.13	12.67	11.94	11.75	12.05	11.9
March	11.1	11.77	10.83	10.65	10.95	11.63
April	9.28	11.17	9.26	9.2	9.45	9.72
May	7.88	8.23	7.77	7.67	7.9	8.37
June	7.22	8.64	6.92	6.76	6.99	7.76
July	6.68	7.16	6.47	6.28	6.47	5.91
August	6.93	8.32	6.84	6.74	6.89	6.39
September	8.44	9.04	8.33	8.31	8.47	7.9
October	9.74	10.99	9.53	9.49	9.65	8.43
November	11.19	12.25	11.18	11.15	11.36	10.8
December	11.86	12.66	11.86	11.88	12.05	11.65
Winter	12.24	13.32	12.15	12.07	12.29	11.86
Spring	9.42	10.25	9.28	9.17	9.43	9.69
Summer	6.94	8.06	6.74	6.59	6.78	6.59
Fall	9.79	10.66	9.68	9.65	9.82	9.18
Annual	9.58	10.35	9.45	9.36	9.57	9.04
Sources: MSC50 database, ICOADS data set						

Table 5.5 Maximum Wind Speed (m/s) Statistics

	East Orphan Basin		West Orphan Basin			
	MSC50 Grid Point 15340	ICOADS	MSC50 Grid Point 16684	MSC50 Grid Point 17322	MSC50 Grid Point 17427	ICOADS
January	32.4	39.6	31.1	31.4	32.8	28.8
February	30.6	38.1	30.8	28.5	29.5	30.9
March	31.2	30.9	29.9	28.3	29.4	23.7
April	26.8	29.0	26.7	27.6	26.6	26.8
May	23.0	24.2	22.0	20.1	21.2	25.7
June	21.6	24.2	22.5	21.4	22.2	22.6
July	18.7	25.2	21.1	16.9	17.9	22.6
August	23.7	22.6	20.6	18.8	19.5	19.0
September	30.4	24.2	29.2	27.9	33.1	24.7
October	28.2	32.0	27.1	28.0	27.5	22.6
November	27.2	30.9	29.2	27.9	28.6	30.0
December	31.4	30.9	31.1	29.7	30.8	26.2
Winter	32.4	39.6	31.1	31.4	32.8	30.9
Spring	31.2	30.9	29.9	28.3	29.4	26.8
Summer	23.7	25.2	22.5	21.4	22.2	22.6
Fall	30.4	32.0	29.2	28.0	33.1	30.0
Annual	32.4	39.6	31.1	31.4	33.1	30.9
Sources: MSC50 database, ICOADS data set						

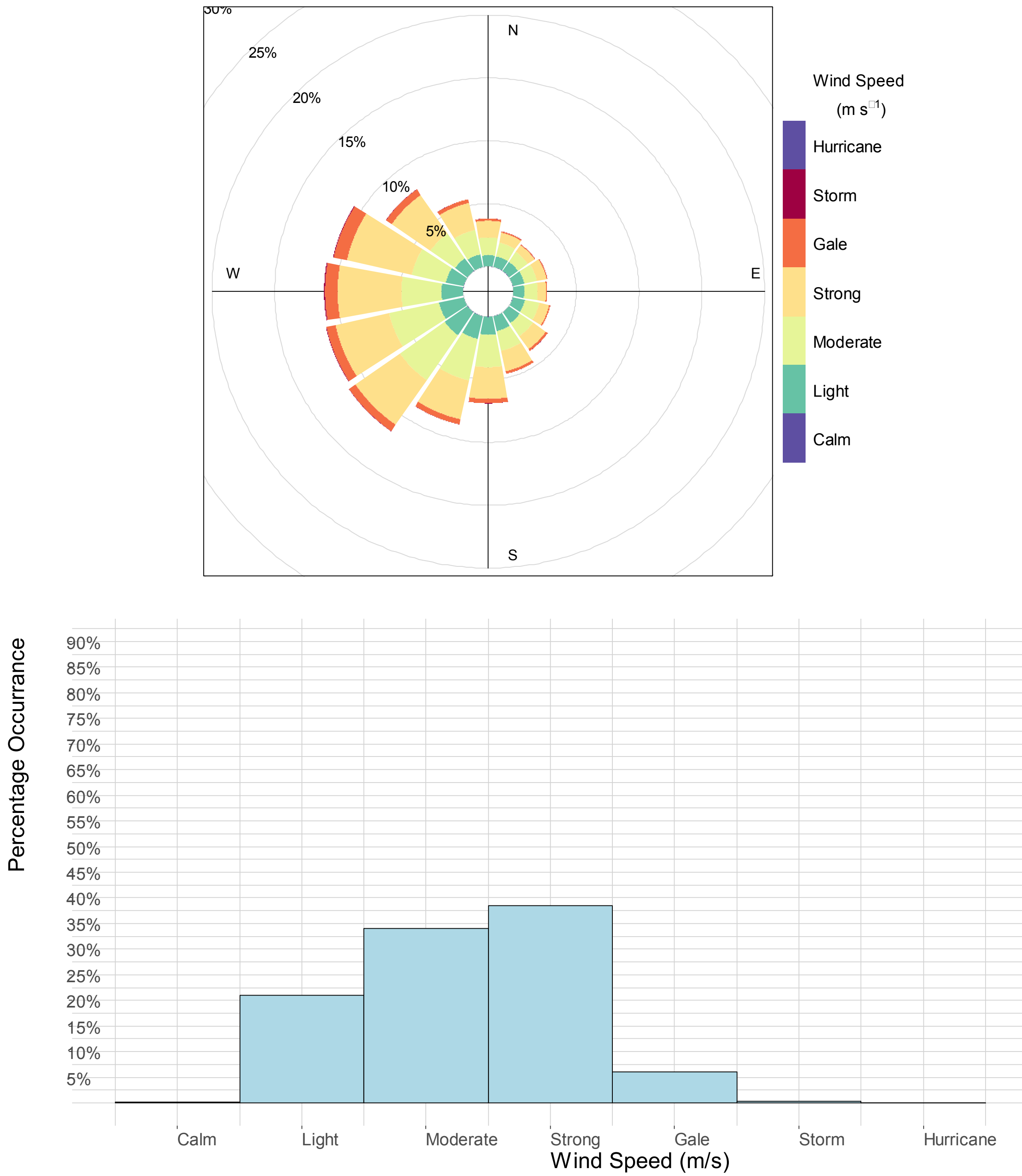

Figure 5.7 Annual Wind Rose and Percentage Frequency of Wind Speeds for MSC50 Grid Point 15340 (1986 – 2015)

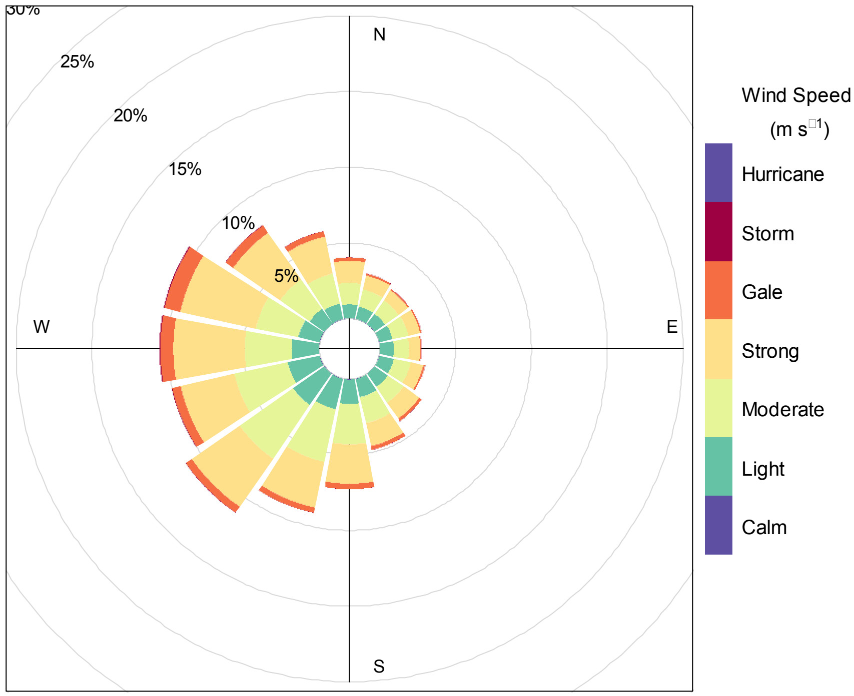

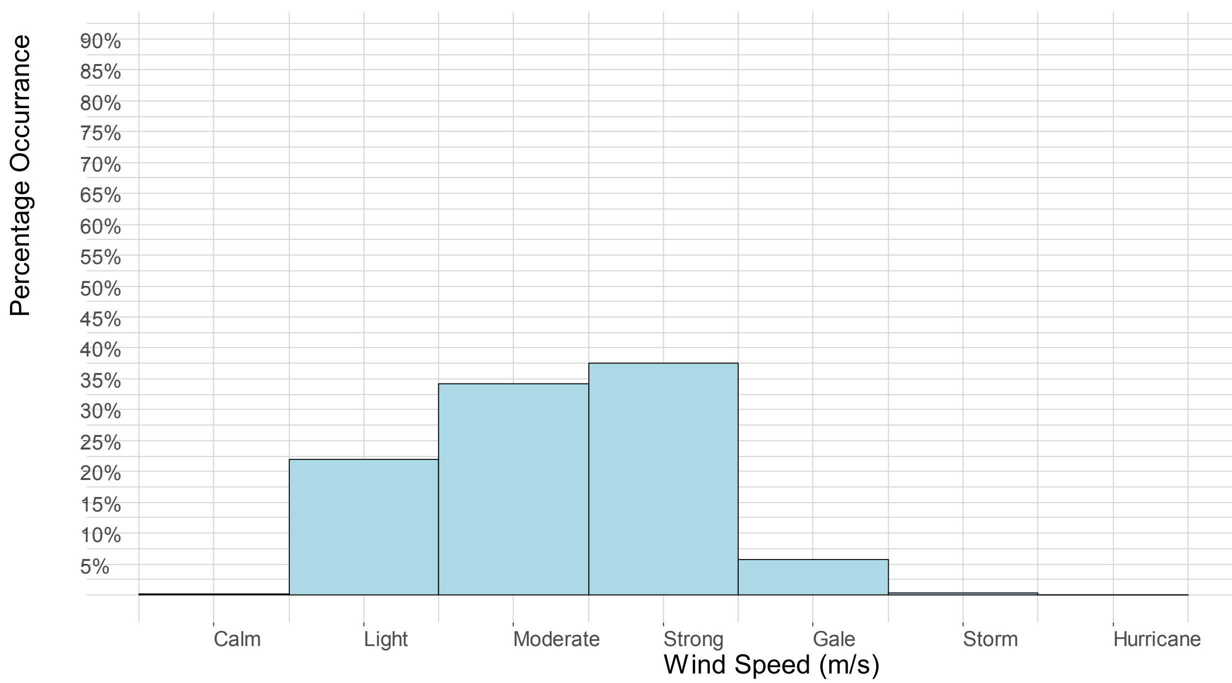

Figure 5.8 Annual Wind Rose and Percentage Frequency of Wind Speeds for MSC50 Grid Point 16684 (1986 – 2015)

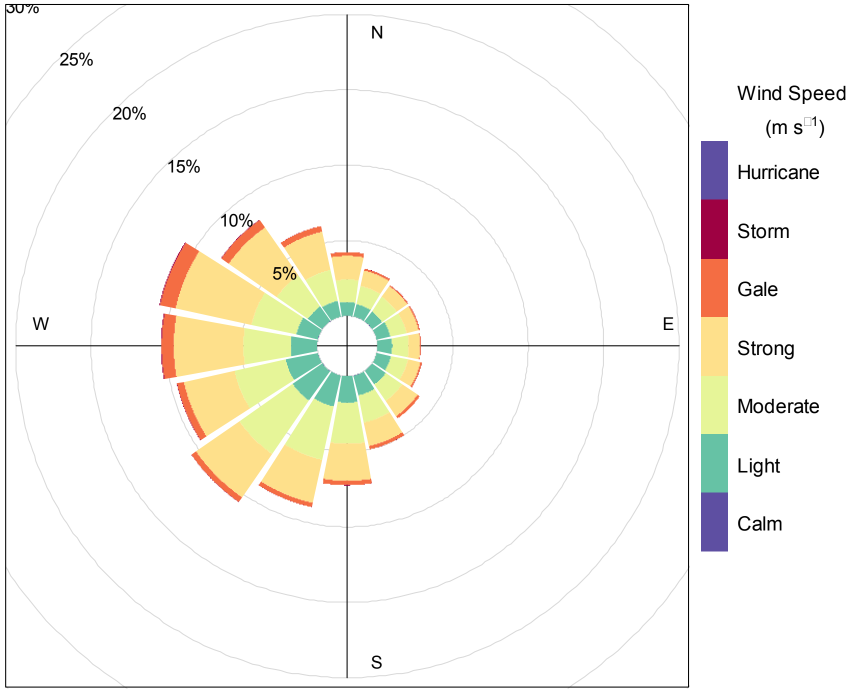

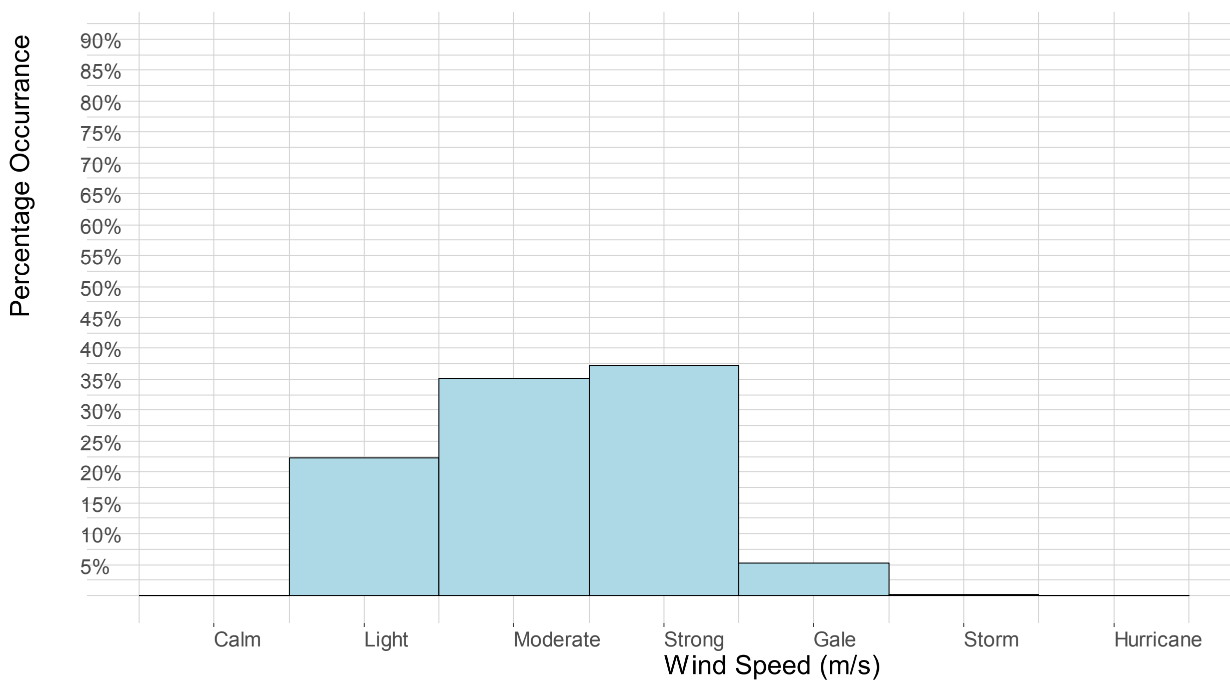

Figure 5.9 Annual Wind Rose and Percentage Frequency of Wind Speeds for Grid Point 17322 (1986 – 2015)

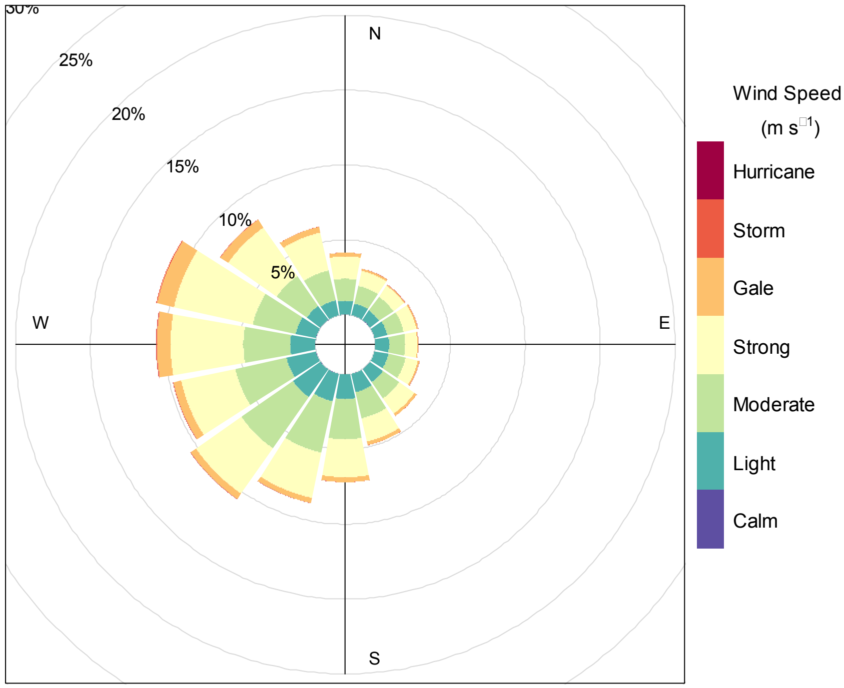

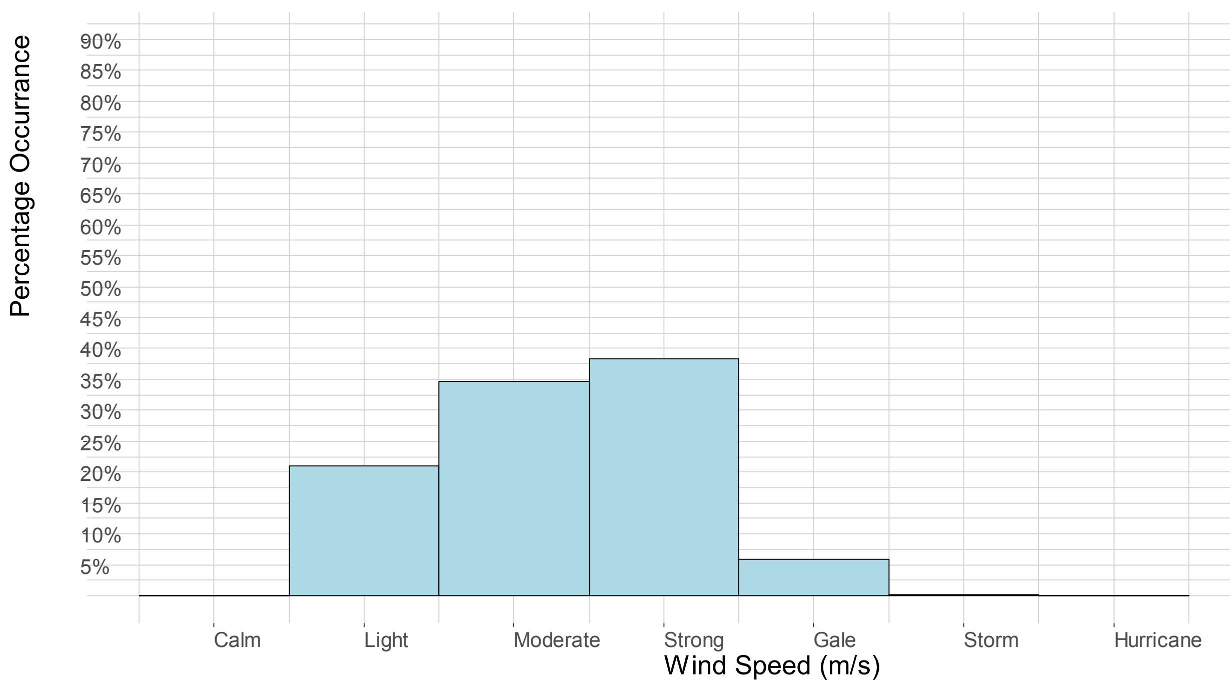

Figure 5.10 Annual Wind Rose and Percentage Frequency of Wind Speeds for MSC50 Grid Point 17427 (1986 – 2015)

Wind directions are in meteorological convention and depict the direction the winds are coming from. Wind speeds are classified according to the following criteria corresponding with the Beaufort Wind Scale:

- Calm: ≤0.5 m/s (1 knot)
- Light: 0.5 m/s (1 knot) - 5.7m/s (11 knots)
- Moderate: 5.7m/s (11 knots) - 10.8 m/s (21 knots)
- Strong: 10.8 m/s (21 knots) - 17.5 m/s (34 knots)
- Gale: 17.5 m/s (34 knots) - 24.7 m/s (48 knots)
- Storm: 24.7 m/s (48 knots) - 32.9 m/s (64 knots)
- Hurricane: >32.9 m/s (64 knots)

Rapidly deepening storm systems known as weather bombs frequent the Orphan Basin. These storm systems typically develop in the warm waters of Cape Hatteras and move northeast across the Grand Banks and the Orphan Basin. At 12Z on January 28, 2007, a 1002 mb low pressure off Cape Hatteras began to move northeast as it deepened to 985 mb south of Newfoundland. The system sustained a central pressure near 985 mb for the next 12 hours as it continued to move northeast. Passing southeast of the Avalon Peninsula near 06Z on January 30th, the low pressure experienced a sudden intensification, with the central pressure decreasing 15 mb in 12 hours to 970 mb. The low pressure continued to deepen as it moved northeast, crossing the Orphan Basin at 18Z on January 30, 2007 with a central pressure of 960 mb. As the system passed, the *Eirik Raude* platform located in the East Orphan Basin region near 49.4°N 48.1°W recorded a wind speed of 39.6 m/s from the southwest at its anemometer. The low pressure maintained a central pressure near 960 mb for the next 12 hours as it moved towards Greenland where it began weakening.

5.3.5 Tropical Storms

In addition to extratropical cyclones, tropical cyclones often retain their tropical characteristics as they enter the study area. Tropical cyclones account for the strongest sustained surface winds observed anywhere on earth. The hurricane season in the North Atlantic normally extends from June through November, although tropical storm systems occasionally occur outside this period. Once formed, a tropical storm or hurricane will maintain its energy as long as a sufficient supply of warm, moist air is available. Tropical storms and hurricanes obtain their energy from the latent heat of vaporization that is released during the condensation process. These systems typically move east to west over the warm water of the tropics; however, some of these systems turn northward and make their way towards Newfoundland. Since the capacity of the air to hold water vapour is dependent on temperature, as the hurricanes move northward over the colder ocean waters, they begin to lose their tropical characteristics. By the time these weakening cyclones reach Newfoundland, they are usually embedded into a mid-latitude low and their tropical characteristics are usually lost.

A considerable number of tropical cyclones that move into the mid-latitudes transform into extratropical cyclones. On average, 46% of tropical cyclones which formed in the Atlantic transform into extratropical cyclones. During this transformation, the system loses tropical characteristics and becomes more extratropical in nature resulting in an increase in size which produces large waves, gale to hurricane force winds and intense rainfall. The likelihood that a tropical cyclone will undergo transition increases toward the second half of the tropical season, with October having the highest probability of transition. In the Atlantic, extratropical transition occurs at lower latitudes in the early and late hurricane season and at higher latitudes during the peak of the season (Hart and Evans 2001).

There has been a significant increase in the number of hurricanes that have developed within the Atlantic Basin during the last 15 years. Figure 5.11 shows the 5-year average of tropical storms which have developed within the Atlantic Basin since 1961. This increase in activity has been attributed to naturally occurring cycles in tropical climate patterns near the equator called the tropical multi-decadal signal (Bell and Chelliah 2006). As a result of the increase in tropical activity in the Atlantic Basin, there has also been an increase in tropical storms or their remnants entering the Canadian Hurricane Centre Response Zone. There is little change in the 5-year trend for hurricanes coming within the Project Area. The unusually high number of tropical storms in 2005 may be skewing the results for the 2001 to 2005 season.

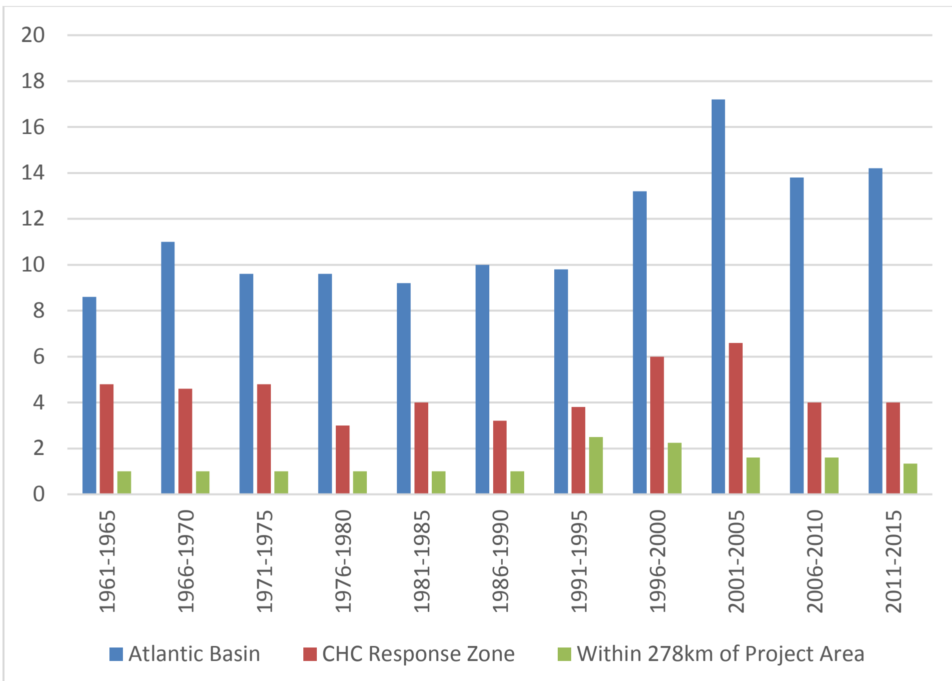

Figure 5.11 Five-Year Average of the Number of Tropical Storms which formed in the Atlantic Basin since 1961

Between 1986 and 2015, 30 tropical systems have passed within 278 km of the Project Area. The names are given in Table 5.6 and the tracks are shown in Figure 5.12. It should be noted that the values are the maximum 1-minute mean wind speeds occurring within the tropical system at the 10-m reference level as it passed within 278 km of the location.

Table 5.6 Tropical Systems Passing within 278 km of the Project Area (1986 to 2015)

Year	Month	Day	Hour	Name	Latitude	Longitude	Wind (m/s)	Pressure	Category
1989	August	9	0000	Dean	50.8	-48.1	20.6	1000	Tropical Storm
1990	September	3	0600	Gustav	48.5	-44.5	28.3	997	Post-Tropical
1991	August	21	1200	Bob	51.6	-51.4	18.0	1009	Post-Tropical
1995	June	9	1200	Allison	50.0	-53.0	20.6	997	Post-Tropical
1995	July	21	0000	Chantal	47.7	-45.2	25.7	1001	Post-Tropical
1995	August	22	1800	Felix	49.0	-46.0	25.7	985	Post-Tropical
1995	September	11	1200	Luis	51.5	-48.5	36.0	960	Post-Tropical
1996	July	15	0600	Bertha	49.0	-52.0	23.1	996	Post-Tropical
1996	October	10	1800	Josephine	50.5	-50.0	23.1	984	Post-Tropical
1998	September	6	1200	Earl	49.0	-52.0	28.3	964	Post-Tropical
1999	September	19	1200	Floyd	49.5	-48.0	20.6	992	Post-Tropical
1999	October	19	1200	Irene	48.0	-48.0	41.2	968	Post-Tropical
2000	October	9	0000	Leslie	51.0	-50.0	18.0	1007	Post-Tropical
2000	October	20	1800	Michael	52.0	-50.5	30.9	970	Post-Tropical
2001	August	29	0600	Dean	49.0	-45.0	23.1	999	Post-Tropical
2001	September	15	0600	Erin	49.0	-51.0	30.9	981	Post-Tropical
2001	September	20	0000	Gabrielle	48.5	-48.5	30.9	988	Post-Tropical
2002	July	18	0000	Arthur	50.5	-52.5	20.6	999	Post-Tropical
2003	October	7	1800	Kate	47.5	-47.2	30.9	980	Tropical Storm
2004	September	2	0600	Gaston	48.5	-44.0	23.1	996	Post-Tropical
2005	July	31	0000	Franklin	47.5	-46.0	20.6	1006	Post-Tropical
2005	September	19	0600	Ophelia	49.0	-48.8	23.1	1001	Post-Tropical
2006	June	16	1800	Alberto	49.3	-51.5	20.6	990	Post-Tropical
2006	July	19	0600	Unnamed	49.2	-49.4	12.9	1012	Tropical Low
2006	September	14	0600	Florence	48.6	-48.3	30.9	967	Post-Tropical
2006	October	3	0600	Isaac	48.6	-49.0	23.1	998	Post-Tropical
2007	August	1	1800	Chantal	49.0	-49.5	30.9	988	Post-Tropical
2008	October	1	1800	Laura	47.5	-46.3	20.6	995	Tropical Low
2009	August	24	1200	Bill	49.2	-47.2	30.9	980	Post-Tropical
2010	September	22	0000	Igor	51.5	-50.5	38.6	950	Post-Tropical
2011	October	3	1800	Ophelia	48.9	-49.2	23.1	994	Post-Tropical
2012	September	11	1800	Leslie	51.6	-51.9	30.9	972	Post-Tropical
2014	August	8	0000	Bertha	47.4	-46.6	18.0	1001	Post-Tropical
2014	October	19	1200	Gonzalo	47.8	-50.1	36.0	970	Category 1

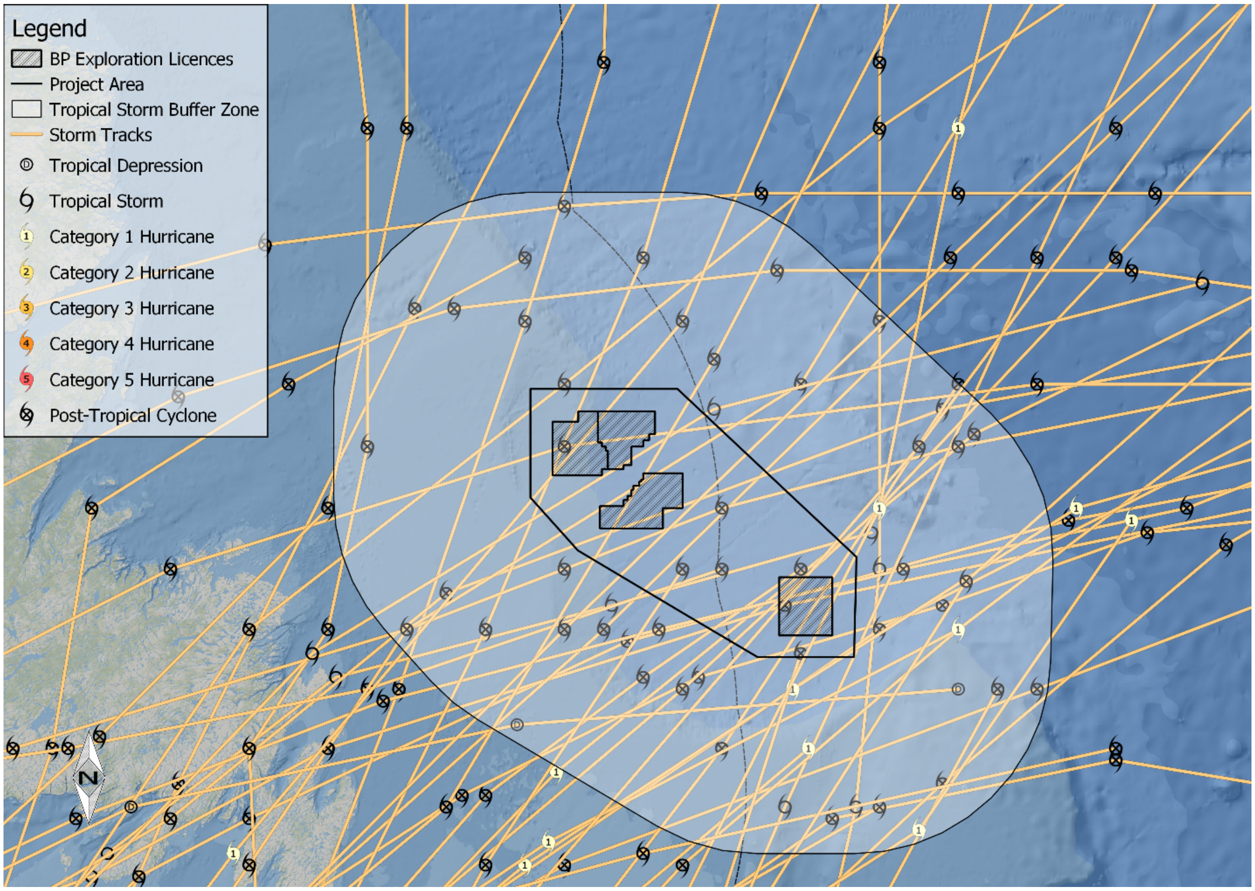

Figure 5.12 Storm Tracks of Tropical Systems Passing within 278 km of 46.9ºN, 47.9ºW (1967 to 2015)

On occasion, these systems still maintain their tropical characteristics when they reach Newfoundland. On October 19, 2014, Category 1 Hurricane Gonzolo passed within 278 km of the Project Area with maximum sustained wind speeds of 36.0 m/s and a central pressure of 970 mb. Tropical Storm Irene, having undergone extratropical transition, had the strongest wind speeds of all the storms. Irene passed near the region with wind speeds of 41.2 m/s and a central pressure of 968 mb on October 19, 1999. There were no observations within the ICOADS during either of these events.

5.3.6 Air and Sea Surface Temperature

The moderating influence of the ocean serves to limit both the diurnal and the annual temperature variation on the Grand Banks. Diurnal temperature variations due to the day/night cycles are very small. Short-term, random temperature changes are due mainly to a change of air mass following a warm or cold frontal passage. In general, air mass temperature contrasts across frontal zones are greater during the winter than during the summer season.

Air and sea surface temperatures for the area were extracted from the ICOADS data set for both the East and West Orphan Basin. Monthly plots of air temperature versus sea surface temperature are presented in

Figures 5.13 and 5.14. Air and sea surface temperature statistics are presented in Tables 5.7 and 5.8. According to these tables, the atmosphere is coldest in the East Orphan Basin in the months of January and February with a mean monthly air temperature of 0.4°C for both months, and warmest in August with a mean monthly air temperature of 12.3°C. The Orphan Basin temperatures range from -2.9°C to 11.6°C between February and August.

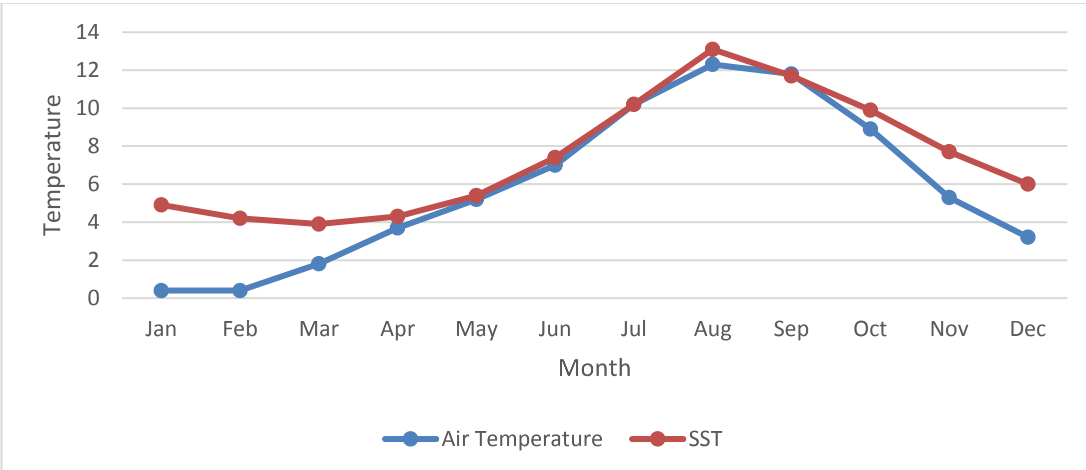

Figure 5.13 Monthly Mean Air and Sea Surface Temperature (°C) for the East Orphan Basin ICOADS Data Set

Table 5.7 East Orphan Basin ICOADS Air Temperature (°C) Statistics

Month	Air Temperature (°C)				Sea Surface Temperature (°C)			
	Mean	Maximum	Minimum	Standard Deviation	Mean	Maximum	Minimum	Standard Deviation
January	0.4	15.0	-11.0	3.5	4.9	11.0	-2.0	1.2
February	0.4	16.2	-10.0	4.2	4.2	13.3	-2.0	1.1
March	1.8	10.7	-10.1	3.5	3.9	12.3	-1.1	0.9
April	3.7	11.9	-2.1	2.2	4.3	11.0	0.0	0.8
May	5.2	13.9	-2.0	1.8	5.4	13.3	0.0	1.1
June	7.0	16.1	0.5	2.0	7.4	15.1	0.5	1.7
July	10.2	17.8	1.4	2.1	10.2	18.6	1.0	1.4
August	12.3	20.0	6.6	1.9	13.1	18.0	5.7	1.3
September	11.8	18.3	5.0	2.0	11.7	20.0	5.0	1.8
October	8.9	18.0	-1.8	2.2	9.9	18.0	1.0	1.5
November	5.3	15.0	-6.1	2.6	7.7	16.1	0.7	1.4
December	3.2	12.5	-5.0	3.0	6.0	15.0	0.0	1.2

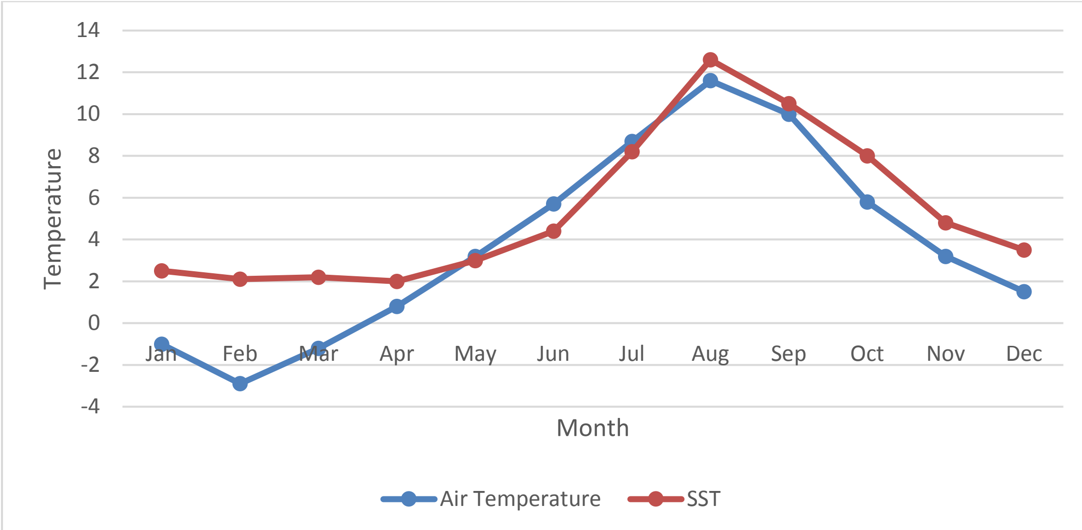

Figure 5.14 Monthly Mean Air and Sea Surface Temperature (°C) for the West Orphan Basin ICOADS Data Set

Table 5.8 West Orphan Basin ICOADS Air Temperature (°C) Statistics

Month	Air Temperature (°C)				Sea Surface Temperature (°C)			
	Mean	Maximum	Minimum	Standard Deviation	Mean	Maximum	Minimum	Standard Deviation
January	-1.0	10.6	-13.0	3.7	2.5	10.8	-2.0	1.1
February	-2.9	12.0	-17.0	5.5	2.1	10.0	-1.8	1.3
March	-1.2	8.7	-12.6	3.9	2.2	10.1	-1.6	1.6
April	0.8	10.5	-4.4	2.4	2.0	9.3	-2.2	1.6
May	3.2	13.8	-1.0	2.0	3.0	10.0	-1.8	1.6
June	5.7	15.0	0.3	2.1	4.4	13.3	-2.2	1.7
July	8.7	18.0	0.6	2.8	8.2	18.5	0.9	2.1
August	11.6	21.0	0.9	2.4	12.6	18.2	2.0	2.0
September	10.0	18.7	0.4	2.6	10.5	17.8	2.3	1.8
October	5.8	15.5	-1.7	3.1	8.0	16.2	0.0	2.3
November	3.2	14.0	-6.0	2.9	4.8	15.0	-0.5	1.6
December	1.5	13.9	-9.3	3.7	3.5	13.0	-0.1	1.5

Sea surface temperatures are warmest in August with a mean monthly temperature of 13.1°C in the East Orphan Basin and 12.6°C in the West Orphan Basin. Sea surface temperatures are coldest in the month of March in the East Orphan Basin and April in the West Orphan Basin.

Mean air temperatures remain above the sea surface temperatures for all months in the East Orphan Basin, while in the West Orphan Basin mean air temperatures decrease below the sea surface temperature during the months of May through July with the greatest difference occurring in the month of July. From August to April, sea surface temperatures are warmer than the mean air temperature. The colder sea surface temperatures for the months of May, June and July have a cooling effect on the atmosphere, while relatively warmer sea surface temperatures for the remainder of the year tend to warm the overlying atmosphere.

Mean temperatures for each month are the mean of all temperatures recorded at the site during that month. The maximum and minimum temperatures are the highest and lowest temperatures, respectively, recorded during the month over the entire data set.

5.3.7 Precipitation

Precipitation can come in three forms and are classified as liquid, freezing or frozen. Included in the three classifications are:

- liquid precipitation
  - drizzle
  - rain
- freezing precipitation
  - freezing drizzle
  - freezing rain
- frozen precipitation
  - snow
  - snow pellets
  - snow grains
  - ice pellets
  - hail
  - ice crystals

The migratory high and low-pressure systems transiting the temperate middle latitude of the Northern Hemisphere cause a variety of precipitation types in their paths. The frequency of precipitation type for the Project Area was calculated using data from the ICOADS data set, with each occurrence counting as one event. Precipitation statistics for these regions may be low due to a fair-weather bias. That is, ships tend to either avoid regions of inclement weather, or simply do not report during these events.

The percentage of occurrences of freezing precipitation data was also calculated from the ICOADS data set. Freezing precipitation occurs when rain or drizzle aloft enters negative air temperatures near the surface and becomes super-cooled so that the droplets freeze upon impact with the surface. This situation typically arises ahead of a warm front extending from low pressure systems passing west of the area. The frequency of freezing precipitation was slightly higher in the winter months than during the spring.

The frequency of precipitation type for each ICOADS region (Tables 5.9 and 5.10) show that annually, precipitation is more frequent in the East Orphan Basin with a frequency of occurrence of 27.9% of the time. Winter has the highest frequency of precipitation with 48.8% of the observations reporting precipitation. Snow accounts for most precipitation during the winter months, accounting for 24.2% of the occurrences of winter precipitation in the East Orphan Basin. Summer has the lowest frequency of precipitation with a total frequency of occurrence of only 15.5%. In the West Orphan Basin, precipitation occurs 20.2% of the time with winter precipitation occurring 39.3% of the time. Of this, 23.3% of winter precipitation falls as snow. Precipitation is only expected within the summer months 10.2% of the time.

Table 5.9 Percentage Frequency (%) Distribution of Precipitation for East Orphan Basin ICOADS Data Set

Month	Rain / Drizzle	Freezing Rain / Drizzle	Rain / Snow Mixed	Snow	Thunder Storm	Hail	Total
January	13.9	1.0	4.4	34.1	0.3	0.3	54.1
February	11.6	0.4	1.8	29.5	0.0	0.0	43.3
March	14.2	0.0	1.6	17.5	0.0	0.0	33.3
April	20.6	0.0	0.7	8.2	0.0	0.0	29.6
May	19.8	0.4	0.9	3.9	0.0	0.0	25.0
June	16.5	0.0	0.5	0.0	0.0	0.0	17.0
July	18.4	0.0	0.0	0.0	0.0	0.0	18.4
August	12.5	0.0	0.0	0.0	0.3	0.0	12.8
September	16.8	0.0	0.0	0.0	0.0	0.0	16.8
October	21.9	0.0	0.3	0.0	0.0	0.3	22.4
November	21.7	0.0	0.3	4.7	0.0	0.6	27.3
December	19.9	1.4	1.8	24.2	0.0	0.4	47.7
Winter	15.3	1.0	2.8	29.4	0.1	0.3	48.8
Spring	18.3	0.1	1.1	9.9	0.0	0.0	29.4
Summer	15.3	0.0	0.1	0.0	0.1	0.0	15.5
Fall	20.1	0.0	0.2	1.5	0.0	0.3	22.0
Annual	17.4	0.3	0.9	9.1	0.1	0.1	27.9

Table 5.10 Percentage Frequency (%) Distribution of Precipitation for West Orphan Basin ICOADS Data Set

Month	Rain / Drizzle	Freezing Rain / Drizzle	Rain / Snow Mixed	Snow	Thunder Storm	Hail	Total
January	12.0	2.0	3.0	33.0	0.0	0.0	50.0
February	7.1	1.2	1.2	32.9	0.0	0.0	42.4
March	19.7	1.5	1.5	15.2	0.0	0.0	37.9
April	17.6	0.0	2.9	1.5	0.0	0.0	22.1
May	15.0	0.8	0.0	0.8	1.5	0.0	18.0
June	18.0	0.0	0.0	0.0	0.0	0.8	18.8
July	9.4	0.0	0.0	0.0	0.7	0.0	10.1
August	5.9	0.0	0.0	0.0	0.6	0.0	6.8
September	17.6	0.0	0.0	0.0	0.0	0.0	17.6
October	14.1	0.0	0.0	0.0	0.0	0.0	14.1
November	18.3	0.0	1.3	7.7	0.0	0.4	27.7
December	14.2	0.0	5.0	10.6	0.0	0.0	29.8
Winter	11.7	0.9	3.4	23.3	0.0	0.0	39.3
Spring	16.9	0.7	1.1	4.5	0.7	0.0	24.0
Summer	9.4	0.0	0.0	0.0	0.5	0.1	10.2
Fall	16.8	0.0	0.5	3.0	0.0	0.2	20.5
Annual	13.1	0.3	0.9	5.5	0.3	0.1	20.2

Thunderstorms occur relatively infrequently over the Project Area though they may occur in any month of the year. Hail only occurs in the presence of severe thunderstorms, yet in Tables 5.9 and 5.10, the frequency of hail is higher than the frequency of thunderstorms for some months. This may be due to observer inexperience, classifying what should be ice pellets (formed through entirely different atmospheric processes) as hail, through coding error or the inability to see the thunderstorms due to low cloud obscuring the sky.

Since negative air temperatures are required for freezing precipitation, statistics show the frequency of freezing precipitation occurs only during the months winter and spring months with winter having a slightly higher percentage occurrence than spring. On a monthly basis, the month of January has the highest frequency of freezing precipitation. Regionally, the West Orphan Basin experiences more freezing precipitation than the East Orphan Basin.

5.3.8 Fog and Visibility

Visibility is defined as the greatest distance at which objects of suitable dimensions can be seen and identified. Horizontal visibility may be reduced by any of the following phenomena, either alone or in combination:

- fog (visibility less than 1 km)
- mist (visibility less than 10 km but greater than 1 km)
- haze
- smoke
- liquid precipitation (e.g., drizzle)
- freezing precipitation (e.g., freezing rain)
- frozen precipitation (e.g., snow)
- blowing snow

During the winter months, the main obstruction is snow; however, mist and fog may also reduce visibilities at times. As spring approaches, the amount of visibility reduction attributed to snow decreases. As the air temperature increases, so does the occurrence of advection fog. Advection fog forms when warm moist air moves over cooler waters. By July, the sea surface temperature is cooler than the surrounding air. As warm moist air from the south moves over the colder sea surface, the air cools and its ability to hold moisture decreases. The air will continue to cool until it becomes saturated and the moisture condenses to form fog. The presence of advection fog increases in June and July. The month of July has the highest percentage of obscuration to visibility, most of which is in the form of advection fog, although frontal fog can also contribute to the reduction in visibility. Frontal fog occurs as relatively warm rain falls through cooler air beneath a frontal surface. Typically, the base of the cloud layer lowers as the air becomes saturated and condensation occurs. If the cloud base reaches the surface, frontal fog occurs. Most frequently, frontal fog occurs ahead of a warm front associated with a frontal disturbance. As the front moves through, clearing of the fog may occur but frequently, frontal fog gives way to advection fog in the warm sector of a low-pressure system.

In August, the air temperature begins to fall below the sea surface temperature. As the air temperature drops, the occurrence of fog decreases. Reduction in visibility during fall and winter is relatively low and is mainly attributed to the passage of low-pressure systems. Fog is the main cause of the reduced visibilities in fall, and snow is the main cause of reduced visibilities in the winter. November has the lowest occurrence of reduced visibility since the air temperature has, on average, decreased below the sea surface temperature and it is not yet cold enough for snow. Typically, fog clears as drier air is adverted into the region from continental source regions to the west.

A plot of the frequency distribution of visibility from the two ICOADS regions are presented in Figures 5.15 and 5.16. These figure shows that obstructions to vision can occur in any month. Annually, 37.8% of the observations had reduced visibilities less than 10 km in the East Orphan Basin. In the West Orphan Basin, 37.3% of the observations have reduced visibilities.

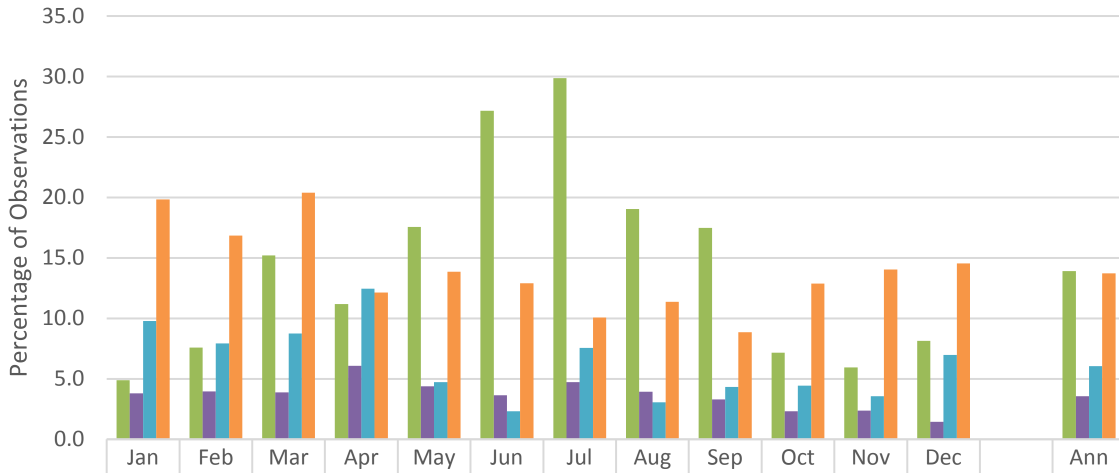

	Jan	Feb	Mar	Apr	May	Jun	Jul	Aug	Sep	Oct	Nov	Dec		Ann
<1	4.9	7.6	15.2	11.2	17.6	27.2	29.9	19.0	17.5	7.2	6.0	8.1		13.9
<2.0	3.8	4.0	3.9	6.1	4.4	3.6	4.7	3.9	3.3	2.3	2.4	1.5		3.6
<4.0	9.8	7.9	8.7	12.5	4.7	2.3	7.5	3.1	4.3	4.4	3.6	7.0		6.1
<10.0	19.8	16.8	20.4	12.1	13.9	12.9	10.1	11.4	8.8	12.9	14.0	14.5		13.7

Figure 5.15 Monthly and Annual Percentage Occurrence of Visibility from the East Orphan Basin ICOADS Data Set (1986-2015)

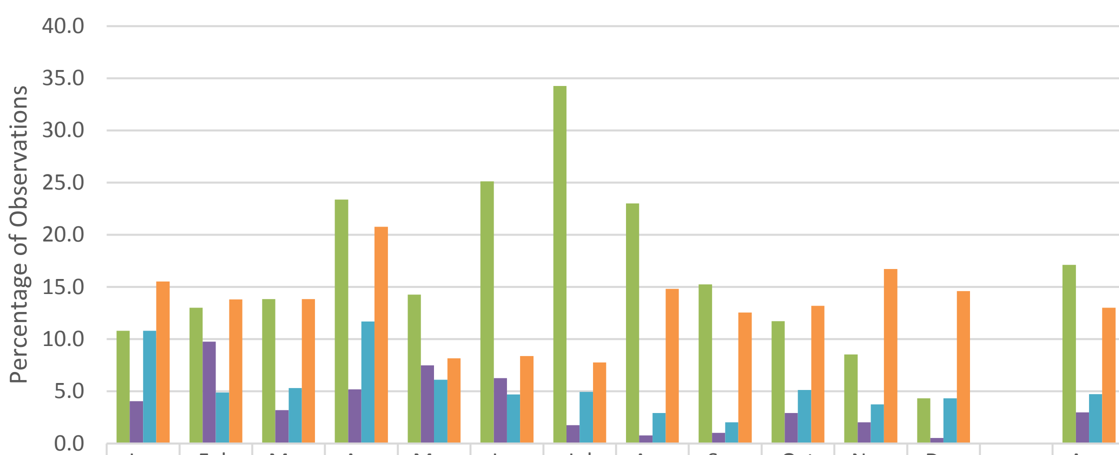

	Jan	Feb	Mar	Apr	May	Jun	Jul	Aug	Sep	Oct	Nov	Dec		Ann
<1	10.8	13.0	13.8	23.4	14.3	25.1	34.3	23.0	15.3	11.7	8.5	4.3		17.1
<2.0	4.1	9.8	3.2	5.2	7.5	6.3	1.8	0.8	1.0	2.9	2.0	0.5		3.0
<4.0	10.8	4.9	5.3	11.7	6.1	4.7	4.9	2.9	2.0	5.1	3.8	4.3		4.7
<10.0	15.5	13.8	13.8	20.8	8.2	8.4	7.8	14.8	12.5	13.2	16.7	14.6		13.0

Figure 5.16 Monthly and Annual Percentage Occurrence of Visibility from the West Orphan Basin ICOADS Data Set (1986-2015)

5.3.9 Lightning

Lightning occurs year-round in offshore Newfoundland. Lightning strikes are stronger during the winter months. Lightning is most commonly produced in thunderstorms and is usually accompanied by thunder (Statoil Canada Ltd. 2017).

Lightning is a localized phenomenon and is difficult to accurately represent in numerical models (Statoil Canada Ltd. 2017). Given its location offshore, there is no specific information on lightning activity in the Project Area. The Canadian Lightning Detection Network provides land-based measurements and statistics for the Newfoundland and Labrador region (Table 5.11); 2013 was the most recent available update.

Table 5.11 Lightning Activity in Newfoundland and Labrador (1999 to 2013)

City	Area (km²)	Total Lightning Strikes from 1999 to 2013	Average Number of Days with Lightning (within 25 km)
Labrador City	38.83	2,231	8.1
Grand Falls-Windsor	54.48	2,747	7.6
Corner Brook	148.30	2,334	7.5
Goose Bay	305.80	1,133	6.8
Gander	104.20	2,579	6.7
Conception Bay South	59.27	644	4.6
Mount Pearl	15.76	580	4.2
Paradise	29.24	590	4.2
St. John's	446.06	566	4.1
Source: ECCC 2016 - Canadian Lightning Detection Network			

5.3.10 Ambient Sound

Sound propagation in the ocean is a complex process that depends on many factors. Sound levels from an omnidirectional point source in the water column are reduced with range, a process known as geometric spreading. Before the sound emanating from the point source reaches the seabed or sea surface boundaries, sound waves propagate in a spherical pattern. In this case, the received levels at a recorder located a distance R from the source are 20×log(R) dB lower than the levels measured at a reference point (1 m from the source). This is known as spherical geometric spreading. Once the sound waves interact with the sea surface and seabed, the spreading becomes cylindrical, with a lower range-dependent decay of 10×log(R) dB. Spherical and cylindrical spreading factors provide rules of thumb for quickly estimating the expected levels from a given source; however, for more realistic scenarios, other factors must also be considered related to losses at the seabed and sea surface, frequency spectrum of the source, and environmental parameters (e.g., bathymetry, water sound speed profile, and seabed geoacoustics).

Bathymetry and seabed conditions of the Project Area are discussed in Sections 5.4 and 5.1, respectively. Their influence on sound propagation is discussed in Section 5.3.10.1.

5.3.10.1 Underwater Sound Speed

As sound speed changes with depth, the sound refracts toward the depth with the lowest sound speed, which results in sound being trapped in a 'duct' and travelling very long distances with minimal attenuation. Conversely, in conditions where the sound speed decreases with depth, sound is refracted toward the seabed and may not reach an intended receiver.

The sound speed changes as a function of the temperature, salinity, and pressure (depth). Colder and fresher water has a lower sound speed and conversely warmer and saltier water has a higher sound speed. As the water depth increases the pressure increases the water density slightly, which increases the sound speed (Jensen et al. 2011). These effects combine with environmental forces, such as solar heating, wind mixing, and currents, to constantly affect the sound speed in the upper 500 m of the water column, which has daily variations around typical seasonal means. The ability of a minimum in the sound speed profile to 'trap' sound depends on the magnitude of the sound speed change at the minimum, the vertical height of the minimum and the sound's wavelength. Ducts must be several times larger than the wavelength for effective trapping of sound (Etter 1996). An outcome of this effect is that higher frequencies are refracted more readily by sound speed changes than lower frequencies that have longer wavelengths.

Sound speed profiles in the Project Area were derived from temperature and salinity profiles from the US Naval Oceanographic Office's Generalized Digital Environmental Model V 3.0 (GDEM; Teague et al. 1990, Carnes 2009). GDEM provides an ocean climatology of temperature and salinity for the world's oceans on a latitude-longitude grid with 0.25° resolution, with a temporal resolution of one month, based on global historical observations from the U.S. Navy's Master Oceanographic Observational Data Set (MOODS). The climatology profiles include 78 fixed depth points to a maximum depth of 6800 m (where the ocean is that deep). The GDEM temperature-salinity profiles were converted to sound speed profiles according to Coppens (1981).

Mean monthly sound speed profiles were derived from the GDEM profiles for the entire year at the two selected model sites (Figure 5.17). The left and middle figures only show the upper 200 m of the sound speed profiles, as this is where the monthly variability is exhibited; below this depth the sound speed exhibits the same uniform positive pressure-based gradient with increasing depth, essentially independent of seasonality. Figure 5.17, right, compares the profiles at both sites, for June, down to a water depth of 1,500 m.

The upper portion of the sound speed profile in the Project Area varies between slightly upward-refracting and isovelocity (December to April) and downward refracting (August to November). A weak sound channel, with a sound speed minimum at approximately 50-75 m, develops in EL 1145 between May and July. In general, the sound emitted in the top 100 m of the water column will tend to refract toward the surface from December to April, toward the seafloor from August to November, but toward the sound speed minimum from May to July. There is little temporal variation in the profiles at depths greater than approximately 100 m. At these depths, the sound speed increases slightly with depth, mainly due to the increase in ambient pressure.

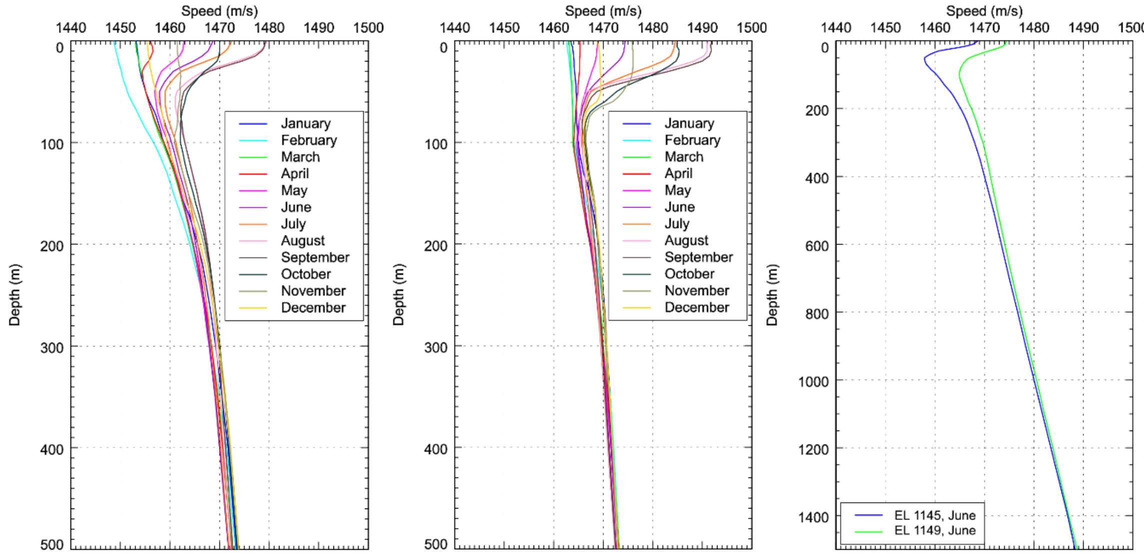

Source: Derived from data obtained from GDEM V 3.0 (Teague et al. 1990; Carnes 200)

Figure 5.17 Mean Monthly Sound Speed Profiles for the a) West Orphan Site EL 1145, b) East Orphan Site EL 1149, c) both Locations in June

To assess transmission loss at sites EL 1145 and EL 1149, a single representative sound speed profile was selected at each location. This profile would be typical of the propagation conditions expected during the months that BP has indicated are preferred for drilling activity (May to October); the sound speed profile for June was selected.

5.3.10.2 Sound Frequency Characteristics

Along with the environmental parameters (bathymetry, sound speed profile, and seabed geoacoustics), a sound's frequency content plays an important role in how it propagates in the ocean. For example, acoustic energy is attenuated by molecular absorption in seawater. The volumetric sound absorption is quantified by an attenuation coefficient, expressed in units of decibels per kilometre (dB/km). This absorption coefficient depends on the temperature, salinity, and pressure of the water, as well as the sound frequency. In general, the absorption coefficient increases with the square of the frequency (i.e., high frequencies are more affected). The absorption of acoustic wave energy has a noticeable effect (>0.05 dB/km) at frequencies above 1 kHz. For example, at 10 kHz the absorption loss over 10 km distance can exceed 10 dB, as computed according to the formulae of François and Garrison (1982b). Another mechanism of absorption in the water column is scattering, which results from the sound wave interacting with non-homogeneities (such as air bubbles) and with the rough boundaries at the air-sea and sea-seabed interfaces. Acoustic energy loss due to scattering is also frequency-dependent, with more noticeable effects when the scatterer is the same size or larger than the sound wavelength. Sounds at low frequencies, therefore, are less affected by scattering than sounds at high frequencies.

Although lower frequency sounds are less affected by absorption and scattering, there are other mechanisms that have the opposite effect (i.e., favour propagation of higher frequency sounds). For example, propagation through a surface duct only applies to frequencies above a certain cut-off. When sound has strong frequency components above this cut-off, acoustic energy is trapped in the surface channel. This trapped energy does not interact with the seabed, so it propagates to farther ranges. Low-frequency sounds, however, tend to interact with the seabed and are attenuated as they propagate through the seabed sediment.

5.3.10.3 Ambient Soundscape

The ambient, or background, sound levels that create the ocean soundscape are comprised of many natural and anthropogenic sources (refer to Figure 5.18). The main environmental sources of sound are wind, precipitation, and sea ice (Matthews et al. 2018; see Appendix C). Sea ice can produce loud sounds that are often the main contributor of acoustic energy in the local soundscape, particularly during ice formation and break up. Precipitation is a common source of sound, with contributions typically concentrated at frequencies above 500 Hz. At low frequencies (<100 Hz), earthquakes and other geological events contribute to the soundscape (Matthews et al. 2018).

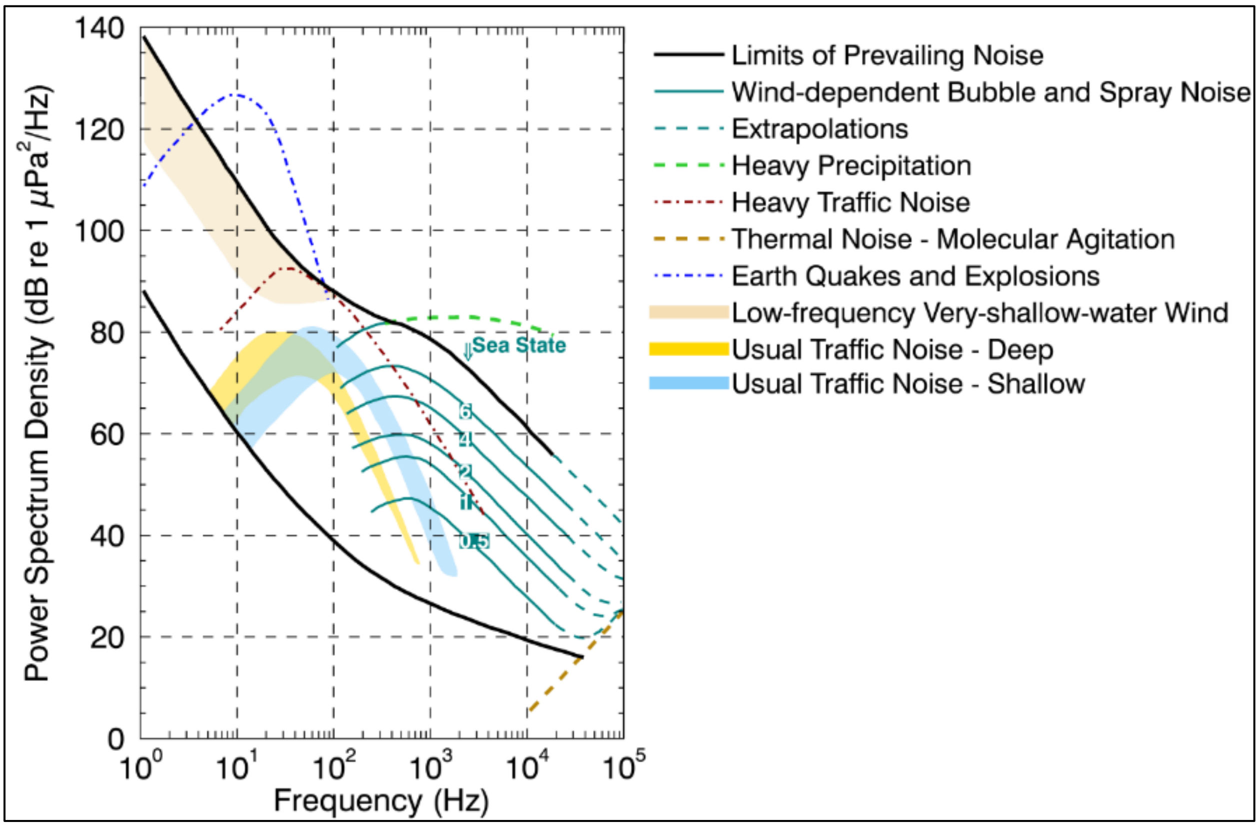

Source: adapted from Wenz (1962), in Matthews et al. (2018)

Figure 5.18 Wenz Curves Describing Pressure Spectral Density Levels of Marine Ambient Noise from Weather, Wind, Geologic Activity, and Commercial Shipping

As reported in Matthews et al. (2018), the Environmental Studies Research Fund (ESRF) funded a two-year program aimed recording the underwater soundscape and the occurrence of marine mammals on Canada's East Coast (hereinafter referred to as the "ESRF Study"). The ESRF Study area includes shallow and deep waters, and it extends from Dawson Canyon off Halifax, NS, to Nain Bank on the Labrador shelf. JASCO deployed 20 acoustic recorders along Canada's east coast for the ESRF Study. The recorders were active for most of 2015-2017. Data from recorder stations 15 and 19 were used in an acoustic assessment undertaken by JASCO for this Project (Matthews et al. 2018) to provide the best available information on the existing soundscape in the Project Area (see Figure 5.19).

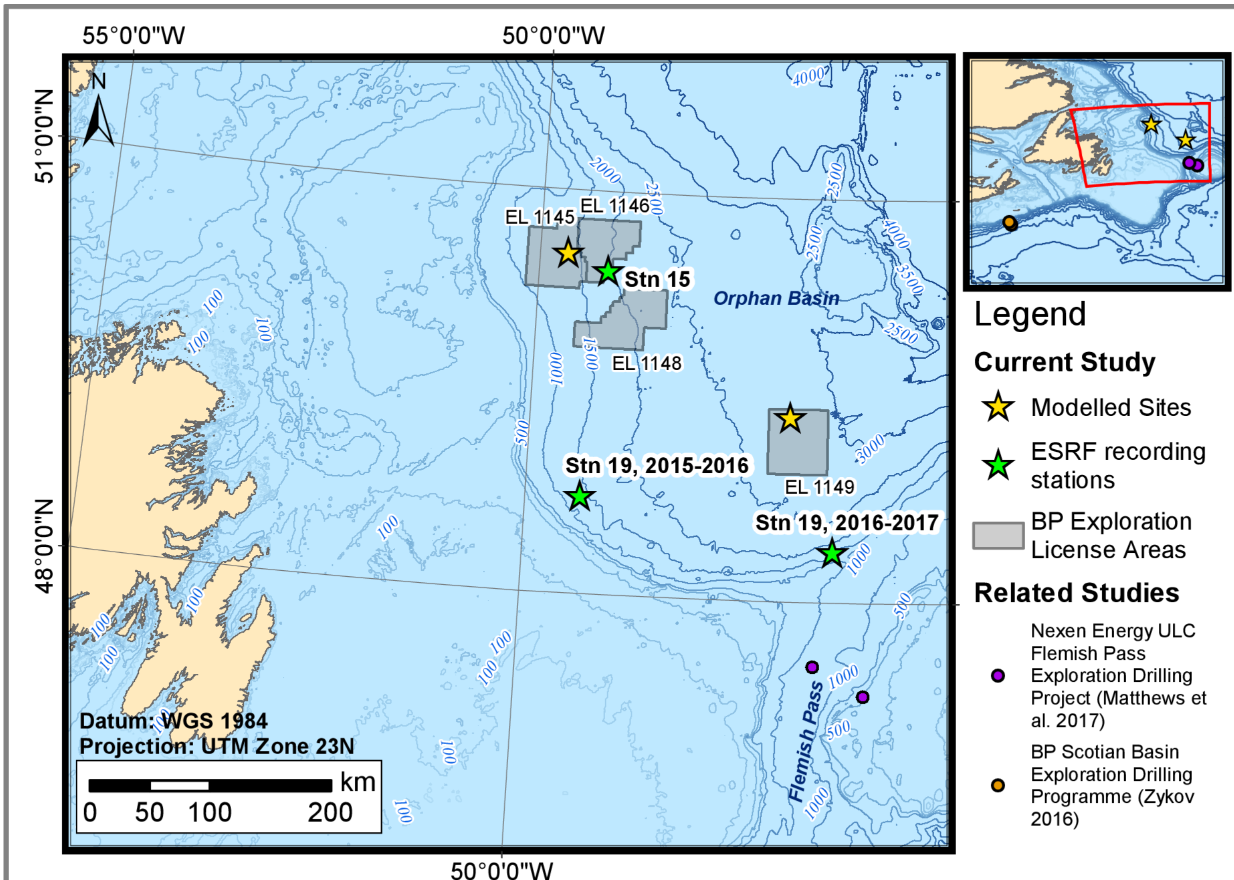

Overview of the Newfoundland Orphan Basin Exploration Drilling Program area, modelled sites, sites of related studies, and recording stations.

Source: Matthews et al. (2018)

Figure 5.19 Location of ESRF Recording Stations Relative to BP's ELs

Station 15 was in 2000 m water depth, approximately between EL 1146 and EL 1148. Station 19 was deployed off the northeastern coast of Newfoundland at slightly different locations in 2015-2016 and 2016-2017. In 2015-2016, it was deployed in the southwestern part of Orphan Basin (1282 m depth) to obtain baseline data ahead of anticipated oil and gas activity. In 2016-2017, the station was moved to the southeastern part of Orphan Basin (1550 m depth) to investigate mammal habitat use after repeated sightings of northern bottlenose whales in the area and due to increased oil and gas interest in the area. It was deployed at a depth of 1547 m (Matthews et al. 2018).

The maximum and minimum broadband sound pressure levels (SPLs) measured at Station 15 in 2015-2016 were 137.6 and 87.9 dB re 1 µPa, respectively (Figure 26 in Appendix C). The maximum and minimum broadband SPLs measured in 2016-2017 were 144.3 and 91.1 dB re 1 µPa, respectively (Matthews et al. 2018).

The maximum and minimum broadband SPL measured at Station 19 in 2015-2016 were 139.5 and 90.6 dB re 1 µPa, respectively (Figure 29 in Appendix C). The maximum and minimum broadband SPL measured in 2016-2017 were 157.6 and 95.5 dB re 1 µPa, respectively (Matthews et al. 2018).

The two main soundscape features at both stations were seismic survey activity from July to October in both years, and fin whale calls. Fin whale 20 Hz notes were detected as early as September 2015, but they were generally masked by seismic survey until the end of the survey in late October 2015. These notes were the main source of identifiable sound at both stations until mid-March 2016. A similar pattern occurred in 2016-2017.

Based on measurements at the ESRF stations, Matthews et al. (2018) found there were several identifiable sources in the Project Area that have long-term effects on the soundscape and these sources are expected to be present in the foreseeable future: fin whales, shipping and oil and gas extraction platforms, and seismic surveys (Matthews et al. 2018).

Fin whales sing from October to March on the Grand Banks, seemingly favoring the shallow waters on the Grand Banks compared to the deeper waters off the continental shelf. Their constant notes raise the total sound level in the 10-45 Hz band by 5-10 dB in winter across the Grand Banks. Whales close to a recorder can temporarily increase the one-minute sound levels to 130 or 140 dB re 1 µPa (Matthews et al. 2018).

Shipping, including supply vessels like PSVs that are proposed to be used for the Project, are generally transient sources that are detectable at any one location over a period of several hours. Closer to the exploration drilling areas and existing oil and gas extraction platforms, the sounds from vessels and dynamic positioning systems are continuously present (Matthews et al. 2018).

Although the seismic surveys detected at Stations 15 and 19 were over 100 km from the recorders, they were still a dominant sound source in the soundscape. The peak frequency of sound from seismic source arrays is near 50 Hz (Dragoset 1984), however the frequency range increases as the source vessel gets closer to a measurement location. The measurements reported in the ESRF Study included energy up to 1 kHz. This sound source is variable in space and time depending on where the seismic source is located. It is expected that 2D and 3D seismic surveys will continue off Newfoundland for the foreseeable future each summer.

5.4 Physical Oceanography

5.4.1 Bathymetry

The Orphan Basin is part of the complex network of connected basins and sub basins formed in offshore Newfoundland and Labrador during Mesozoic lithospheric extension, continental rifting, and continental breakup (Enachescu et al. 2005). These basins are separated by basin-bounding faults or by sediment-covered ridges or basement ridges devoid of sediment (Enachescu et al. 2005). Large north-south and northeast-southwest trending basement ridges with intervening troughs were identified on seismic data and were interpreted as basement highs or sediment-covered ridges (Enachescu et al. 2005). The main sedimentary basins in the Project Area and RAA include the East and West Orphan Basin, the Flemish Pass, and Jeanne d'Arc Basin (Amec 2014).

The Orphan Basin is bounded by the Newfoundland Shelf to the west, the Flemish Cap to the south, and the Orphan Knoll to the northeast (Campbell 2005). The floor of Orphan Basin is relatively flat and slopes gently towards the east, with the exceptions of the Sackville Spur and broad submarine channels that merge in the gap between the Flemish Pass and Orphan Knoll (Campbell 2005). The Grand Banks extend to the Northeast Newfoundland Shelf with depths generally between 200 to 300 m (Statoil Canada Ltd. 2017). The Orphan Basin lies to the northeast of the Grand Banks shelf. Water depths in the Orphan Basin range from approximately 1,200 m at the edge of the continental shelf to 3,300 m south of the Orphan Knoll (Statoil Canada Ltd. 2017). To the north and east of the Orphan Basin, the Labrador Basin and deeper water lie farther offshore with depths from 3,000 to over 4,000 m (Statoil Canada Ltd. 2017). The minimum, maximum and average water depth of ELs 1145, 1146, 1148, and 1149 are shown in Table 5.12.

Table 5.12 Minimum, Maximum, and Average Depth of ELs

EL	Minimum Depth (m)	Maximum Depth (m)	Average Depth (m)
1145	970	1,540	1,257
1146	1,360	2,275	1,843
1148	1,250	2,400	1,846
1149	2,595	2,910	2,752

The transit routes for PSVs to and from the Project Area will cross portions of the northeast Grand Banks, the Northeast Newfoundland Shelf and Slope, and the southern part of the Orphan Basin (see Figure 2.11 in Section 2.4.5.2). The northeast Grand Banks have a water depth of approximately 200 m, which deepens to 300 m where the Grand Banks extend north to the Northeast Newfoundland Shelf (Figure 5.20) (Statoil Canada Ltd. 2017). Water depths in the southern part of the Orphan Basin where it extends from the Northeast Newfoundland Slope range from 1,000 to 1,500 in the West Orphan Basin and from 1,500 to 3,000 in the East Orphan Basin (Enachescu 2006).

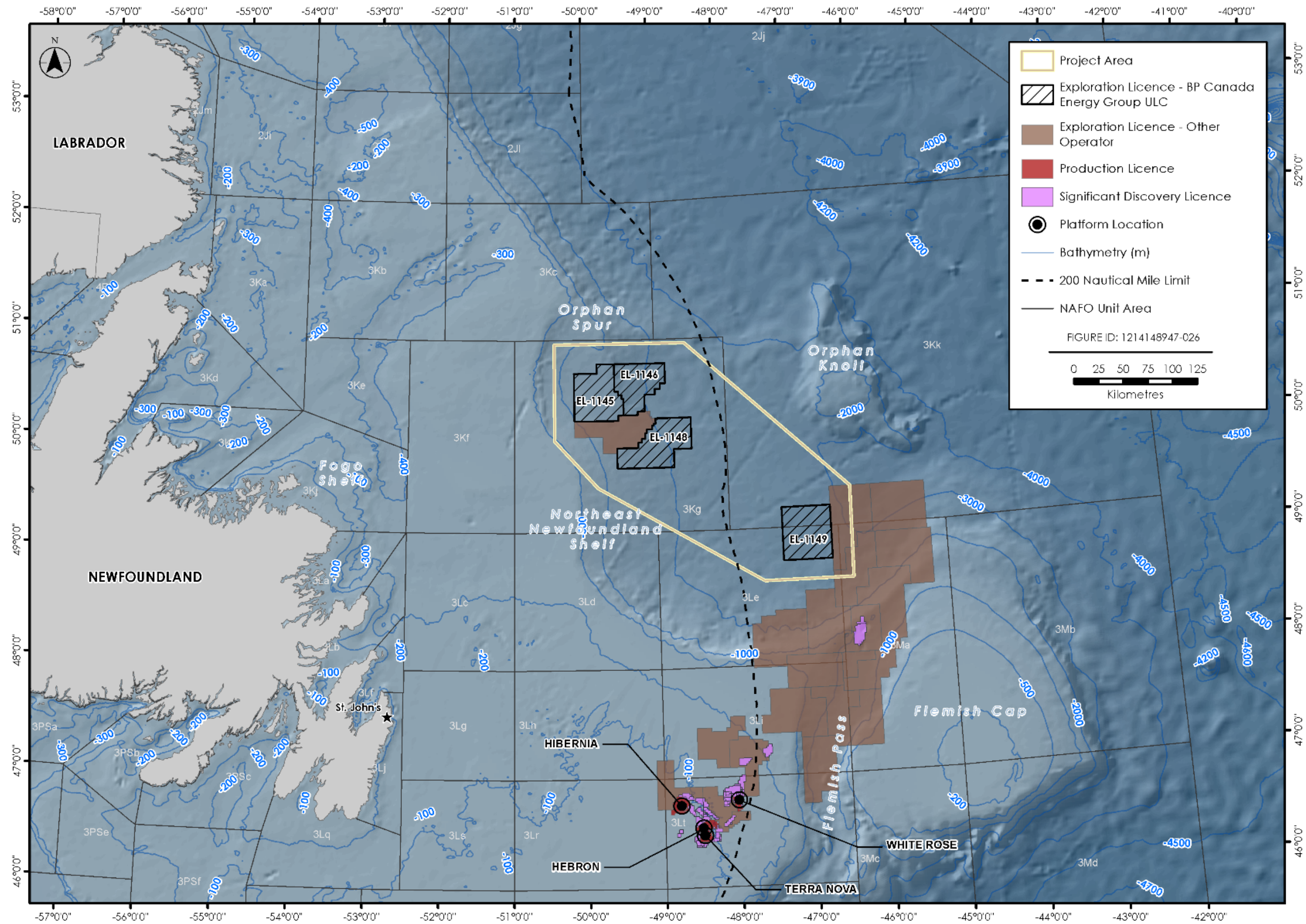

Figure 5.20 Orphan Basin Bathymetry

bp

5.4.2 Ocean Currents

5.4.2.1 General Description

The Labrador Current (Figure 5.21) is the dominant current in the RAA. The Labrador Current is composed of the West Greenland, Baffin Island Currents and Irminger Current. The Labrador Current originates from the Hudson Strait at 60°N and flows southward over the Labrador and Newfoundland Shelf and Slope to the tail end of the Grand Banks at 43°N (Lazier and Wright 1993). The Labrador Current becomes two branches on the southern Labrador Shelf: an inshore branch with approximately 15% of the transport and a main offshore branch, with approximately 85% of the transport (Lazier and Wright 1993). The main branch of the offshore Labrador Current typically flows along the Continental Slope between 300 and 1,500 m (Lazier and Wright 1993). The inshore branch is a weaker flow, not well defined, except in specific regions where bathometry effects are dominate such as in the Avalon Channel (Narayanan et al. 1996). The mean surface water velocities of the offshore branch typically range from 25 to 50 cm/s, and those of the inshore branch are weaker and range from 5 to 20 cm/s (Fissel and Lemon 1991; Lazier and Wright 1993; Colbourne 2000). The currents on the Newfoundland Slope are highly variable due to the influences of strong atmospheric forcing, large inflows of sea ice, and interactions with the Gulf Stream and North Atlantic Current (Han and Li 2004). This results in the Labrador Current having seasonal and interannual variations in velocity and transport. Typically, the upper waters of the Labrador Current are stronger in fall and winter and weaker in spring (Lazier and Wright 1993; Han and Tang 1999; Han and Li 2004). Lazier and Wright (1993) found seasonal variations in the upper 400 m level circulation and no significant variations deeper than the 1,000 m level.

The Labrador Current flows southward until it reached the southern part of Orphan Basin, where it is diverted eastward by the bathymetry. Upon reaching the entrance to Flemish Pass, the current divides into two branches. One branch continues to flow eastward north of Flemish Cap and the other branch flows southward through Flemish Pass.

East of the Tail of the Grand Banks, the Gulf Stream loses its characteristics and divides into branches. One of these branches flows northward (Figure 5.21) on the eastern side of Flemish Cap to the Orphan Basin region. Greenan et al. (2010) found that the waters in the Orphan Knoll region of Orphan Basin were warmer in 2009 than in 2008 from an incursion of a filament from a meander of the North Atlantic Current.

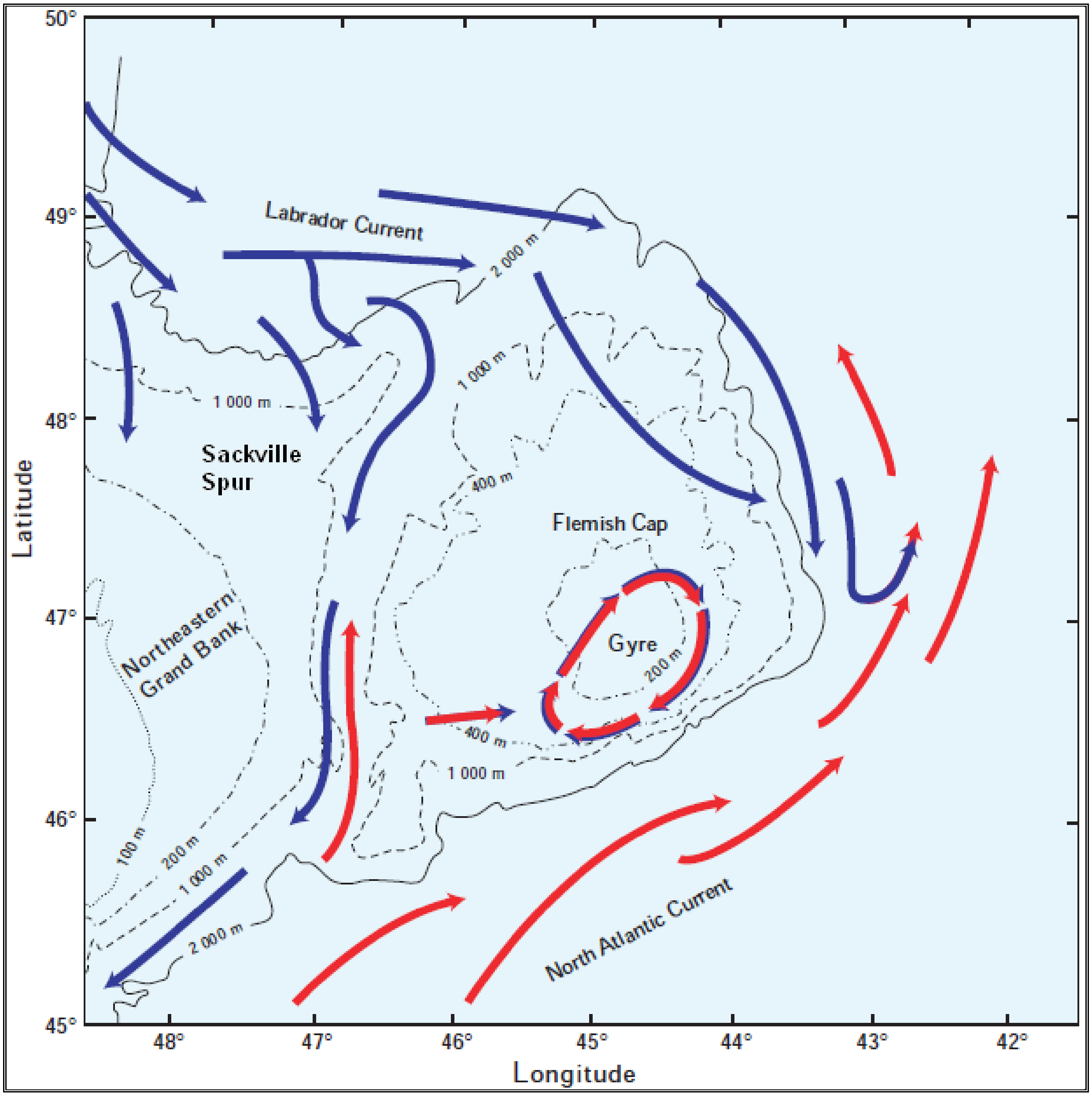

Source: (modified from Colbourne & Foote 2000
Note: Blue arrows represent the Labrador Current; red arrows represent the North Atlantic Current.

Figure 5.21 The Major Circulation Features East Orphan Basin

5.4.2.2 Current Measurements in Orphan Basin

Moored current measurements in Orphan Basin have been carried out by the Bedford Institute of Oceanography (BIO) in the past decades and by Oceans Ltd at the exploration drill sites Great Barasway F-66 in 2006 and Lona O-55 in 2010. The Project Area was divided into two sub-areas: West Orphan Basin (EL 1145, EL 1146 and EL 1148) and East Orphan Basin (EL 1149). Moorings selected for this report in West Orphan Basin and East Orphan Basin are described in the following section.

West Orphan Basin

Two moored current measurements were made in West Orphan Basin between May 11, 1991 and May 25, 1992. Both mooring sites are close to EL 1148. The locations of these moorings are listed in Table 5.13 and shown in Figure 5.22.

Table 5.13 Current Meter Data for the Project Area - West Orphan Basin

Mooring #	Date	Instrument Depth (m)	Latitude	Longitude
WOB_1	May 11, 1991 – Nov. 03, 1991	200	49.7485N	49.7465W
WOB_1	May 11, 1991 – Nov. 03, 1991	400	49.7485N	49.7465W
WOB_1	May 11, 1991 – Nov. 03, 1991	900	49.7485N	49.7465W
WOB_2	Nov. 03, 1991 – May 25, 1992	400	49.7467N	49.7388W
WOB_2	Nov. 03, 1991 – May 25, 1992	900	49.7467N	49.7388W

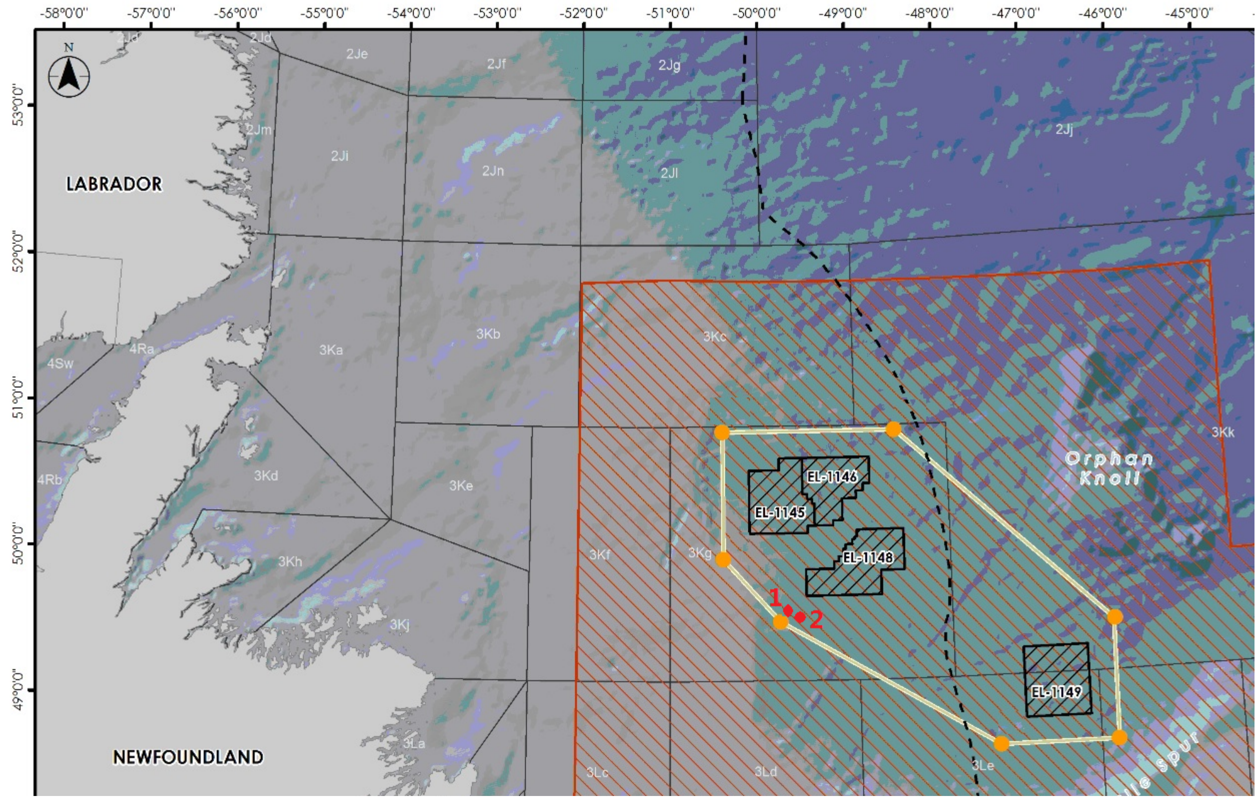

Figure 5.22 BIO Mooring Locations (mooring WOB_ 1 and WOB_2) at West Orphan Basin

At mooring stations 1 (200, 400, and 900 m) and 2 (400 and 900 m) (Figure 5.22), current was flowing towards the south-southeast at all depths throughout the year.

From May 1991 to November 1991, mean current speed decreased with depths, with values of 11.7 cm/s at 200 m, 9.1 cm/s at 400 m, and 8.2 cm/s at 900 m. The maximum speed of current occurred in October, September, and May, with values of 30.7 cm/s, 22.0 cm/s and 19.7 cm/s at 200 m, 400 m, and 900 m, respectively.

From November 1991 to May 1992, mean current speeds at 400 m and 900 m depths were 7.6 and 7.4 cm/s, respectively. The maximum current speeds occurred in December at 400 m and April at 900 m, with values of 23.2 and 23.1 cm/s, respectively.

Table 5.14 summarizes the statistics for current data collected from May 11, 1991 to May 25, 1992.

Table 5.14 Statistics of Current at West Orphan Basin at 200 m, 400 m and 900 m, from May 11, 1991 to May 25, 1992

Duration	Depth (m)	Mean Speed (cm/s)	Mean Direction	Maximum Speed (cm/s)	Mean Velocity (cm/s)
May 11, 1991 – Nov. 03, 1991	200	11.7	SSE	30.7	11.1
	400	9.1	SSE	22.0	8.4
	900	8.2	S	19.7	7.1
Nov. 03, 1991 – May 25, 1992	400	7.6	S	23.2	4.1
	900	7.4	S	23.1	4.3

Rose plots for mooring station 1 (Figure 5.22) at 200 m, 400 m, and 900 m from May 1991 to November 1991 indicate that currents at all depths at West Orphan Basin flow towards southern-southeast directions (Figure 5.23). Rose plots are in oceanographic convention.

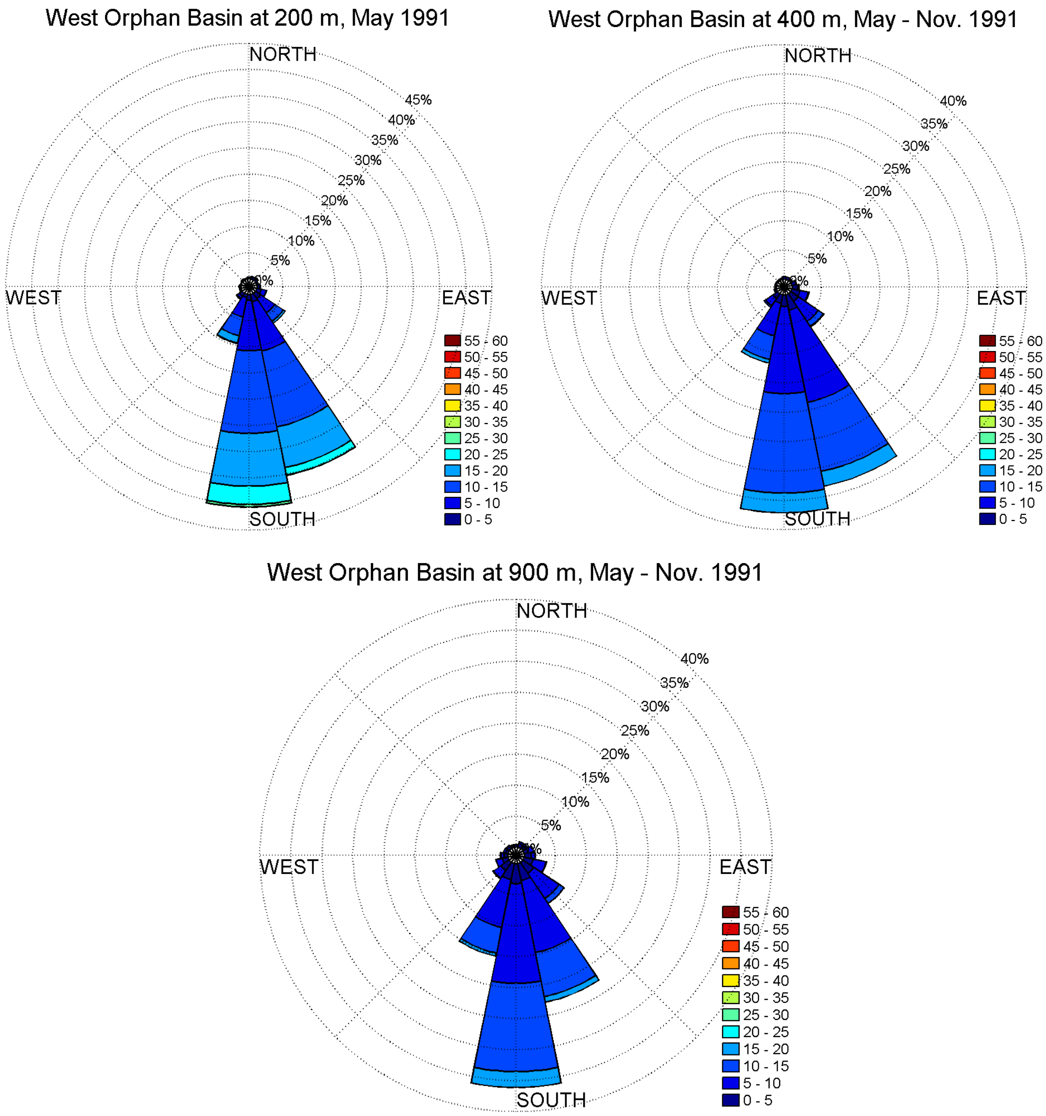

Figure 5.23 Rose Plot for Currents at West Orphan Basin at 200, 400, and 900 m depths, May 1991 – November 1991

East Orphan Basin

Five moored current measurements were made in East Orphan Basin between June 05, 2004 and May 07, 2010. The locations of these moorings are listed in Table 5.15 and shown in Figure 5.24.

Table 5.15 Current Meter Data for the Project Area - East Orphan Basin

Mooring #	Date	Instrument Depth (m)	Latitude	Longitude
EOB_1	Jun. 05, 2004 – Dec. 26, 2004	362	49.2969N	48.3162W
EOB_1	Jun. 05, 2004 – Dec. 10, 2005	712	49.2969N	48.3162W
EOB_1	Jun. 05, 2004 – Jul. 21, 2004	1112	49.2969N	48.3162W
EOB_1	Jun. 05, 2004 – May 22, 2005	1912	49.2969N	48.3162W
EOB_1	Jun. 05, 2004 – May 22, 2005	2237	49.2969N	48.3162W
EOB_2	Jun. 04, 2004 – May 22, 2005	2227	48.8321N	47.4544W
EOB_3	May 12, 2008 – Mar. 10, 2009	2455	48.8315N	47.4544W
EOB_4	May 14, 2008 – May 10, 2009	2719	49.1375N	46.9211W
EOB_5	May 10, 2009 – Mar. 28, 2010	2474	49.1382N	46.9229W
EOB_5	May 10, 2009 – May 07, 2010	2724	49.1382N	46.9229W

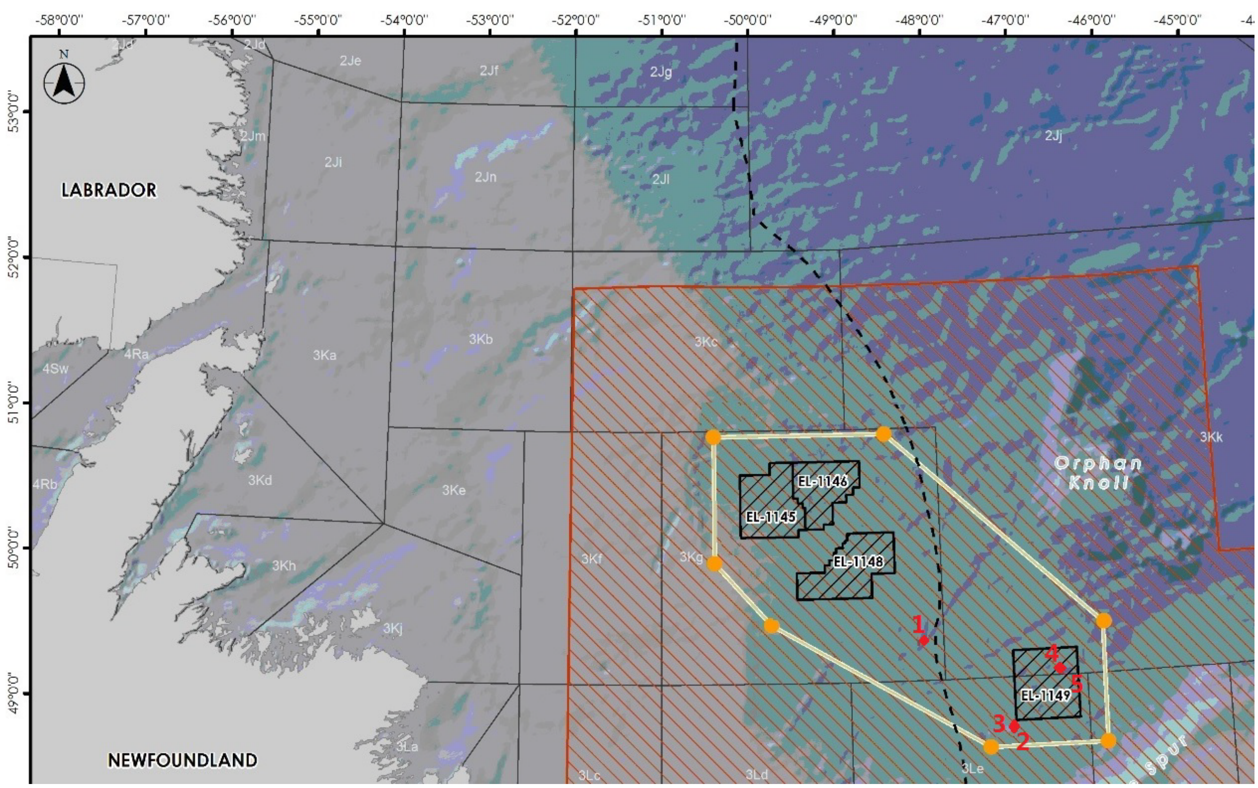

Figure 5.24 BIO Monitoring Locations at East Orphan Basin

At 362 m depth at mooring station 1 (Figure 5.24), current flowed southerly in June and July months, while it changed to a western direction from August and remained in a western direction for the rest of the measuring period. At 712 m depth, current was mainly in a southward direction with slight fluctuations from southwest to southeast. At 1,112 m and 1,192 m, current flowed in a south-southeast direction and at 2,237 m current was toward a south-southwest direction.

At 2,227 m at mooring station 2 (Figure 5.24), current flowed to a southeast direction throughout the year, with a mean velocity of 6.6 cm/s. At 2,455 m at mooring station 3 (Figure 5.24), current flowed to a southeast direction throughout the year, with a mean velocity of 6.1 cm/s. At 2,719 m at mooring station 4 (Figure 5.24), current flowed to a south-southeast direction throughout the year, with a mean velocity of 10.2 cm/s. At 2,724 m at mooring station 5 (Figure 5.24), current flowed to a south-southeast direction throughout the year, with a mean velocity of 8.4 cm/s and 12.4 cm/s at 2,474 m and 2,724 m, respectively.

From June 2004 to December 2004 at 362 m depth at mooring station 1, the mean current speed was 8.3 cm/s with the maximum speed 30.7 cm/s that occurred in November 2004. Mean speed at 712 m depth at mooring station 1 was 8.0 cm/s with the maximum speed 21.7 cm/s in November 2004 as well. From June 2004 to July 2004, the mean current speed at 1,112 m depth at mooring station 1 was 8.5 cm/s. The maximum speed in June and July months were 21.4 cm/s and 20.0 cm/s, respectively. From June 2004 to May 2005, the mean current speeds at 1,912 m and 2,237 m at mooring station 1 were 7.8 cm/s and 7.3 cm/s, respectively. The maximum current speeds occurred in June and March at 1,912 m with a value of 21.7 cm/s. At 2,237 m depth at mooring station 1, the maximum current speed occurred in June with a value of 31.4 cm/s.

From June 2004 to May 2005, the mean current speed at 2,227 m at mooring station 2 was 8.3 cm/s, with the maximum speed of 30.5 cm/s in April. From May 2008 to March 2009, the mean current speed at 2,455 m at mooring station 3 was 8.4 cm/s, with the maximum speed of 32.0 cm/s in June. From May 2008 to May 2009, the mean current speed at 2,719 m at mooring station 4 was 11.9 cm/s, with the maximum speed of 37.5 cm/s in August. From May 2009 to March 2010, the mean current speed at 2,474 m at mooring station 5 was 10.3 cm/s, with the maximum speed of 40.4 cm/s in June. From May 2009 to May 2010, the mean current speed at 2,724 m at mooring station 5 was 14.2 cm/s, with the maximum speed of 39.5 cm/s in April.

Table 5.16 summarizes the statistics for current data collected from June 04, 2004 to May 07, 2010.

Table 5.16 Statistics of Current at East Orphan Basin from June 04, 2004 to May 07, 2010

Duration	Depth (m)	Max Speed (cm/s)	Mean Speed (cm/s)	Mean Velocity (cm/s)	Direction of Mean Velocity (degree)
Jun. 05, 2004 – Dec. 26, 2004	362	8.3	SW	30.7	5.0
Jun. 05, 2004 – Dec. 10, 2005	712	8.0	S	21.7	5.0
Jun. 05, 2004 – Jul. 21, 2004	1112	8.5	S	21.4	7.4
Jun. 05, 2004 – May 22, 2005	1912	7.8	SSE	21.7	5.7
Jun. 05, 2004 – May 22, 2005	2237	7.3	S	31.4	4.6
Jun. 04, 2004 – May 22, 2005	2227	8.3	SE	30.5	6.6
Jun. 04, 2004 – May 22, 2005	2455	8.4	SSE	32.0	6.1
May 14, 2008 – May 10, 2009	2719	11.9	SSE	37.5	10.2
May 10, 2009 – Mar. 28, 2010	2474	10.3	SSE	40.4	8.4
May 10, 2009 – May 07, 2010	2724	14.2	SSE	39.5	12.4

Rose plots for mooring station 1 at 362 m, 712 m, 1112 m, 1,912 m, and 2,237 m June 2004 to May 2005 are presented in Figure 5.25. Rose plots are in oceanographic convention.

The rose plots indicate that current at 362 m was toward a westerly direction with fluctuations to southwest. At 712 m and 2,237 m, currents flowed to a southerly direction with a slight deviation to southwest; at 1,112 m and 1,192 m, the rose plots indicate that currents were mainly in a southerly direction with slight fluctuations from southwest to southeast.

The harmonic analysis for currents at East Orphan Basin 362 m, 712 m, 1,112 m, 1,912 m, and 2,237 m, June 2004 to May 2005 (mooring station 1) indicated that from June 2004 to December 2004 at 362 m depth, M2 (the principal lunar semidiurnal), K1 (solar diurnal constituent), S2 (principal solar semidiurnal constituents), and O1 (lunar diurnal constituent) had values of 0.6 cm/s, 0.2 cm/s, 0.3 cm/s and 0.2 cm/s, respectively. At 712 m depth, M2, K1, S2, and O1 had values of 1.4 cm/s, 0.4 cm/s, 0.6 cm/s and 0.1 cm/s, respectively. From June 2004 to July 2004 at 1,112 m depth, the tidal constituents M2, K1, S2, and O1 had values of 1.5 cm/s, 0.4 cm/s, 0.6 cm/s and 0.2 cm/s, respectively. From June 2004 to May 2005, M2 were 2.1 cm/s and 1.8 cm/s at depths of 1,912 m and 2,237 m depths, respectively. At 1,912 m depth, K1, S2, and O1 had values of 0.3 cm/s, 0.6 cm/s, and 0.1 cm/s; at 2,237 m, K1 and S2 had values of 0.2 cm/s and 0.5 cm/s with O1 close to 0 cm/s.

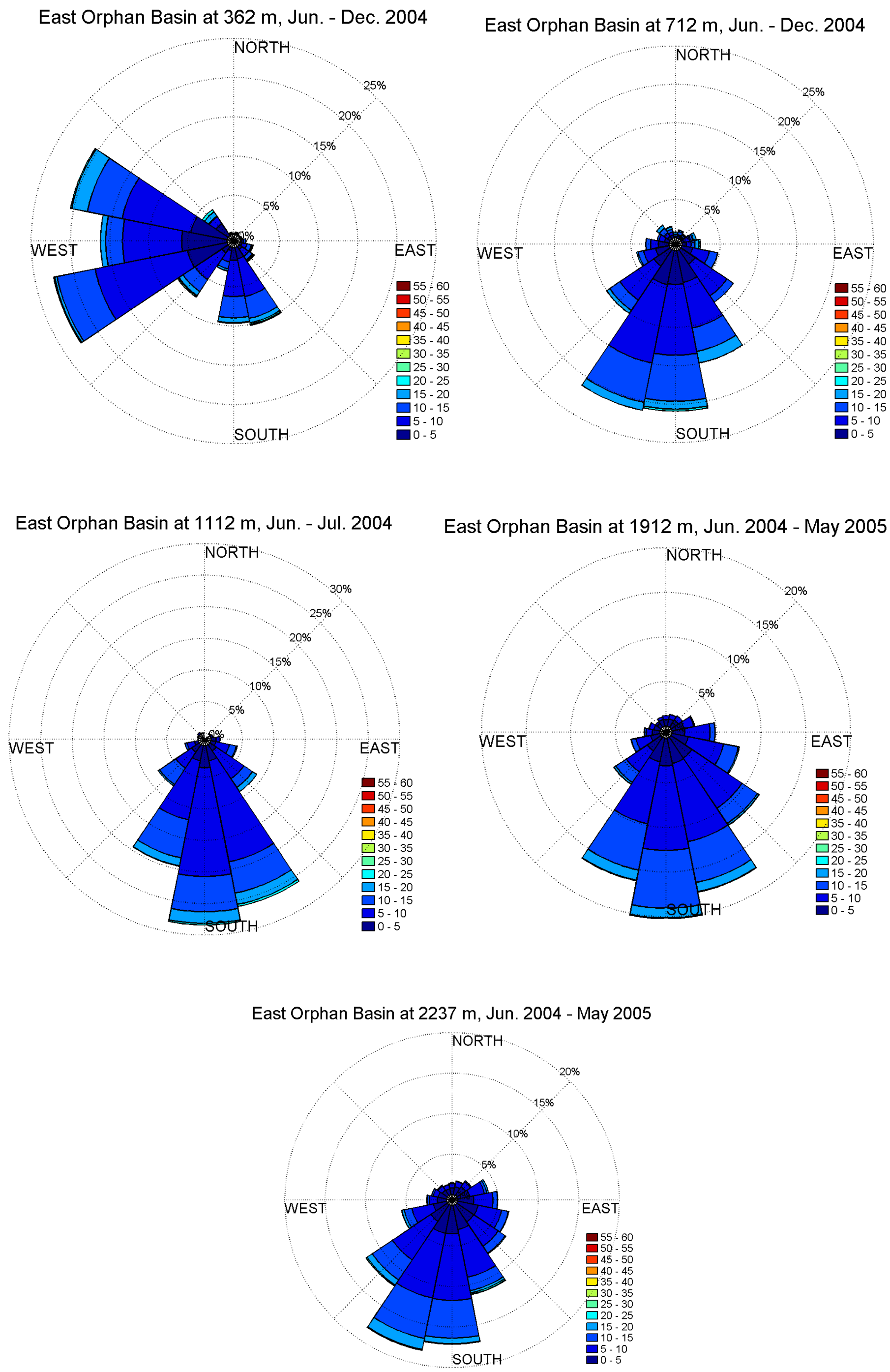

Figure 5.25 Rose Plot for Currents at East Orphan Basin 362 m, 712 m, 1,112 m, 1,912 m, and 2,237 m, June 2004 to May 2005 (Mooring EOB_1)

Oceans Current Measurements

Oceans Ltd placed current meter moorings in the Orphan Basin at the Great Barasway F-66 and Lona O-55 wellsites during the period of exploration drilling between 2006 and 2007. The locations are shown in Figure 5.26.

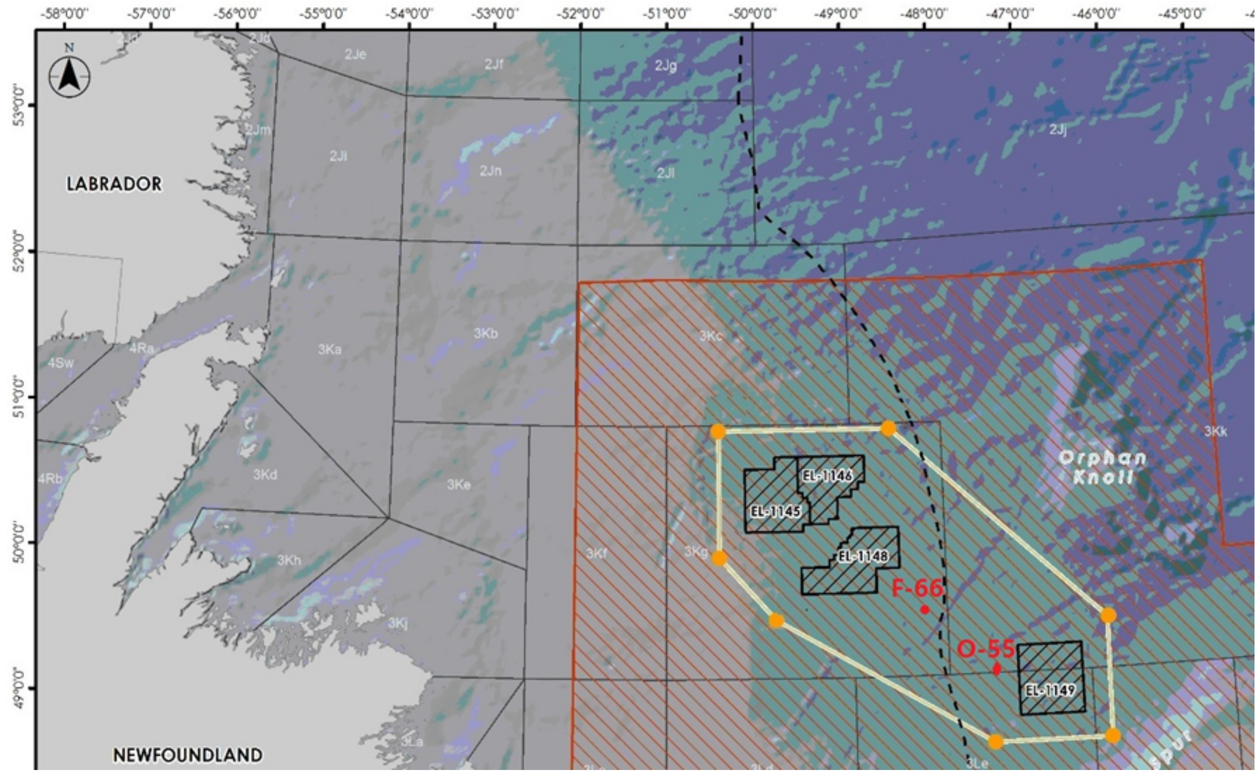

Figure 5.26 Locations of Current Moorings at Great Barasway F-66 and Lona O-55

Great Barasway F-66

Oceans Ltd measured the currents near drill site Great Barasway F-66 at depths of 300 m, 650 m, 1,850 m, and 2,328 m (2 m above bottom) between September 18, 2006 and April 7, 2007. The mooring was located at 49°24'42"N; 48°11'24"W. The mean flow was towards the south southeast at 300 m, 650 m, and 1,850 m and towards the southeast near the bottom. There were occasions when the current direction changed abruptly from southeast to southwest and then flowed in the new direction for several days. Such shifts occurred on September 28, October 23 and November 1 of 2006. The abrupt changes in current direction may be associated with the eddy motion in the Orphan Basin identified by BIO in their data.

Histograms of the current speed and direction at the four depths are presented in Figure 5.27. The mean current speeds were 11.6 cm/s, 10.21 cm/s, 8.9 cm/s, and 7.1 cm/s at depths of 300 m, 650 m, 1,850 m, and 2,328 m, respectively. The maximum current speeds were 36.3 cm/s, 31.3 cm/s, 24.0 cm/s and 23.6 cm/s at depths of 300m, 650 m, 1,850 m, and 2,328 m, respectively.

300 m

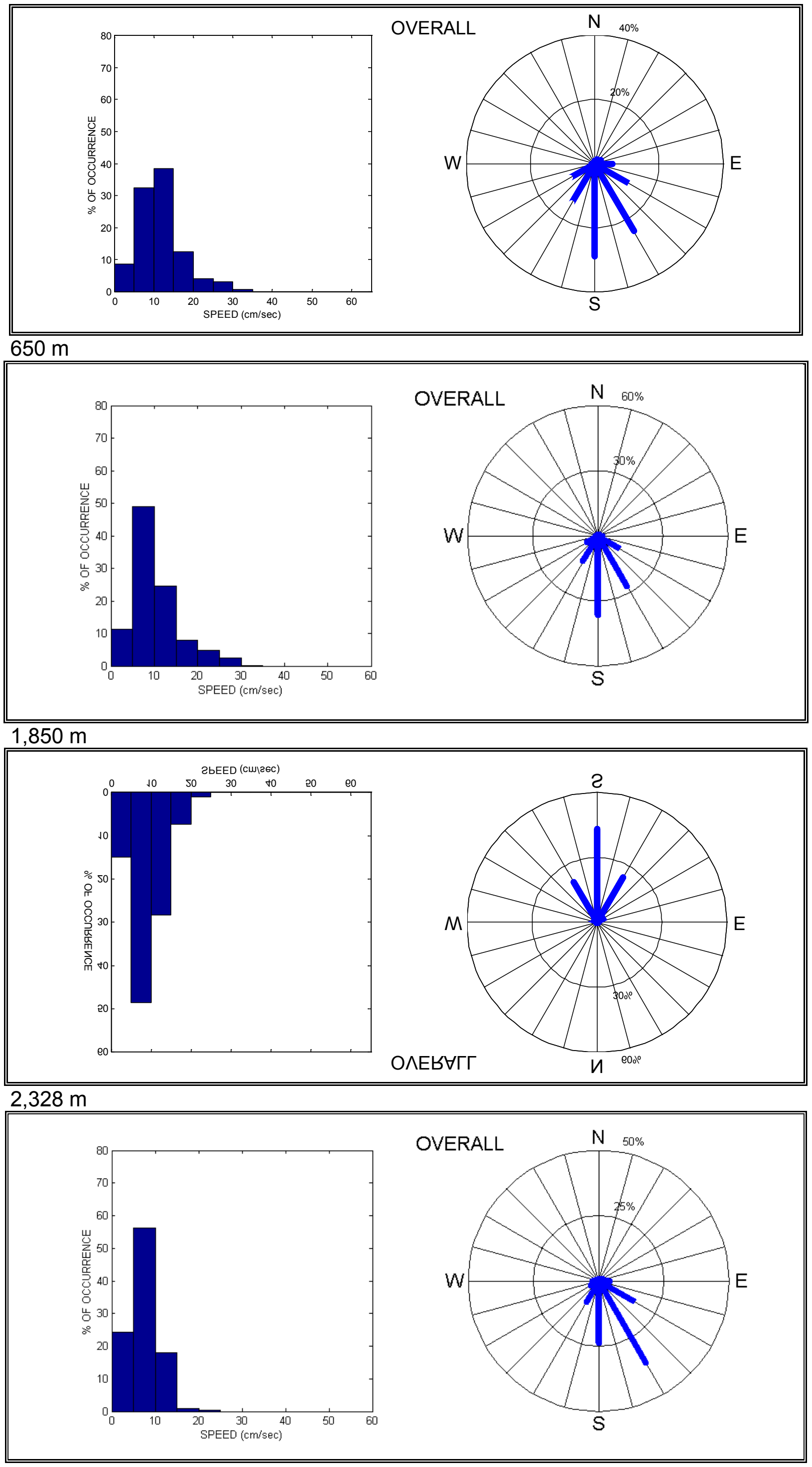

Figure 5.27 Histograms of Current Speed and Direction for Orphan Basin

Lona O-55

Oceans Ltd measured the currents near the drill site Lona O-55 at depths of 1,135 m and 2,485 m with Neil Brown current meters and in the upper 300 m of the water column with a 75 kHz Long Ranger ADCP using a bin size of 8 m. The mooring was located at 49°04.2'N; 47°22.3'W. The mean flow was towards the northeast at a depth of 20 m, towards the southeast at 100 m and towards the south at 1,135 m and 2,485 m as; there is a significant amount of variability in flow.

Histograms of the current speed and direction are presented in Figure 5.28. The mean current speeds were 75.4 cm/s, 11.7 cm/s, 8.1 cm/s and 20.6 cm/s at depth of 20 m, 100 m, 1,135 m, and 2,488 m, respectively. The maximum current speeds were 162.1 cm/s, 38.5 cm/s, 24.5 cm/s and 49.3 cm/s at depths of 20 m, 100 m, 1,135 m, and 2,485 m, respectively.

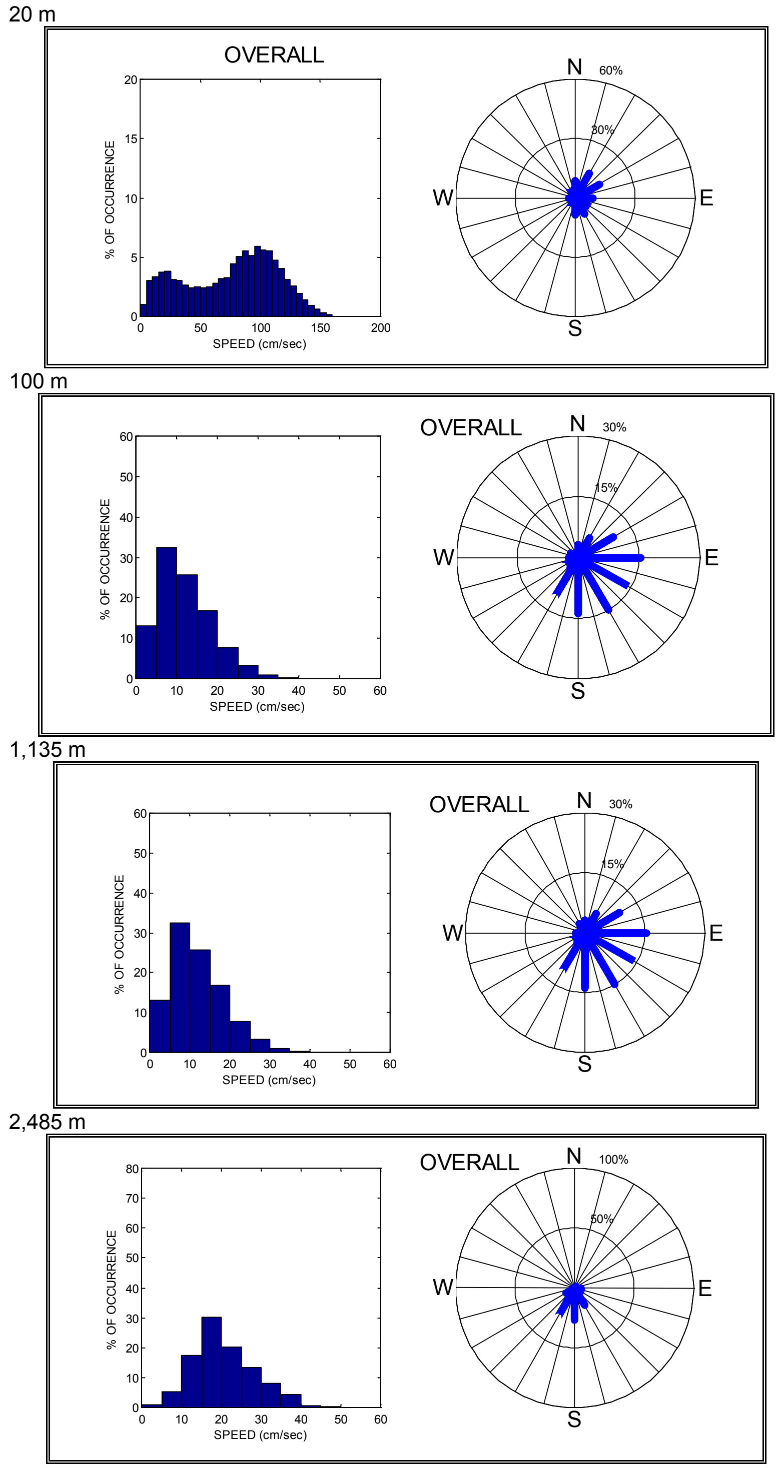

Figure 5.28 Histograms of Current Speeds and Directions at Lona O-55

5.4.3 Waves

5.4.3.1 Wave Climate Overview

The main parameters for describing wave conditions are the significant wave height, the maximum wave height, the peak spectral period, and the characteristic period. The significant wave height is defined as the average height of the 1/3 highest waves, and its value roughly approximates the characteristic height observed visually. The maximum height is the greatest vertical distance between a wave crest and adjacent trough. The spectral peak period is the period of the waves with the largest energy levels, and the characteristic period is the period of the 1/3 highest waves. The characteristic period is the wave period reported in ship observations, and the spectral peak period is reported in the MSC50 data set.

A sea state may be composed of the wind wave alone, swell alone, or the wind wave in combination with one or more swell groups. A swell is a wave system not produced by the local wind blowing at the time of observation and may have been generated within the local weather system, or from within distant weather systems. The former situation typically arises when a front, trough, or ridge crosses the point of concern, resulting in a marked shift in wind direction. Swells generated in this manner are usually of low period. Swells generated by distant weather systems may propagate in the direction of the winds that originally produced the waves to the vicinity of the observation area. These swells may travel for thousands of miles before dying away. As the swell advances, its crest becomes rounded and its surface smooth. As a result of the latter process, swell energy may propagate through a point from more than one direction at a particular time.

The wave climate is dominated by extra-tropical storms, primarily during October through March. Severe storms may, on occasion, occur outside these months. Storms of tropical origin may occur during the early summer and early winter, but most often from late August through October. Hurricanes are usually reduced to tropical storm strength or evolve into extra-tropical storms by the time they reach the Project Area but they are still capable of producing storm force winds and high waves.

During fall and winter, the dominant direction of the combined significant wave height is from the west. This corresponds with a higher frequency of occurrence of the wind wave during these months, suggesting that during the late fall and winter, the wind wave is the main contributor to the combined significant wave height. During the months of March and April, the wind wave remains predominately westerly while the swell begins to come from a southerly direction, resulting in the vector mean direction of the combined significant wave heights being south-westerly. A mean south-westerly direction for the combined significant wave heights during the summer months is a result of a mainly south-westerly wind wave and a south-westerly swell. As winter approaches again, during the months of September and October, the wind wave will veer to the west and become the more dominant component of the combined significant wave height. This will result in the frequency of occurrence of the combined significant wave heights being westerly once again.

5.4.3.2 Wave Statistics

Significant Wave Height

Annual wave roses and their associated percentage frequency of significant wave heights from the four MSC50 grid points are presented in Figures 5.29 to 5.32. The wave roses are in meteorological convention and depict the direction the waves are coming from. Therefore, these wave roses show that the majority of wave energy comes from the southwest to south.

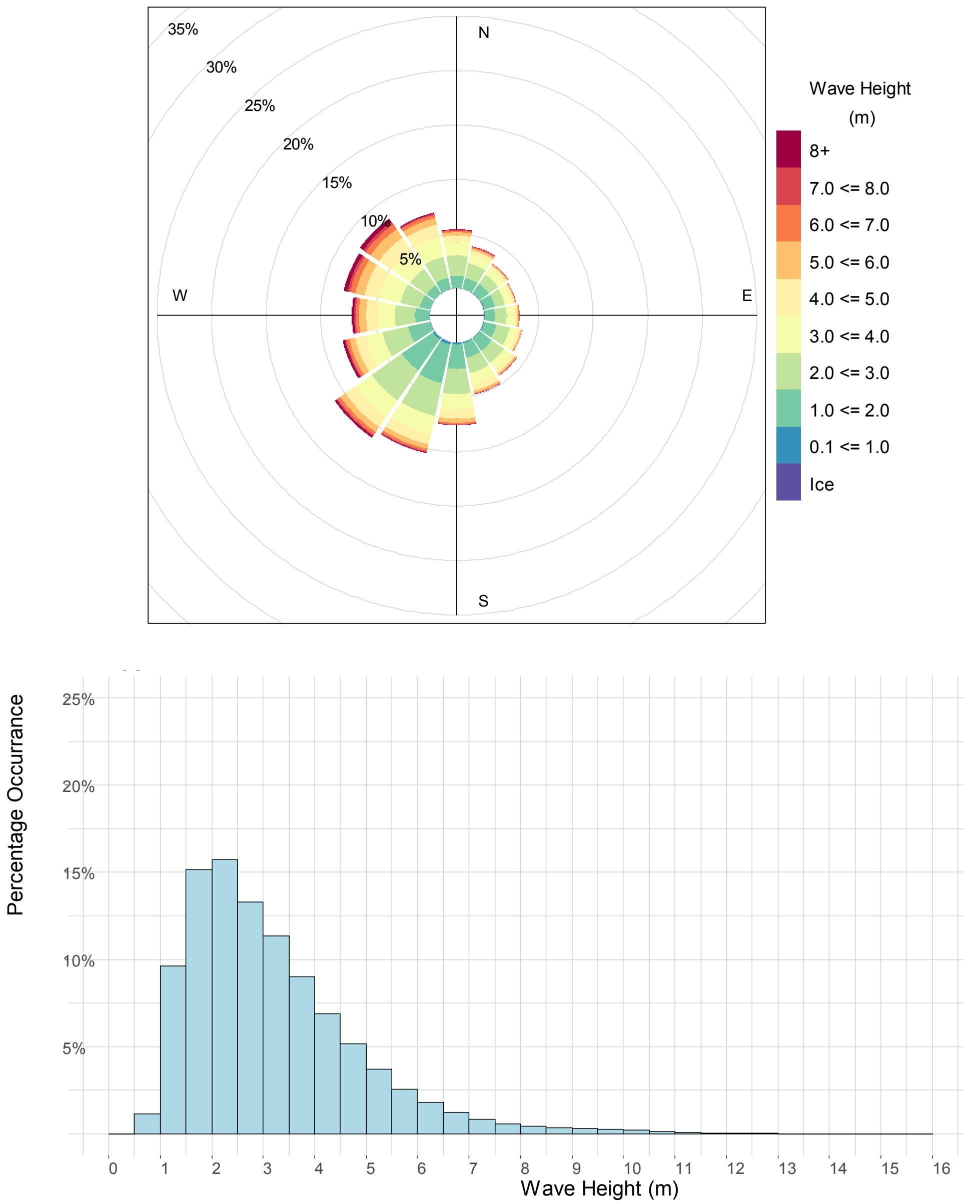

Figure 5.29 Annual Wave Rose and Percentage Frequency of Significant Wave Height for MSC50 Grid Point 15340 (1986 – 2015)

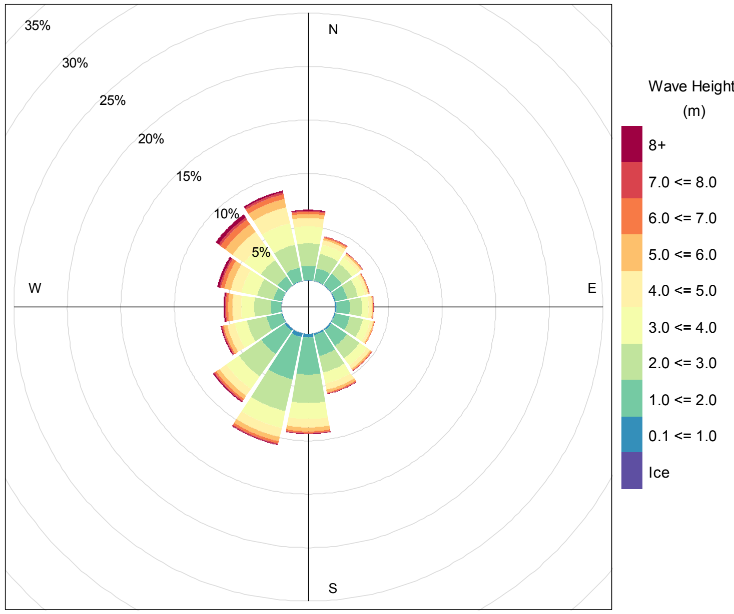

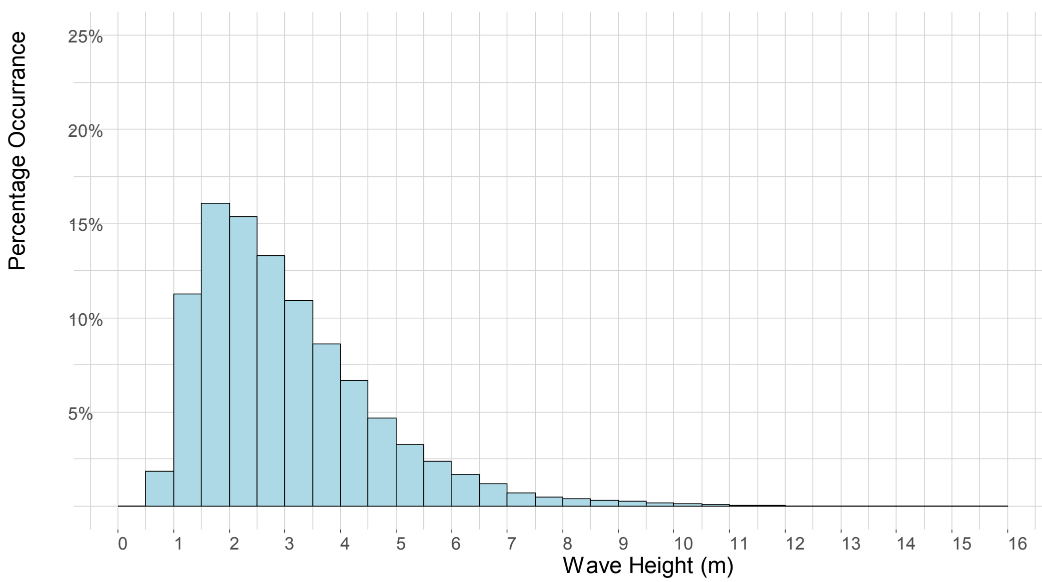

Figure 5.30 Annual Wave Rose and Percentage Frequency of Significant Wave Height for MSC50 Grid Point 16684 (1986 – 2015)

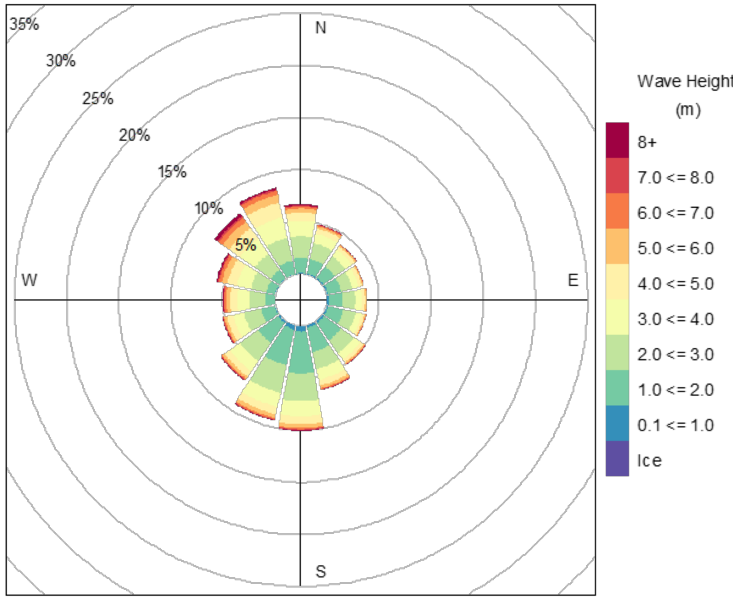

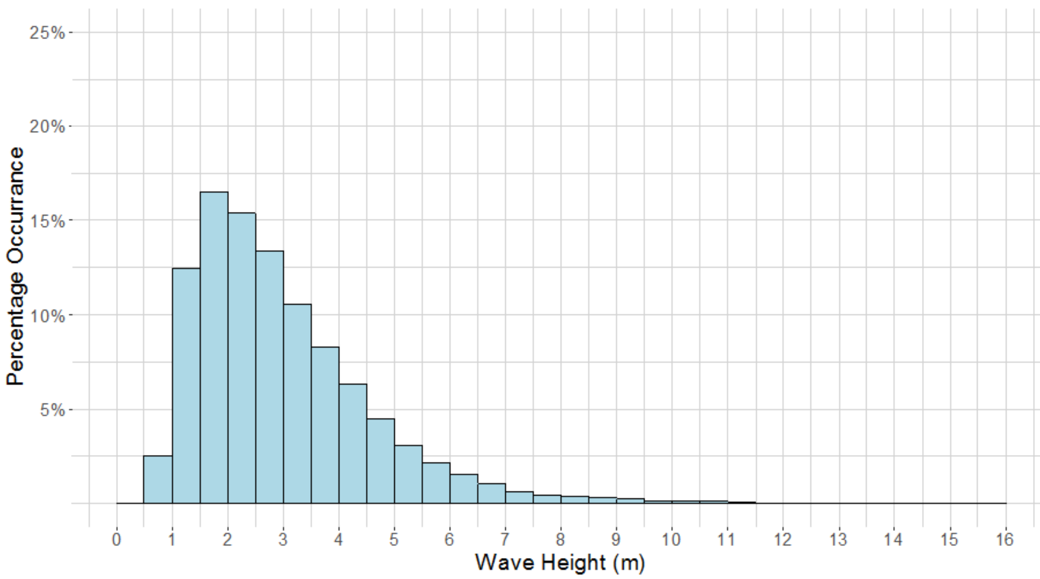

Figure 5.31 Annual Wave Rose and Percentage Frequency of Significant Wave Height for MSC50 Grid Point 17322 (1986 – 2015)

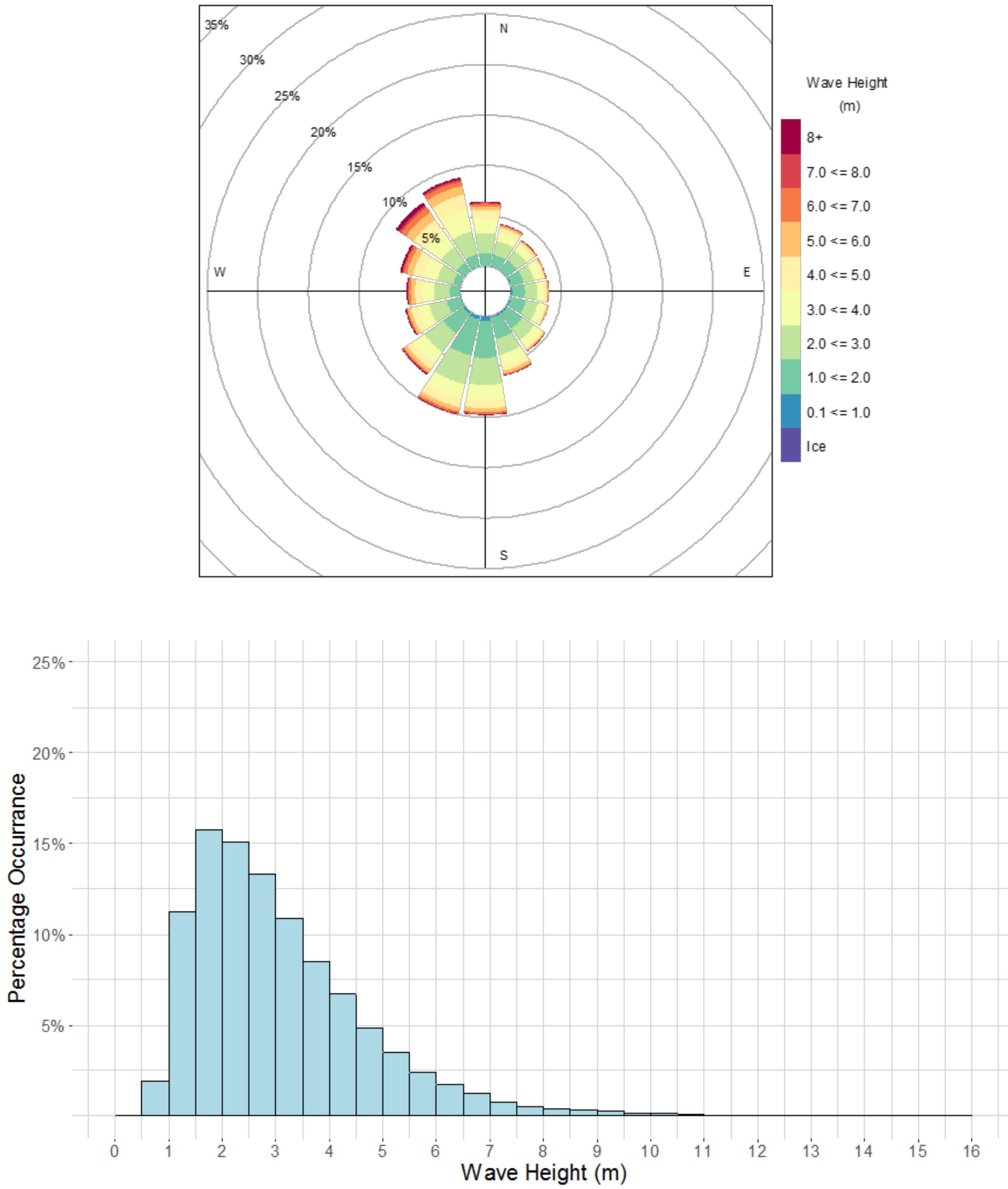

Figure 5.32 Annual Wave Rose and Percentage Frequency of Significant Wave Height for MSC50 Grid Point 17427 (1986 – 2015)

Most significant wave heights lie between 1.0 and 3.0 m. There is a gradual decrease in frequency of wave heights above 2.5 m and only a small percentage of the wave heights exceed 7.0 m.

Significant wave heights in the Orphan Basin peak during the winter months with the MSC50 Grid Points having a mean monthly significant wave height in January ranging from 4.4 to 4.6 m in the West Orphan Basin and 4.8 m in the East Orphan Basin. The lowest significant wave heights occur in the summer, with

July having a mean monthly significant wave height of 1.7 m for the three grid points within the West Orphan Basin and a mean monthly significant wave height of 1.8 m in the East Orphan Basin (Table 5.17).

Table 5.17 Mean Significant Wave Height Statistics (m)

	East Orphan Basin		West Orphan Basin			
	MSC50 Grid Point 15340	ICOADS	MSC50 Grid Point 16684	MSC50 Grid Point 17322	MSC50 Grid Point 17427	ICOADS
January	4.8	3.3	4.6	4.4	4.6	2.3
February	4.3	2.5	3.8	3.4	3.8	2.6
March	3.8	1.8	3.3	2.9	3.4	2.1
April	3.1	2.4	2.8	2.6	2.7	1.3
May	2.4	1.4	2.4	2.3	2.4	1.6
June	2.1	1.3	2.0	2.0	2.0	1.1
July	1.8	1.1	1.7	1.7	1.7	0.8
August	1.9	1.2	1.9	1.8	1.9	0.9
September	2.6	1.5	2.6	2.5	2.6	1.5
October	3.2	2.0	3.2	3.1	3.2	1.5
November	3.9	2.3	3.8	3.7	3.8	2.1
December	4.4	2.7	4.3	4.2	4.4	2.0
Winter	4.5	2.9	4.2	4.0	4.3	2.2
Spring	3.1	1.9	2.8	2.6	2.8	1.6
Summer	2.0	1.2	1.9	1.8	1.9	0.9
Fall	3.2	1.9	3.2	3.1	3.2	1.7
Annual	3.2	1.9	3.0	2.9	3.0	1.4
Source: ICOADS data set, MSC50 database						

Combined significant wave heights of 10.0 m or more occurred in each month between September and April in both the West Orphan Basin and the East Orphan Basin, with the highest waves occurring during the months of December and January (Table 5.18). The highest significant wave height of 15.3 m in the MSC50 data set occurred in the East Orphan Basin on December 16, 1997. While the maximum significant wave heights tend to peak during the winter months, a tropical system could pass through the area and produce high wave heights during any month.

Table 5.18 Maximum Combined Significant Wave Height Statistics (m)

	East Orphan Basin		West Orphan Basin			
	MSC50 Grid Point 15340	ICOADS	MSC50 Grid Point 16684	MSC50 Grid Point 17322	MSC50 Grid Point 17427	ICOADS
January	14.9	11.0	14.5	14.5	15.1	6.0
February	13.8	11.5	12.2	12.3	12.0	12.0
March	12.6	7.5	11.2	11.6	11.5	5.0
April	11.8	7.5	11.3	11.2	11.7	8.0
May	9.5	5.0	7.7	7.6	8.1	5.5
June	8.4	6.0	7.4	7.2	7.2	3.5
July	6.7	3.0	5.7	5.3	5.5	3.5
August	7.0	7.0	6.1	5.9	6.0	7.0
September	12.7	5.5	11.5	10.7	10.8	8.5
October	12.0	6.5	11.3	12.3	12.0	5.0
November	13.6	9.5	12.8	12.5	12.8	8.0
December	15.3	9.0	14.4	13.8	14.6	7.0
Winter	15.3	11.5	14.5	14.5	15.1	12.0
Spring	12.6	7.5	11.3	11.6	11.7	8.0
Summer	8.4	7.0	7.4	7.2	7.2	7.0
Fall	13.6	9.5	12.8	12.5	12.8	8.5
Annual	15.3	11.5	14.5	14.5	15.1	12.0
Source: ICOADS dataset, MSC50 database						

The spectral peak period of waves varies with season with the most common period varying from 7 seconds during summer to 11 seconds in winter. Annually, the most common spectral peak period is 9 seconds for all grid points. The most common wave at all Grid Points within the West Orphan Basin is 2 m with a peak spectral period of 7 seconds. Within the East Orphan Basin, the probability of having a 2-m wave with either at 7 second peak spectral period or a 9 second peak spectral period is 7.01%.

Wind Wave

Annual wind wave roses and their associated percentage frequency of wind wave heights from the four MSC50 grid points are presented in Figures 5.33 to 5.36. The wave roses are in meteorological convention and depict the direction the waves are coming from. Therefore, these wave roses show that the majority of wind wave energy comes from the southwest to northwest.

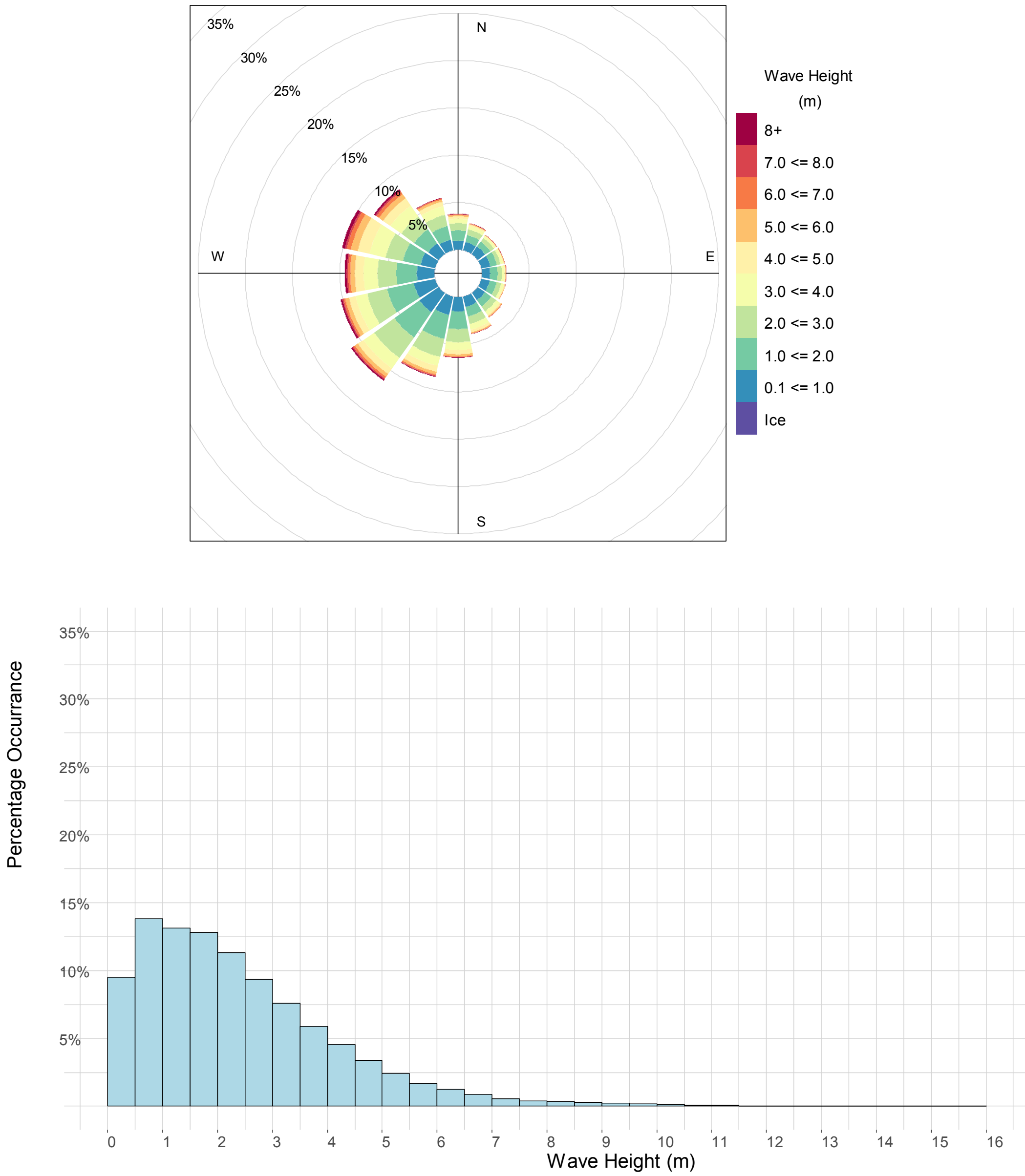

Figure 5.33 Annual Wind Wave Rose and Percentage Frequency of Wind Wave Height for MSC50 Grid Point 15340 (1986 – 2015)

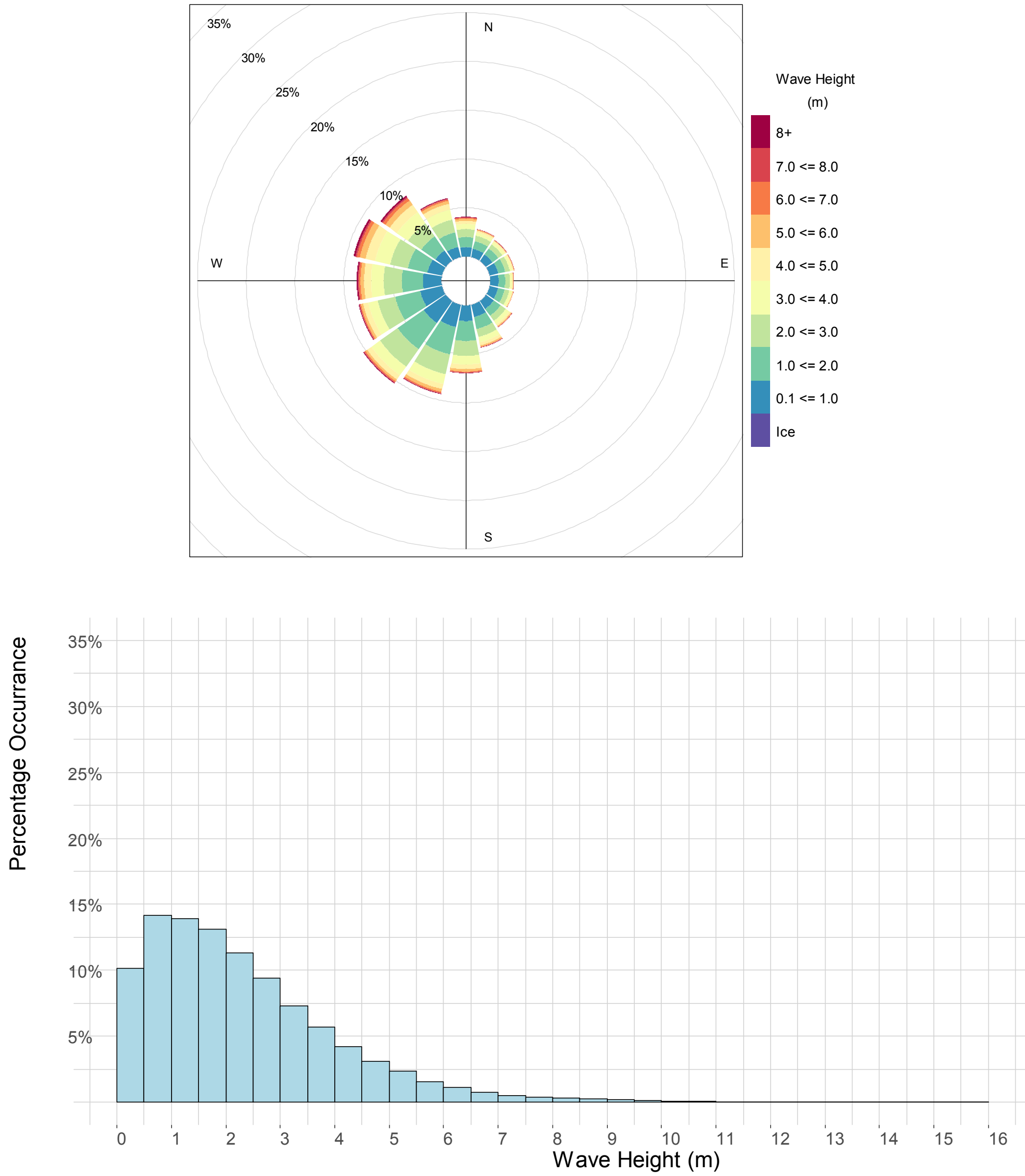

Figure 5.34 Annual Wind Wave Rose and Percentage Frequency of Wind Wave Height for MSC50 Grid Point 16684 (1986 – 2015)

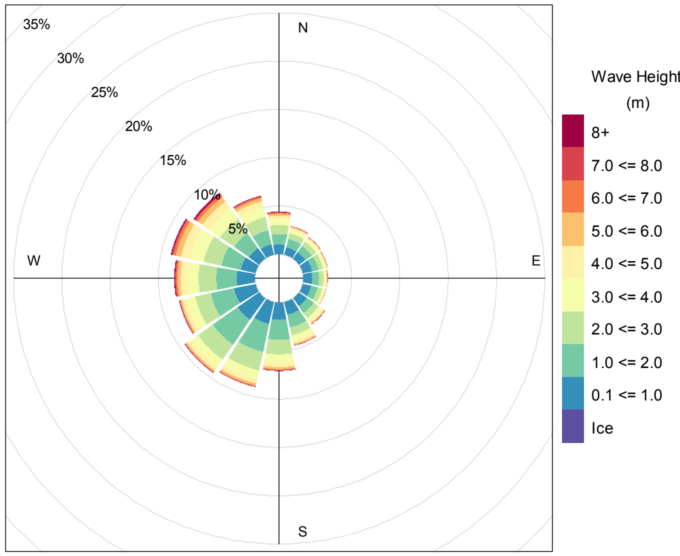

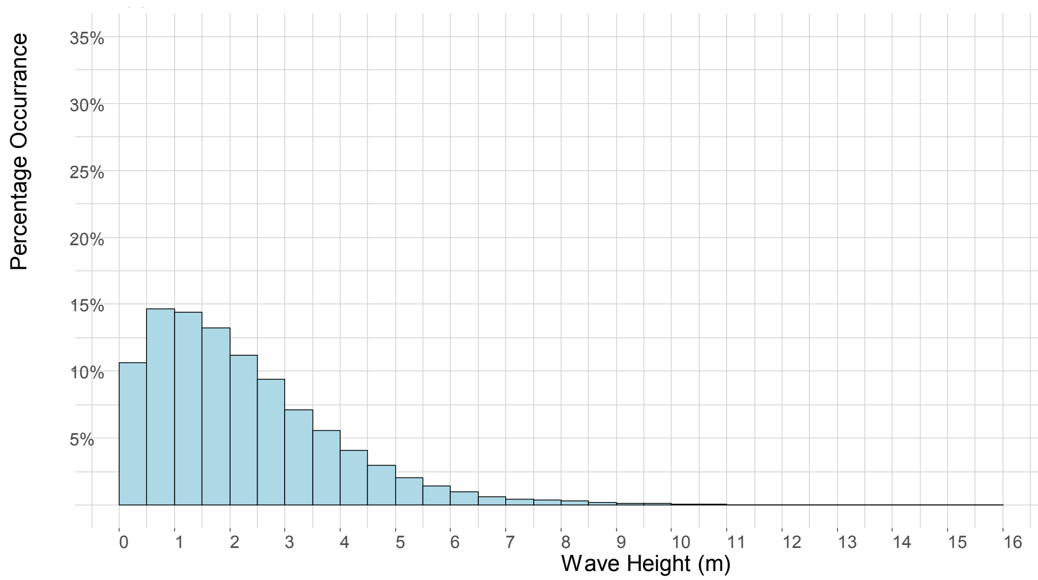

Figure 5.35 Annual Wind Wave Rose and Percentage Frequency of Wind Wave Height for MSC50 Grid Point 17322 (1986 – 2015)

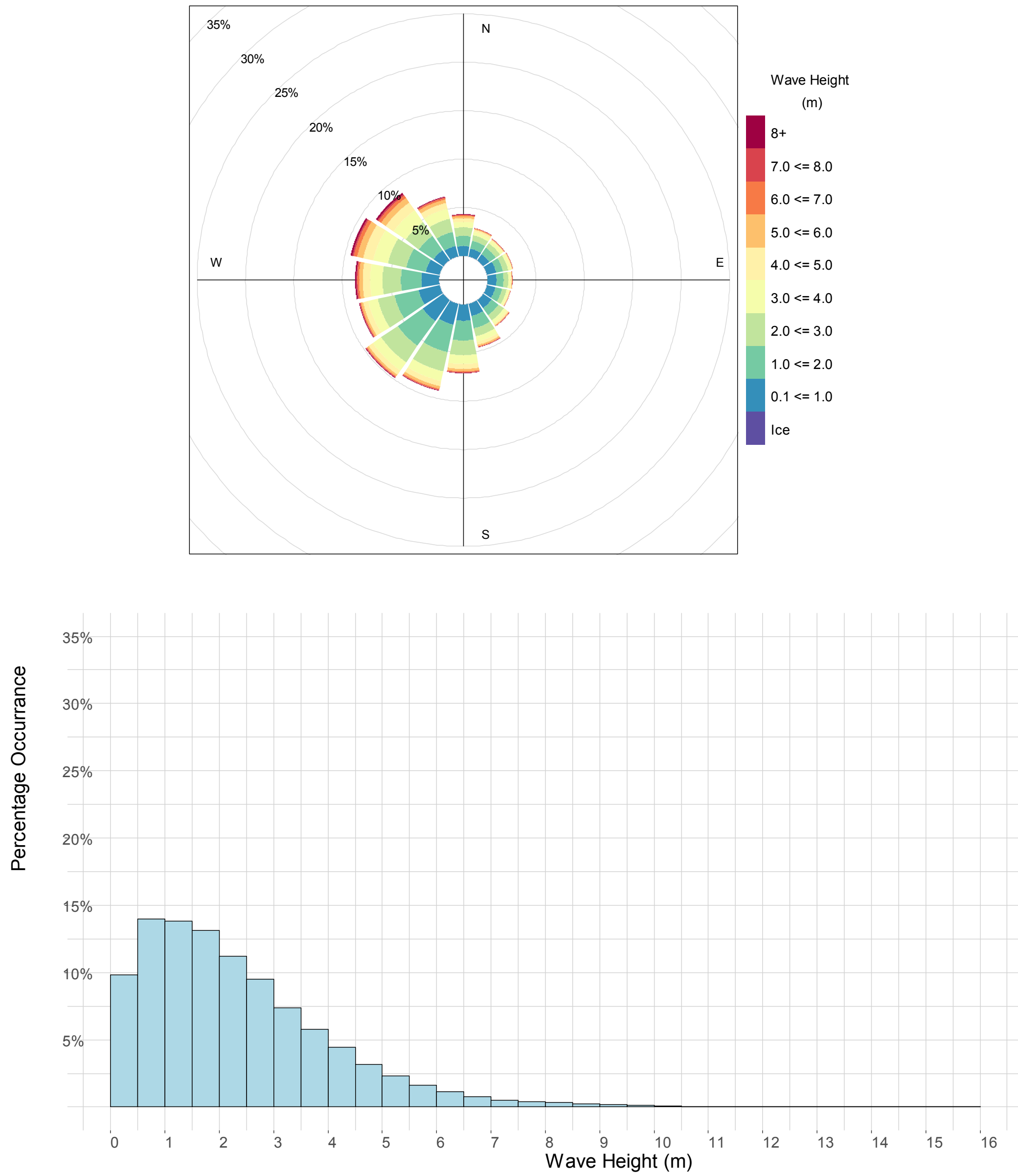

Figure 5.36 Annual Wind Wave Rose and Percentage Frequency of Wind Wave Height for MSC50 Grid Point 17427 (1986 – 2015)

Wind wave heights in the Orphan Basin peak during the winter months with the MSC50 Grid Points having a mean monthly wind wave height in January ranging from 3.2 to 3.3 m in the West Orphan Basin and 3.5 m in the East Orphan Basin. The lowest significant wave heights occur in the summer, with July having a mean monthly wind wave height ranging from 1.0 to 1.2 m (Table 5.19).

Table 5.19 Mean Wind Wave Height Statistics (m)

Month	East Orphan Basin	West Orphan Basin		
	MSC50 Grid Point 15340	MSC50 Grid Point 16684	MSC50 Grid Point 17322	MSC50 Grid Point 17427
January	3.5	3.3	3.2	3.3
February	3.2	2.7	2.4	2.7
March	2.7	2.2	1.9	2.3
April	2.1	1.9	1.8	2.0
May	1.6	1.5	1.5	1.6
June	1.3	1.2	1.2	1.2
July	1.2	1.1	1.0	1.1
August	1.2	1.2	1.2	1.2
September	1.8	1.7	1.7	1.8
October	2.3	2.3	2.2	2.3
November	2.8	2.7	2.7	2.8
December	3.2	3.2	3.2	3.2
Winter	3.3	3.1	2.9	3.1
Spring	2.1	1.9	1.7	2.0
Summer	1.2	1.2	1.1	1.2
Fall	2.3	2.2	2.2	2.3
Annual	2.2	2.1	2.0	2.1

Wind wave heights of 10.0 m or more occurred in each month between September and May in both the East Orphan Basin and the West Orphan Basin, with the highest waves occurring during the month of December in the East Orphan Basin and January in the West Orphan Basin (Table 5.20). The highest significant wave height of 14.8 m in the MSC50 data set occurred in the East Orphan Basin on December 16, 1997. While the maximum significant wave heights tend to peak during the winter months, a tropical system could pass through the area and produce high wave heights during any month.

Table 5.20 Maximum Wind Wave Height Statistics (m)

Month	East Orphan Basin	West Orphan Basin		
	MSC50 Grid Point 15340	MSC50 Grid Point 16684	MSC50 Grid Point 17322	MSC50 Grid Point 17427
January	14.6	13.8	13.7	14.3
February	13.4	12.4	12.5	12.7
March	12.2	11.9	12.0	11.4
April	11.1	11.0	11.0	11.4
May	11.0	10.8	10.4	10.8
June	9.6	9.3	8.4	8.5
July	6.6	6.4	6.6	6.4
August	6.9	9.6	11.3	11.0
September	12.6	11.3	11.1	11.3
October	12.7	11.6	11.9	11.8
November	13.2	12.6	12.4	12.6
December	14.8	13.7	13.5	13.8
Winter	14.8	13.8	13.7	14.2
Spring	12.2	11.9	12.0	11.4
Summer	9.6	9.6	11.3	11.0
Fall	13.2	12.6	12.4	12.6
Annual	14.8	13.8	13.7	14.3

Swell

Annual swell roses and their associated percentage frequency of swell heights from the four MSC50 grid points are presented in Figures 5.37 to 5.40. The swell roses are in meteorological convention and depict the direction the waves are coming from. Therefore, these swell roses show that the majority of swell energy comes from the southwest to northwest.

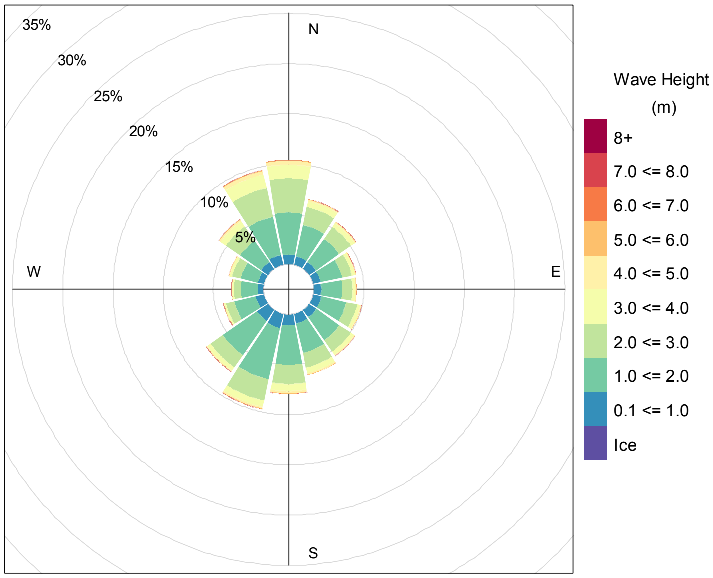

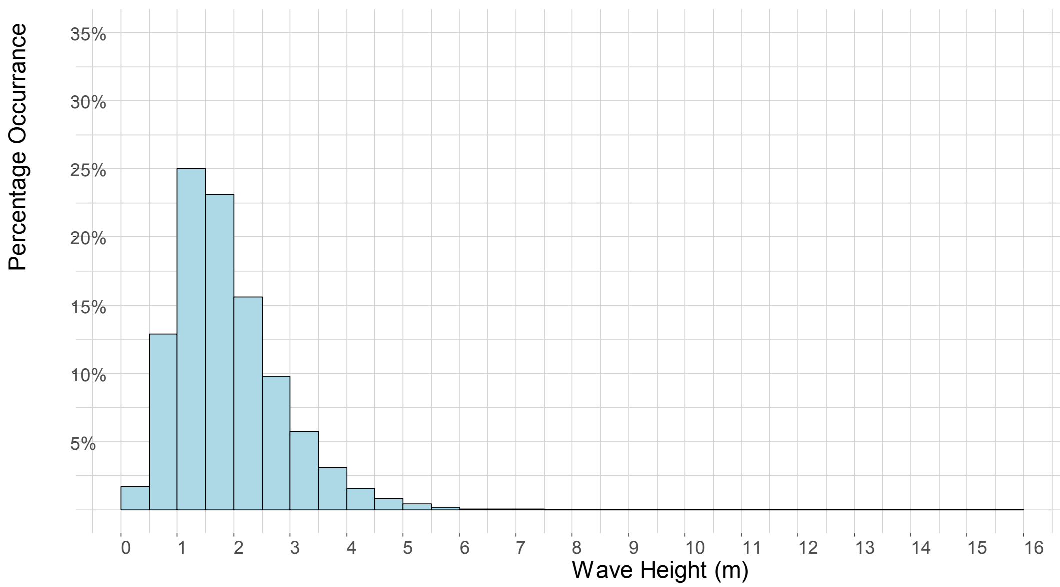

Figure 5.37 Annual Swell Rose and Percentage Frequency of Swell Height for MSC50 Grid Point 15340 (1986 – 2015)

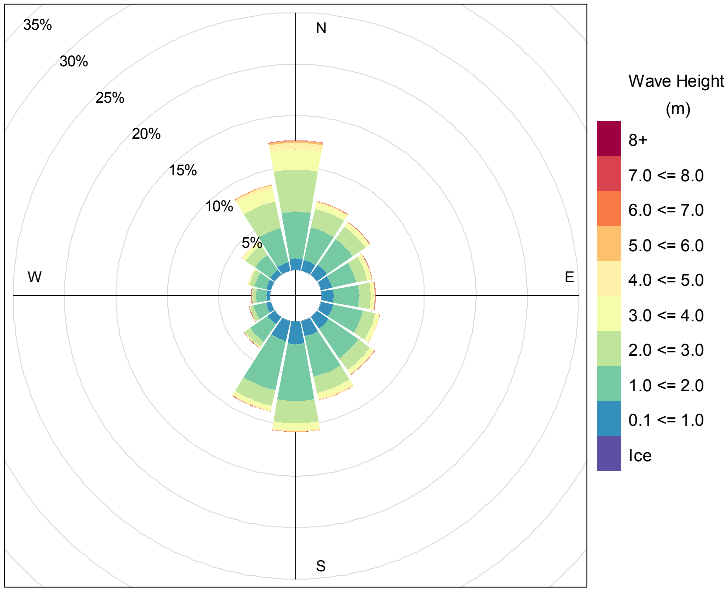

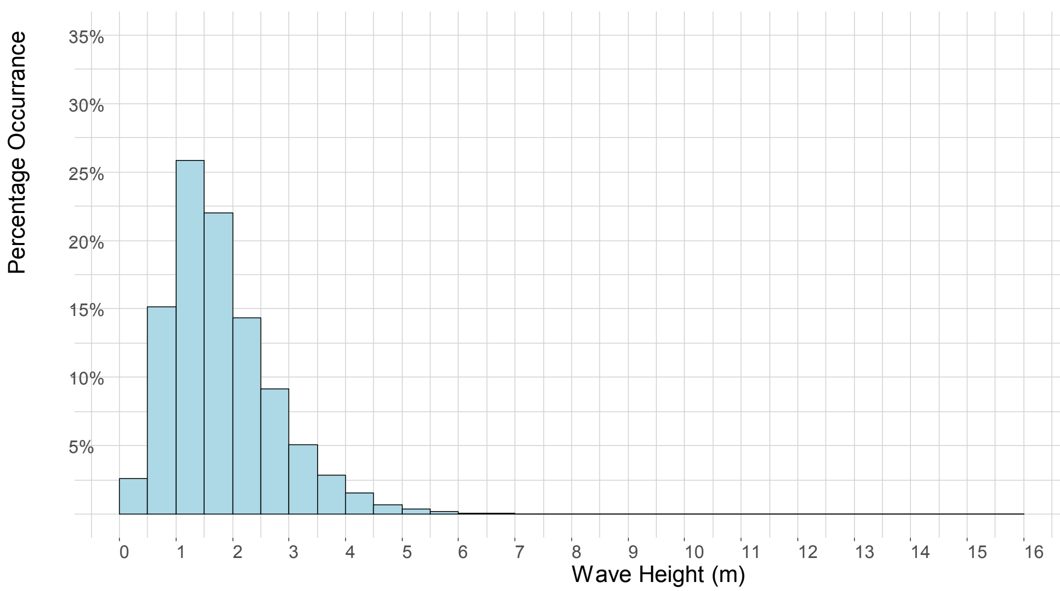

Figure 5.38 Annual Swell Rose and Percentage Frequency of Swell Height for MSC50 Grid Point 16684 (1986 – 2015)

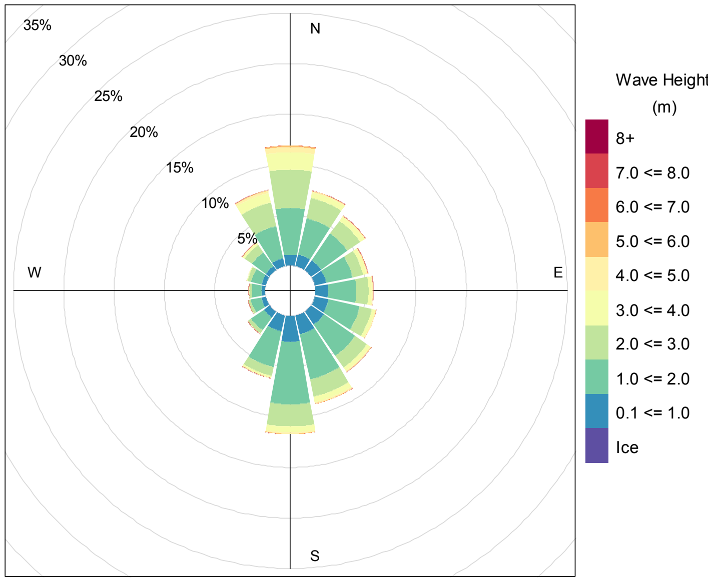

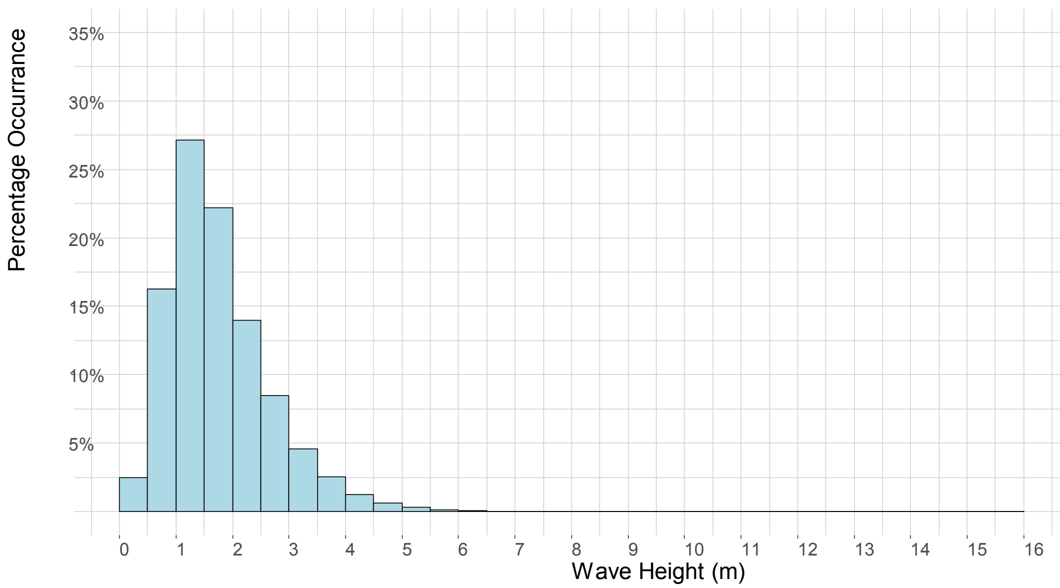

Figure 5.39 Annual Swell Rose and Percentage Frequency of Swell Height for MSC50 Grid Point 17322 (1986 – 2015)

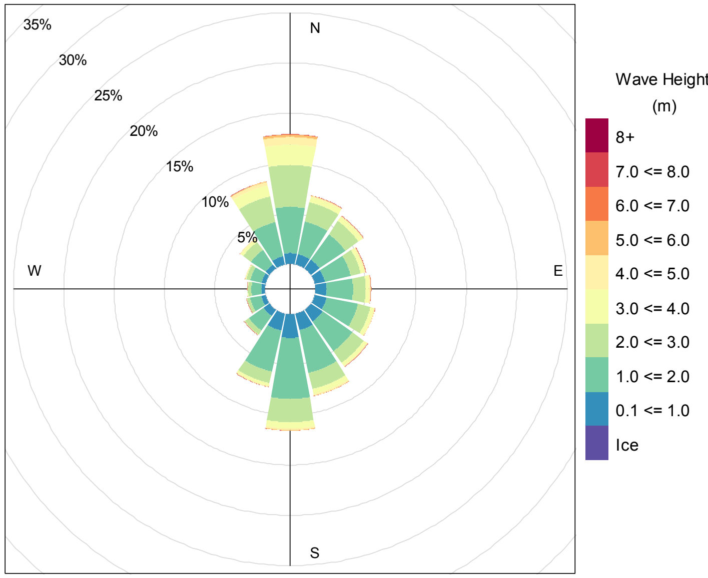

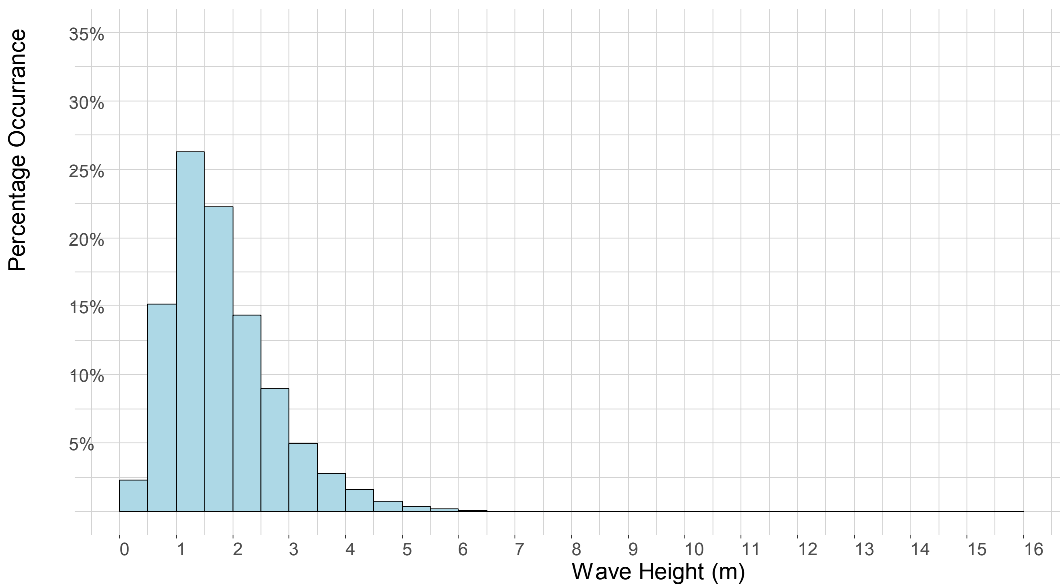

Figure 5.40 Annual Swell Rose and Percentage Frequency of Swell Height for MSC50 Grid Point 17427 (1986 – 2015)

Swell heights in the Orphan Basin peak during the winter months with December and January having mean monthly swell heights ranging from 2.3 to 2.5 m. Swell heights in the East Orphan Basin are slightly higher than those in the West Orphan Basin. The lowest swell heights occur in the summer, with July having a mean monthly swell height of 1.1 m for all locations (Table 5.21).

Table 5.21 Mean Swell Height Statistics (m)

Month	East Orphan Basin	West Orphan Basin		
	MSC50 Grid Point 15340	MSC50 Grid Point 16684	MSC50 Grid Point 17322	MSC50 Grid Point 17427
January	2.5	2.4	2.3	2.3
February	2.3	2.0	1.8	2.0
March	2.1	1.8	1.5	1.8
April	1.9	1.7	1.5	1.6
May	1.5	1.5	1.4	1.4
June	1.3	1.3	1.2	1.3
July	1.1	1.1	1.1	1.1
August	1.2	1.2	1.2	1.2
September	1.6	1.6	1.5	1.6
October	1.9	1.9	1.8	1.9
November	2.1	2.1	2.0	2.0
December	2.5	2.4	2.3	2.4
Winter	2.4	2.2	2.1	2.2
Spring	1.8	1.6	1.4	1.6
Summer	1.2	1.2	1.2	1.2
Fall	1.9	1.8	1.8	1.8
Annual	1.8	1.7	1.6	1.7

Maximum swell heights occurred in the month of September for Grid Point 15340 and 16684 (Table 5.22). These maximum swells correspond with the passage of Post-Tropical Storm Florence with a central pressure of 967 mb and maximum sustained winds of 30.9 m/s.

Table 5.22 Maximum Swell Height Statistics (m)

Month	East Orphan Basin	West Orphan Basin		
	MSC50 Grid Point 15340	MSC50 Grid Point 16684	MSC50 Grid Point 17322	MSC50 Grid Point 17427
January	8.2	8.4	8.2	8.5
February	8.3	9.3	8.5	8.9
March	7.4	8.0	7.8	8.1
April	6.5	6.5	6.4	6.6
May	5.4	5.4	5.3	5.4
June	4.6	5.1	5.6	5.0
July	4.4	4.7	4.1	4.2
August	5.0	4.5	5.9	5.2
September	10.6	9.7	8.5	8.5
October	7.3	7.6	6.7	6.9
November	7.2	6.9	7.1	6.7
December	8.7	7.7	7.1	7.4
Winter	8.7	9.3	8.5	8.9
Spring	7.4	8.0	7.8	8.1
Summer	5.0	5.1	5.9	5.2
Fall	10.6	9.7	8.5	8.5
Annual	10.6	9.7	8.5	8.9

Extreme wind and waves were calculated for the Project Area using the MSC50 hindcast data set. This data set was determined to be the most representative of the available data sets, as it provides a continuous wind and wave hindcast in 1-hour time steps from January 1954 to December 2015, on a 0.1° latitude by 0.1° longitude grid. All extremes are specified for return periods of 1-yr, 10-yr, 50-yr and 100-yr. All wind speeds are referenced to the 10 m height.

The extreme value analysis for wind speeds was carried out using the peak-over-threshold method. For the extreme wave analysis, two methods were used; the peak-over-threshold method and the joint probability method.

After considering four different distributions, the Gumbel distribution was chosen to be the most representative for the peak-over-threshold method as it provided the best fit to the data. Since extreme values can vary depending on how well the data fits the distribution, a sensitivity analysis was carried out to determine the number storms to use, whereby the number of storms, the 100-year extreme value, the correlation coefficient and storm threshold were all compared on an annual and monthly basis.

5.4.3.3 Wind

Gumbel Extreme Value Analysis

The extreme value estimates for wind were calculated using Oceanweather's Osmosis software program for the return periods of 1-year, 10-years, 25-years, 50-years and 100-years. The analysis used hourly wind values for the reference height of 10 m above sea level. These values were converted to 10-minute and 1-minute wind values using a constant ration of 1.06 and 1.22, respectively (U.S. Geological Survey 1979).

A comparison of these values, with actual values measured by platforms in the Project Area was not possible. Logarithmic profiles for adjusting wind speeds from anemometer height to the surface are valid only in neutral or unstable conditions. Observations from platforms on the Grand Banks over the past ten years frequently show stable conditions in which the surface layer wind speed profiles are not valid. Using a logarithmic profile to adjust wind speeds between the 10 m and anemometer level would therefore introduce an unnecessary source of error in the results.

The calculated annual and monthly values for each grid point for 1-hour, 10-minutes and 1-minute are presented in Tables 5.23 to 5.26. The annual 100-year extreme 1-hour wind speed was determined to range from 32.5 to 34.0 m/s in the West Orphan Basin and 33.8 m/s in the East Orphan Basin.

Table 5.23 Extreme Wind Speed Estimates (m/s) for Grid Point 15340 (East Orphan Basin) for Return Periods of 1, 10, 25, 50 and 100 Years

	Wind Speed 1-hr (m/s)					Wind Speed 10-min (m/s)					Wind Speed 1-min (m/s)				
Month	**1**	**10**	**25.0**	**50.0**	**100.0**	**1.0**	**10.0**	**25.0**	**50.0**	**100.0**	**1.0**	**10.0**	**25.0**	**50.0**	**100.0**
January	23.4	27.4	28.9	30.0	31.1	24.8	29.1	30.6	31.8	32.9	28.5	33.5	35.2	36.6	37.9
February	23.1	28.1	29.9	31.2	32.6	24.4	29.8	31.7	33.1	34.6	28.1	34.2	36.5	38.1	39.8
March	21.5	26.2	27.8	29.1	30.4	22.8	27.7	29.5	30.9	32.2	26.2	31.9	34.0	35.5	37.1
April	19.3	23.4	24.8	25.9	27.0	20.4	24.8	26.3	27.5	28.7	23.5	28.5	30.3	31.6	33.0
May	16.9	20.9	22.4	23.4	24.5	17.9	22.2	23.7	24.8	26.0	20.6	25.5	27.3	28.6	29.9
June	15.4	18.9	20.2	21.2	22.1	16.3	20.0	21.4	22.4	23.4	18.7	23.1	24.6	25.8	27.0
July	13.8	16.9	18.0	18.8	19.7	14.7	17.9	19.1	19.9	20.8	16.9	20.6	21.9	23.0	24.0
August	15.0	19.2	20.8	22.0	23.1	15.9	20.4	22.0	23.3	24.5	18.3	23.5	25.4	26.8	28.2
September	18.0	23.1	25.0	26.4	27.8	19.1	24.5	26.5	28.0	29.4	21.9	28.2	30.5	32.2	33.9
October	19.6	25.1	27.0	28.5	30.0	20.8	26.6	28.7	30.2	31.8	23.9	30.6	33.0	34.8	36.6
November	21.1	25.3	26.8	27.9	29.1	22.4	26.8	28.4	29.6	30.8	25.7	30.8	32.7	34.1	35.4
December	22.8	27.5	29.2	30.5	31.8	24.2	29.2	31.0	32.3	33.7	27.8	33.6	35.6	37.2	38.7
All	26.2	30.0	31.5	32.6	33.8	27.8	31.8	33.4	34.6	35.8	31.9	36.6	38.5	39.8	41.2

Table 5.24 Extreme Wind Speed Estimates (m/s) for Grid Point 16684 (West Orphan Basin) for Return Periods of 1, 10, 25, 50 and 100 Years

	Wind Speed 1-hr (m/s)					Wind Speed 10-min (m/s)					Wind Speed 1-min (m/s)				
Month	**1.0**	**10.0**	**25.0**	**50.0**	**100.0**	**1.0**	**10.0**	**25.0**	**50.0**	**100.0**	**1.0**	**10.0**	**25.0**	**50.0**	**100.0**
January	23.3	27.6	29.1	30.1	31.2	24.7	29.3	30.8	31.9	33.1	28.4	33.7	35.5	36.8	38.1
February	22.6	28.8	30.9	32.4	33.9	24.0	30.6	32.7	34.3	35.9	27.6	35.2	37.6	39.5	41.3
March	21.3	26.2	27.8	29.0	30.2	22.6	27.8	29.5	30.8	32.0	26.0	32.0	34.0	35.4	36.9
April	19.3	23.2	24.5	25.4	26.3	20.5	24.6	25.9	26.9	27.9	23.6	28.3	29.8	31.0	32.1
May	16.9	21.1	22.6	23.7	24.8	17.9	22.4	23.9	25.1	26.3	20.6	25.7	27.5	28.9	30.2
June	15.3	19.1	20.5	21.5	22.5	16.2	20.3	21.7	22.8	23.8	18.6	23.3	25.0	26.2	27.4
July	13.9	17.0	18.1	19.0	19.8	14.7	18.0	19.2	20.1	21.0	17.0	20.8	22.1	23.1	24.1
August	14.8	18.9	20.3	21.4	22.5	15.7	20.0	21.6	22.7	23.8	18.1	23.1	24.8	26.1	27.4
September	18.3	23.6	25.5	26.8	28.2	19.4	25.0	27.0	28.4	29.9	22.4	28.8	31.0	32.7	34.4
October	19.7	24.3	25.9	27.1	28.3	20.9	25.7	27.4	28.7	29.9	24.0	29.6	31.6	33.0	34.5
November	21.4	25.4	26.8	27.8	28.9	22.7	26.9	28.4	29.5	30.6	26.1	31.0	32.7	33.9	35.2
December	23.1	27.8	29.5	30.8	32.0	24.4	29.5	31.3	32.6	33.9	28.1	34.0	36.0	37.5	39.0
All	26.2	30.1	31.7	32.8	34.0	27.8	31.9	33.5	34.8	36.0	32.0	36.8	38.6	40.0	41.4

Table 5.25 Extreme Wind Speed Estimates (m/s) for Grid Point 17322 (West Orphan Basin) for Return Periods of 1, 10, 25, 50 and 100 Years

	Wind Speed 1-hr (m/s)					Wind Speed 10-min (m/s)					Wind Speed 1-min (m/s)				
Month	**1.0**	**10.0**	**25.0**	**50.0**	**100.0**	**1.0**	**10.0**	**25.0**	**50.0**	**100.0**	**1.0**	**10.0**	**25.0**	**50.0**	**100.0**
January	22.8	26.6	28.0	29.1	30.1	24.2	28.2	29.7	30.8	31.9	27.8	32.5	34.2	35.5	36.7
February	22.4	27.3	29.1	30.4	31.8	23.7	28.9	30.8	32.2	33.7	27.3	33.2	35.4	37.1	38.7
March	20.9	24.7	26.1	27.1	28.2	22.1	26.1	27.6	28.8	29.9	25.4	30.1	31.8	33.1	34.4
April	19.0	22.9	24.4	25.5	26.6	20.2	24.3	25.9	27.0	28.2	23.2	28.0	29.8	31.1	32.4
May	16.5	20.3	21.7	22.8	23.8	17.5	21.5	23.0	24.1	25.3	20.1	24.8	26.5	27.8	29.1
June	14.8	18.5	19.9	21.0	22.0	15.7	19.6	21.1	22.2	23.3	18.0	22.6	24.3	25.6	26.9
July	13.5	16.3	17.4	18.1	18.9	14.3	17.3	18.4	19.2	20.1	16.4	19.9	21.2	22.1	23.1
August	14.5	18.4	19.8	20.9	22.0	15.4	19.5	21.0	22.2	23.3	17.7	22.4	24.2	25.5	26.8
September	17.9	22.7	24.5	25.9	27.2	19.0	24.1	26.0	27.4	28.8	21.9	27.7	29.9	31.5	33.2
October	19.5	23.6	25.1	26.3	27.5	20.6	25.0	26.6	27.9	29.1	23.8	28.8	30.7	32.1	33.5
November	20.9	24.7	26.1	27.2	28.3	22.1	26.2	27.7	28.8	30.0	25.5	30.1	31.9	33.2	34.5
December	22.5	27.0	28.6	29.9	31.1	23.9	28.6	30.3	31.6	33.0	27.5	32.9	34.9	36.4	37.9
All	25.3	28.9	30.4	31.4	32.5	26.8	30.7	32.2	33.3	34.5	30.8	35.3	37.0	38.4	39.7

Table 5.26 Extreme Wind Speed Estimates (m/s) for Grid Point 17427 (West Orphan Basin) for Return Periods of 1, 10, 25, 50 and 100 Years

Month	Wind Speed 1-hr (m/s)					Wind Speed 10-min (m/s)					Wind Speed 1-min (m/s)				
	1.0	10.0	25.0	50.0	100.0	1.0	10.0	25.0	50.0	100.0	1.0	10.0	25.0	50.0	100.0
January	23.1	26.9	28.4	29.4	30.5	24.5	28.5	30.1	31.2	32.4	28.2	32.8	34.6	35.9	37.2
February	22.7	27.6	29.5	30.9	32.3	24.1	29.3	31.3	32.7	34.2	27.7	33.7	36.0	37.7	39.4
March	21.2	25.3	26.8	28.0	29.2	22.5	26.8	28.5	29.7	30.9	25.9	30.9	32.7	34.2	35.6
April	19.2	23.2	24.7	25.8	26.9	20.4	24.6	26.1	27.3	28.5	23.4	28.3	30.1	31.5	32.8
May	16.8	20.6	22.1	23.2	24.2	17.8	21.8	23.4	24.5	25.7	20.4	25.1	26.9	28.2	29.6
June	15.0	18.8	20.2	21.3	22.4	15.9	19.9	21.4	22.6	23.7	18.3	22.9	24.7	26.0	27.3
July	13.7	16.6	17.7	18.5	19.3	14.5	17.6	18.7	19.6	20.5	16.7	20.2	21.5	22.5	23.6
August	14.7	18.3	19.7	20.7	21.7	15.6	19.4	20.9	21.9	23.0	17.9	22.3	24.0	25.3	26.5
September	18.3	23.4	25.4	26.8	28.3	19.4	24.8	26.9	28.4	30.0	22.3	28.6	30.9	32.7	34.5
October	19.6	23.8	25.3	26.5	27.7	20.8	25.2	26.9	28.1	29.4	23.9	29.0	30.9	32.4	33.8
November	21.1	25.0	26.5	27.6	28.7	22.3	26.5	28.1	29.3	30.5	25.7	30.5	32.3	33.7	35.1
December	22.8	27.2	28.9	30.2	31.5	24.1	28.9	30.7	32.0	33.4	27.8	33.2	35.3	36.9	38.4
All	25.5	29.4	30.9	32.0	33.1	27.1	31.1	32.7	33.9	35.1	31.2	35.8	37.6	39.0	40.4

5.4.3.4 Waves

Gumbel Extreme Value Analysis

The maximum individual wave heights were calculated within Oceanweather's OSMOSIS software by evaluating the Borgman integral (Borgman 1973), which was derived from a Raleigh distribution function. The variant of this equation used in the software has the following form (Forristall 1978):

$$\Pr\{H > h\} = \exp\left[-1.08311\left(\frac{h^2}{8M_0}\right)^{1.063}\right];\ T = \frac{M_0}{M_1}$$

where h is the significant wave height, T is the wave period, and M0 and M1 are the first and second spectral moments of the total spectrum. The associated peak periods are calculated by plotting the peak periods of the chosen storm peak values versus the corresponding significant wave heights. This plot is fitted to a power function (y = axb), and the resulting equation is used to calculate the peak periods associated with the extreme values of significant wave height.

The annual and monthly extreme value estimates for significant wave height, maximum individual wave height and extreme associated peak period for return periods of 1-year, 10-years, 25-years, 50-years and 100-years are given in Tables 5.27 to 5.30. The annual 100-year extreme significant wave height ranges from 14.7 to 15.2 m in the West Orphan Basin and 16.1 m for Grid Point 15340 in the East Orphan Basin.

In order to examine the period ranges of storm events, an environmental contour plot was produced showing the probability of the joint occurrence of significant wave heights and the spectral peak periods using the methodology of Winterstein et al. (1993). The wave heights were fitted to a Weibull distribution and the peak periods to a lognormal distribution. The wave data was divided into bins of 1 m for significant wave heights and 1 second for peak periods. Since the lower wave values were having too much of an impact on the wave extremes, the wave heights below 2 m were modeled separately in a Weibull distribution. The two Weibull curves were combined near 2 m, the point where both functions had the same probability.

Three-parameter Weibull distributions were used with a scaling parameter α, shape parameter β, and location parameter γ. The three parameters were solved by using a least square method, the maximum log likelihood, and the method of moments. The following equation was minimized to get the coefficients:

$$LS(\alpha,\beta,\gamma) := \sum_{i=0}^{13}\left[\ln\left(-\ln\left(1-FP_i\right)\right) - \beta\cdot\ln\left[\frac{\left(h_i-\gamma\right)}{\alpha}\right]\right]^2$$

where hi is the endpoint of the height bin (0.5, 1.5, …) and FPi is the cumulative probability of the height bin. Using a minimizing function, the three parameters α, β, and γ were calculated.

Table 5.27 Extreme Significant Wave Height, Maximum Wave Height and Associated Peak Period Estimates (m) for Grid Point 15340 (East Orphan Basin) for Return Periods of 1, 10, 25, 50 and 100 Years

	Significant Wave Height (m)					Maximum Wave Height (m)					Associated Peak Period (sec)				
Month	**1.0**	**10.0**	**25.0**	**50.0**	**100.0**	**1.0**	**10.0**	**25.0**	**50.0**	**100.0**	**1.0**	**10.0**	**25.0**	**50.0**	**100.0**
January	10.0	12.7	13.6	14.3	14.9	18.3	23.5	25.2	26.4	27.7	13.3	14.8	15.3	15.6	15.9
February	9.4	12.4	13.4	14.1	14.8	17.2	23.0	24.9	26.3	27.6	12.6	14.5	15.1	15.5	15.9
March	7.7	10.6	11.5	12.2	12.9	14.1	19.6	21.4	22.7	24.0	12.0	13.2	13.5	13.7	13.9
April	6.5	9.5	10.5	11.2	11.9	12.1	17.5	19.2	20.5	21.8	11.4	13.0	13.5	13.8	14.1
May	5.0	8.1	9.1	9.9	10.6	9.3	14.9	16.7	18.1	19.4	10.1	12.1	12.7	13.1	13.5
June	4.2	6.5	7.2	7.8	8.3	7.8	12.0	13.4	14.4	15.4	9.1	11.1	11.6	12.0	12.4
July	3.6	5.4	6.0	6.4	6.8	6.7	10.0	11.0	11.8	12.6	8.5	10.5	11.0	11.4	11.8
August	4.1	6.0	6.6	7.1	7.6	7.7	11.1	12.2	13.0	13.8	9.4	10.9	11.3	11.6	11.9
September	5.7	10.1	11.5	12.6	13.6	10.5	18.3	20.8	22.7	24.5	10.9	13.4	14.0	14.4	14.9
October	6.7	10.9	12.3	13.3	14.3	12.4	20.0	22.5	24.3	26.2	11.9	13.5	14.0	14.3	14.6
November	8.1	11.7	12.9	13.8	14.6	14.9	21.5	23.6	25.2	26.8	12.2	13.8	14.3	14.6	14.9
December	9.7	13.0	14.0	14.8	15.6	17.8	23.8	25.7	27.2	28.6	12.9	14.5	15.0	15.4	15.7
All	11.6	13.9	14.8	15.4	16.1	21.4	25.7	27.3	28.6	29.8	13.9	15.2	15.6	16.0	16.3

Table 5.28 Extreme Significant Wave Height, Maximum Wave Height and Associated Peak Period Estimates (m) for Grid Point 16684 (West Orphan Basin) for Return Periods of 1, 10, 25, 50 and 100 Years

	Significant Wave Height (m)					Maximum Wave Height (m)					Associated Peak Period (sec)				
Month	**1.0**	**10.0**	**25.0**	**50.0**	**100.0**	**1.0**	**10.0**	**25.0**	**50.0**	**100.0**	**1.0**	**10.0**	**25.0**	**50.0**	**100.0**
January	9.4	11.8	12.6	13.2	13.8	17.4	22.0	23.6	24.8	25.9	12.9	14.3	14.8	15.1	15.4
February	8.5	11.6	12.6	13.4	14.2	15.8	21.8	23.9	25.4	26.9	12.1	14.0	14.5	15.0	15.3
March	7.4	10.1	11.0	11.7	12.4	13.8	19.2	21.1	22.5	23.9	11.9	13.3	13.7	14.0	14.3
April	6.6	9.1	9.9	10.6	11.2	12.3	16.8	18.4	19.5	20.7	11.4	13.1	13.6	13.9	14.3
May	5.1	7.8	8.7	9.4	10.1	9.7	15.0	16.8	18.1	19.5	10.1	12.0	12.6	13.0	13.4
June	4.3	6.3	7.1	7.6	8.1	8.1	11.9	13.2	14.1	15.1	9.3	11.0	11.5	11.8	12.2
July	3.6	5.1	5.6	6.0	6.4	6.9	9.7	10.6	11.3	12.0	8.7	9.9	10.3	10.6	10.8
August	4.0	6.0	6.7	7.3	7.8	7.7	11.3	12.5	13.5	14.4	9.2	10.9	11.4	11.7	12.1
September	5.9	9.4	10.6	11.6	12.5	11.1	17.6	19.8	21.5	23.2	10.6	13.2	13.9	14.4	15.0
October	6.9	10.0	11.0	11.8	12.6	12.9	18.9	20.9	22.5	24.0	11.5	13.2	13.7	14.1	14.4
November	8.0	11.1	12.1	12.9	13.7	14.9	20.5	22.4	23.8	25.3	12.1	13.5	13.9	14.3	14.6
December	9.3	12.1	13.0	13.8	14.5	17.5	22.8	24.6	26.0	27.3	12.6	14.1	14.5	14.9	15.2
All	10.9	12.9	13.6	14.2	14.8	20.2	24.0	25.4	26.5	27.6	13.6	14.7	15.1	15.4	15.7

Table 5.29 Extreme Significant Wave Height, Maximum Wave Height and Associated Peak Period Estimates (m) for Grid Point 17322 (West Orphan Basin) for Return Periods of 1, 10, 25, 50 and 100 Years

Month	Significant Wave Height (m)					Maximum Wave Height (m)					Associated Peak Period (sec)				
	1.0	10.0	25.0	50.0	100.0	1.0	10.0	25.0	50.0	100.0	1.0	10.0	25.0	50.0	100.0
January	9.1	11.6	12.4	13.0	13.6	16.9	21.5	23.1	24.3	25.4	12.8	14.2	14.7	15.0	15.3
February	8.0	11.3	12.4	13.2	14.0	15.0	21.3	23.4	25.0	26.6	11.9	13.9	14.5	14.9	15.4
March	6.9	10.0	11.0	11.8	12.6	13.2	19.5	21.7	23.3	24.9	11.8	13.2	13.6	13.9	14.2
April	6.3	9.1	10.0	10.7	11.4	11.9	17.0	18.7	20.0	21.3	11.2	12.9	13.4	13.8	14.1
May	5.0	7.6	8.5	9.2	9.9	9.5	14.6	16.4	17.7	19.0	10.0	11.9	12.4	12.8	13.1
June	4.2	6.2	6.9	7.4	7.9	8.0	11.6	12.9	13.8	14.7	9.2	10.8	11.2	11.6	11.9
July	3.5	5.0	5.5	5.8	6.2	6.8	9.3	10.2	10.8	11.5	8.5	10.0	10.5	10.8	11.1
August	3.8	6.1	6.9	7.5	8.1	7.4	11.4	12.8	13.8	14.8	8.9	10.9	11.5	11.9	12.3
September	5.7	9.0	10.2	11.0	11.9	10.7	16.6	18.7	20.2	21.7	10.5	12.9	13.7	14.2	14.7
October	6.7	9.8	10.9	11.6	12.4	12.6	18.4	20.4	21.9	23.4	11.2	13.1	13.6	14.0	14.4
November	7.8	10.9	11.9	12.7	13.5	14.5	20.1	22.1	23.5	25.0	11.8	13.4	13.8	14.1	14.5
December	9.2	11.8	12.7	13.3	14.0	17.1	22.0	23.7	25.0	26.3	12.6	13.8	14.2	14.5	14.8
All	10.6	12.7	13.5	14.1	14.7	19.7	23.7	25.2	26.3	27.5	13.4	14.5	14.9	15.2	15.5

Table 5.30 Extreme Significant Wave Height, Maximum Wave Height and Associated Peak Period Estimates (m) for Grid Point 17427 (West Orphan Basin) for Return Periods of 1, 10, 25, 50 and 100 Years

	Significant Wave Height (m)					Maximum Wave Height (m)					Associated Peak Period (sec)				
Month	**1.0**	**10.0**	**25.0**	**50.0**	**100.0**	**1.0**	**10.0**	**25.0**	**50.0**	**100.0**	**1.0**	**10.0**	**25.0**	**50.0**	**100.0**
January	9.4	11.9	12.8	13.4	14.0	17.4	22.1	23.7	24.9	26.1	12.9	14.4	14.8	15.2	15.5
February	8.4	11.7	12.8	13.7	14.5	15.8	22.0	24.0	25.6	27.1	12.1	14.0	14.5	14.9	15.3
March	7.5	10.3	11.2	11.9	12.6	13.8	19.6	21.6	23.0	24.5	12.0	13.4	13.9	14.2	14.5
April	6.5	9.3	10.3	11.0	11.7	12.4	17.5	19.2	20.4	21.7	11.3	13.1	13.7	14.1	14.4
May	5.1	7.9	8.8	9.5	10.2	9.7	15.1	17.0	18.4	19.7	10.0	12.0	12.6	13.0	13.4
June	4.3	6.3	7.0	7.5	8.0	8.1	11.9	13.2	14.2	15.2	9.4	10.9	11.4	11.7	12.0
July	3.6	5.1	5.6	5.9	6.3	7.0	9.5	10.3	11.0	11.6	8.6	10.1	10.5	10.9	11.2
August	3.8	6.2	7.0	7.6	8.2	7.4	11.4	12.8	13.8	14.8	9.0	11.0	11.6	12.0	12.4
September	5.9	9.4	10.6	11.5	12.4	11.0	17.3	19.5	21.0	22.6	10.5	13.1	13.8	14.3	14.8
October	6.9	10.0	11.1	11.9	12.7	12.9	18.9	20.9	22.4	23.9	11.5	13.1	13.6	14.0	14.3
November	8.1	11.1	12.1	12.9	13.6	15.0	20.6	22.5	23.9	25.3	12.1	13.4	13.7	14.0	14.2
December	9.4	12.2	13.1	13.8	14.5	17.5	22.8	24.6	25.9	27.3	12.7	14.0	14.4	14.7	15.0
All	10.9	13.1	13.9	14.6	15.2	20.4	24.6	26.2	27.4	28.6	13.5	14.5	14.9	15.1	15.4

A lognormal distribution was fitted to the spectral peak periods in each wave height bin. The coefficient of the lognormal distribution was then calculated. Using the coefficients and the two distribution functions, the joint wave height and period combinations were calculated for the various return periods.

Contour plots depicting these values for return periods of 1-year, 10-years, 25-years, 50-years, and 100-years is presented for each grid point in Figures 5.41 to 5.44. The annual values for the significant wave height estimates and the associated spectral peak periods are given in Table 5.31. The extreme wave height for all return periods was higher using the Weibull distribution when compared to the Gumbel distribution.

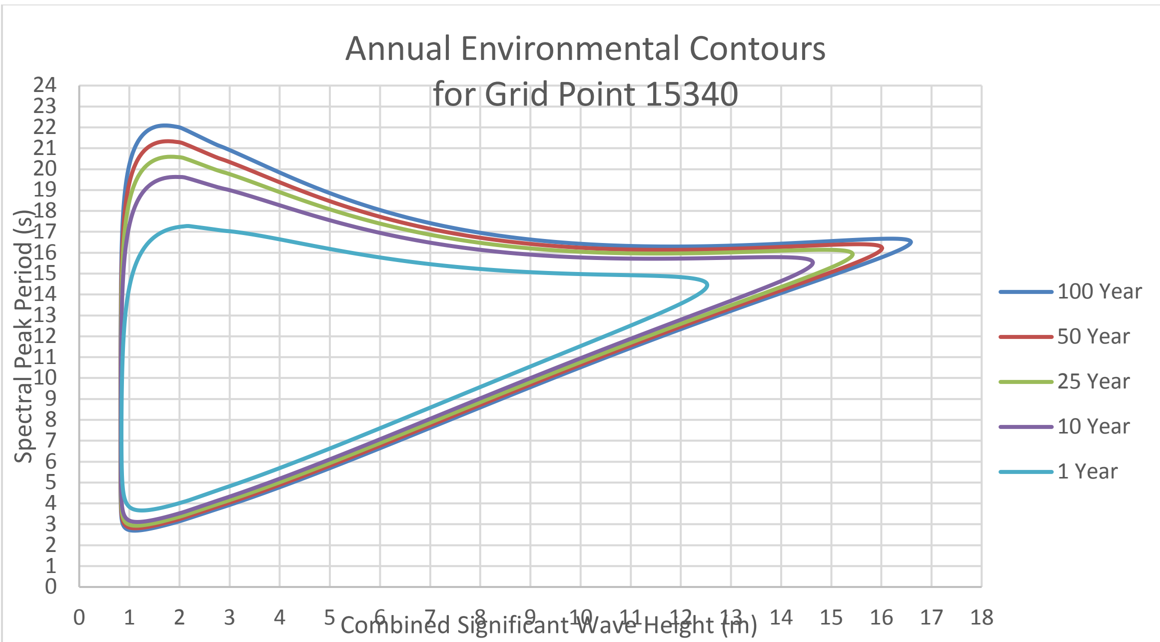

Figure 5.41 Environmental Contour Plot of 1, 10, 25, 50 and 100-year Return Periods for Grid Point 15340

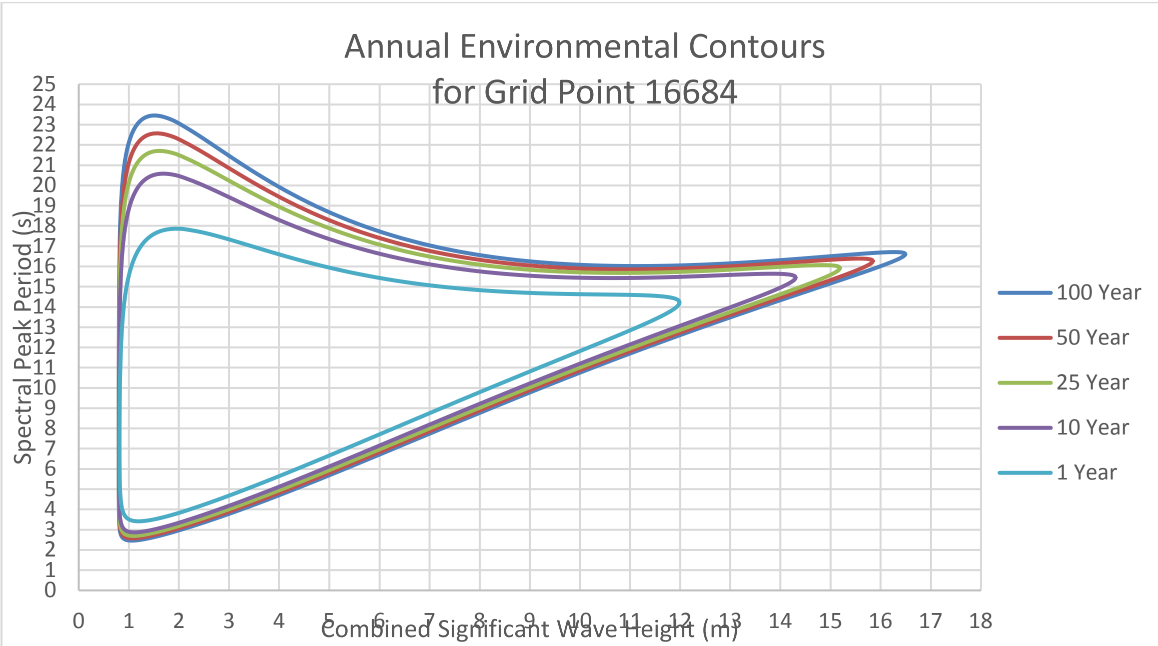

Figure 5.42 Environmental Contour Plot of 1, 10, 25, 50 and 100-year Return Periods for Grid Point 16684

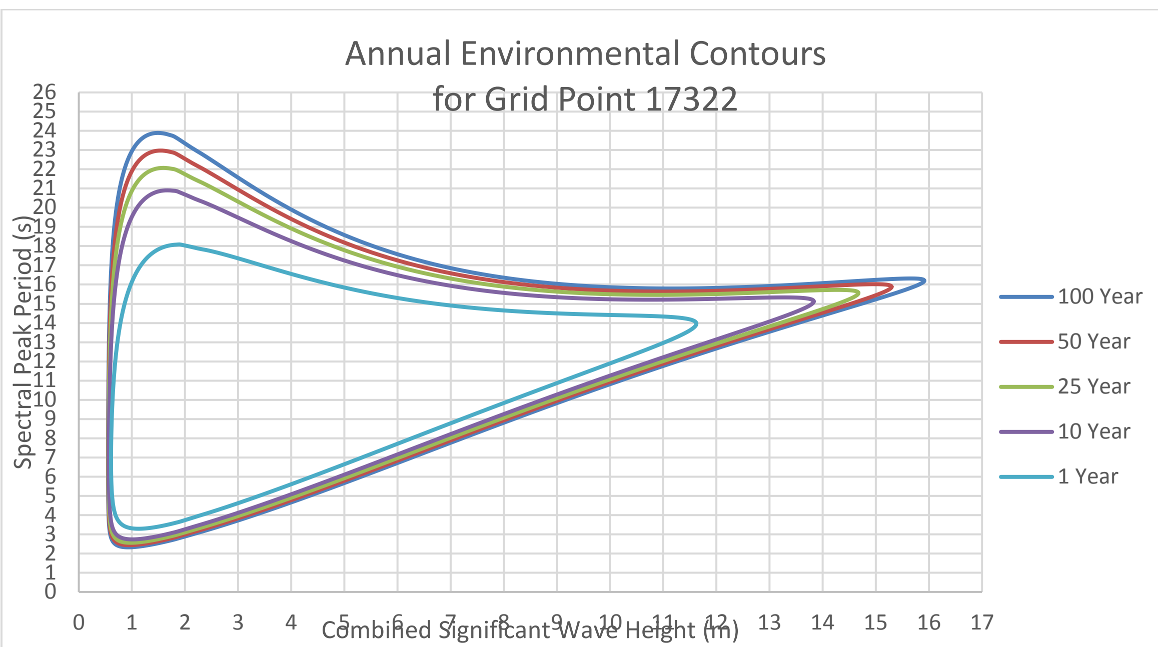

Figure 5.43 Environmental Contour Plot of 1, 10, 25, 50 and 100-year Return Periods for Grid Point 17322

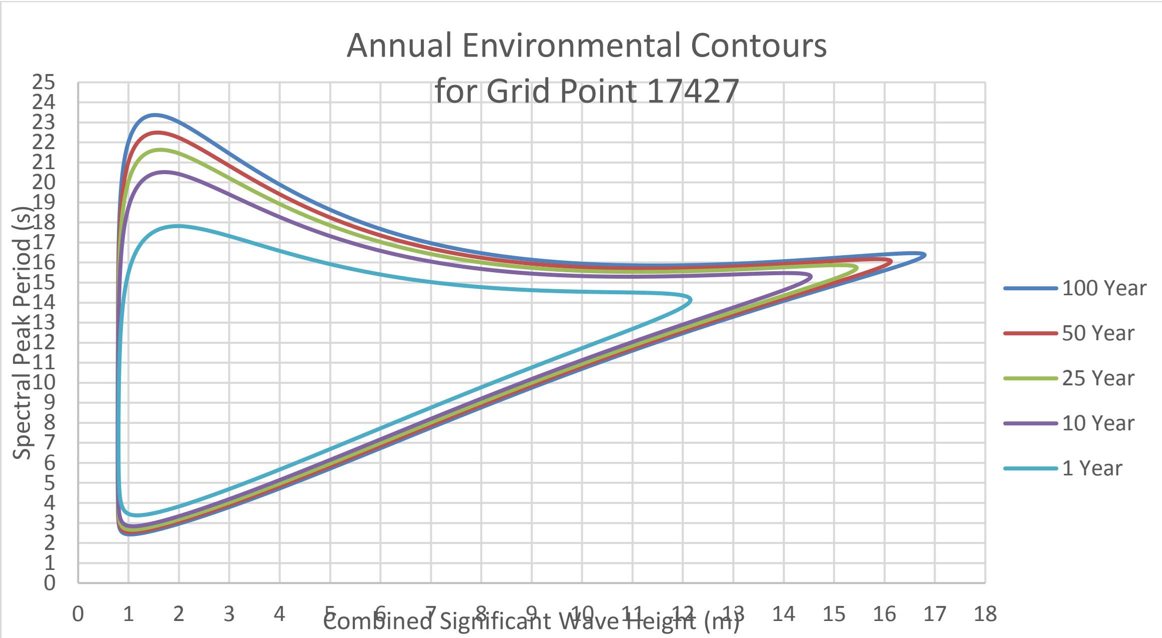

Figure 5.44 Environmental Contour Plot of 1, 10, 25, 50 and 100-year Return Periods for Grid Point 17427

Table 5.31 Annual Extreme Significant Wave Estimates and Spectral Peak Periods for Return Periods of 1, 10, 25, 50 and 100 Years

Grid Point	Significant Wave Height (m)					Spectral Peak Period Median Value (s)				
	1.0	10.0	25.0	50.0	100.0	1.0	10.0	25.0	50.0	100.0
15340	12.5	14.6	15.4	16.0	16.6	14.5	15.5	15.9	16.2	16.5
16684	12.0	14.3	15.2	15.8	16.5	14.2	15.4	15.9	16.3	16.6
17322	11.6	13.8	14.7	15.3	15.9	14.0	15.1	15.6	15.9	16.2
17427	12.1	14.5	15.4	16.1	16.8	14.1	15.3	15.7	16.1	16.4

5.4.4 Seawater Properties

Temperatures and salinity data from historical measurements were extracted from the Bedford Institute of Oceanography archive. Locations of these measurements are shown on Figure 5.45. These data are presented as monthly statistics. The Project Area was divided into two sub-areas: West Orphan Basin (EL 1145, EL 1146, and EL 1148) and East Orphan Basin (EL 1149).

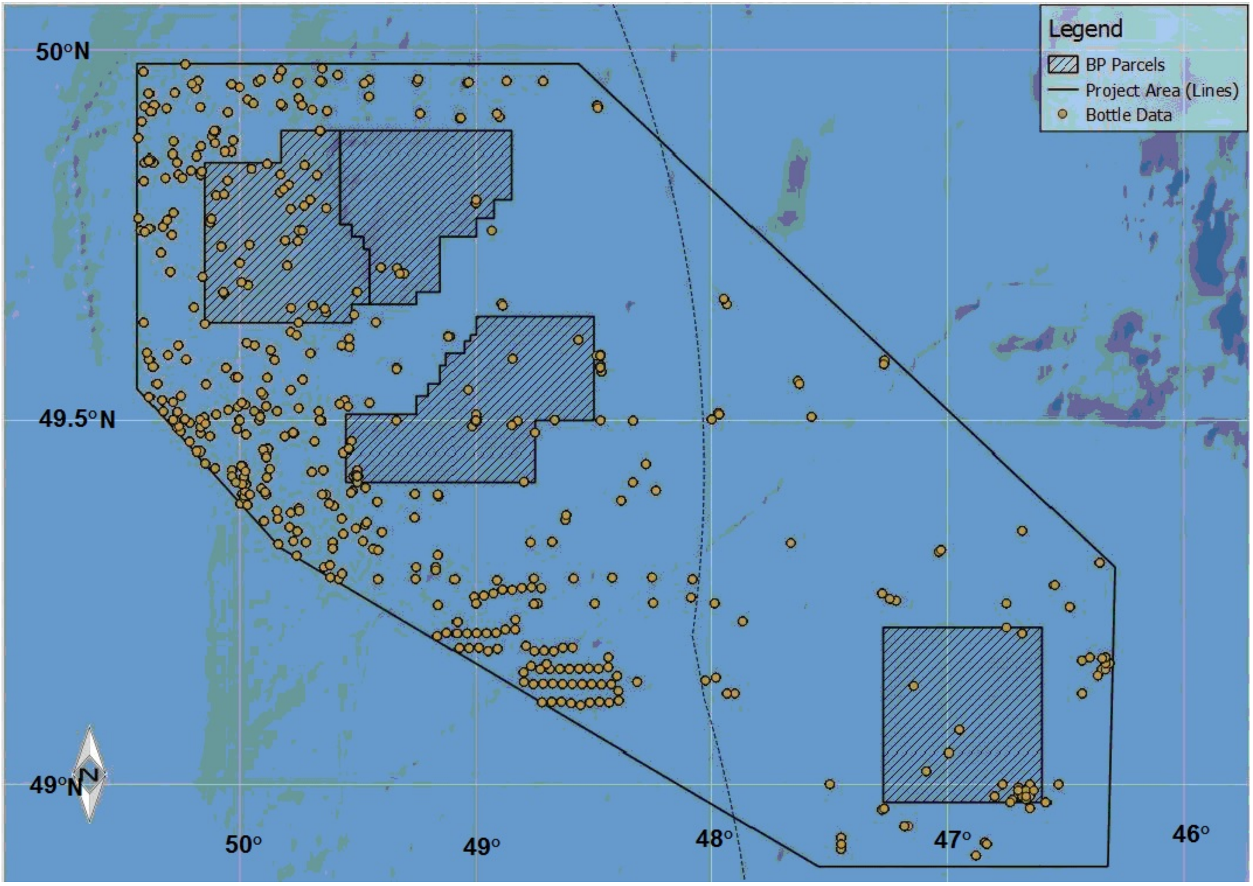

Figure 5.45 BIO Conductivity, Temperature, Depth (CTD) Mooring Locations in the Orphan Basin

5.4.4.1 West Orphan Basin

Summarized statistics of sea water temperature and salinity at depths of 0 m, 50 m, 100 m, 200m, 300 to 900 m, and 1,000 to 3,000 m at West Orphan Basin are provided in Tables 5.32 to 5.37. The surface waters were warmest during the months of July to September with mean temperatures ranging from 6.62°C to 8.59°C. The coldest temperatures were in March and April with mean temperatures of -0.10°C and 0.02°C, respectively. The mean salinities ranged between 32.97 psu in October and 34.07 psu in December. At a depth of 50 m, the mean temperatures ranged between 0.78°C in March to 4.01°C in October. The mean salinities ranged between 33.82 psu in August and 34.46 psu in July. At a depth of 100 m, the mean temperatures ranged between 1.95°C in September and 3.60°C in December. The salinity had a standard deviation of less than 0.30 and mean salinity values that ranged from 34.26 psu in September to 34.47 psu in November. At a depth of 200 m, the mean temperatures ranged between 2.56°C in April to 4.13°C in December. The salinity had a standard deviation of less than 0.20 and mean salinity values that ranged from 34.62 psu in April and 34.80 psu in December. At a depth of 300 to 900 m, the mean temperatures ranged between 3.21°C in March to 4.03°C in February. The salinity had a standard deviation of less than 0.10 and mean salinity values that ranged from 34.78 psu in April and 34.89 psu in February and November.

At a depth of 1,000 to 3,000 m, the mean temperatures ranged between 3.04°C in March to 3.47°C in January and November. The salinity had a standard deviation of less than 0.08 and mean salinity values that ranged between 34.84 psu and 34.90 psu.

Table 5.32 Monthly Temperature and Salinity Statistics for the Surface Water in West Orphan Basin from Historical CTD Data

Surface Temperature (0 m)					
Month	**#OBS**	**Mean (°C)**	**Stdev (°C)**	**Max(°C)**	**Min(°C)**
January	319	1.92	0.65	3.16	-0.04
February	3	0.06	0.00	0.06	0.06
March	160	-0.10	1.38	2.82	-1.68
April	471	0.02	1.43	5.30	-1.71
May	331	2.23	1.47	5.16	-0.05
June	288	2.37	0.85	4.54	0.42
July	561	6.80	2.64	12.31	-1.17
August	209	8.59	1.70	11.50	3.39
September	23	6.62	2.19	11.48	4.87
October	8	3.31	0.03	3.35	3.28
November	803	3.97	0.96	7.39	1.10
December	1035	2.92	0.85	5.38	-0.29
Overall	4211	3.33	2.67	12.31	-1.71
Surface Salinity (0 m)					
Month	**#OBS**	**Mean (psu)**	**Stdev (psu)**	**Max (psu)**	**Min (psu)**
January	319	34.06	0.19	34.57	33.60
February	3	33.32	0.00	33.32	33.32
March	160	33.76	0.44	34.64	33.18
April	471	33.73	0.40	34.83	32.25
May	331	33.88	0.44	34.74	30.48
June	288	33.55	0.49	34.63	32.19
July	561	33.37	0.58	34.65	31.47
August	209	33.32	0.65	34.55	31.49
September	23	33.46	0.58	34.47	33.05
October	8	32.97	0.38	33.15	32.05
November	803	33.82	0.42	34.61	32.48
December	1035	34.07	0.27	34.53	32.55
Overall	4211	33.78	0.49	34.83	30.48

Table 5.33 Monthly Temperature and Salinity Data for a Depth of 50 m in West Orphan Basin from Historical CTD Data

Temperature (50 m)					
Month	**#OBS**	**Mean (°C)**	**Stdev (°C)**	**Max(°C)**	**Min(°C)**
January	931	2.11	0.55	3.36	-0.01
February	674	0.81	1.34	2.91	-1.69
March	1333	0.78	1.45	5.31	-1.59
April	1238	1.80	1.07	3.97	-0.41
May	1323	1.16	1.17	4.12	-1.65
June	1476	2.62	1.81	8.65	-1.37
July	537	3.35	1.14	8.90	-1.00
August	114	2.06	2.52	9.86	-0.36
September	54	3.21	0.38	3.83	2.68
October	2179	4.01	0.89	7.33	0.70
November	2900	3.20	0.83	5.23	-0.44
Overall	12759	2.46	1.62	9.86	-1.69
Salinity (50 m)					
Month	**#OBS**	**Mean (psu)**	**Stdev (psu)**	**Max (psu)**	**Min (psu)**
January	931	34.13	0.17	34.61	33.57
February	674	34.10	0.41	34.69	33.25
March	1333	34.09	0.41	34.83	33.17
April	1238	34.13	0.31	34.75	33.14
May	1323	34.08	0.32	34.71	33.11
June	1476	34.27	0.33	34.75	32.65
July	537	34.46	0.28	34.78	32.81
August	114	33.82	0.28	34.52	33.37
September	54	33.91	0.15	34.15	33.37
October	2179	34.05	0.27	34.68	32.98
November	2900	34.19	0.19	34.53	33.17
Overall	12759	34.14	0.31	34.83	32.65

Table 5.34 Monthly Temperature and Salinity Data for a Depth of 100 m in West Orphan Basin from Historical CTD Data

Temperature (100 m)					
Month	**#OBS**	**Mean (°C)**	**Stdev (°C)**	**Max(°C)**	**Min(°C)**
January	1567	2.74	0.71	4.31	0.44
March	945	1.96	0.94	3.58	-1.22
April	2148	1.82	0.80	5.17	-0.62
May	1736	2.48	0.81	4.70	0.33
June	1775	2.03	0.98	3.75	-1.20
July	1779	2.73	1.11	4.71	-1.17
August	629	3.24	0.57	3.87	-0.04
September	154	1.95	1.07	6.14	0.17
October	50	2.69	0.15	3.10	2.49
November	3407	3.56	0.80	5.46	1.09
December	4857	3.60	0.69	5.24	-0.44
Overall	19047	2.88	1.07	6.14	-1.22
Salinity (100 m)					
Month	**#OBS**	**Mean (psu)**	**Stdev (psu)**	**Max (psu)**	**Min (psu)**
January	1567	34.28	0.18	34.71	33.61
March	945	34.48	0.25	34.81	33.50
April	2148	34.39	0.22	34.82	33.55
May	1736	34.46	0.18	34.75	33.82
June	1775	34.42	0.23	34.78	33.56
July	1779	34.55	0.24	34.84	33.37
August	629	34.69	0.15	34.81	33.49
September	154	34.26	0.23	34.96	33.83
October	50	34.36	0.11	34.59	34.15
November	3407	34.47	0.22	34.84	33.68
December	4857	34.41	0.19	35.03	33.63
Overall	19047	34.44	0.22	35.03	33.37

Table 5.35 Monthly Temperature and Salinity Data for a Depth of 200 m in West Orphan Basin from Historical CTD Data

Temperature (200 m)					
Month	**#OBS**	**Mean (°C)**	**Stdev (°C)**	**Max (°C)**	**Min (°C)**
January	1535	3.82	0.65	4.76	1.71
March	728	2.83	0.36	3.38	1.37
April	1420	2.56	0.38	4.00	0.88
May	1239	3.08	0.38	3.92	2.17
June	1131	3.25	0.54	4.03	0.91
July	1233	3.41	0.37	4.07	1.71
August	540	3.38	0.20	4.31	2.70
September	69	3.33	0.45	4.81	2.68
October	20	3.71	0.08	3.82	3.55
November	2871	4.09	0.32	4.82	2.69
December	4730	4.13	0.35	4.72	1.33
Overall	15516	3.65	0.68	4.82	0.88
Salinity (200 m)					
Month	**#OBS**	**Mean (psu)**	**Stdev (psu)**	**Max (psu)**	**Min (psu)**
January	1535	34.65	0.15	34.87	34.23
March	728	34.71	0.09	34.83	34.37
April	1420	34.62	0.11	34.84	34.20
May	1239	34.69	0.09	34.86	34.45
June	1131	34.73	0.10	34.87	34.27
July	1233	34.76	0.09	34.86	34.36
August	540	34.79	0.05	34.87	34.36
September	69	34.69	0.14	34.97	34.47
October	20	34.77	0.02	34.81	34.73
November	2871	34.79	0.08	34.98	34.34
December	4730	34.80	0.09	35.53	34.09
Overall	15516	34.74	0.12	35.53	34.09

Table 5.36 Monthly Temperature and Salinity Data for a Depth of 300 to 900 m in West Orphan Basin from Historical CTD Data

Temperature (300 to 900 m)					
Month	**#OBS**	**Mean (°C)**	**Stdev (°C)**	**Max (°C)**	**Min (°C)**
January	15364	3.99	0.23	4.60	2.86
February	12	4.03	0.03	4.06	4.00
March	3157	3.21	0.22	3.87	2.23
April	3258	3.16	0.27	4.04	1.10
May	4629	3.32	0.16	3.95	2.82
June	2637	3.37	0.23	4.01	2.78
July	5148	3.35	0.19	4.41	2.89
August	3849	3.34	0.13	4.25	2.85
September	214	3.70	0.30	4.46	3.28
October	39	3.65	0.07	3.74	3.55
November	29413	3.97	0.27	4.86	3.21
December	54341	3.90	0.27	4.75	3.12
Overall	122061	3.82	0.36	4.86	1.10
Salinity (300 to 900 m)					
Month	**#OBS**	**Mean (psu)**	**Stdev (psu)**	**Max (psu)**	**Min (psu)**
January	15364	34.85	0.05	34.89	34.55
February	12	34.89	0.02	34.91	34.87
March	3157	34.81	0.04	34.89	34.60
April	3258	34.78	0.06	34.91	34.26
May	4629	34.82	0.03	34.92	34.67
June	2637	34.83	0.03	34.89	34.72
July	5148	34.83	0.02	35.07	34.69
August	3849	34.83	0.01	34.93	34.70
September	214	34.82	0.08	35.03	34.64
October	39	34.84	0.01	34.86	34.82
November	29413	34.89	0.07	35.10	34.62
December	54341	34.87	0.03	35.96	34.67
Overall	122061	34.86	0.05	35.96	34.26

Table 5.37 Monthly Temperature and Salinity Data for a Depth of 1.000 to 3,000 m in West Orphan Basin from Historical CTD Data

Temperature (1,000 to 3,000 m)					
Month	**#OBS**	**Mean (°C)**	**Stdev (°C)**	**Max (°C)**	**Min (°C)**
January	3002	3.47	0.15	3.82	2.99
March	11	3.04	0.05	3.13	3.00
April	330	3.19	0.26	3.73	2.78
May	258	3.28	0.17	3.72	2.91
June	17	3.40	0.02	3.43	3.38
July	434	3.21	0.19	3.81	2.85
August	202	3.20	0.21	3.82	2.80
September	52	3.18	0.29	3.82	2.80
October	4	3.34	0.01	3.35	3.33
November	9113	3.47	0.17	3.91	2.91
December	13967	3.44	0.14	3.88	2.88
Overall	27390	3.45	0.16	3.91	2.78
Salinity (1,000 to 3,000 m)					
Month	**#OBS**	**Mean (psu)**	**Stdev (psu)**	**Max (psu)**	**Min (psu)**
January	3002	34.87	0.01	34.90	34.84
March	11	34.85	0.01	34.85	34.83
April	330	34.87	0.04	34.95	34.83
May	258	34.86	0.01	34.90	34.84
June	17	34.90	0.02	34.92	34.87
July	434	34.86	0.02	34.96	34.83
August	202	34.87	0.04	34.95	34.81
September	52	34.91	0.01	34.92	34.88
October	4	34.84	0.01	34.85	34.84
November	9113	34.90	0.07	35.08	34.74
December	13967	34.87	0.02	34.94	34.84
Overall	27390	34.88	0.05	35.08	34.74

Figure 5.46 and Figure 5.47 indicate the monthly mean temperature and mean salinity at West Orphan Basin at depth of 0 m, 50 m, 100 m, 200 m, 300 to 900 m, and 1,000 to 3,000 m, representatively.

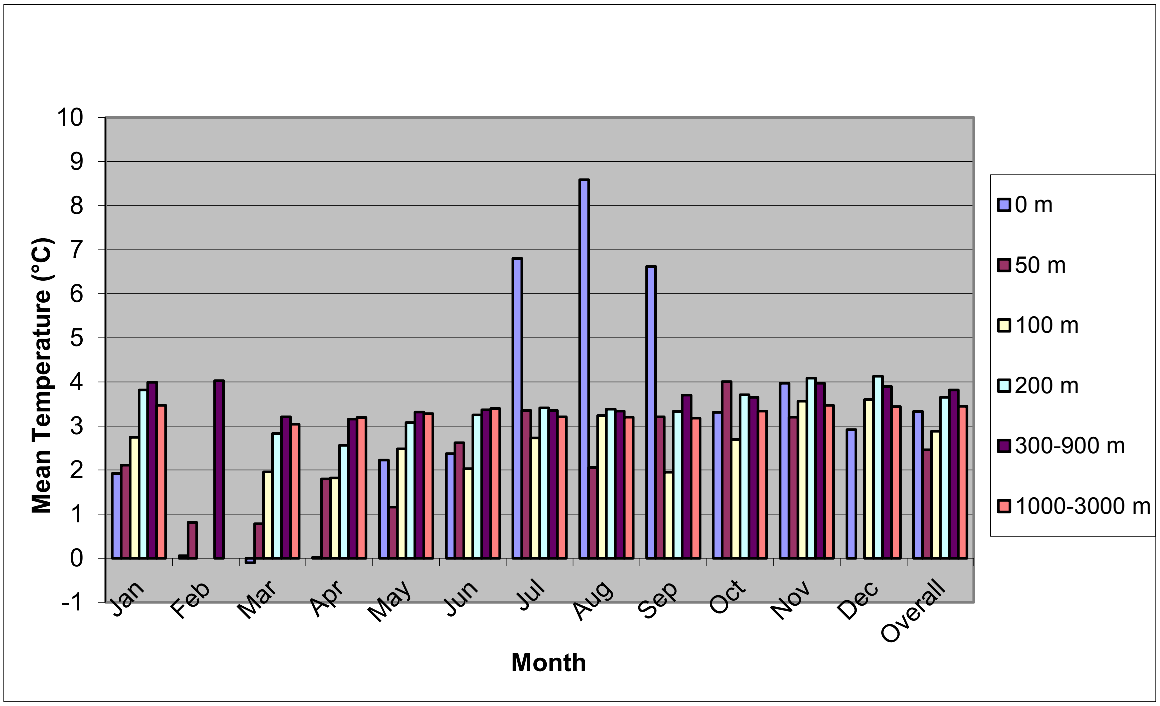

Figure 5.46 Mean Temperature at West Orphan Basin from Historical CTD Data

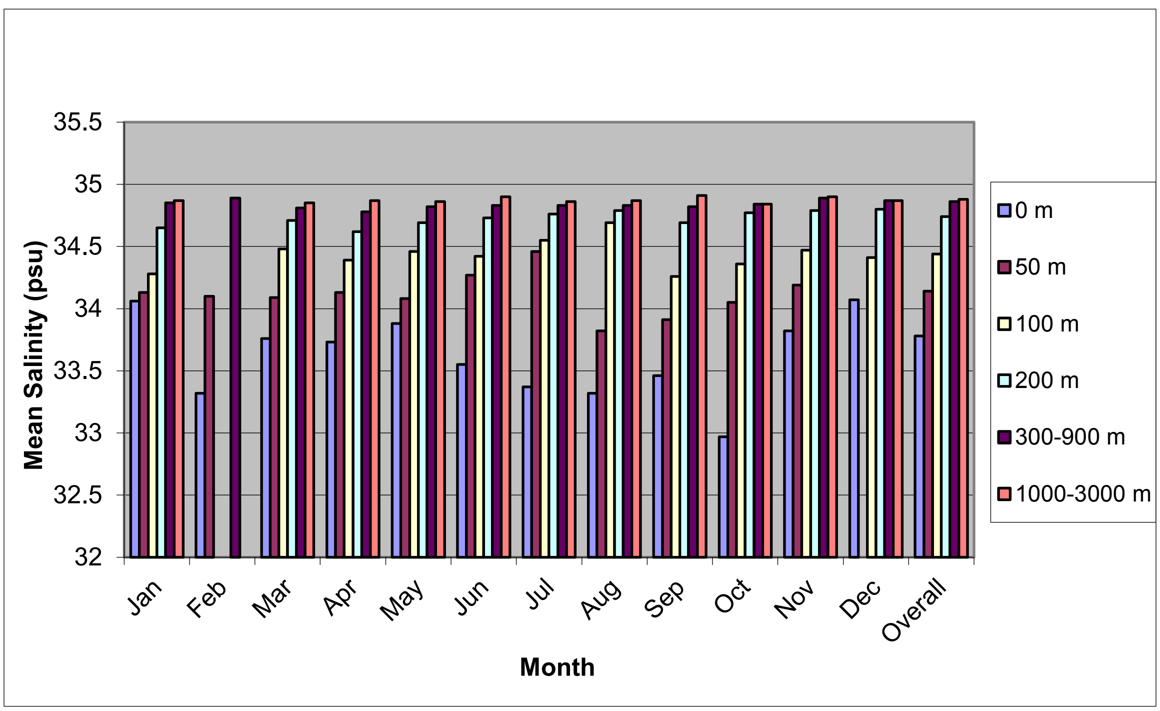

Figure 5.47 Mean Salinity at West Orphan Basin from Historical CTD Data

5.4.4.2 East Orphan Basin

Summarized statistics of sea water temperature and salinity at depths of 0 m, 50 m, 100 m, 200, 300 to 900 m, and 1,000 to 3,000 m at East Orphan Basin are provided in Tables 5.38 to 5.43. The surface waters were warmest during the months of July to September with mean temperatures ranging from 8.80°C to 12.40°C. The coldest temperatures were in March and April with mean temperatures of 1.45°C and 2.50°C, respectively. The mean salinities ranged between 33.75 psu in August and 34.49 psu in May with a mean salinity of 34.31 psu throughout the year. At a depth of 50 m, the mean temperatures ranged between 2.24°C in March to 5.71°C in August. The mean salinities ranged between 34.28 psu in September and 34.58 psu in March and April. At a depth of 100 m, the mean temperatures ranged between 2.77°C in March and 4.67°C in November. The salinity had no significant difference among the months throughout the year with mean salinity values that ranged from 34.54 psu in January to 34.71 psu in September. At a depth of 200 m, the mean temperatures ranged between 3.07°C in March to 4.24°C in November. The salinity had a standard deviation of less than 0.10 and mean salinity values that ranged from 34.75 psu in April and 34.85 psu in November. At a depth of 300 to 900 m, the mean temperatures ranged between 3.00°C in July to 3.89°C in October. The salinity had a standard deviation of less than 0.05 and mean salinity values that ranged from 34.82 psu to 34.87 psu. At a depth of 1000 to 3000 m, the mean temperatures ranged between 2.83°C in November to 3.42°C in July. The salinity had a standard deviation of less than 0.04 and mean salinity values that ranged between 34.85 psu and 34.95 psu.

Figure 5.48 and Figure 5.49 indicate the monthly mean temperature and mean salinity at East Orphan Basin at depth of 0 m, 50 m, 100 m, 200 m, 300 to 900 m, and 1,000 to 3,000 m, respectively.

Table 5.38 Monthly Temperature and Salinity Data for Surface Seawater in East Orphan Basin from Historical CTD Data

Surface Temperature (0 m)					
Month	**#OBS**	**Mean (°C)**	**Stdev (°C)**	**Max (°C)**	**Min (°C)**
January	4	3.55	0.65	4.18	2.64
March	69	1.45	1.35	2.98	-0.81
April	93	2.50	1.74	5.40	-1.05
May	62	4.50	1.05	7.08	3.26
June	33	7.05	1.46	9.89	4.08
July	76	8.80	2.01	13.04	5.50
August	15	12.40	1.13	14.55	10.37
September	2	11.93	0.00	11.93	11.93
October	60	6.14	1.22	8.90	4.63
November	8	5.82	0.54	7.15	5.56
Overall	422	5.10	3.32	14.55	-1.05
Surface Salinity (0 m)					
Month	**#OBS**	**Mean (psu)**	**Stdev (psu)**	**Max (psu)**	**Min (psu)**
January	4	34.48	0.02	34.50	34.46
March	69	34.26	0.46	34.71	33.32
April	93	34.33	0.42	34.86	33.40
May	62	34.49	0.19	34.78	34.25
June	33	34.46	0.24	34.78	33.80
July	76	34.28	0.29	34.72	33.55
August	15	33.75	0.24	34.29	33.40
September	2	34.00	0.00	34.00	34.00
October	60	34.26	0.15	34.56	33.98
November	8	34.33	0.09	34.47	34.19
Overall	422	34.31	0.35	34.86	33.32

Table 5.39 Monthly Temperature and Salinity Data for a Depth of 50 m in East Orphan Basin from Historical CTD Data

Temperature (50 m)					
Month	**#OBS**	**Mean (°C)**	**Stdev (°C)**	**Max (°C)**	**Min (°C)**
January	12	3.44	0.64	4.19	2.63
March	147	2.24	0.57	2.99	0.89
April	295	3.00	1.06	5.40	0.21
May	224	4.10	0.80	6.51	2.94
June	114	5.06	1.09	8.07	3.02
July	306	4.38	1.11	10.00	1.84
August	47	5.71	1.81	9.30	1.19
September	167	5.60	0.96	8.64	4.54
October	24	5.44	0.21	5.68	4.94
Overall	1336	4.06	1.47	10.00	0.21
Salinity (50 m)					
Month	**#OBS**	**Mean (psu)**	**Stdev (psu)**	**Max (psu)**	**Min (psu)**
January	12	34.48	0.01	34.51	34.47
March	147	34.58	0.15	34.71	34.14
April	295	34.58	0.18	34.84	33.93
May	224	34.50	0.18	34.78	34.25
June	114	34.51	0.12	34.80	34.15
July	306	34.55	0.17	34.92	34.06
August	47	34.42	0.23	34.69	33.57
September	167	34.28	0.14	34.56	34.00
October	24	34.47	0.08	34.64	34.35
Overall	1336	34.51	0.19	34.92	33.57

Table 5.40 Monthly Temperature and Salinity Data for a Depth of 100 m in East Orphan Basin from Historical CTD Data

Temperature (100 m)					
Month	**#OBS**	**Mean (°C)**	**Stdev (°C)**	**Max (°C)**	**Min (°C)**
January	53	3.53	0.45	4.19	2.65
March	270	2.77	0.35	3.29	1.98
April	443	3.09	0.62	5.41	1.47
May	278	3.39	0.62	5.22	2.60
June	95	4.20	0.98	8.03	2.50
July	352	3.28	0.34	5.04	1.96
August	32	3.76	0.79	4.91	1.80
September	4	3.59	0.01	3.59	3.58
October	285	4.37	0.54	9.23	3.69
November	21	4.69	0.27	5.63	4.44
Overall	1833	3.43	0.77	9.23	1.47
Salinity 100 m					
Month	**#OBS**	**Mean (psu)**	**Stdev (psu)**	**Max (psu)**	**Min (psu)**
January	53	34.54	0.04	34.69	34.47
March	270	34.69	0.04	34.78	34.61
April	443	34.64	0.09	34.80	34.17
May	278	34.64	0.10	34.89	34.34
June	95	34.66	0.10	34.97	34.37
July	352	34.69	0.07	34.79	34.33
August	32	34.63	0.12	34.79	34.28
September	4	34.71	0.00	34.71	34.71
October	285	34.60	0.14	34.78	34.13
November	21	34.69	0.06	34.74	34.47
Overall	1833	34.65	0.10	34.97	34.13

Table 5.41 Monthly Temperature and Salinity Data for a Depth of 200 m in East Orphan Basin from Historical CTD Data

Temperature (200 m)					
Month	**#OBS**	**Mean (°C)**	**Stdev (°C)**	**Max (°C)**	**Min (°C)**
January	49	3.91	0.30	4.15	2.75
March	193	3.07	0.29	3.51	2.44
April	444	3.30	0.47	5.11	2.42
May	192	3.48	0.30	4.58	2.74
June	60	3.78	0.47	4.95	3.02
July	245	3.26	0.34	3.85	2.91
August	17	3.54	0.36	4.12	3.16
September	4	3.43	0.00	3.43	3.43
October	137	3.88	0.20	4.74	3.55
November	10	4.24	0.05	4.33	4.17
Overall	1351	3.40	0.45	5.11	2.42
Salinity (200 m)					
Month	**#OBS**	**Mean (psu)**	**Stdev (psu)**	**Max (psu)**	**Min (psu)**
January	49	34.76	0.07	34.82	34.53
March	193	34.77	0.04	34.87	34.69
April	444	34.75	0.06	34.87	34.63
May	192	34.78	0.04	34.89	34.61
June	60	34.79	0.04	34.85	34.68
July	245	34.80	0.02	34.84	34.77
August	17	34.78	0.05	34.85	34.70
September	4	34.81	0.00	34.81	34.81
October	137	34.80	0.03	34.90	34.70
November	10	34.85	0.00	34.86	34.85
Overall	1351	34.78	0.05	34.90	34.53

Table 5.42 Monthly Temperature and Salinity Data for a Depth of 300 to 900 m in East Orphan Basin from Historical CTD Data

Temperature (300 to 900 m)					
Month	**#OBS**	**Mean (°C)**	**Stdev (°C)**	**Max (°C)**	**Min (°C)**
January	129	3.66	0.13	3.92	3.43
March	893	3.19	0.18	3.60	2.72
April	1872	3.55	0.17	4.43	2.96
May	400	3.63	0.22	4.24	3.11
June	159	3.58	0.22	4.17	3.09
July	266	3.00	0.22	3.91	2.92
August	40	3.44	0.23	3.94	3.20
September	30	3.38	0.04	3.45	3.30
October	89	3.89	0.30	4.51	3.47
November	21	3.88	0.13	4.03	3.57
Overall	3899	3.45	0.28	4.51	2.72
Salinity (300 to 900 m)					
Month	**#OBS**	**Mean (psu)**	**Stdev (psu)**	**Max (psu)**	**Min (psu)**
January	129	34.87	0.03	34.91	34.81
March	893	34.82	0.04	34.92	34.74
April	1872	34.86	0.03	34.92	34.68
May	400	34.84	0.03	34.91	34.74
June	159	34.85	0.03	34.90	34.75
July	266	34.82	0.01	34.88	34.81
August	40	34.83	0.04	34.89	34.76
September	30	34.84	0.00	34.84	34.83
October	89	34.85	0.04	34.91	34.76
November	21	34.87	0.00	34.87	34.86
Overall	3899	34.85	0.04	34.92	34.68

Table 5.43 Monthly Temperature and Salinity Data for a Depth of 1,000 to 3,000 m in East Orphan Basin from Historical CTD Data

Temperature (1,000 to 3,000 m)					
Month	**#OBS**	**Mean (°C)**	**Stdev (°C)**	**Max (°C)**	**Min (°C)**
January	64	3.33	0.08	3.42	3.06
March	1	3.11	0.00	3.11	3.11
April	3583	3.08	0.37	3.56	2.04
May	143	3.06	0.56	3.71	2.07
June	53	3.35	0.20	3.56	2.76
July	27	3.42	0.13	3.53	3.14
August	2	3.33	0.00	3.33	3.33
September	56	2.79	0.46	3.45	2.20
October	40	2.84	0.47	3.63	2.16
November	18	2.83	0.54	3.46	1.99
Overall	3987	3.08	0.38	3.71	1.99
Salinity (1,000 to 3,000 m)					
Month	**#OBS**	**Mean (psu)**	**Stdev (psu)**	**Max (psu)**	**Min (psu)**
January	64	34.92	0.03	34.97	34.87
March	1	34.85	0.00	34.85	34.85
April	3583	34.95	0.02	34.98	34.85
May	143	34.90	0.02	34.95	34.86
June	53	34.90	0.03	34.94	34.83
July	27	34.88	0.01	34.90	34.86
August	2	34.90	0.00	34.90	34.90
September	56	34.91	0.01	34.92	34.88
October	40	34.89	0.02	34.92	34.81
November	18	34.89	0.01	34.91	34.86
Overall	3987	34.94	0.03	34.98	34.81

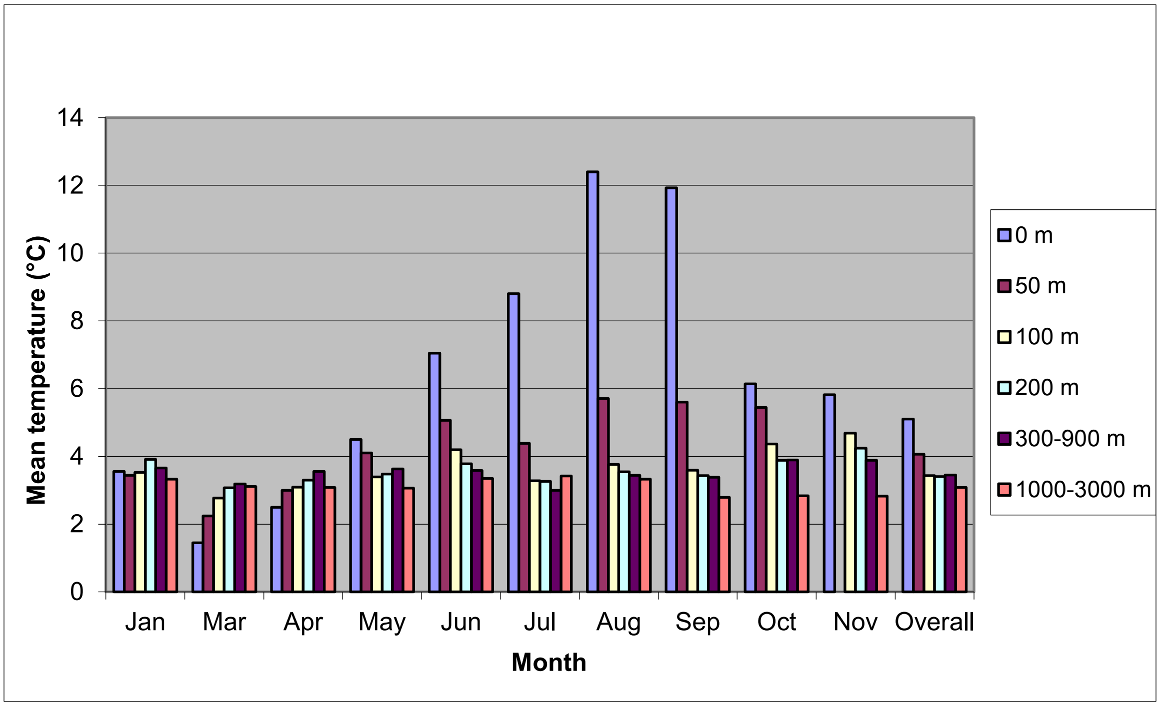

Figure 5.48 Mean Temperature at East Orphan Basin from Historical CTD Data

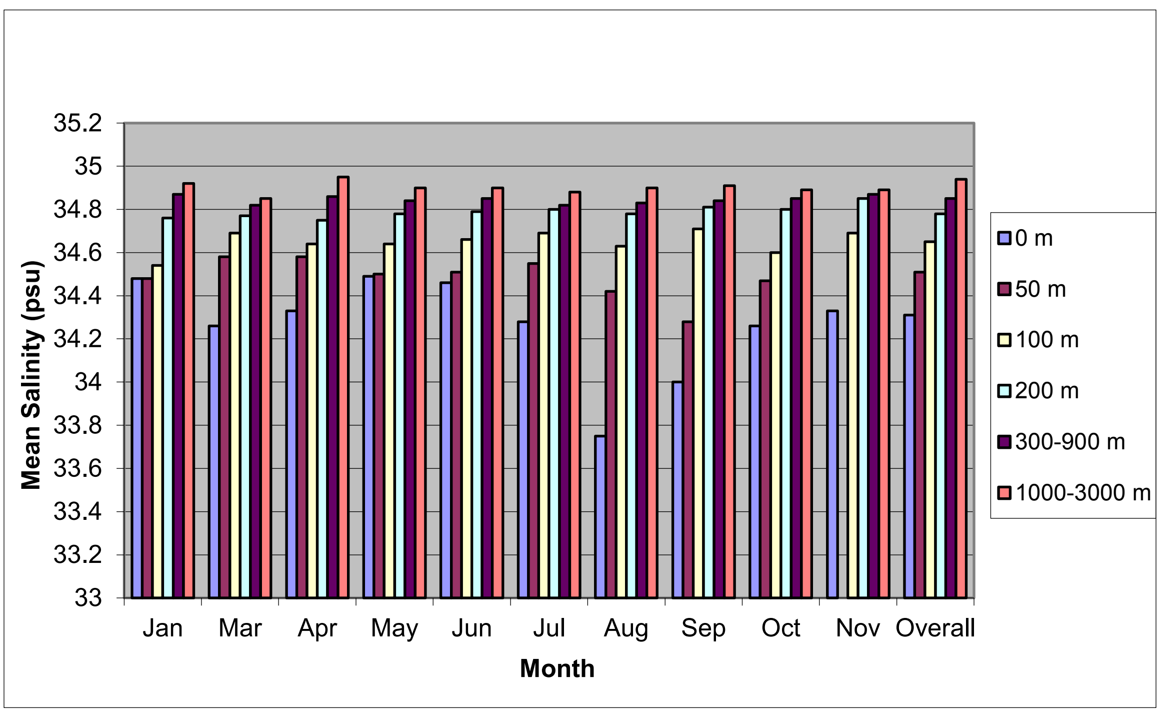

Figure 5.49 Mean Salinity at East Orphan Basin from Historical CTD Data

5.4.5 Tides

There are no tidal measurements for Orphan Basin. Tidal information for the Grand Banks comes from a tidal study carried out by the Bedford Institute of Oceanography (BIO) in 1983-84. From the BIO data, Petrie et al. (1987) prepared co-range and co-phase tidal charts for the Grand Banks for constituents M2, S2 and K1. By extrapolating the co-range lines, the M2 constituent for Orphan Basin is 25 cm and S2 and K1 has values of approximately 10 cm each. This means that the tidal height in Orphan Basin is expected to be approximately 50 cm.

5.4.6 Storm Surge

The water level due to storm surge is the inverse barometer effect due to the variation in atmospheric pressure plus the rise in sea level as a result of wind stress on the surface of the ocean. Severe storm surges can cause the ocean to rise by a few meters in coastal regions, but much smaller in the absence of a boundary. The extreme 100-year return period storm surge value near Terra Nova was calculated by Seaconsult (1988) as being 73 cm above mean water level.

The inverse barometer effect causes a sea level rise of 1 cm/1 millibar as the atmospheric pressure drops. The minimum atmospheric pressure measured in Orphan Basin over the last 15 years was 952.0 mb on February 20, 2007, and again during Hurricane Igor on September 22, 2010. This gives a sea level rise of approximately 56 cm. The total storm surge level will be somewhat higher due to the effect of wind stress.

Bernier and Thompson (2006) conducted a modelling study of storm surges and extreme sea levels in the Northwest Atlantic. Figure 5.50 of the shows that the 40-year return level of extreme storm surges in Orphan Basin is 70 to 80 cm for this return period.

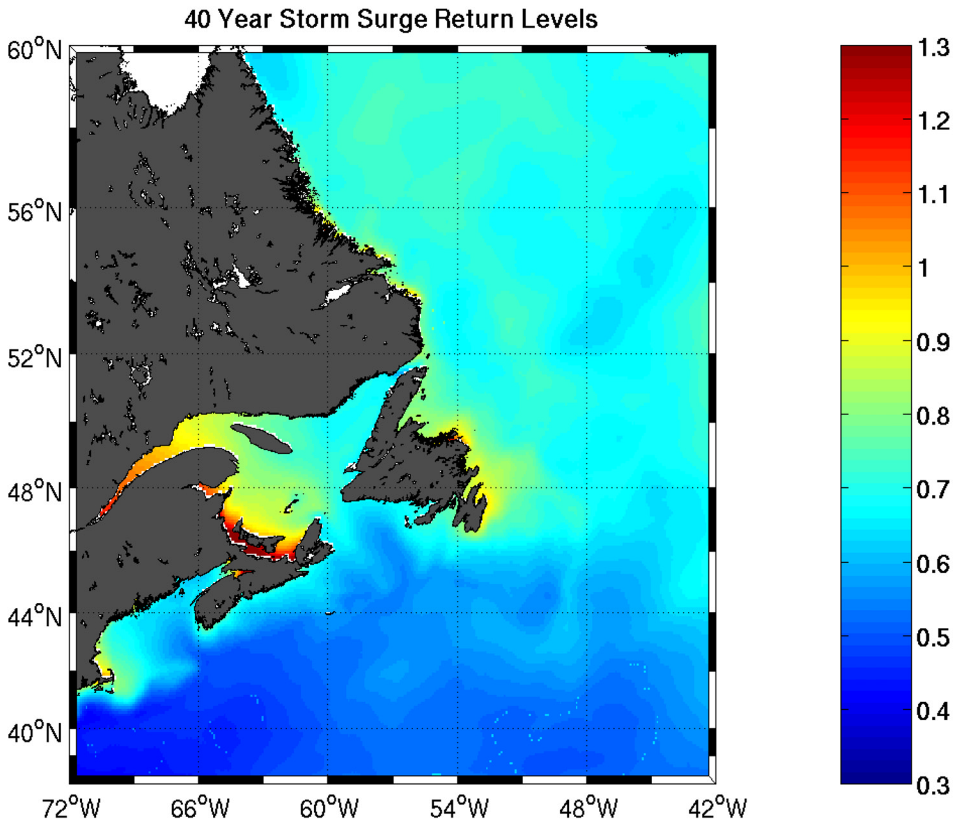

Source: Bernier and Thompson (2006)
Note: Colour bar indicates the 40-year return levels in metres

Figure 5.50 40-year Return Level of Extreme Storm Surges based on the Surge Hindcast

5.5 Ice Conditions

5.5.1 Sea Ice

5.5.1.1 Terminology

Classification of ice commonly found in the waters along Canada's Eastern Seaboard according to internationally accepted terminology (ECCC2018b) is provided in Table 5.44.

5.5.1.2 Frequency of Presence

The "Frequency of Presence of Sea Ice (%)" charts consider the likelihood of total concentration of ice greater than or equal to 1/10 throughout the course of a year and provides an indication of the likelihood that ice will occur at a particular location for the appropriate date.

Table 5.44 Sea Ice Terminology

Sea Ice Age	Concentration of Sea Ice	Forms of Sea Ice	Surface Features of Sea Ice
New Ice A general term for recently formed ice which includes frazil ice, grease ice, slush and shuga. These types of ice are composed of ice crystals which are only weakly frozen together (if at all) and have a definite form only while they are afloat. In Canada, the term 'new ice' is applied to all recently formed sea ice having thickness up to 10 cm. This includes ice rind, light nilas and dark nilas. *Frazil Ice* – Fine spicules or plates of ice suspended in water. *Grease Ice* – A later stage of freezing than Frazil Ice when crystals have coagulated to form a soupy layer on the surface. Grease ice reflects little light, giving the sea a matt appearance. *Slush* – Snow which is saturated and mixed with water on land or ice surfaces, or as a viscous floating mass in water after a heavy snowfall. *Shuga* – An accumulation of spongy white ice lumps, a few centimeters across; they are formed from grease ice or slush and sometimes from anchor ice rising to the surface. Nilas A thin elastic crust of ice, easily bending on the waves and swell and under pressure, thrusting in a pattern of interlocking 'fingers' (finger rafting). Has a matt surface and may be subdivided into darl nilas and light nilas. *Dark Nilas* – Nilas which is under 5 cm in thickness and is very dark in colour. *Light Nilas* – Nilas which is more than 5 cm in thickness and rather lighter in colour than dark nilas.	Concentration is the ratio expressed in tenths describing the amount of the sea surface covered by ice as a fraction of the whole area being considered. Total concentration includes all stages of development that are present, partial concentration may refer to the amount of a particular stage or a particular form of ice and represents only a part of the total. The following terms are used: *Compact Ice* - Floating ice in which the concentration is 10/10 and no water is visible. *Consolidated Ice* - Floating ice in which the concentration is 10/10 and the floes are frozen together. *Very Close Ice* - Floating ice in which the concentration is 9/10 to less than 10/10. *Close Ice* - Floating ice, in which the concentration is 7/10 to less than 8/10, composed of floes mostly in contact. *Open Ice* - Floating ice in which the concentration is 4/10 to less than 6/10 with many leads and polynyas, and the floes are generally not in contact with one another. *Very Open Water* - Floating ice in which the concentration is 1/10 to less than 3/10 and water preponderates over ice. *Open Water* - A large area of freely navigable water in which sea ice is present in concentration less than 1/10. No ice of land origin is present. *Ice Free* - No ice present. *Bergy Water* - An area of freely navigable water in which ice of land origin is present in concentrations less than 1/10. There may be sea ice present, although the total concentration of all ice shall not exceed 1/10.	*Ice Floe* - Any relatively flat piece of sea ice 20 m or more across.	*Rafted Ice* - Type of deformed ice formed by one piece of ice overriding another. *Ridge* - A line or wall of broken ice forced up by pressure. May be fresh or weathered. The submerged volume of broken ice under a ridge, forced downwards by pressure is termed an ice keel.

Sea Ice Age	Concentration of Sea Ice	Forms of Sea Ice	Surface Features of Sea Ice
<u>Young Ice</u> Ice in the transition stage between nilas and first year ice, 10 -30 cm in thickness. May be subdivided into grey ice and grey-white ice. *Grey Ice* - Young ice 10-15 cm thick. Less elastic than nilas and breaks in swell. Usually rafts under pressure *Grey-white Ice* - Young ice 15-30 cm thick. Under pressure is more likely to ridge than raft. <u>First Year Ice</u> Sea ice of not more than one winter's growth, developing from young ice; thickness 30 cm to 2 m, and sometimes slightly more. May be subdivided into thin first-year ice/white ice, medium first-year ice and thick first-year ice. *Thin First-year Ice/white ice* First-year ice 30-70 cm thick. May be subdivided into thin first-year ice of the first stage 30-50 cm thick and thin first-year ice of the second stage 50-70 cm thick. *Medium First-year Ice* - First-year ice 70-120 cm thick. *Thick First-year Ice*: First-year ice over 120 cm thick. <u>Old Ice</u> - Sea ice which has survived at least one summer's melt. Most topographic features are smoother than first-year ice.			

The charts can be interpreted as the "odds of encountering sea ice for the dataset". The charts depict above normal extent (1 to 33%), near normal extent (34 to 66%) and below normal extent (67 to 99%). The 0% line represents the maximum extent of sea ice, beyond it no ice was reported in the dataset; the 100% line represents the minimum extent of sea ice, within it there has always been ice reported in the dataset. (ECCC 2018b).

Project Area

A weekly analysis of the Canadian Ice Service's Frequency of Presence of Sea Ice for the period of 1981 to 2010 was determined for the Project Area. These results are presented in Table 5.45 and Figure 5.51. These statistics show that the Project Area is primarily affected by sea ice beginning the week of January 08 and lasting until the week beginning July 02, with the highest frequency of sea ice observed the week of March 12 (Figure 5.52).

Table 5.45 Frequency of Presence of Sea Ice within the Project Area (1981 - 2010)

Date	Ice Free	1-15%	16-33%	34-50%	51-66%	67-84%	85-99%	100%
Nov 19	100.00	0.00	0.00	0.00	0.00	0.00	0.00	0.00
Nov 26	100.00	0.00	0.00	0.00	0.00	0.00	0.00	0.00
Dec 04	100.00	0.00	0.00	0.00	0.00	0.00	0.00	0.00
Dec 11	100.00	0.00	0.00	0.00	0.00	0.00	0.00	0.00
Dec 18	100.00	0.00	0.00	0.00	0.00	0.00	0.00	0.00
Dec 25	100.00	0.00	0.00	0.00	0.00	0.00	0.00	0.00
Jan 01	100.00	0.00	0.00	0.00	0.00	0.00	0.00	0.00
Jan 08	77.74	22.26	0.00	0.00	0.00	0.00	0.00	0.00
Jan 15	82.84	17.16	0.00	0.00	0.00	0.00	0.00	0.00
Jan 22	65.15	30.07	4.79	0.00	0.00	0.00	0.00	0.00
Jan 29	30.81	37.22	31.98	0.00	0.00	0.00	0.00	0.00
Feb 05	31.77	44.69	23.54	0.00	0.00	0.00	0.00	0.00
Feb 12	26.27	37.93	35.72	0.07	0.00	0.00	0.00	0.00
Feb 19	28.52	44.34	15.59	11.55	0.00	0.00	0.00	0.00
Feb 26	14.68	60.78	18.34	6.19	0.00	0.00	0.00	0.00
Mar 05	26.97	51.51	9.82	10.33	1.37	0.00	0.00	0.00
Mar 12	11.59	62.53	16.31	9.54	0.04	0.00	0.00	0.00
Mar 19	25.42	48.09	17.21	9.15	0.12	0.00	0.00	0.00
Mar 26	22.90	39.97	29.95	7.18	0.00	0.00	0.00	0.00
Apr 02	45.62	21.41	27.22	5.75	0.00	0.00	0.00	0.00
Apr 09	38.09	44.19	17.06	0.67	0.00	0.00	0.00	0.00
Apr 16	58.90	34.66	6.44	0.00	0.00	0.00	0.00	0.00
Apr 23	66.74	26.39	6.86	0.00	0.00	0.00	0.00	0.00
Apr 30	70.74	29.26	0.00	0.00	0.00	0.00	0.00	0.00

Date	Ice Free	1-15%	16-33%	34-50%	51-66%	67-84%	85-99%	100%
May 07	72.33	26.61	1.06	0.00	0.00	0.00	0.00	0.00
May 14	77.80	22.20	0.00	0.00	0.00	0.00	0.00	0.00
May 21	94.72	5.28	0.00	0.00	0.00	0.00	0.00	0.00
May 28	99.25	0.75	0.00	0.00	0.00	0.00	0.00	0.00
Jun 04	99.90	0.10	0.00	0.00	0.00	0.00	0.00	0.00
Jun 11	93.20	6.80	0.00	0.00	0.00	0.00	0.00	0.00
Jun 18	100.00	0.00	0.00	0.00	0.00	0.00	0.00	0.00
Jun 25	91.21	8.79	0.00	0.00	0.00	0.00	0.00	0.00
Jul 02	98.67	1.33	0.00	0.00	0.00	0.00	0.00	0.00
Jul 09	100.00	0.00	0.00	0.00	0.00	0.00	0.00	0.00
Jul 16	100.00	0.00	0.00	0.00	0.00	0.00	0.00	0.00
Jul 23	100.00	0.00	0.00	0.00	0.00	0.00	0.00	0.00
Jul 30	100.00	0.00	0.00	0.00	0.00	0.00	0.00	0.00
Aug 06	100.00	0.00	0.00	0.00	0.00	0.00	0.00	0.00
Aug 13	100.00	0.00	0.00	0.00	0.00	0.00	0.00	0.00
Aug 20	100.00	0.00	0.00	0.00	0.00	0.00	0.00	0.00
Aug 27	100.00	0.00	0.00	0.00	0.00	0.00	0.00	0.00

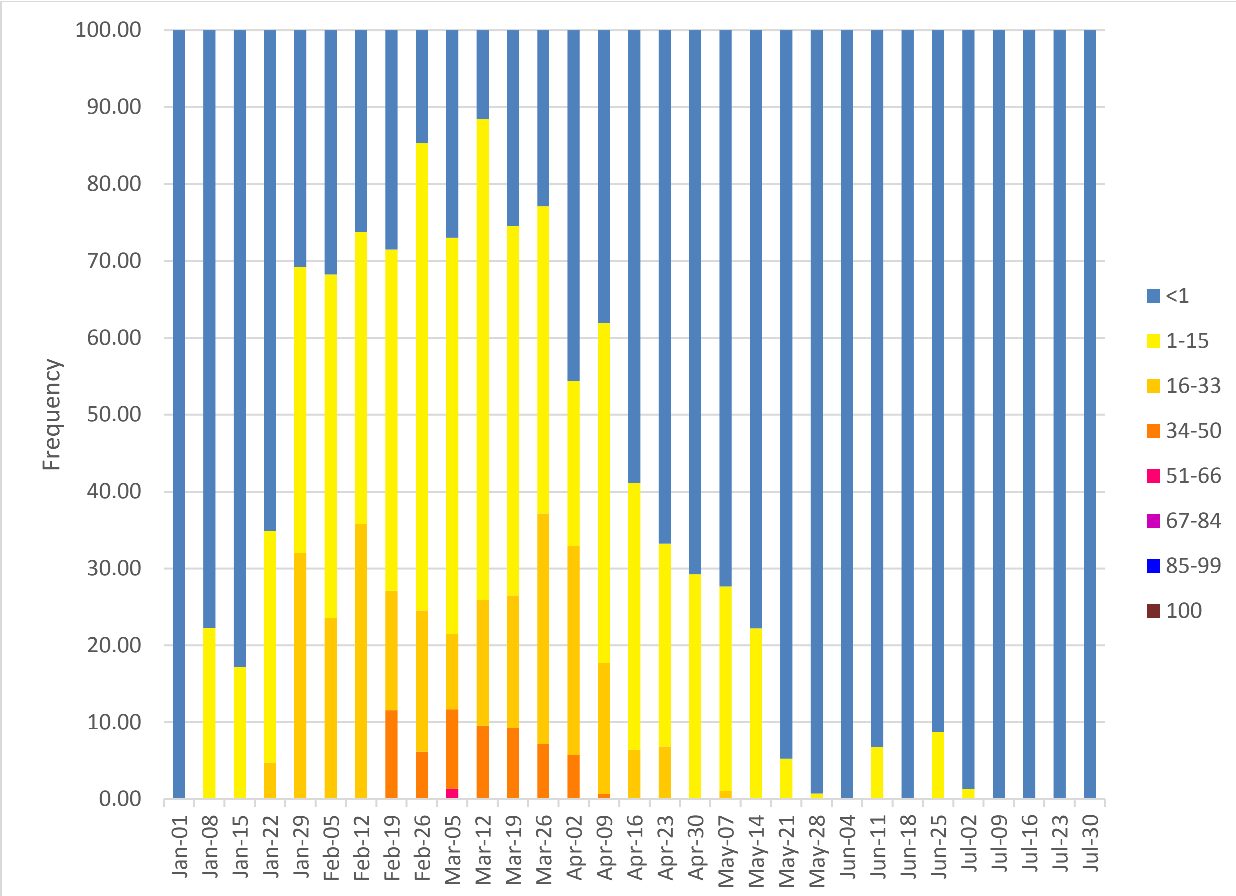

Figure 5.51 Plot of Frequency of Presence of Sea Ice within the Project Area (1981 - 2010)

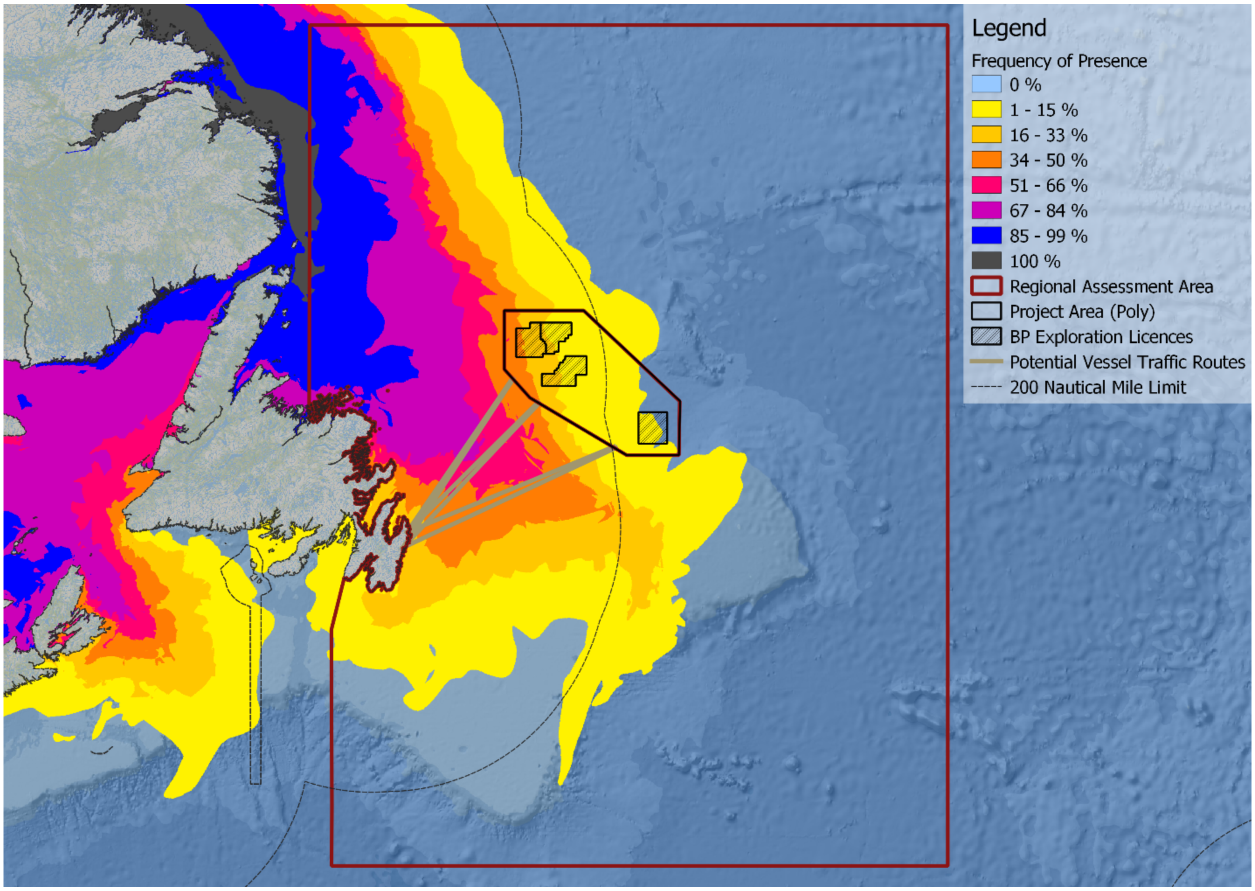

Figure 5.52 Frequency of Presence of Sea Ice in the Project Area for the Week of March 12 (1981 - 2010)

Regional Assessment Area

A weekly analysis of the Canadian Ice Service's Frequency of Presence of Sea Ice for the period of 1981 to 2010 within the Regional Assessment Area is presented in Table 5.46 and Figure 5.53. These statistics show that sea ice begins to affect the Regional Assessment Area beginning the week of December 04 and lasts until the week beginning August 06.

Table 5.46 Frequency of Presence of Sea Ice within the Regional Assessment Area (1981 - 2010)

Date	Ice Free	1-15%	16-33%	34-50%	51-66%	67-84%	85-99%	100%
Nov 12	100.00	0.00	0.00	0.00	0.00	0.00	0.00	0.00
Nov 19	100.00	0.00	0.00	0.00	0.00	0.00	0.00	0.00
Nov 26	100.00	0.00	0.00	0.00	0.00	0.00	0.00	0.00
Dec 04	99.98	0.02	0.00	0.00	0.00	0.00	0.00	0.00
Dec 11	99.85	0.15	0.00	0.00	0.00	0.00	0.00	0.00

Date	Ice Free	1-15%	16-33%	34-50%	51-66%	67-84%	85-99%	100%
Dec 18	99.18	0.73	0.09	0.00	0.00	0.00	0.00	0.00
Dec 25	98.02	1.67	0.31	0.00	0.00	0.00	0.00	0.00
Jan 01	95.04	2.78	2.02	0.14	0.02	0.00	0.00	0.00
Jan 08	93.15	3.84	1.87	0.82	0.26	0.07	0.00	0.00
Jan 15	91.04	5.32	1.78	0.82	0.70	0.32	0.00	0.00
Jan 22	90.02	4.42	2.80	0.82	0.71	1.06	0.17	0.00
Jan 29	89.11	3.61	3.24	1.07	1.27	1.25	0.45	0.01
Feb 05	86.86	5.63	2.66	1.21	0.84	1.84	0.97	0.00
Feb 12	86.11	4.86	3.30	1.20	1.03	2.09	1.41	0.00
Feb 19	85.44	5.26	2.71	1.54	0.84	1.71	2.49	0.00
Feb 26	85.65	5.58	2.31	1.08	1.23	2.18	1.97	0.00
Mar 05	86.24	4.37	2.68	1.42	1.26	2.65	1.38	0.00
Mar 12	84.45	6.27	2.63	1.82	1.07	2.06	1.63	0.07
Mar 19	85.31	5.22	3.11	1.53	1.98	2.36	0.45	0.03
Mar 26	86.85	4.07	2.75	1.72	1.26	2.94	0.41	0.00
Apr 02	86.53	4.72	2.70	2.07	1.33	2.36	0.29	0.00
Apr 09	87.03	5.42	2.73	1.93	1.52	1.33	0.03	0.00
Apr 16	88.77	4.66	2.64	1.68	1.36	0.85	0.03	0.00
Apr 23	88.86	4.89	2.69	1.91	0.96	0.68	0.02	0.00
Apr 30	90.67	4.16	2.42	1.39	1.05	0.31	0.00	0.00
May 07	91.93	3.70	2.12	1.43	0.75	0.08	0.00	0.00
May 14	92.77	3.30	2.03	1.48	0.36	0.07	0.00	0.00
May 21	92.84	3.60	2.42	0.84	0.28	0.03	0.00	0.00
May 28	92.87	4.54	1.94	0.62	0.03	0.00	0.00	0.00
Jun 04	94.66	3.56	1.45	0.32	0.00	0.00	0.00	0.00
Jun 11	95.46	3.02	1.40	0.12	0.00	0.00	0.00	0.00
Jun 18	95.94	3.36	0.70	0.00	0.00	0.00	0.00	0.00
Jun 25	96.06	3.81	0.13	0.00	0.00	0.00	0.00	0.00
Jul 02	97.45	2.51	0.03	0.00	0.00	0.00	0.00	0.00
Jul 09	98.96	1.04	0.00	0.00	0.00	0.00	0.00	0.00
Jul 16	99.27	0.73	0.00	0.00	0.00	0.00	0.00	0.00
Jul 23	99.85	0.15	0.00	0.00	0.00	0.00	0.00	0.00
Jul 30	100.00	0.00	0.00	0.00	0.00	0.00	0.00	0.00
Aug 06	99.99	0.01	0.00	0.00	0.00	0.00	0.00	0.00
Aug 13	100.00	0.00	0.00	0.00	0.00	0.00	0.00	0.00
Aug 20	100.00	0.00	0.00	0.00	0.00	0.00	0.00	0.00
Aug 27	100.00	0.00	0.00	0.00	0.00	0.00	0.00	0.00

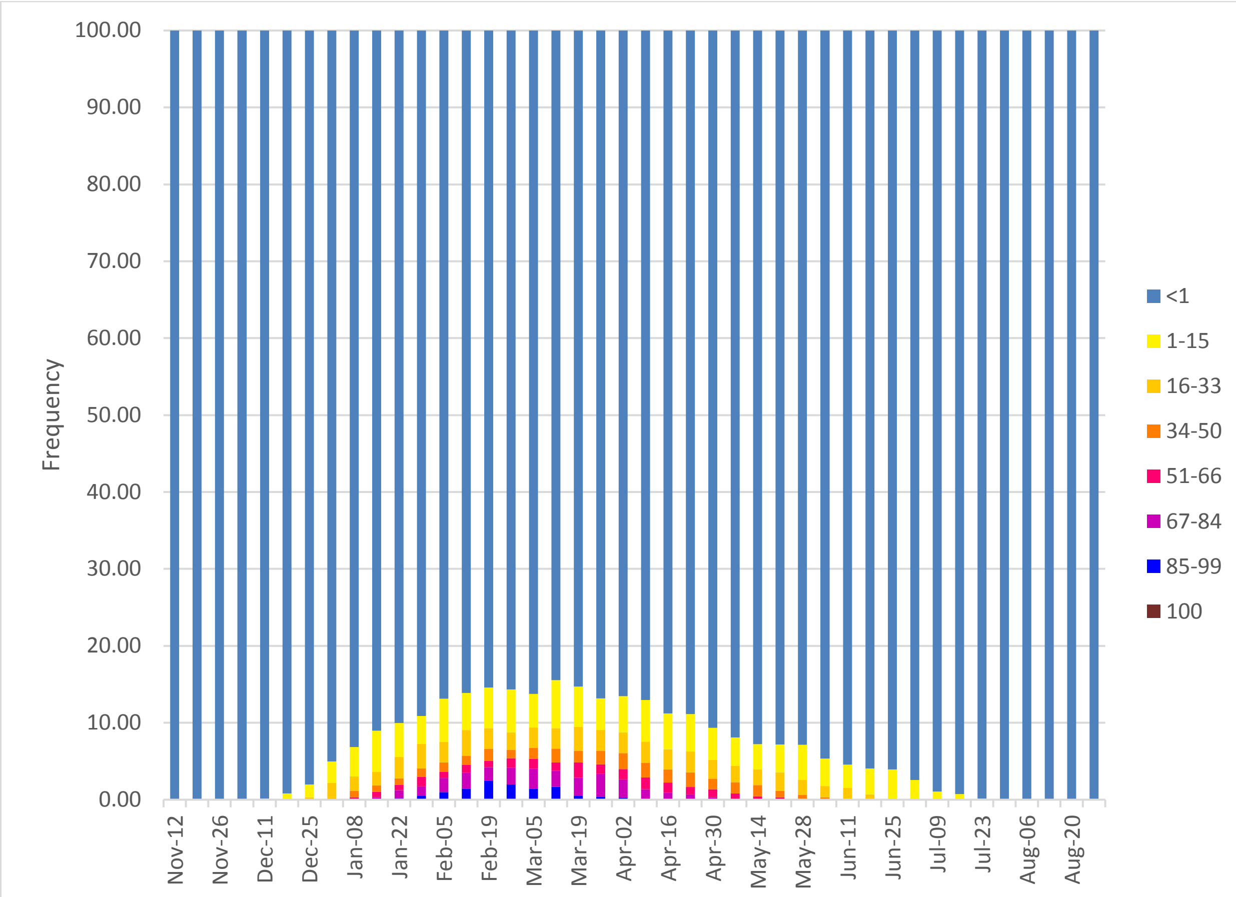

Figure 5.53 Plot of Frequency of Presence of Sea Ice within the Regional Assessment Area (1981 - 2010)

Marine Transportation Route Area

A weekly analysis of the Canadian Ice Service's Frequency of Presence of Sea Ice for the period of 1981 to 2010 within the marine transportation route area is presented in Table 5.47 and Figure 5.54. The marine transportation route area is defined as an area between the Project Area and the St. John's region (Northeast Avalon) and bounded by the most northerly transportation route and the most southerly transportation route. These statistics show that sea ice begins to affect the marine transportation route area beginning the week of January 08 and lasts until the week beginning July 02.

Table 5.47 Frequency of Presence of Sea Ice within the Marine Transportation Route Area (1981 - 2010)

Date	Ice Free	1-15%	16-33%	34-50%	51-66%	67-84%	85-99%	100%
Nov 12	100.00	0.00	0.00	0.00	0.00	0.00	0.00	0.00
Nov 19	100.00	0.00	0.00	0.00	0.00	0.00	0.00	0.00
Nov 26	100.00	0.00	0.00	0.00	0.00	0.00	0.00	0.00
Dec 04	100.00	0.00	0.00	0.00	0.00	0.00	0.00	0.00
Dec 11	100.00	0.00	0.00	0.00	0.00	0.00	0.00	0.00
Dec 18	100.00	0.00	0.00	0.00	0.00	0.00	0.00	0.00
Dec 25	100.00	0.00	0.00	0.00	0.00	0.00	0.00	0.00
Jan 01	100.00	0.00	0.00	0.00	0.00	0.00	0.00	0.00
Jan 08	78.70	21.30	0.00	0.00	0.00	0.00	0.00	0.00
Jan 15	55.87	44.13	0.00	0.00	0.00	0.00	0.00	0.00
Jan 22	58.92	32.50	8.59	0.00	0.00	0.00	0.00	0.00
Jan 29	51.45	15.02	33.53	0.00	0.00	0.00	0.00	0.00
Feb 05	51.45	9.63	38.90	0.02	0.00	0.00	0.00	0.00
Feb 12	51.93	2.23	32.66	12.76	0.42	0.00	0.00	0.00
Feb 19	51.45	0.36	11.50	30.20	5.74	0.75	0.00	0.00
Feb 26	51.45	4.82	9.33	15.14	15.72	3.54	0.00	0.00
Mar 05	51.45	3.92	6.83	16.69	17.48	3.62	0.00	0.00
Mar 12	51.45	3.39	5.49	21.59	16.81	1.27	0.00	0.00
Mar 19	51.45	2.71	11.38	21.16	13.29	0.00	0.00	0.00
Mar 26	51.45	2.01	9.91	24.15	12.36	0.12	0.00	0.00
Apr 02	52.27	2.70	11.13	27.33	6.57	0.00	0.00	0.00
Apr 09	51.45	8.21	30.27	10.07	0.00	0.00	0.00	0.00
Apr 16	51.77	15.30	30.65	2.28	0.00	0.00	0.00	0.00
Apr 23	57.35	14.54	27.93	0.18	0.00	0.00	0.00	0.00
Apr 30	56.05	37.55	6.39	0.00	0.00	0.00	0.00	0.00
May 07	68.25	31.63	0.11	0.00	0.00	0.00	0.00	0.00
May 14	70.95	29.03	0.02	0.00	0.00	0.00	0.00	0.00
May 21	82.62	17.38	0.00	0.00	0.00	0.00	0.00	0.00
May 28	85.64	14.36	0.00	0.00	0.00	0.00	0.00	0.00
Jun 04	93.17	6.83	0.00	0.00	0.00	0.00	0.00	0.00
Jun 11	100.00	0.00	0.00	0.00	0.00	0.00	0.00	0.00
Jun 18	100.00	0.00	0.00	0.00	0.00	0.00	0.00	0.00
Jun 25	99.87	0.13	0.00	0.00	0.00	0.00	0.00	0.00
Jul 02	97.09	2.91	0.00	0.00	0.00	0.00	0.00	0.00
Jul 09	100.00	0.00	0.00	0.00	0.00	0.00	0.00	0.00

Date	Ice Free	1-15%	16-33%	34-50%	51-66%	67-84%	85-99%	100%
Jul 16	100.00	0.00	0.00	0.00	0.00	0.00	0.00	0.00
Jul 23	100.00	0.00	0.00	0.00	0.00	0.00	0.00	0.00
Jul 30	100.00	0.00	0.00	0.00	0.00	0.00	0.00	0.00
Aug 06	100.00	0.00	0.00	0.00	0.00	0.00	0.00	0.00
Aug 13	100.00	0.00	0.00	0.00	0.00	0.00	0.00	0.00
Aug 20	100.00	0.00	0.00	0.00	0.00	0.00	0.00	0.00
Aug 27	100.00	0.00	0.00	0.00	0.00	0.00	0.00	0.00

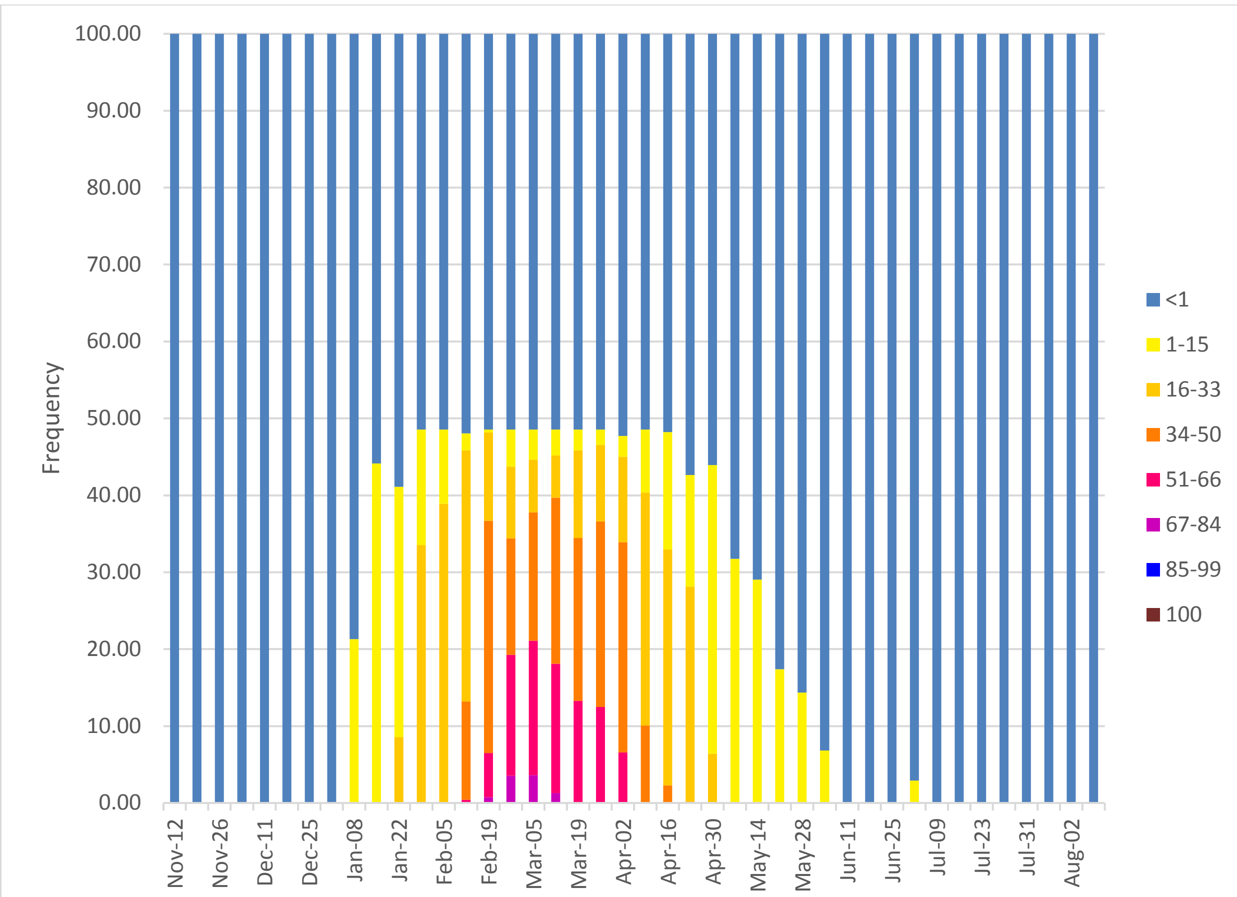

Figure 5.54 Plot of Frequency of Presence of Sea Ice within the Marine Transportation Route Area (1981 - 2010)

5.5.1.3 Median Concentration of Sea Ice

The "Median of Ice Concentration" database considers total concentration of ice on a weekly period from January 01 to July 30. The charts do not represent any real ice season but rather a statistical composite of all available seasons. The charts represent the statistical "normal" ice concentration for the appropriate date. (ECCC 2018b).

Project Area

The Project Area analysis results are presented in Table 5.48 and Figure 5.55. The 30-year median concentration of sea ice reaches its maximum over the Project Area the week of March 19 (Figure 5.56), with 42.5% of the region covered in 7/10ths or greater sea ice.

Table 5.48 Median Concentration of Sea Ice within the Project Area (1981 - 2010)

Date	Ice Free	1/10 - 3/10	4/10 - 6/10	7/10 - 8/10	9/10 - 9+/10	10/10	Total Ice
Nov 12	100.00	0.00	0.00	0.00	0.00	0.00	0.00
Nov 19	100.00	0.00	0.00	0.00	0.00	0.00	0.00
Nov 26	100.00	0.00	0.00	0.00	0.00	0.00	0.00
Dec 04	100.00	0.00	0.00	0.00	0.00	0.00	0.00
Dec 11	100.00	0.00	0.00	0.00	0.00	0.00	0.00
Dec 18	100.00	0.00	0.00	0.00	0.00	0.00	0.00
Dec 25	100.00	0.00	0.00	0.00	0.00	0.00	0.00
Jan 01	100.00	0.00	0.00	0.00	0.00	0.00	0.00
Jan 08	77.74	0.14	16.51	0.42	5.18	0.00	22.26
Jan 15	82.84	14.03	0.00	0.00	3.13	0.00	17.16
Jan 22	65.15	18.82	2.14	11.76	2.13	0.00	34.85
Jan 29	30.81	8.15	31.94	5.49	23.61	0.00	69.19
Feb 05	31.77	18.24	16.99	11.90	21.10	0.00	68.23
Feb 12	26.27	0.06	27.99	35.63	10.05	0.00	73.73
Feb 19	28.52	19.15	43.21	5.72	3.40	0.00	71.48
Feb 26	14.68	0.89	38.57	2.86	43.00	0.00	85.32
Mar 05	26.97	0.76	36.44	5.89	29.94	0.00	73.03
Mar 12	11.59	19.83	26.05	32.43	10.10	0.00	88.41
Mar 19	25.42	19.57	37.81	17.20	0.00	0.00	74.58
Mar 26	22.90	22.72	32.40	14.60	7.39	0.00	77.10
Apr 02	45.62	6.37	41.49	4.73	1.78	0.00	54.38
Apr 09	38.09	25.35	17.52	14.67	4.37	0.00	61.91
Apr 16	58.90	18.05	19.66	1.91	1.48	0.00	41.10
Apr 23	66.74	21.74	11.52	0.00	0.00	0.00	33.26
Apr 30	70.74	20.03	7.86	1.37	0.00	0.00	29.26

Date	Ice Free	1/10 - 3/10	4/10 - 6/10	7/10 - 8/10	9/10 - 9+/10	10/10	Total Ice
May 07	72.33	14.24	13.42	0.00	0.00	0.00	27.67
May 14	77.80	0.05	22.11	0.05	0.00	0.00	22.20
May 21	94.72	0.08	5.20	0.00	0.00	0.00	5.28
May 28	99.25	0.22	0.53	0.00	0.00	0.00	0.75
Jun 04	99.90	0.00	0.10	0.00	0.00	0.00	0.10
Jun 11	93.20	1.27	0.00	5.53	0.00	0.00	6.80
Jun 18	100.00	0.00	0.00	0.00	0.00	0.00	0.00
Jun 25	91.21	0.00	0.00	8.79	0.00	0.00	8.79
Jul 02	98.67	1.33	0.00	0.00	0.00	0.00	1.33
Jul 09	100.00	0.00	0.00	0.00	0.00	0.00	0.00
Jul 16	100.00	0.00	0.00	0.00	0.00	0.00	0.00
Jul 23	100.00	0.00	0.00	0.00	0.00	0.00	0.00
Jul 30	100.00	0.00	0.00	0.00	0.00	0.00	0.00
Aug 06	100.00	0.00	0.00	0.00	0.00	0.00	0.00
Aug 13	100.00	0.00	0.00	0.00	0.00	0.00	0.00
Aug 20	100.00	0.00	0.00	0.00	0.00	0.00	0.00
Aug 27	100.00	0.00	0.00	0.00	0.00	0.00	0.00

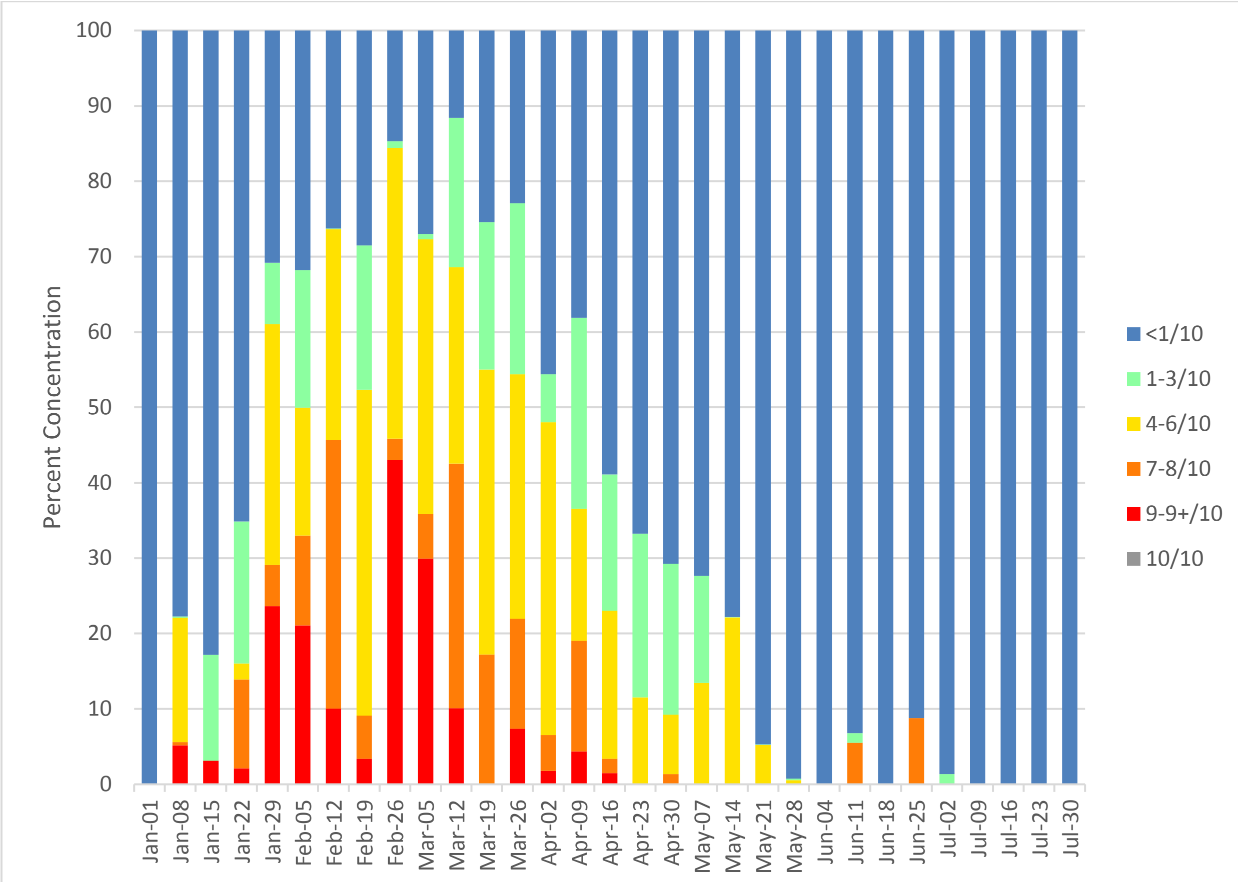

Figure 5.55 Plot of Median Concentration of Sea Ice with the Project Area (1981 - 2010)

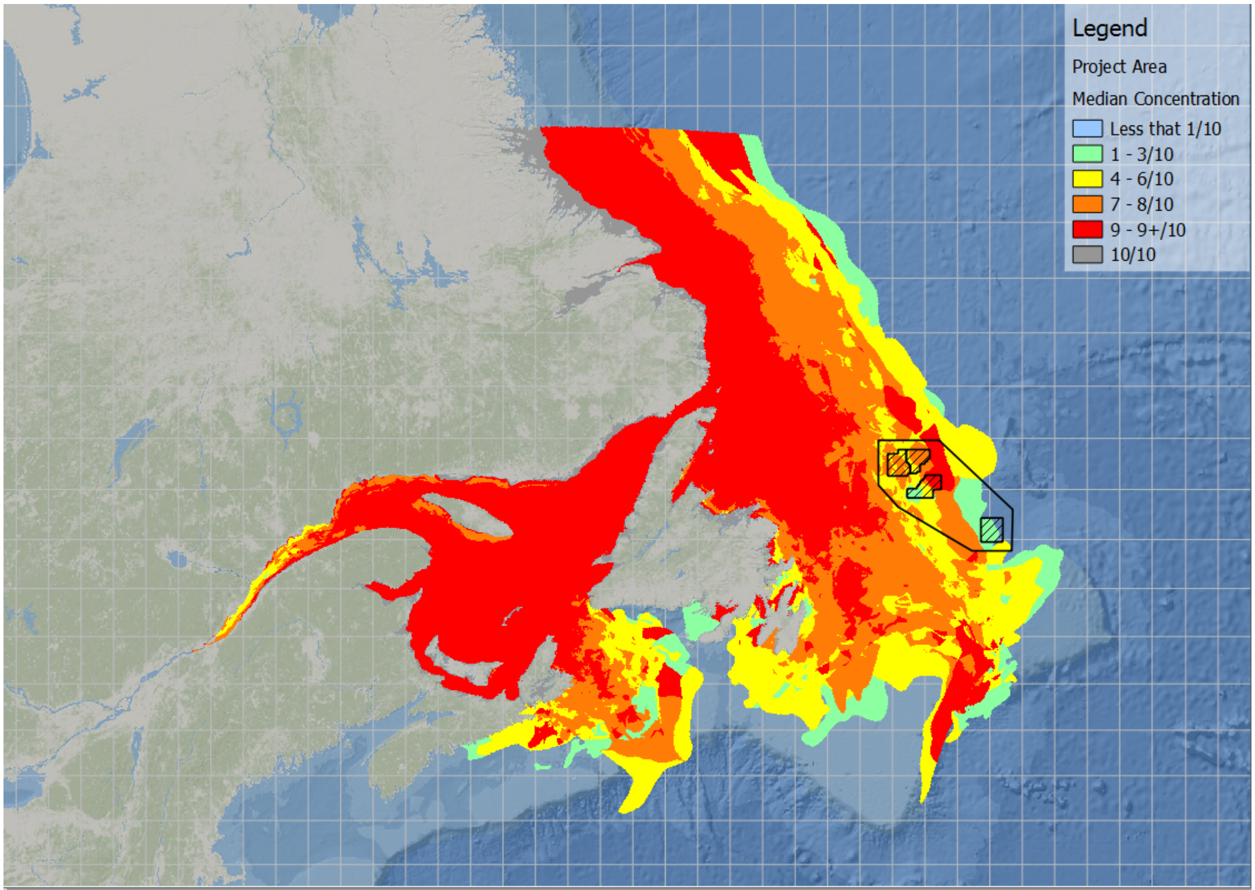

Figure 5.56 Median Concentration of Sea Ice in the Project Area for the Week of March 12 (1981 - 2010)

Regional Assessment Area

Results for the Regional Assessment Area are presented in Table 5.49 and Figure 5.57. The 30-year median concentration of sea ice reaches its maximum over the area the week of March 12, with 9.7% of the region covered in 7/10ths or greater sea ice.

Table 5.49 Median Concentration of Sea Ice within the Regional Assessment Area (1981 - 2010)

Date	Ice Free	1/10 - 3/10	4/10 - 6/10	7/10 - 8/10	9/10 - 9+/10	10/10	Total Ice
Nov 12	100.00	0.00	0.00	0.00	0.00	0.00	0.00
Nov 19	100.00	0.00	0.00	0.00	0.00	0.00	0.00
Nov 26	100.00	0.00	0.00	0.00	0.00	0.00	0.00
Dec 04	99.98	0.00	0.01	0.00	0.01	0.00	0.02
Dec 11	99.85	0.11	0.01	0.03	0.00	0.00	0.15
Dec 18	99.10	0.21	0.46	0.10	0.13	0.00	0.90

Date	Ice Free	1/10 - 3/10	4/10 - 6/10	7/10 - 8/10	9/10 - 9+/10	10/10	Total Ice
Dec 25	98.02	0.06	0.16	0.16	1.60	0.00	1.98
Jan 01	95.04	0.39	1.47	0.78	2.32	0.01	4.96
Jan 08	93.15	0.36	1.40	0.88	4.21	0.01	6.85
Jan 15	91.04	2.57	0.44	1.47	4.46	0.02	8.96
Jan 22	90.02	0.57	1.56	2.77	5.07	0.01	9.98
Jan 29	89.11	0.48	2.33	3.29	4.78	0.02	10.89
Feb 05	86.86	0.78	2.58	2.74	7.01	0.03	13.14
Feb 12	86.11	1.32	3.33	3.44	5.77	0.03	13.89
Feb 19	85.44	1.77	3.77	4.53	4.46	0.04	14.56
Feb 26	85.65	0.94	3.24	3.41	6.73	0.04	14.35
Mar 05	86.24	1.14	2.69	3.62	6.28	0.04	13.76
Mar 12	84.45	1.47	4.35	5.06	4.63	0.05	15.55
Mar 19	85.26	1.92	3.26	4.79	4.73	0.05	14.74
Mar 26	86.85	0.95	3.76	4.74	3.64	0.05	13.15
Apr 02	86.53	1.11	4.76	4.02	3.54	0.04	13.47
Apr 09	87.03	3.51	3.23	4.19	1.98	0.05	12.97
Apr 16	88.77	2.05	5.29	2.53	1.30	0.05	11.23
Apr 23	88.86	2.24	4.50	3.03	1.32	0.06	11.14
Apr 30	90.67	3.00	3.41	2.18	0.70	0.03	9.33
May 07	91.93	1.00	3.78	2.31	0.94	0.04	8.07
May 14	92.77	1.16	4.85	1.09	0.09	0.05	7.23
May 21	92.84	1.43	4.36	1.32	0.06	0.00	7.16
May 28	92.87	2.16	3.58	1.17	0.22	0.00	7.13
Jun 04	94.66	1.26	2.69	0.72	0.67	0.00	5.34
Jun 11	95.46	0.88	1.93	1.06	0.67	0.00	4.54
Jun 18	95.94	2.48	0.98	0.26	0.35	0.00	4.06
Jun 25	96.06	2.04	0.83	1.00	0.07	0.00	3.94
Jul 02	97.45	1.62	0.76	0.09	0.07	0.00	2.55
Jul 09	98.96	0.63	0.39	0.03	0.00	0.00	1.04
Jul 16	99.27	0.66	0.00	0.07	0.00	0.00	0.73
Jul 23	99.85	0.15	0.00	0.00	0.00	0.00	0.15
Jul 30	100.00	0.00	0.00	0.00	0.00	0.00	0.00
Aug 06	99.99	0.01	0.00	0.00	0.00	0.00	0.01
Aug 13	100.00	0.00	0.00	0.00	0.00	0.00	0.00
Aug 20	100.00	0.00	0.00	0.00	0.00	0.00	0.00
Aug 27	100.00	0.00	0.00	0.00	0.00	0.00	0.00

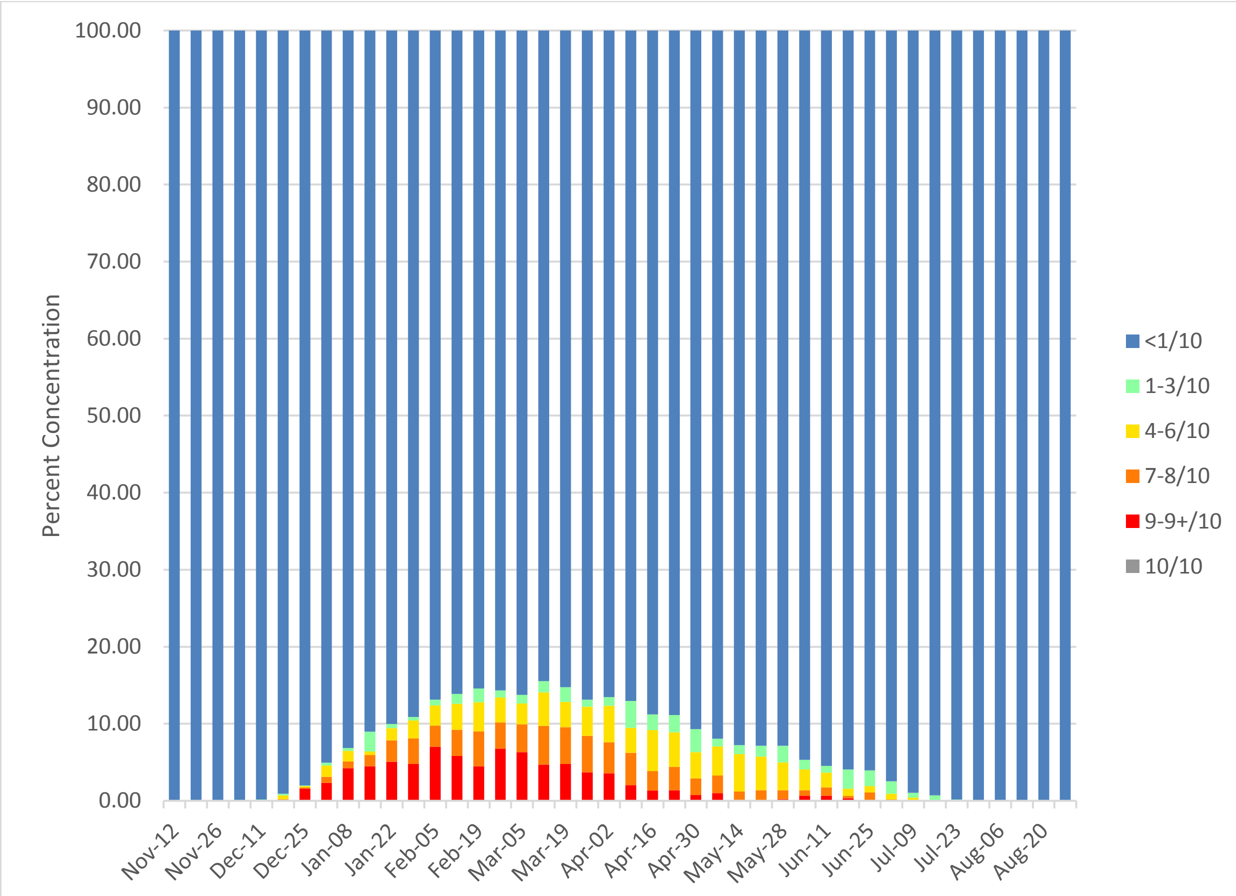

Figure 5.57 Plot of Median Concentration of Sea Ice with the Regional Assessment Area (1981 - 2010)

Marine Transportation Route Area

Results for the marine transportation route area are presented in Table 5.50 and Figure 5.58. The 30-year median concentration of shows that the week of February 19 has 45.8% of the area covered in 7/10ths ice.

Table 5.50 Median Concentration of Sea Ice within the Marine Transportation Route Area (1981 - 2010)

Date	Ice Free	1/10 - 3/10	4/10 - 6/10	7/10 - 8/10	9/10 - 9+/10	10/10	Total Ice
Nov 12	100.00	0.00	0.00	0.00	0.00	0.00	0.00
Nov 19	100.00	0.00	0.00	0.00	0.00	0.00	0.00
Nov 26	100.00	0.00	0.00	0.00	0.00	0.00	0.00
Dec 04	100.00	0.00	0.00	0.00	0.00	0.00	0.00
Dec 11	100.00	0.00	0.00	0.00	0.00	0.00	0.00
Dec 18	100.00	0.00	0.00	0.00	0.00	0.00	0.00
Dec 25	100.00	0.00	0.00	0.00	0.00	0.00	0.00

Date	Ice Free	1/10 - 3/10	4/10 - 6/10	7/10 - 8/10	9/10 - 9+/10	10/10	Total Ice
Jan 01	100.00	0.00	0.00	0.00	0.00	0.00	0.00
Jan 08	78.70	10.13	3.64	6.56	0.97	0.00	21.30
Jan 15	55.87	32.21	0.22	0.57	11.13	0.00	44.13
Jan 22	58.92	1.90	17.20	9.48	12.51	0.00	41.08
Jan 29	51.45	0.67	4.75	28.18	14.95	0.00	48.55
Feb 05	51.45	0.21	8.29	7.98	32.07	0.00	48.55
Feb 12	51.93	0.04	5.83	31.01	11.19	0.00	48.07
Feb 19	51.45	0.00	2.75	36.74	9.05	0.00	48.55
Feb 26	51.45	0.22	13.10	20.56	14.67	0.00	48.55
Mar 05	51.45	1.50	10.34	18.85	17.85	0.00	48.55
Mar 12	51.45	0.57	8.22	29.01	10.75	0.00	48.55
Mar 19	51.45	4.02	5.45	32.16	6.92	0.00	48.55
Mar 26	51.45	2.52	11.61	30.89	3.52	0.00	48.55
Apr 02	52.27	2.97	17.86	21.18	5.72	0.00	47.73
Apr 09	51.45	12.19	24.47	7.72	4.16	0.00	48.55
Apr 16	51.77	5.50	36.72	4.39	1.61	0.00	48.23
Apr 23	57.35	9.03	19.09	13.53	0.67	0.34	42.65
Apr 30	56.05	33.58	9.46	0.25	0.65	0.00	43.95
May 07	68.25	7.83	6.30	11.93	5.62	0.06	31.75
May 14	70.95	6.17	9.09	13.79	0.00	0.00	29.05
May 21	82.62	4.81	6.64	5.93	0.00	0.00	17.38
May 28	85.64	7.22	7.14	0.00	0.00	0.00	14.36
Jun 04	93.17	1.29	5.55	0.00	0.00	0.00	6.83
Jun 11	100.00	0.00	0.00	0.00	0.00	0.00	0.00
Jun 18	100.00	0.00	0.00	0.00	0.00	0.00	0.00
Jun 25	99.87	0.00	0.00	0.13	0.00	0.00	0.13
Jul 02	97.09	2.91	0.00	0.00	0.00	0.00	2.91
Jul 09	100.00	0.00	0.00	0.00	0.00	0.00	0.00
Jul 16	100.00	0.00	0.00	0.00	0.00	0.00	0.00
Jul 23	100.00	0.00	0.00	0.00	0.00	0.00	0.00
Jul 30	100.00	0.00	0.00	0.00	0.00	0.00	0.00
Aug 06	100.00	0.00	0.00	0.00	0.00	0.00	0.00
Aug 13	100.00	0.00	0.00	0.00	0.00	0.00	0.00
Aug 20	100.00	0.00	0.00	0.00	0.00	0.00	0.00
Aug 27	100.00	0.00	0.00	0.00	0.00	0.00	0.00

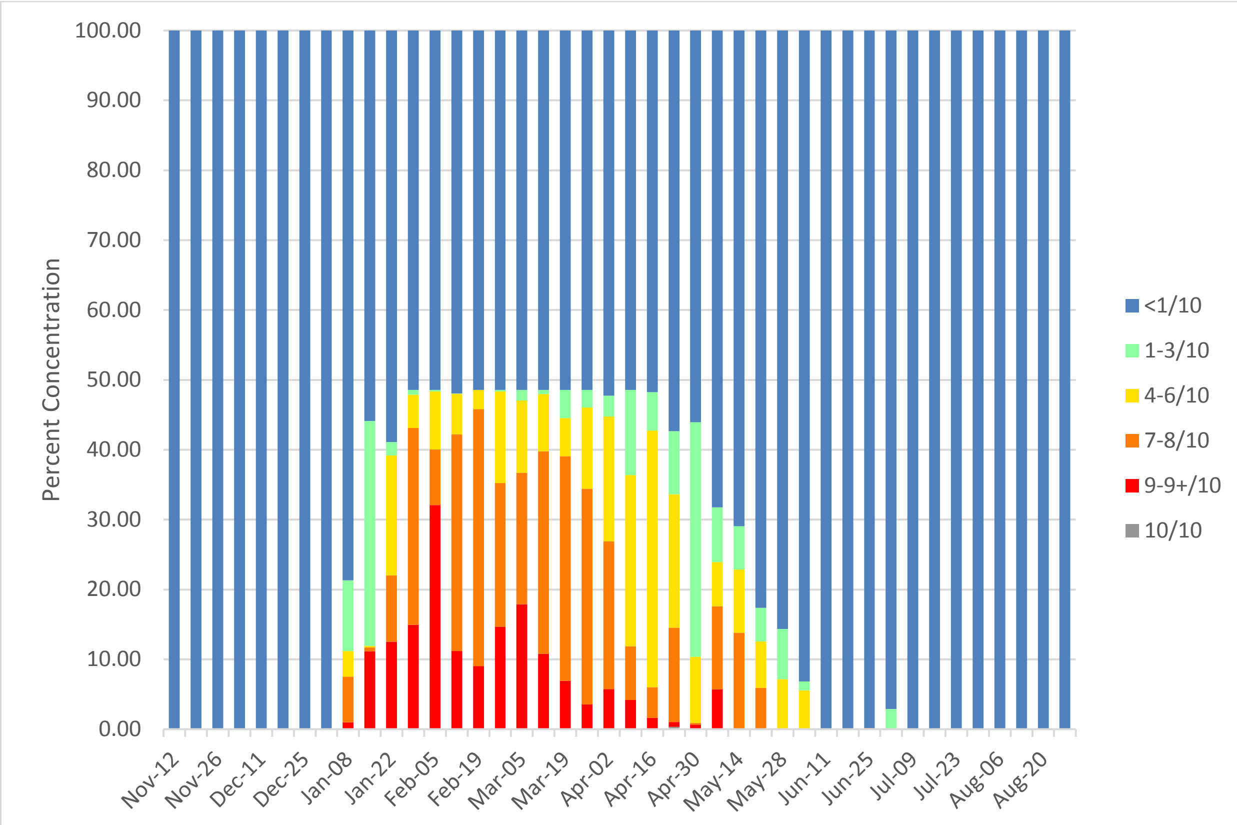

Figure 5.58 Plot of Median Concentration of Sea Ice with the Marine Transportation Route Area (1981 - 2010)

5.5.2 Icebergs

Glacial ice is formed from the accumulation of snow, which gradually changes form as it is compressed into a solid mass of large granular ice. This process produces a structure quite different from pack ice. The principal origins of the icebergs that reach the Project Area are the 100 tidewater glaciers of West Greenland. Between 10,000 and 15,000 icebergs are calved each year, primarily from 20 major glaciers between the Jacobshaven and Humboldt glaciers. These glaciers account for 85% of the icebergs that reach the Grand Banks. Of the remaining icebergs, 10% come from the East Greenland glaciers and 5% from the glaciers and ice shelves of Ellesmere Island.

The International Ice Patrol (IIP) Iceberg Sightings databasease from 1986-2015 was used in this analysis (National Snow and Ice Data Center 2015).

5.5.2.1 Iceberg Sightings

Overall there is a good distribution of iceberg sightings in the Project Area ranging from 286 in 2014 to none in other years (Figure 5.59). Monthly, icebergs were observed within the Project Area for each month of the year (Figure 5.60). The peak in iceberg sightings is between the months of March, April, and May with over 300 sightings within each month.

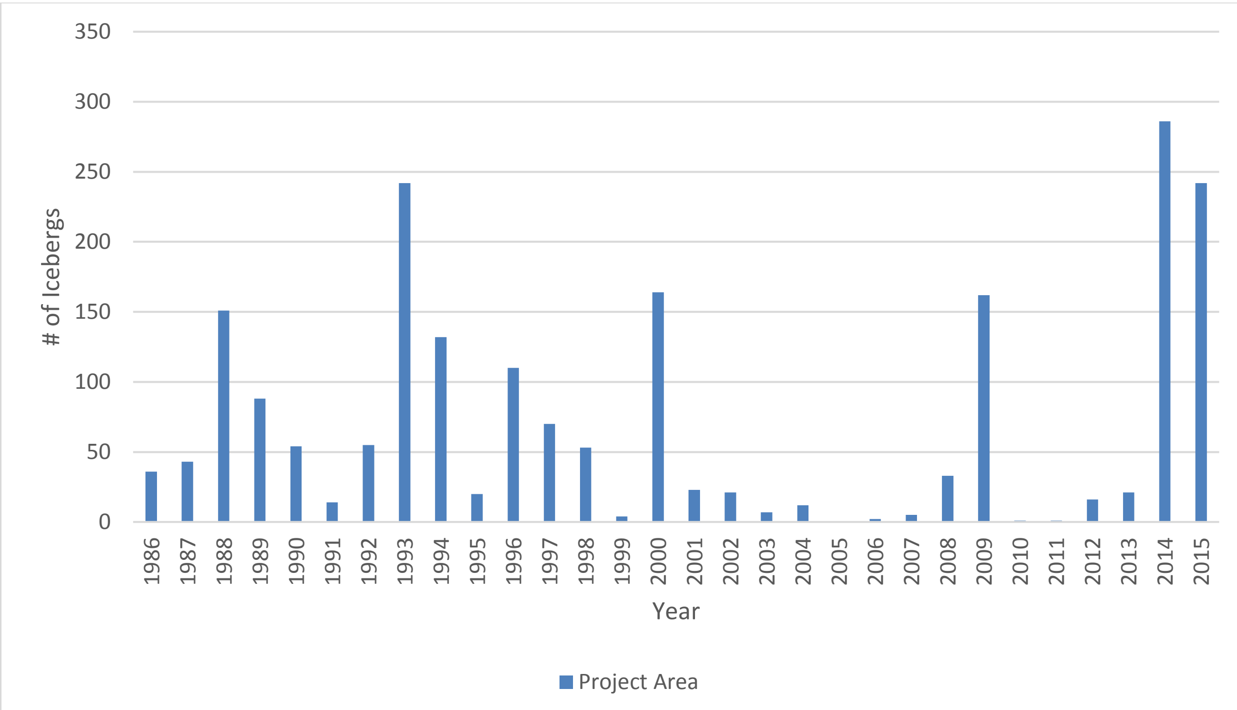

Source: National Snow and Ice Data Centre 2015

Figure 5.59 Number of Iceberg Sightings Annually within the Project Area

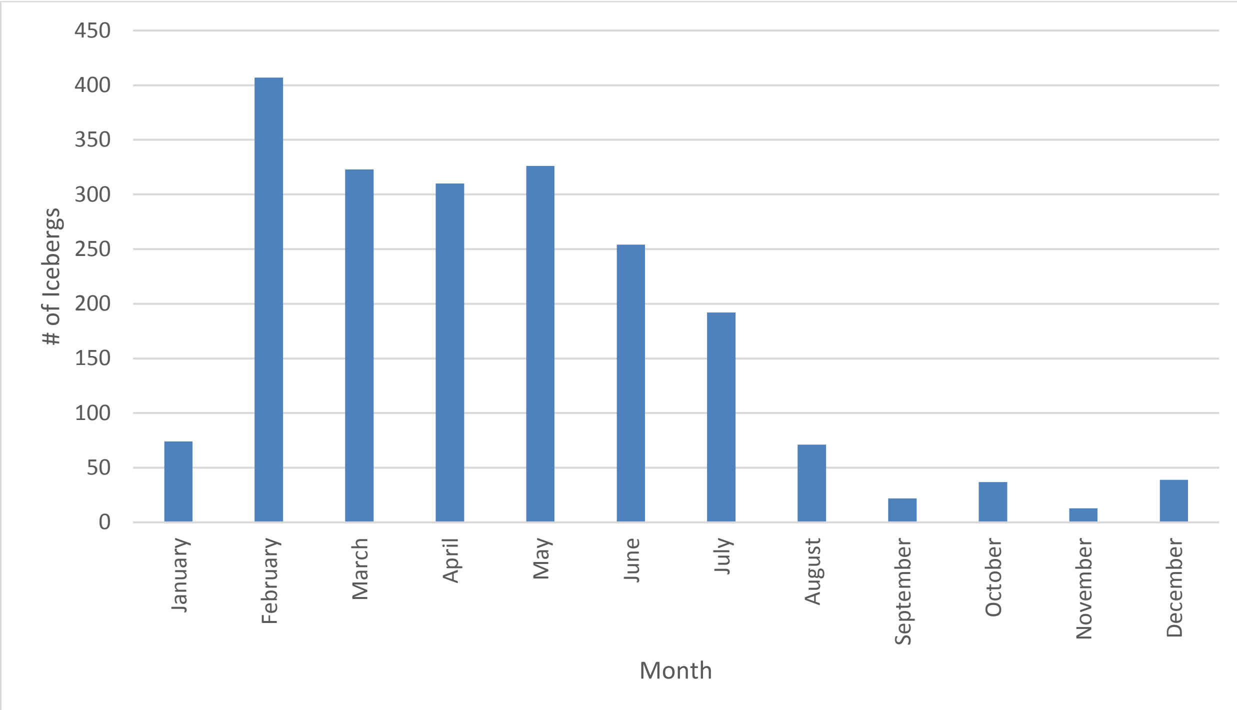

Source: IIP

Figure 5.60 Number of Iceberg Sightings Monthly within the Project Area

Figure 5.61 shows the positions of all icebergs within the Project Area from 1986-2015. Over the 30 years studied, there have been 2,068 icebergs sightings inside the Project Area. The highest number of icebergs on the field occurred in 2014 with 286 iceberg sightings. The second highest was in 1993 and 2015 when there were 242 icebergs sighted. The mean number of iceberg sightings within the Project Area is 71. Environmental factors such as iceberg concentration, ocean currents and wind determine how icebergs drift through the area.

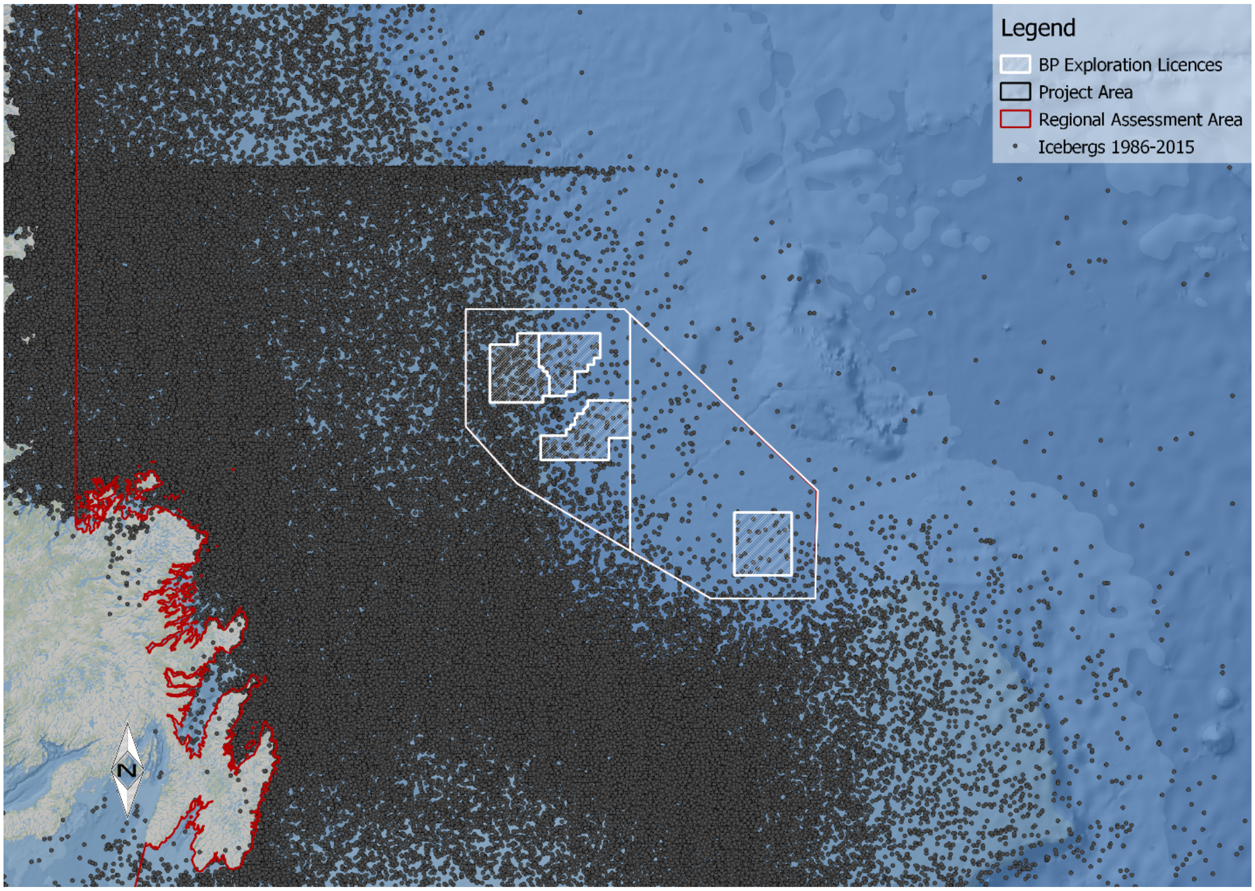

Source: from IIP data

Figure 5.61 Locations of Iceberg Sightings for 1986-2015

5.5.2.2 Iceberg Size

Icebergs are categorized by size, as defined in Table 5.51. These general size classifications have been in use for the past 30 years. However, the accuracy of size distributions extracted from the various databases may not be reliable, because most data are based on visual estimations and unspecified selection criteria.

Table 5.51 Iceberg Size

Category	Height (m)	Length (m)	Approx. Mass (T)
Very Large	> 75	>200	>10 Million
Large	46 -75	121 - 200	2 - 10 Million
Medium	16 - 45	61 - 120	100,000 - <2 Million
Small	5 - 15	15 - 60	100,000
Bergy Bit	1.0 - < 5	5 - <15	10,000
Growler	< 1.0	< 5	1,000
Source: MANICE (June 2005)			

A monthly analysis (Figure 5.62) shows that icebergs have been spotted within the Project Area from January to September and they are most prominent during the months of April and May. The most prominent icebergs are small, accounting for 26.1% of observed icebergs within the Project Area. Large icebergs occur 11.3% of the time and very large occur 0.8% of the time. 30.2% of the icebergs are classified as General. All iceberg reports were included in this analysis, regardless of the number of times they were reported.

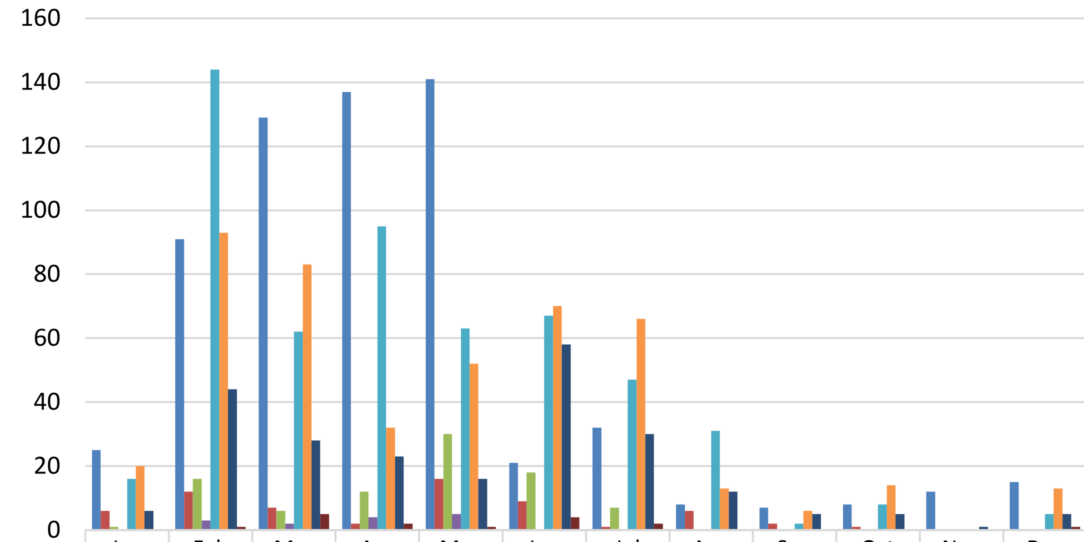

	Jan	Feb	Mar	Apr	May	Jun	Jul	Aug	Sep	Oct	Nov	Dec
General	25	91	129	137	141	21	32	8	7	8	12	15
Unidentified	6	12	7	2	16	9	1	6	2	1	0	0
Growler	1	16	6	12	30	18	7	0	0	0	0	0
Bergy Bit	0	3	2	4	5	0	0	0	0	0	0	0
Small	16	144	62	95	63	67	47	31	2	8	0	5
Medium	20	93	83	32	52	70	66	13	6	14	0	13
Large	6	44	28	23	16	58	30	12	5	5	1	5
Very Large	0	1	5	2	1	4	2	0	0	0	0	1

Source: IIP

Figure 5.62 Iceberg Size by Month within the Project Area

Figures 5.63 to 5.66 show the iceberg distribution along the East Coast for icebergs ranging from “small” to “very large”. The icebergs tend to follow the bathymetric contours and as a result, very few are found towards the East Orphan Basin portion of the Project Area.

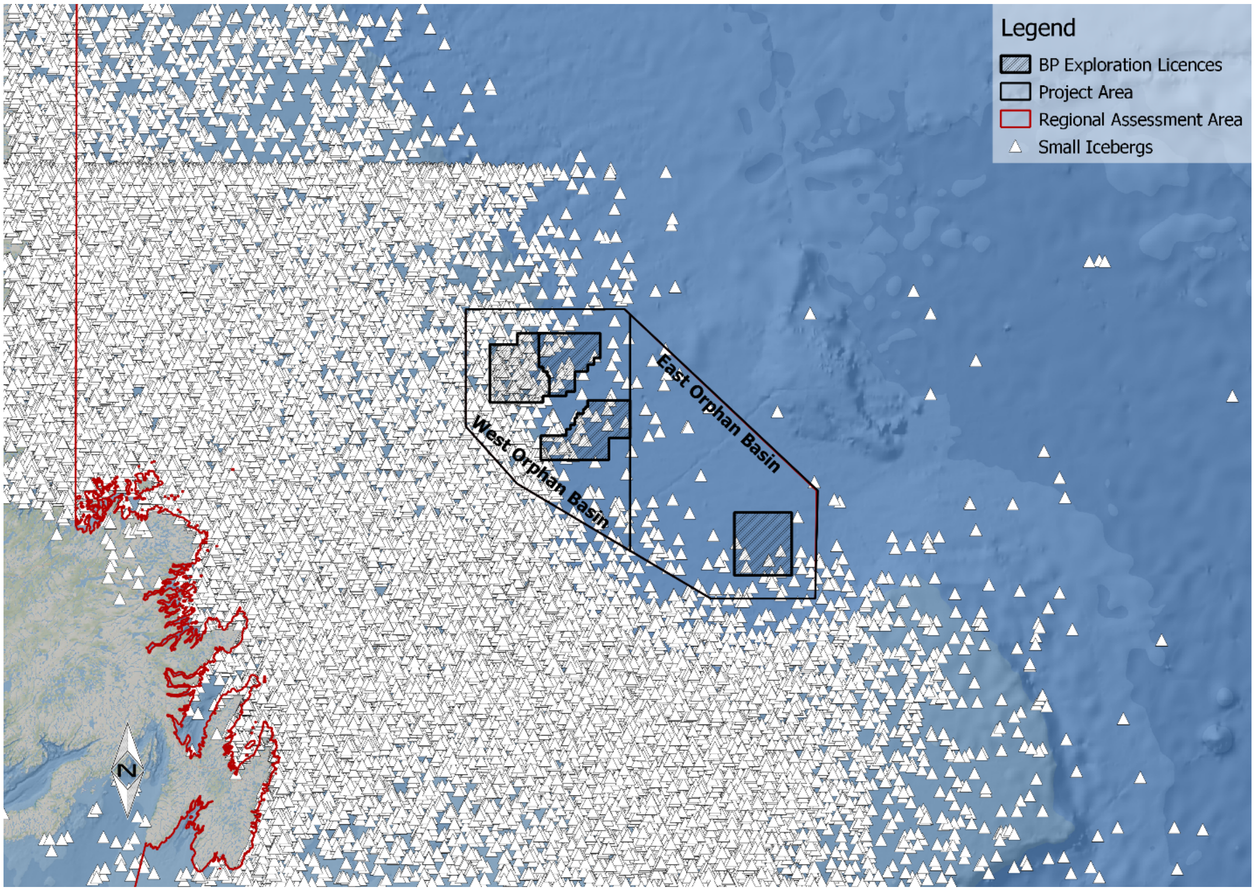

Source: IIP

Figure 5.63 Distribution of Small Icebergs (1986 - 2015)

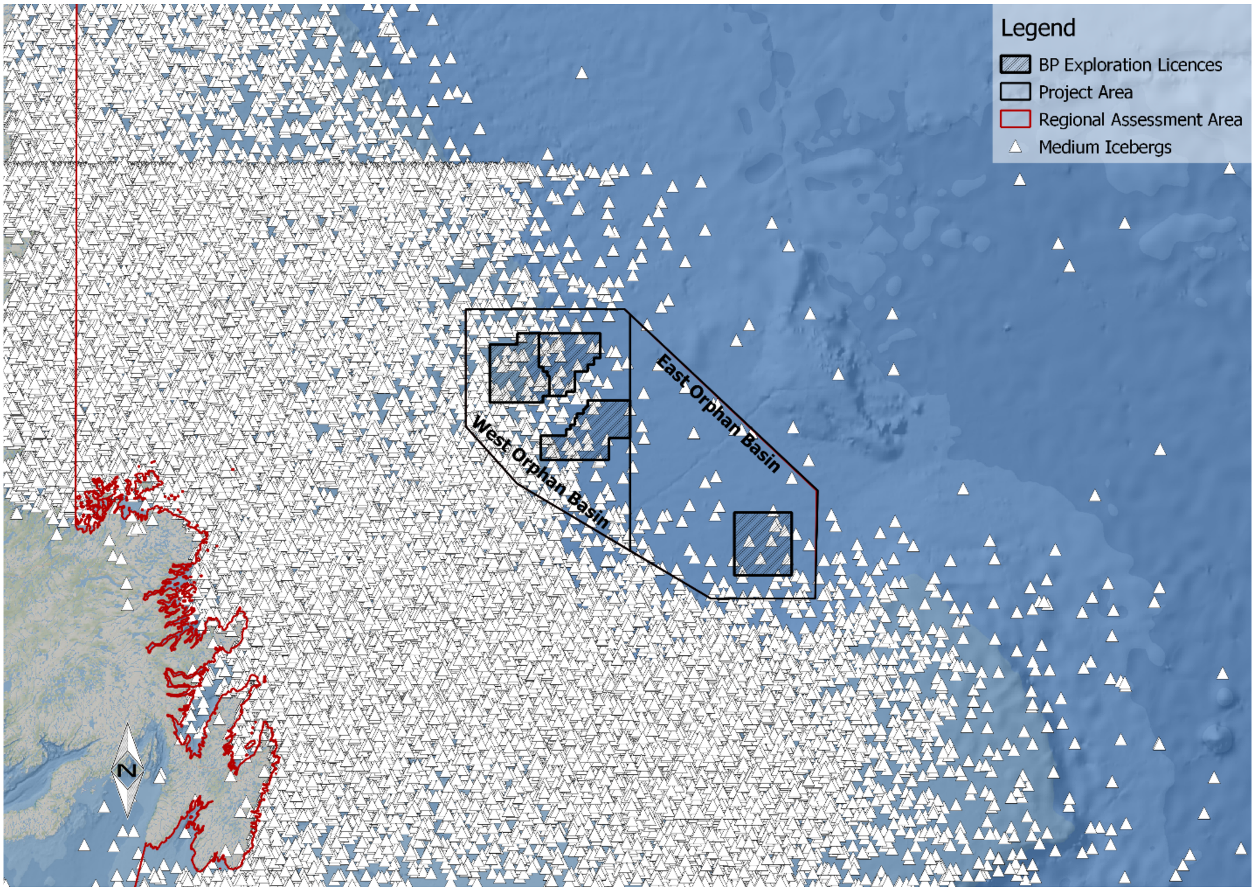

Source: IIP

Figure 5.64 Distribution of Medium Icebergs (1986 - 2015)

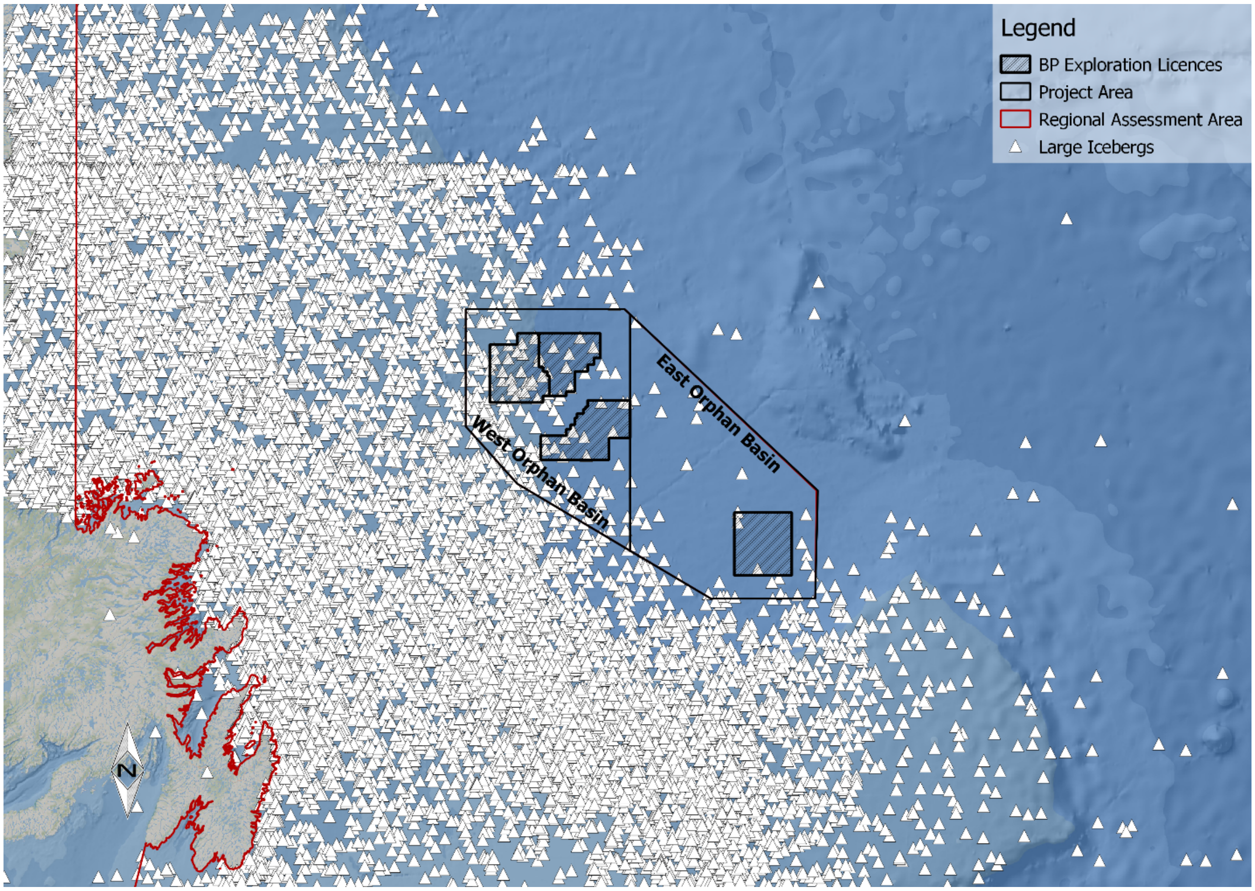

Source: IIP

Figure 5.65 Distribution of Large Icebergs (1986 - 2015)

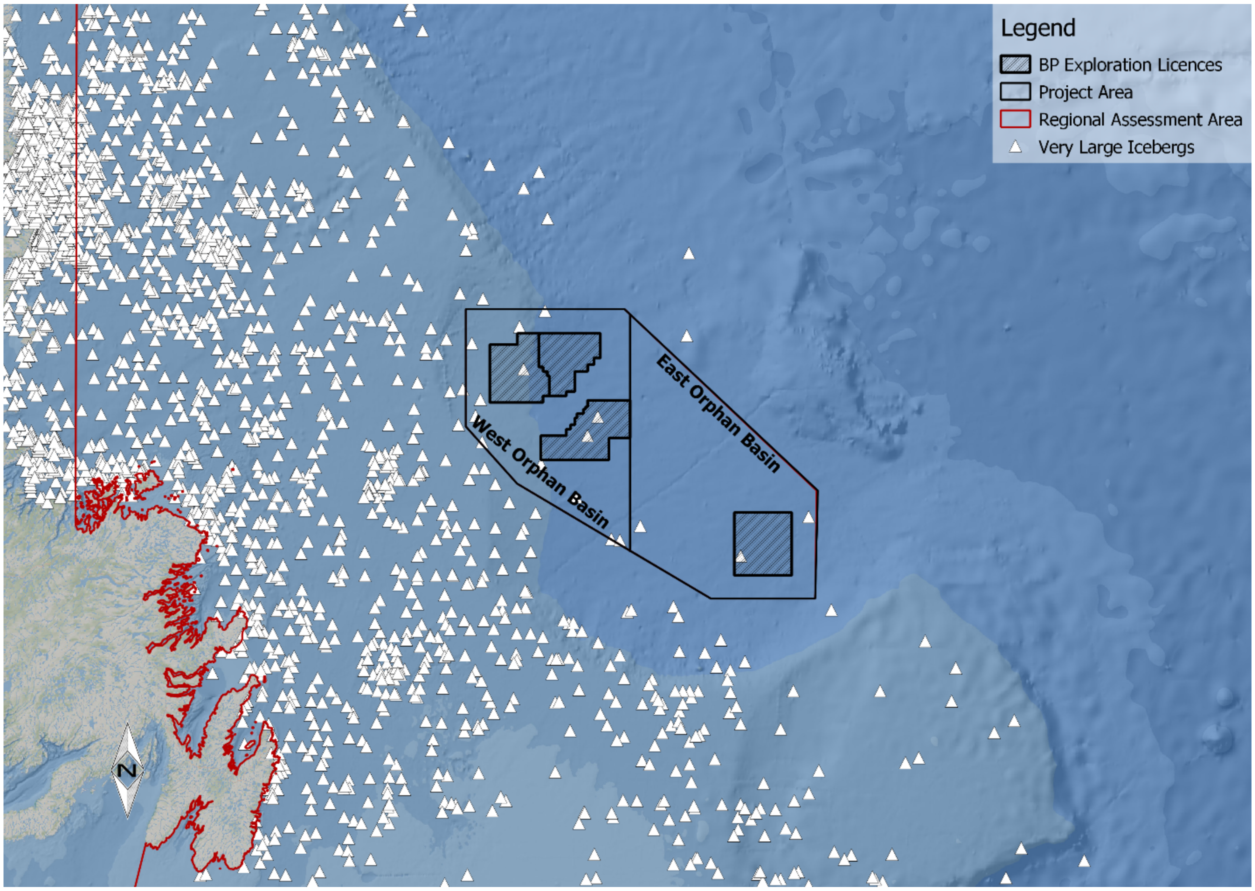

Source: IIP

Figure 5.66 Distribution of Very Large Icebergs (1960 - 2015)

5.5.3 Marine Icing

Spray icing can accumulate on vessels and shore structures when air temperatures are below the freezing temperature of water and there is potential for spray generation. In addition to air temperature, icing severity depends on water temperature, water salinity, wave conditions, and wind speed which influence the amount of spray and the cooling rate of droplets. A review of the spray icing hazard is provided by Minsk (1977). The frequency of potential icing conditions and its severity was estimated from the algorithm proposed by Overland et al. (1986) and subsequently updated by Overland (1990). Vessel icing rates for freezing spray forecasts are shown in Table 5.52. These rates and terminology are used when forecasting freezing spray on the Grand Banks.

Table 5.52 Intensity of Freezing Spray

Intensity Term	Icing Rate (cm per hour)
Light	less than 0.7 cm/hr
Moderate	0.7 to 2.0 cm/hr inclusive
Heavy	2.0 – 4.0 cm/hr
Extreme	greater than 4.0 cm/hr

Potential icing rates were computed using wind speed and air sea surface temperature observations from the ICOADS data set. Monthly, seasonal, and annual summaries are presented in Figures 5.67 and 5.68.

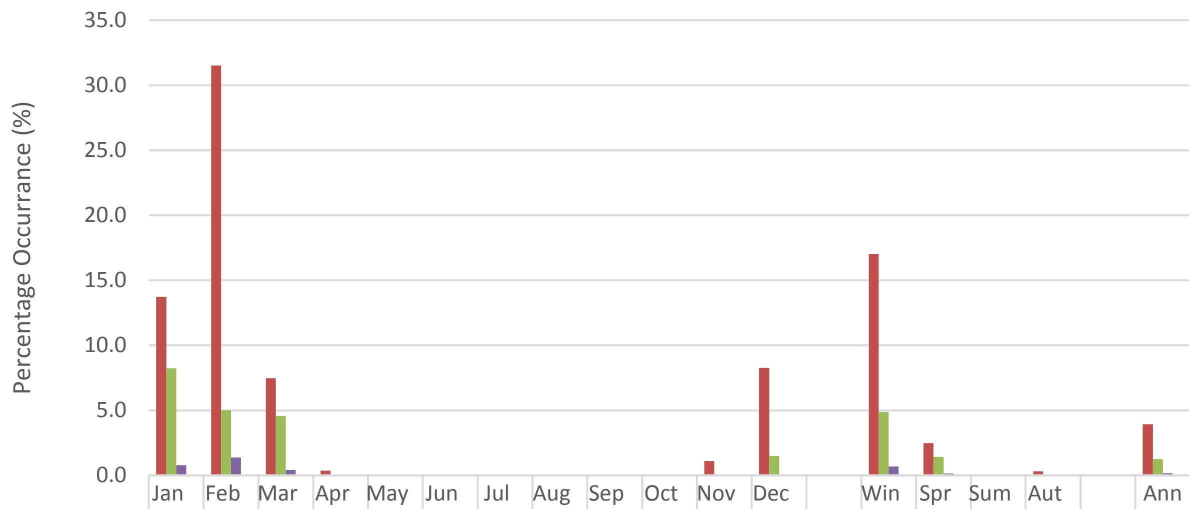

	Jan	Feb	Mar	Apr	May	Jun	Jul	Aug	Sep	Oct	Nov	Dec		Win	Spr	Sum	Aut		Ann
Light	13.7	31.5	7.5	0.4	0.0	0.0	0.0	0.0	0.0	0.0	1.1	8.3		17.0	2.5	0.0	0.3		3.9
Moderate	8.2	5.0	4.6	0.0	0.0	0.0	0.0	0.0	0.0	0.0	0.0	1.5		4.9	1.4	0.0	0.0		1.2
Heavy	0.8	1.4	0.4	0.0	0.0	0.0	0.0	0.0	0.0	0.0	0.0	0.0		0.7	0.1	0.0	0.0		0.2
Extreme	0.0	0.0	0.0	0.0	0.0	0.0	0.0	0.0	0.0	0.0	0.0	0.0		0.0	0.0	0.0	0.0		0.0

Figure 5.67 Frequency of Occurrence of Potential Spray Icing Conditions in the East Orphan Basin

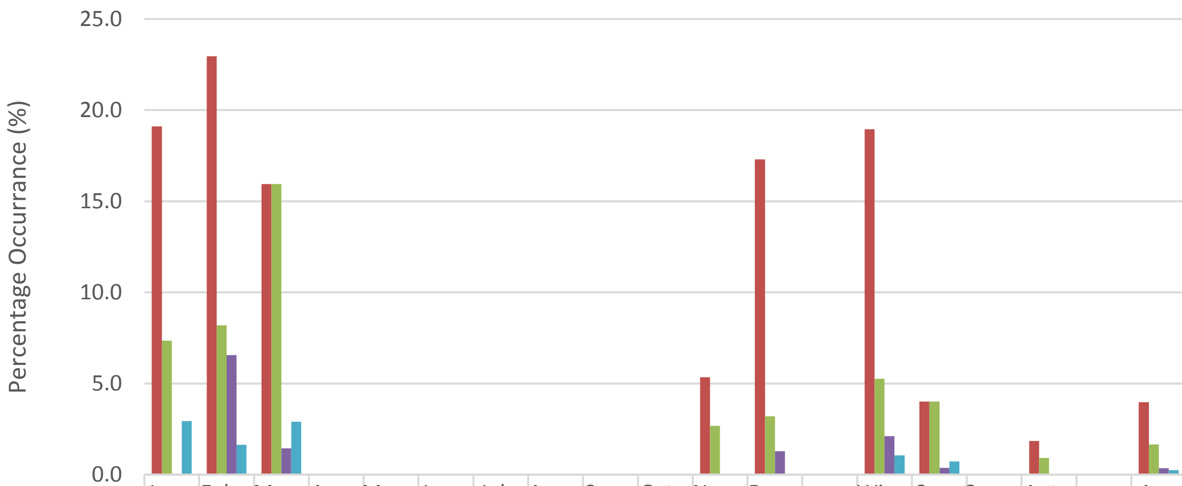

	Jan	Feb	Mar	Apr	May	Jun	Jul	Aug	Sep	Oct	Nov	Dec		Win	Spr	Sum	Aut		Ann
Light	19.1	23.0	15.9	0.0	0.0	0.0	0.0	0.0	0.0	0.0	5.3	17.3		18.9	4.0	0.0	1.8		4.0
Moderate	7.4	8.2	15.9	0.0	0.0	0.0	0.0	0.0	0.0	0.0	2.7	3.2		5.3	4.0	0.0	0.9		1.7
Heavy	0.0	6.6	1.4	0.0	0.0	0.0	0.0	0.0	0.0	0.0	0.0	1.3		2.1	0.4	0.0	0.0		0.4
Extreme	2.9	1.6	2.9	0.0	0.0	0.0	0.0	0.0	0.0	0.0	0.0	0.0		1.1	0.7	0.0	0.0		0.3

Figure 5.68 Frequency of Occurrence of Potential Spray Icing Conditions in the West Orphan Basin

Potential sea spray icing conditions start during the month of November with a frequency of icing potential of only 1.1% in the East Orphan Basin and 8% in the West Orphan Basin. As temperatures cool throughout the winter, the frequency of icing potential increases to a maximum in February. Extreme sea spray icing conditions were calculated to occur during the months of January through March in the West Orphan Basin only.

5.6 Climate Change

Climate conditions and climate change are presently the focus of much concern globally. While “climate” refers to average weather conditions over a 30-year period, “climate change” is an acknowledged change in climate that has been documented over two or more periods, each with a minimum of 30 years (Catto 2006). The Intergovernmental Panel on Climate Change (IPCC) defines climate change as a change in the state of the climate that can be identified (e.g., by using statistical tests) by changes in the mean and/or the variability of its properties and that persists for an extended period, typically decades or longer. Climate change may be due to natural internal processes or external forcings, or to persistent anthropogenic changes in the composition of the atmosphere or in land use (IPCC 2012). The temporal scope of the Project activities extend from 2020 to 2026, which is near term, and a relatively short timeframe. However, effects of climate change, including changing precipitation patterns, higher temperatures, more storm events, and increasing storm intensity are already being observed in current climate conditions and therefore must be taken into account for Project planning.

To assess the environmental effects of climate on the Project, current climate and climate change must both be considered. Current climate conditions are established by compiling relevant historical data and establishing a climatological background for the eastern Newfoundland offshore area (Section 5.3). Climate change effects projected over the life of the Project (2020 to 2026) are determined through review of climate modelling research.

Numerous climate-related conditions, linked primarily to global warming, have been observed across Atlantic Canada, the entire country, and globally. Evidence of climate change is being observed globally; climate warming has been demonstrated by observed increases in global average air and ocean temperatures, extensive melting snow and ice, and rising sea levels (IPCC 2007a, 2013).

Many researchers believe that changes to the climate regime will accelerate over the next century, as has been the case with global temperatures over the past two decades (IPCC 2007a, 2007b). Several changes have been projected to affect infrastructure in Atlantic Canada, including changing precipitation patterns, higher temperatures, more storm events, increasing storm intensity, and rising sea levels (Vasseur and Catto 2008).

Extreme environmental events associated with climate change must be taken into account in the design of marine structures, to ensure that the structural integrity can be maintained throughout the intended life of the structure (Vanem 2017).

Those most relevant climate-related changes to the Project can be broken down into two categories: i) atmospheric changes in temperature, precipitation patterns, wind and storms; and ii) oceanographic changes in ocean water temperature, waves, currents, sea level, sea ice, and icebergs.

5.6.1 Atmospheric Changes

5.6.1.1 Temperature

There are two atmospheric patterns that tend to influence the weather conditions in the area: the North Atlantic Oscillation (NAO) and the Atlantic Multidecadal Oscillation (AMO). The NAO results from the difference in atmospheric pressure between the Subtropical (Azores) High-pressure area and the Subpolar Low-pressure area (National Oceanic and Atmospheric Administration [NOAA] 2018). The AMO is a result of ongoing large-scale multidecadal fluctuations in sea surface temperature in the North Atlantic Ocean. Cool and warm phases can last for 20 to 40 years with differences in temperatures of approximately 0.6°C between extremes (NOAA 2005). In addition to these patterns, ocean currents in the Atlantic Ocean also influence the local meteorology and climate. These differences in pressures and temperatures and ocean currents are the primary drivers of the meteorological conditions experienced off the Northeast Newfoundland Slope in the East and West Orphan Basin. For further information on current climatology please see Section 5.3.

Air temperatures have been increasing over the last century on the east coast of Newfoundland and Labrador. The average warming over the 100-year period between 1900-2010 was 0.90±0.37°C and 0.75±0.34°C for coastal and Atlantic Ocean stations, respectively (Savard et al. 2016).

Temperatures for Newfoundland and Labrador are projected to increase by 1.6 to 3.8°C by 2050 (Savard et al. 2016) (Table 5.53), which is in line with projected increases presented in other studies (Finnis 2013; Galbraith and Larouche 2013), who concluded the increases in temperature are expected to be of higher magnitude in the winter than in summer and fall (Finnis 2013).

Table 5.53 Projected Change of Near-surface Air Temperature in the East Coast Canada Region for 30-year Period, Centered on 2020, 2050, and 2080, Relative to the 1970-2000 Period

Season	Change by 2020	Change by 2050	Change by 2080
Winter	1.4 to 2.2°C	2.5 to 3.8°C	3.4 to 5.0°C
Spring	0.8 to 1.5°C	1.6 to 2.7°C	2.2 to 4.1°C
Summer	0.9 to 1.6°C	1.7 to 2.7°C	2.2 to 3.8°C
Fall	1.1 to 1.6°C	1.9 to 2.8°C	2.3 to 4.1°C
Source: Savard et al. 2016			

5.6.1.2 Precipitation

Historical precipitation data may not demonstrate a distinct historical trend, as observed with temperature increases, but precipitation is expected to increase in winter and spring and remain stable or decrease slightly in summer and fall (Table 5.54) (Savard et al. 2016). Like temperature projections, mean precipitation rates for the region are expected to be highest in winter (Ouranos 2010). According to Finnis (2013), although snow is expected to continue as a common occurrence into the future, higher temperatures in the winter indicate more precipitation as rain than snow (Finnis 2013).

Table 5.54 Projected Precipitation in the East Coast Canada Region for 30-year Period, Centered on 2020, 2050, and 2080, Relative to the 1970-2000 Period

Season	Change by 2020	Change by 2050	Change by 2080
Winter	2.8 to 9.7%	6.5 to 15.4%	12.6 to 22.9%
Spring	0.3 to 8.1%	3.1 to 11.5%	8.8 to 18.5%
Summer	–1.9 to 5.2%	–1.4 to 5.7%	–4.0 to 7.1%
Fall	–2.8 to 3.6%	–2.0 to 7.1%	–0.9 to 10.1%
Source: Savard et al. 2016			

The effect of climate change on precipitation must also consider the expected increase in intensity and multi-day precipitation events. Because mean event intensity is expected to increase, the snow events that do occur are expected to be heavier on average. More intense snow events could have larger effects, than more frequent lighter events (Finnis 2013).

Projected increases in winter temperature and precipitation, would suggest that the proportion of winter precipitation falling as snow is likely to decrease, and freezing rain increase.

In eastern Newfoundland, freezing rain is mostly associated with southeast surface winds from the Atlantic, which form a warm layer above a shallow subfreezing layer over a cold surface (Stuart and Isaac 1999). Freezing rain and freezing drizzle, even at low intensities, can result in natural hazards that cause damage to infrastructure and be a hazard to transportation. Historically (1953-2007), eastern Newfoundland has the highest amount of freezing rain in all of Canada (Figure 5.69) (Cheng et al. 2011).

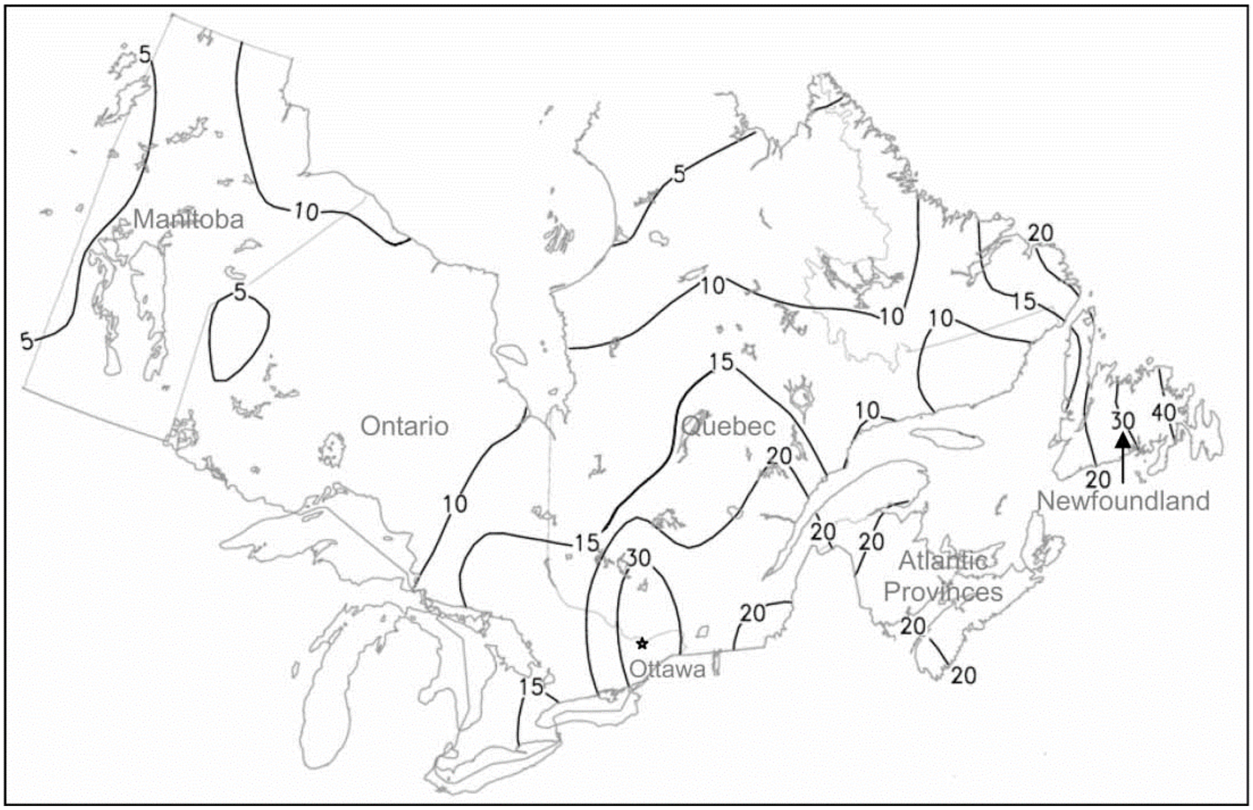

Source: Cheng et al. 2011

Figure 5.69 Approximate Contour Locations for Seasonal Total Freezing Rain Hours over Eastern Canada (October-May, 1953-2007)

5.6.1.3 Wind and Storms

Determining historical trends in wind velocity and direction are far more difficult than with previously discussed climate variables, because wind data sets are not as complete. Wind is affected by topography; any movement of the wind monitoring stations, or maintenance on equipment, would lead to substantive changes in the data that were not related to climate change (Savard et al. 2016).

The use of satellite data in the early 1960s has allowed for analysis of high wind events. Based on satellite observational data, over the 57-year period between 1961-2000, the Northwestern Atlantic Ocean was one of the stormiest areas in North America (Savard et al. 2016) (Figure 5.70).

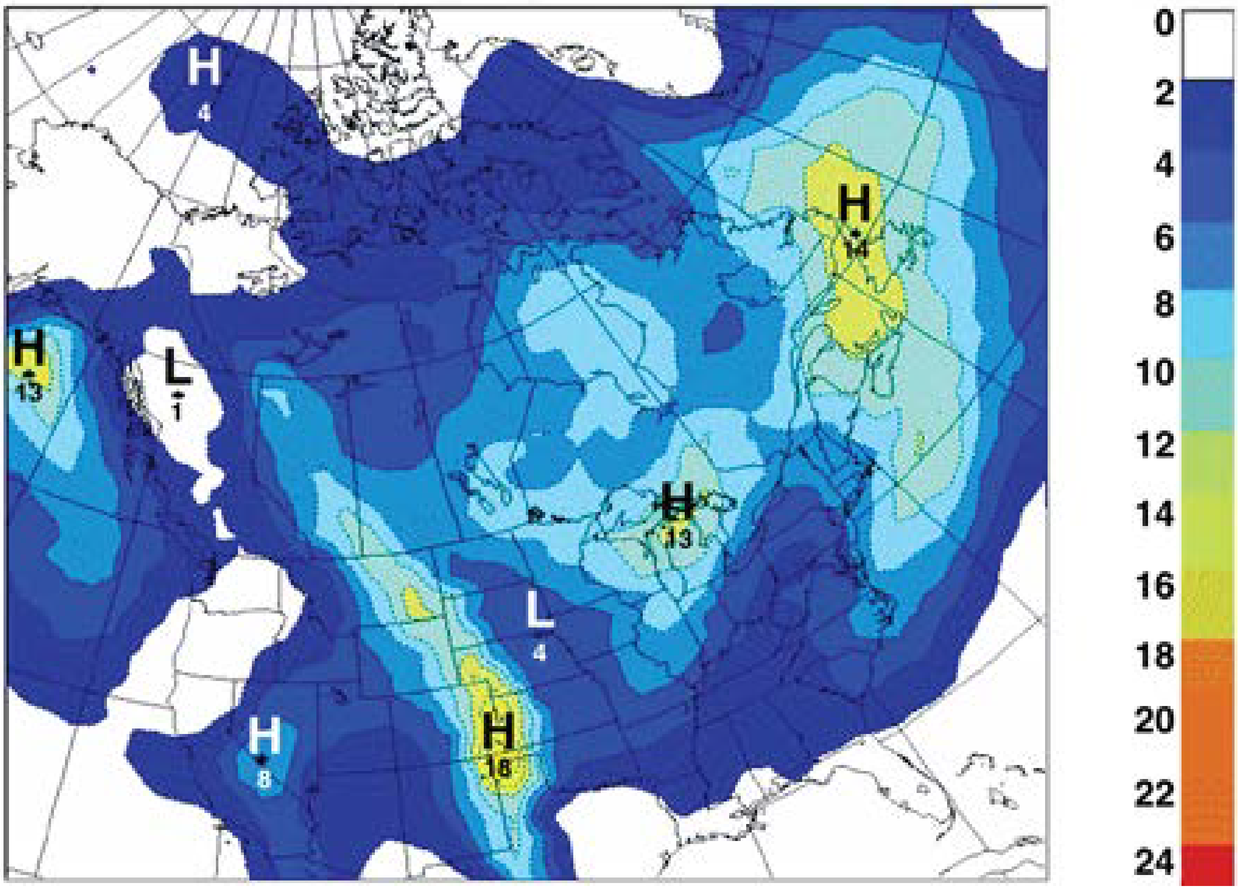

Source: Savard et al. 2016

Figure 5.70 Spatial Distribution of the Annual Average Density of Storm Tracks for the 1961-2000 Time Period

According to the IPCC (2012), climate change can lead to changes in the frequency, intensity, spatial extent, duration, and timing of extreme weather and climate events, and can result in unprecedented storms. Although substantial uncertainty, and thus low confidence, remains in projecting changes in storm frequency for the North Atlantic basin, according to the IPCC, analyses show the frequency of storms decreasing in projected climates, though the occurrence of strong storms may increase (Collin et al. 2013).

Recent climate change projections suggest that substantive changes in windspeed are unlikely because of climate warming (Salon et al. 2017). This agrees with a recent study (Amec Foster Wheeler 2017), where wind speeds, were projected to decrease slightly or remain unchanged, and mean monthly wind directions were not expected to change significantly from present conditions. However, climate change projections do suggest there will likely be northward shift in storm tracks that will affect storm frequency in the region (Salon et al. 2017).

Climate change affects storm surge, storm frequency, and intensity (Savard et al. 2016). Increased storm intensity may result in higher associated peak wave heights and more frequent occurrence of extreme wave or storm surge events; however, climate simulations for the next century show almost no change in peak significant wave heights for the western North Atlantic, consistent with recent trends in observed data (Husky Energy 2012).

Atlantic hurricanes are tropical storms, or cyclones, that form in the Atlantic Ocean near the Equator, usually in the summer or fall. Subjective measurements and variable procedures make existing tropical cyclone databases insufficiently reliable to detect trends in the frequency of extreme cyclones. Climate researchers are reanalyzing existing tropical cyclone datasets to mitigate the problems in applying the present observational tropical cyclone databases to trend analyses (Landsea et al. 2006). Although it seems warmer sea temperatures generate longer and more intense cyclones, scientists remain careful to link hurricanes and climate change (Ocean and Climate Platform 2018).

5.6.2 Oceanographic Changes

5.6.2.1 Ocean Water Temperatures

Ocean warming accounts for 90% of the energy accumulated between 1971 and 2010, with only approximately 1% stored in the atmosphere (IPCC 2014). Globally, ocean warming is largest near the surface, and the upper 75 m warmed by 0.11°C per decade over the period 1971 to 2010. While the IPCC (2014) is "virtually certain that the upper ocean (0-700 m) warmed from 1971 to 2010", it also suggests warming at this depth between 1870s and 1971 is also likely (IPCC 2014).

Based on recent regional downscaling results[1], the annual mean surface temperature will increase generally with time from 2011 to 2069; the surface temperature will increase 1.4°C, and the bottom will increase by 1.6°C. The linear rates are estimated to be approximately 0.023 ±0.002°C per year at the surface, and 0.023 ±0.001°C per year at the bottom, with the latter data set having much less inter-annual variability (Han et al. 2018).

5.6.2.2 Waves and Currents

Wave climate modelling is commonly being used in vulnerability assessments and the planning and design of offshore infrastructure project (Savard et al. 2016). According to Rhein et al. (2013), mean significant wave height has increased since the 1950s over much of the North Atlantic north of 45°N, with typical winter season trends of up to 20 cm per decade.

[1] Predicting climate change for a specific area using global data sets is problematic due to generic data and larger scale model outputs that do not take into account local climate. Accurate regional and local projections require the development of specific regional and local climate variables and climate change scenarios (Lines et al. 2005). As a result, regional downscaling techniques are used to introduce micro-scale interactions by including local climate variables. Downscaling techniques are particularly important for Atlantic Canada due to the inherent variability associated with this predominantly coastal climate. Statistical downscaling uses global climate model projections as well as historical data from weather stations across the region and studies the relationship between these sets of data. Downscaling produces more detailed predictions and has allowed for a better understanding of future climate scenarios based on precise and accurate historic data sets.

The wind, along with other forces (temperature, salinity differences), affect ocean currents. Ocean currents flow long distances in a manner similar to a conveyor belt that moves warm and cold water around the globe. As such, ocean currents play a key role in determining the climate of many regions.

Since climate change is warming the water of the Atlantic Ocean (Section 5.6.2.1), and warmer water is less likely to sink, it logically follows that climate change will have an effect on ocean currents. Although observations of ocean circulation are more limited than those of temperature, making predictions difficult and uncertain, there is growing evidence of variability and change of ocean current patterns related to climate (Rhein et al. 2013). The Labrador Current, for instance, has been observed to weaken in strength, but extend toward the equator for the period from 1992 to 2012 (Han et al. 2014).

5.6.2.3 Sea Level

Over the period 1901 to 2010, global mean sea level rose by 0.19 m, and the rate of sea level rise since the mid-19th century has been larger than the mean rate during the previous two millennia (IPCC 2014). The sea level has been slowly and steadily rising in most of Atlantic Canada for centuries due to crustal subsidence, warming trends, and the melting of polar ice caps (Government of Newfoundland and Labrador 2003).

In Atlantic Canada, particularly off the coast of Newfoundland, spatial differences in sinking land produce regional differences that global models do not consider (Savard et al. 2016). Recent regional downscaled results predict that sea level will rise by 0.11 m at the St. Johns tidal gauge station from 2011 to 2069 (Han et al. 2018).

5.6.2.4 Sea Ice

Climate change may affect ocean and ice conditions and thus have substantive effects on marine navigation and infrastructure (Han et al. 2018). Warmer average winter temperatures have decreased ice cover, thickness, and duration of the ice-covered season. Annual average sea ice cover in the east coast region has decreased by 1.53% per year over the period of 1998 to 2013 (Savard et al. 20126).

Sea ice cover is important as it stops wave formation, and thus the shortening of the ice cover season increases the energy of storm waves (Savard et al. 2016). Model simulations for the Gulf of St. Lawrence, comparing past (1982-2011) and future (2041-2070) conditions, suggest that sea ice cover will decrease by 36 days and the number of days the ice foot protects the coast line will decrease by an average of 33.4 days (Senneville et al. 2014).

5.6.2.5 Icebergs

Icebergs are a major hazard for shipping in the Northwest Atlantic, around the Grand Banks (Marsh et al. 2018). In April 2017, media outlets from around the globe reported unusually high number of icebergs (approximately 450) affecting the shipping lanes, causing inconvenience to ship navigation. In 2016, 687 icebergs were detected south of 48ºN on the Northern Grand Bank (0.1 SD below the 1981-2010 average of 767) (Coulbourne et al. 2017).

According to Bigg (2015), the number of icebergs vary immensely from year to year; while some years have recorded no icebergs passing across 48°N, other years recorded more than 1,000 icebergs. The largest number of icebergs between 1997 to and 2007 is 1,380 icebergs in 1998; however, since at the time the closest iceberg to the Hibernia platform was estimated 30 nautical miles north northwest, the presence of icebergs on the Grand Banks was not sufficient to effect drilling operations in the area (NRCan 2007).

Over the 10-year period between 1997 and 2007, the annual average iceberg count was 543 over this 10- year period and the annual mean was 553 icebergs. The monthly mean ranges from 8 (August) to 18 (February), to 71 (March) and 90 (June), with the highest averages in April (130) and May (143). During the main portion of the season from March to June, the median ranges from 31 (March) to 70 (April).

5.7 References

Amec (Amec Environment & Infrastructure). 2014. Eastern Newfoundland and Labrador Offshore Area Strategic Environmental Assessment Update. Submitted to Canada-Newfoundland and Labrador Offshore Petroleum Board, St. John's, NL.

Amec Foster Wheeler. 2017. ARP Pilot Area 4 Climatological Report: Port Hawkesbury and the Strait of Canso. Environment and Climate Change Canada.

Archer, C. and K. Caldeira. 2008. Historical trends in the jet streams. Geophysical. Research Letters, 35(L08803).

Bell, G. and M Chelliah. 2006. Leading Tropical Modes Associated with Interannual and Multidecadal Fluctuations in North Atlantic Hurricane Activity. Journal of Climate, 19: 590-612.

Bernier, N.B. and K.T. Thompson. 2006. Predicting the frequency of storm surges and extreme sea levels in the Northwest Atlantic. Journal of Geophysical Research, 111(C10009).

Bigg, G. 2015. Icebergs and the future. Pp. 220-236. In: G.R. Bigg (ed.). Icebergs: Their Science and Links to Global Change, Cambridge: Cambridge University Press. doi:10.1017/CBO9781107589278.011

Borgman, L.E. 1973. Probabilities for highest wave in hurricane, J. Waterways, Harbors and Coastal Engineering, ASCE 99 (WW2), 185-207.

Cameron, G.D.M. and M.A. Best. 1985. Surface Features of the Continental Margin of Eastern Canada. Map compilation for the Atlantic. Geoscience Centre, Bedford Institute of Oceanography.

Campbell, D.C. 2005. Major Quaternary Mass-transport Deposits in Southern Orphan Basin, Offshore Newfoundland and Labrador. GSC Current Research 2005-D3: 10 pp. Available at: https://www.researchgate.net/publication/234036596_Major_Quaternary_mass-transport_deposits_in_southern_Orphan_Basin_offshore_Newfoundland_and_Labrador.

Carnes, M.R. 2009. Description and Evaluation of GDEM-V 3.0. Document Number NRL Memorandum Report 7330-09-9165. US Naval Research Laboratory, Stennis Space Center, MS. 21 pp.

Catto, N.R. 2006. Impacts of Climate Change and Variation on the Natural Areas of Newfoundland and Labrador. Newfoundland and Labrador Department of Environment and Conservation, St. John's NL. 160 pp.

CBC. 2018. 4.2 Magnitude Earthquake Recorded off Newfoundland Coast. Available at: https://www.cbc.ca/news/canada/newfoundland-labrador/earthquake-off-bonavista-1.4808601

Cheng, C.S., Guilong L. and H. Auld. 2011. Possible Impacts of Climate Change on Freezing Rain Using Downscaled Future Climate Scenarios: Updated for Eastern Canada, Atmosphere-Ocean, 49:1, 8-21, DOI: 10.1080/07055900.2011.555728. Available at: https://doi.org/10.1080/07055900.2011.555728

Colbourne, E. 2000. Interannual variations in the stratification and transport of the Labrador Current on the Newfoundland Shelf. Northwest Atlantic Fisheries Centre, International Council for the Exploration of the Sea. Department of Fisheries and Oceans.

Colbourne, E.B. and K.D. Foote. 2000. Variabiliy of the stratification and circulation on the Flemish Cap during the decades of the 1950's - 1990's. Journal of Northwest Atlantic Fishery Science, 26: 103-122.

Colbourne, E., J. Holden, S. Snook, G. Han, S. Lewis, D. Senciall, W. Bailey, J. Higdon and N. Chen. 2017. Physical oceanographic conditions on the Newfoundland and Labrador Shelf during 2016 - Erratum. DFO Can. Sci. Advis. Sec. Res. Doc., 2017/079: v + 50 pp. Available at: http://www.dfo-mpo.gc.ca/csas-sccs/Publications/ResDocs-DocRech/2017/2017_079-eng.pdf

Collins, M., R. Knutti, J. Arblaster, J.-L. Dufresne, T. Fichefet, P. Friedlingstein, X. Gao, W.J. Gutowski, T. Johns, G. Krinner, M. Shongwe, C. Tebaldi, A.J. Weaver and M. Wehner, 2013: Long-term Climate Change: Projections, Commitments and Irreversibility. In: Climate Change 2013: The Physical Science Basis. Contribution of Working Group I to the Fifth Assessment Report of the Intergovernmental Panel on Climate Change [Stocker, T.F., D. Qin, G.-K. Plattner, M. Tignor, S.K. Allen, J. Boschung, A. Nauels, Y. Xia, V. Bex and P.M. Midgley (eds.)]. Cambridge University Press, Cambridge, United Kingdom and New York, NY, USA.

Dafoe, L.T., C.E. Keen, G.L. Williams and S.A. Dehler. 2013. A tectonostratigraphic history of Orphan Basin, offshore Newfoundland, Canada. GeoConvention 2013: Integration. 6 pp.

Dragoset, W.H. 1984. A comprehensive method for evaluating the design of airguns and airgun arrays. Pp. 75-84. In: Proceedings, 16th Annual Offshore Technology Conference Volume 3, May 7-9, 1984. OTC 4747, Houston, TX.

Edinger, E.N., O.A. Sherwood, D.J.W. Piper, V.E. Wareham, K.D. Baker, K.D. Gilkinson and D.B. Scott. 2011. Geological features supporting deep-sea coral habitat in Atlantic Canada. Continental Shelf Research, 31:569-584.

Enachescu, M.E., 2004, Conspicuous submarine mounds in the north-eastern Orphan Basin and on the Orphan Knoll, offshore Newfoundland: The Leading Edge, 23 , 1290-1294.

Enachescu, M. 2006. Structural Setting and Petroleum Potential of the Orphan Basin, offshore Newfoundland and Labrador. CSEG Recorder, 31(2). Available at: https://csegrecorder.com/articles/view/structural-setting-and-petroleum-potential-of-orphan-basin-offshore-nfld.

Enachescu, M., S. Kearsey, V. Hardy, J.-C. Sibuet, J. Hogg, S.P. Srivastava, A. Fagan, T. Thompson and R. Ferguson. 2005. Evolution and Petroleum Potential of Orphan Basin, Offshore Newfoundland, and Its Relation to the Movement and Rotation of Flemish Cap based on Plate Kinematics of the North Atlantic. Gulf Coast Section Society for Sedimentary Geology, Pp: 75-131. Conference Paper: Petroleum Systems of Divergent Continental Margin Basins, 25th Annual GCSSEPM Foundation - Bob F. Perkins Research Conference, Houston, TX. DOI: 10.5724/gcs.05.25.0075.

ECCC (Environment and Climate Change Canada). 2016. Lightning Activity in Canadian cities. Available at: https://www.canada.ca/en/environment-climate-change/services/lightning/statistics/activity-canadian-cities.html

ECCC (Environment and Climate Change Canada). 2017. Greenhouse Gas Reporting Program data search. Available at: https://climate-change.canada.ca/facility-emissions/

ECCC (Environment and Climate Change Canada). 2018a. National Pollutant Release Inventory (NPRI) Data Search. Available at: https://pollution-waste.canada.ca/national-release-inventory/archives/index.cfm?do=query&lang=en. Data as of June 14, 2018.

ECCC (Environment and Climate Change Canada). 2018b. Environment and Climate Change Canada - Weather and Meteorology - Ice Glossary. Retrieved from Environment and Climate Change Canada: https://www.ec.gc.ca/glaces-ice/default.asp?lang=En&n=501D72C1-1&def=hide1B6894C57

Etter, P.C. 1996. Underwater Acoustic Modeling - Principles, Techniques, and Applications. Second edition. E & FN Spon, London, UK. 344 pp.

ExxonMobil (ExxonMobil Canada Properties). 2011. Hebron Project Comprehensive Study Report. Submitted to the Canada-Newfoundland and Labrador Offshore Petroleum Board, St. John's, NL.

Fader, G.B., G.D.M. Cameron and M.A. Best. 1989. Geology of the Continental Margin of Eastern Canada, Geological Survey of Canada. Map 1705A.

Finnis, J. 2013. Projected Impacts of Climate Change for the Province of Newfoundland and Labrador, Report prepared for the Office of Climate Change, Energy Efficiency and Emissions Trading, St John's, NL, 134 pp. Available at: http://www.turnbackthetide.ca/tools-and-resources/whatsnew/2013/climate_projections.pdf

Fissel, D.B. and D.D. Lemon. 1991. Analysis of the physical oceanographic data from the Labrador Shelf, summer 1980. Canadian Contractor Report of Hydrography and Ocean Sciences, No. 39.

Forristall, G.Z. 1978, On the statistical distribution of wave heights in a storm, J. Geophys. Res., 83, 2353-2358.

François, R.E. and G.R. Garrison. 1982a. Sound absorption based on ocean measurements: Part II: Boric acid contribution and equation for total absorption. Journal of the Acoustical Society of America 72(6): 1879-1890.

François, R.E. and G.R. Garrison. 1982b. Sound absorption based on ocean measurements: Part I: Pure water and magnesium sulfate contributions. Journal of the Acoustical Society of America 72(3): 896-907.

Freeman, E., S.D. Woodruff, S.J. Worley, S.J. Lubker, E.C, Kent, W.E. Angel, D.I. Berry, P. Brohan, R. Eastman, L. Gates, W. Gloeden, Z. Ji. J. Lawrimore, N.A. Rayner, G. Rosenhagen and S.R. Smith. 2017. ICOADS Release 3.0: A major update to the historical marine climate record. International Journal of Climatology (CLIMAR_IV Special Issue), 37, 2211-2237. doi:doi:10.1002/joc.4775

Galbraith, P.S. and P. Larouche. 2013. Trends and variability in air and sea surface temperatures in eastern Canada; Pp. 1-18. In: J.W. Loder, G. Han, P.S. Galbraith, J. Chassé, and A. van der Baaren (eds.). Aspects of Climate Change in the Northwest Atlantic off Canada, Can. Tech. Rep. Fish. Aquat. Sci., 3045: 190 pp. Available at: http://publications.gc.ca/collections/collection_2014/mpo-dfo/Fs97-6-3045-eng.pdf

Government of Newfoundland and Labrador. 2003. Newfoundland and Labrador Climate Change Discussion Paper, Department of the Environment. 28 pp. Available at: http://www.env.gov.nl.ca/env/Env/PollPrev/pdf/climatechange_paper.pdf

Greenan, B.J.W, I. Yashaysey, E. Head, W. Harrison, K. Azetsu-Scott, W.K.W. Li, J.W. Loder and Y. Geshlin, Y. 2010. Interdisciplinary oceanographic observation of Orphan Knoll. NAFO SCR Doc 10/19: 32 pp.

Han, G. and J. Li. 2004. Sea surface height and current variability on the Newfoundland Slope from TOPES/Poseidon Altimetry. Canadian Technical Report of Hydrography and Ocean Sciences, 234.

Han, G. and C.L. Tang. 1999. Velocity and transport of the Labrador Current determined from altimetric, hydrographic and wind data. Journal of Geophysical Research, 104: 18.

Han, G., N. Chen and Z. Ma. 2014. Is there a north-south phase shift in the surface Labrador Current on the interannual-todecadal scale, J. Geophys. Res. Oceans, 119: 276-287, doi:10.1002/2013JC009102. Available at; https://agupubs.onlinelibrary.wiley.com/doi/pdf/ 10.1002/2013JC009102

Han, G., Z. Ma, Z. Long, W. Perrie and J. Chassé. 2018: Climate Change on Newfoundland and Labrador Shelves: Results from a Regional Downscaled Ocean and Sea-Ice Model Under an A1B Forcing Scenario 2011–2069, Atmosphere-Ocean, DOI: 10.1080/07055900.2017.1417110. Available at: https://www.tandfonline.com/doi/pdf/10.1080/07055900.2017.1417110?needAccess=true

Hart, R. and J. Evans. 2001. A Climatology of extratropical transition of Atlantic tropical cyclones. Journal of Climate, 14: 546-564.

Husky Energy. 2012. Husky Energy White Rose Extension Project Environmental Assessment. Prepared by Stantec Consulting Ltd., St. John's, NL for Husky Energy, St. John's, NL.

IPCC (Intergovernmental Panel on Climate Change). 2007a. Climate Change 2007a: The Physical Science Basis, Summary for Policymakers. Contribution of Working Group I to the Fourth Assessment Report of the Intergovernmental Panel on Climate Change, IPCC Secretariat, Geneva, 21p. Available at: https://www.ipcc.ch/pdf/assessment-report/ar4/wg1/ar4-wg1-spm.pdf

IPCC (Intergovernmental Panel on Climate Change). 2007b. Appendix I: Glossary. Pp. 869-883. In: M.I. Parry, O.F. Canziani, J.P. Palutidof, P.J. van der Linden and C.E. Hanson (eds.). Climate Change 2007: Impacts, Adaptation and Vulnerability (Contribution of Working Group II to the Fourth Assessment Report of the Intergovernmental Panel on Climate Change), Cambridge University Press, Cambridge United Kingdom. Available at: http://www.ipcc.ch/pdf/assessment-report/ar4/wg2/ar4-wg2-app.pdf

IPCC (Intergovernmental Panel on Climate Change). 2012. Summary for Policymakers. Pp. 1-19. In: C.B. Field, V. Barros, T.F. Stocker, D. Qin, D.J. Dokken, K.L. Ebi, M.D. Mastrandrea, K.J. Mach, G.-K. Plattner, S.K. Allen, M. Tignor, and P.M. Midgley (eds.). Managing the Risks of Extreme Events and Disasters to Advance Climate Change Adaptation: A Special Report of Working Groups I and II of the Intergovernmental Panel on Climate Change. Cambridge University Press, Cambridge, UK, and New York, NY.

IPCC (Intergovernmental Panel on Climate Change). 2013. Climate Change 2013: The Physical Science Basis. Contribution of Working Group I to the Fifth Assessment Report of the Intergovernmental Panel on Climate Change [Stocker, T.F., D. Qin, G.-K. Plattner, M. Tignor, S.K. Allen, J. Boschung, A. Nauels, Y. Xia, V. Bex and P.M. Midgley (eds.)]. Cambridge University Press, Cambridge, United Kingdom and New York, NY, USA, 1535 pp. Available at: https://www.ipcc.ch/pdf/assessment-report/ar5/wg1/WG1AR5_Frontmatter_FINAL.pdf

IPCC (Intergovernmental Panel on Climate Change). 2014. Climate Change 2014: Synthesis Report. Contribution of Working Groups I, II and III to the Fifth Assessment Report of the Intergovernmental Panel on Climate Change [Core Writing Team, R.K. Pachauri and L.A. Meyer (eds.)]. IPCC, Geneva, Switzerland, 151 pp. Available at: http://ar5-syr.ipcc.ch/ipcc/ipcc/resources/pdf/IPCC_SynthesisReport.pdf

Jensen, F.B., W.A. Kuperman, M.B. Porter, and H. Schmidt. 2011. Computational Ocean Acoustics. 2nd edition. AIP Series in Modern Acoustics and Signal Processing. AIP Press - Springer, New York. 794 pp.

Kent, E., P. Taylor, B. Truscott and J. Hopkins. 1993. The Accuracy of Voluntary Observing Ships' Meteorological Observations – Results of the VSOP-NA. Journal of Atmospheric Oceanic Technology, 10: 591-608.

King, L.H., G.B.J. Fader, W.A.M. Jenkins, and E.L. King. 1986. Occurrence and regional geological setting of Paleozoic rocks on the Grand Banks of Newfoundland. Canadian Journal of Earth Sciences, 23:504–526.

Landsea, C.W., B. Harper, K. Hoarau and J.A. Knaff. 2006. Can We Detect Trends in Extreme Tropical Cyclones? Science, 313: 452-454. 10.1126/science.1128448. Available at: http://www.aoml.noaa.gov/hrd/Landsea/landseaetal-science06.pdf

Lazier, J.R., and D. Wright. 1993. Annual velocity variations in the Labrador current. Journal of Physical Oceanography, 23: 659-678.

LGL Limited. 2003. Orphan Basin Strategic Environmental Assessment. Report Prepared for Canada-Newfoundland Offshore Petroleum Board, St. John's, NL. Project No. SA767.

Lines, G.S., M. Pancura and C. Lander. 2005. Building Climate Change Scenarios of Temperature and Precipitation in Atlantic Canada using the Statistical Downscaling Model (SDSM). Environment Canada, Meteorological Service of Canada, Atlantic Region. Science Report Series No. 2005-9.

Lowe, D.G., P.J. Sylvester and M.E. Enchescu. 2011. Provenance and paleodrainage patterns of upper Jurassic and Lower Cretaceous synrift sandstones in the Flemish Pass Basin, offshore Newfoundland, east coast of Canada. AAPG Bulletin, 95(8): 1295-1320.

Marsh, R., G. Bigg, Y. Zhao, M. Martin, J. Blundell, S. Josey, E. Hanna and V. Ivchenko. 2018. Prospects for seasonal forecasting of iceberg distributions in the North Atlantic. Natural Hazards, 91(2): 447-471. Available at: https://link.springer.com/content/pdf/10.1007%2Fs11069-017-3136-4.pdf

Matthews, M-N, T.J. Deveau, C. Whitt and B. Martin. 2018. Underwater Sound Assessment for Newfoundland Orphan Basin Exploration Drilling Program. Document 01592, Version 4.0. Technical report by JASCO Applied Sciences for Stantec.

McCabe, G., M. Clark and M. Serreze. 2001. Trends in Northern Hemisphere Surface Cyclone Frequency and Intensity. Journal of Climate, 14: 2763-2768.

Minsk, L.D. 1977. Ice Accumulation on Ocean Structures. Cold Regions Research and Engineering Laboratory, Hanover, NH.

Narayanan, S., S. Prinsenberg and P.C. Smith. 1996. Current meter observations from the Labrador and Newfoundland Shelves and comparisons with barotropica model predictions and IIP surface currents. Atmosphere and Ocean, 34(1): 227-255.

National Snow and Ice Data Center. 2015. International Ice Patrol (IIP) Iceberg Sightings Database. (Digital Media). Boulder, Colorado, USA: National Snow and Ice Data Center / World Data Center for Glaciology.

NRCan (Natural Resources Canada). 2007. Grand Banks Iceberg. Management." PERD/CHC Report 20-84. Report prepared for PERD/CHC, National. Research Council Canada, Ottawa, ON. Report prepared by AMEC Americas. AMEC Earth and Environmental; R. F. McKenna and Associates; PETRA International Ltd. Available at: https://nparc.nrc-cnrc.gc.ca/eng/view/fulltext/?id=754dda8b-6c1c-4712-bdc8-a8844324ccaa

NRCan (Natural Resources Canada). 2016. Seismic Hazard Map # 5 (of 5): 2010 National Building Code of Canada. Available at: http://www.earthquakescanada.nrcan.gc.ca/hazard-alea/zoning-zonage/images/NBCC2010canPGApdf_e.pdf.

NRCan (Natural Resources Canada). 2018. Search of the Earthquakes Canada Database. Available at; http://www.earthquakescanada.nrcan.gc.ca/stndon/NEDB-BNDS/bull-en.php?shape_type=region&region_north=89.99&region_east=-50&region_south=40&region_west=-150.

NOAA (National Oceanic and Atmospheric Administration) 2005. Frequently Asked Questions about the Atlantic Multidecadal Oscillation (AMO). Atlantic Oceanographic and Meteorological Laboratory (AOML). United States Department of Commerce. Available at: http://www.aoml.noaa.gov/phod/amo_faq.php

NOAA (National Oceanic and Atmospheric Administration). 2018. North Atlantic Oscillation (NAO). Available at https://www.ncdc.noaa.gov/about

Ocean and Climate Platform. 2018. Cyclones and climate change. Available at: https://ocean-climate.org/?p=4832&lang=en#_ftn3

Ouranos. 2010. Élaborer un plan d'adaptation aux changements climatiques – Guide destiné au milieu municipal québécois; Ouranos, Montréal, Québec, 45 pp., In: J.-P. Savard, D. van Proosdij and S. O'Carroll (eds.) 2016. Perspectives on Canada's East Coast region. Pp. 99-152. Chapter 4 in D.S. Lemmen, F.J. Warren, T.S. James and C.S.L. Mercer Clarke (eds.). Canada's Marine Coasts in a Changing Climate, Government of Canada, Ottawa, ON. Available at: http://www.nrcan.gc.ca/sites/www.nrcan.gc.ca/files/earthsciences/files/pdf/NRCAN_fullBook%20%20accessible.pdf

Overland, J.E. 1990. Prediction of vessel icing for near-freezing sea temperatures. Weather and Climate, 5: 62-77.

Overland, J.E., C.H. Pease, R.W. Priesendorfer and A.L. Comiskey. 1986. Prediction of vessel icing. Journal of Climate and Applied Meteorology, 25: 1793-1806.

Parson, L.M., D.G. Mason, R.G. Rothwell and A.C. Grant. 1984. Remnants of a submerge pre-Jurassic (Devonian?) landscape on Orphan Knoll, offshore eastern Canada. Can. J. Earth. Sci., 21: 61-66.

Petrie, B., K. Lank and S. de Margerie. 1987. Tides on the Newfoundland Grand Banks. Atmosphere and Ocean, 25(1): 10-21.

Piper, D.J.W, A.W.A. MacDonald, S. Ingram, G.L. Williams and C. McCall. 2005. Late Cenzoic architecture of the St. Pierre Slope. Can. J. Earth Sci., 42: 1987-2000.

Rhein, M., S.R. Rintoul, S. Aoki, E. Campos, D. Chambers, R.A. Feely, S. Gulev, G.C. Johnson, S.A. Josey, A. Kostianoy, C. Mauritzen, D. Roemmich, L.D. Talley and F. Wang, 2013: Observations: Ocean. In: Climate Change 2013: The Physical Science Basis. Contribution of Working Group I to the Fifth Assessment Report of the Intergovernmental Panel on Climate Change [Stocker, T.F., D. Qin, G.-K. Plattner, M. Tignor, S.K. Allen, J. Boschung, A. Nauels, Y. Xia, V. Bex and P.M. Midgley (eds.)]. Cambridge University Press, Cambridge, United Kingdom and New York, NY, USA. Available at: https://www.ipcc.ch/pdf/assessment-report/ar5/wg1/WG1AR5_Chapter03_FINAL.pdf

Rogers, E. and L. Bosart. 1986. An Investigation of Explosively Deepening Oceanic Cyclones. Monthly Weather Review, 114: 702-718.

Ruffman, A.R. 2011. Orphan Knoll as a Window on the Paleozoic: Seemingly Ignored by the Petroleum Industry for Over 40 Years. 2011 CSPG CSEG CWLS Convention. 5 pp.

Salon, F, T. Tamarin, I. Rehovot, and Y. Kaspi. 2017.The Poleward Shift of Storm Tracks Under Climate Change: A Lagrangian Perspective. Available at: https://ams.confex.com/ams/21Fluid19Middle/webprogram/Paper319195.html

Savard, J.-P., van Proosdij, D. and O'Carroll, S. 2016. Perspectives on Canada's East Coast region; Pp. 99-152. In: D.S. Lemmen, F.J. Warren, T.S. James and C.S.L. Mercer Clarke (eds.). Canada's Marine Coasts in a Changing Climate, Government of Canada, Ottawa, ON. Available at: http://www.nrcan.gc.ca/sites/www.nrcan.gc.ca/files/earthsciences/files/pdf/NRCAN_fullBook%20%20accessible.pdf

Schrag, D.P., J.A. Higgins, F.A. MacDonald. and D.T. Johnson. 2013. Authigenic carbonate and the history of the global carbon cycle. Science, 339(6119): 540-543.

Seaconsult Ltd. 1998/ Physical Environmental Data for Production Systems at Terra Nova. Report prepared for Petro-Canada Inc.

Senneville, S., S. St-Onge, D. Dumont, M.-C. Bihan-Poudec, Z. Belemaalem, M. Corriveau, P. Bernatchez, S. Bélanger, S. Tolszczuk-Leclerc and R. Villeneuve. 2014. Rapport final Modélisation des glaces dans l'estuaire et le golfe du Saint-Laurent dans la perspective des changements climatiques. In: J.-P. Savard, D. van Proosdij and S. O'Carroll (eds.) 2016. Perspectives on Canada's East Coast region. Pp. 99-152. Chapter 4 in D.S. Lemmen, F.J. Warren, T.S. James and C.S.L. Mercer Clarke (eds.). Canada's Marine Coasts in a Changing Climate, Government of Canada, Ottawa, ON. Available at: http://www.nrcan.gc.ca/sites/www.nrcan.gc.ca/files/earthsciences/files/pdf/NRCAN_fullBook%20%20accessible.pdf

Statoil Canada Ltd. 2017. Flemish Pass Exploration Drilling Program- Environmental Impact Statement. Prepared by Amec Foster Wheeler and Stantec Consulting Ltd. St. John's, NL Canada, November 2017. 1484 pp.

Stuart, R.A. and G.A. Isaac. 1999. Freezing precipitation in Canada. *In* Cheng, Chad Shouquan, Guilong Li & Heather Auld. 2011. Possible Impacts of Climate Change on Freezing Rain Using Downscaled Future Climate Scenarios: Updated for Eastern Canada, Atmosphere-Ocean, 49:1, 8-21, DOI: 10.1080/07055900.2011.555728. Available at: https://doi.org/10.1080/07055900.2011.555728

Swail, V.R., V.J. Cardone, M. Ferguson, D.J. Gummer, E.L. Harris, E.A. Orelup and A.T. Cox. 2006. The MSC50 Wind and Wave Reanalysis. 9th International Wind and Wave Workshop, September 25-29, 2006. Victoria, B.C.

Teague, W.J., M.J. Carron, and P.J. Hogan. 1990. A comparison between the Generalized Digital Environmental Model and Levitus climatologies. Journal of Geophysical Research 95(C5): 7167-7183.

Vanem, E. 2017. A regional extreme value analysis of ocean waves in a changing climate. Ocean Engineering, 144(1): 277–295. Available at: https://www.sciencedirect.com/science/article/pii/S0029801817304808/pdfft?md5=3e087a7fe1f1ad3377d866317dc36125&pid=1-s2.0-S0029801817304808-main.pdf

van Hinte, J.E., A. Ruffman, M. van den Boogaard, J. Jansonius, T.M.G. van Kempen, M.J. Melchin. and T.H. Miller. 1995. Paleozoic fossils from Orphan Knoll, NW Atlantic Ocean. Scr. Geol., 109: 1-63.

Vasseur, L. and N. Catto. 2008. Atlantic Canada. Pp. 119-170. In: D.S. Lemmen, F.J. Warren, J. Lacroix and E. Bush (eds.). From Impacts to Adaptation: Canada in a Changing Climate 2007, Government of Canada, Ottawa, ON. 448 pp.

Weitzman, J., S. Ledger, C.D. Stacey, G. Strathdee, D.J.W. Piper, K.A. Jarret, and J. Higgins. 2014. Logs of short push cores, deep-water margin of Flemish Cap and the eastern Grand Banks of Newfoundland; Geological Survey of Canada, Open File 7148, 389 p.

Wenz, G.M. 1962. Acoustic ambient noise in the ocean: Spectra and sources. Journal of the Acoustical Society of America, 34(12): 1936-1956. https://doi.org/10.1121/1.1909155.

Winterstein, S., T. Ude, C. Cornell, P. Jarager and S. Haver. 1993. Environmental Parameters for Extreme Response: Inverse FORM with Omission Factors. ICOSSar-3, Paper No 509/11/3. Innsbruck.

Woodruff, S.D., S.J. Worley, S.J. Lubker, Z. Ji, J.E. Freeman, D.I. Berry, P. Brohan, E.C. Kent, R.W. Reynolds, S.R. Smith, and C. Wilkinson. 2011. ICOADS Release 2.5: extensions and enhancements to the surface marine meteorological archive. International Journal of Climatology, 31(7), 951-967 (DOI: 10.1002/joc.2103).